

A Thesis Submitted for the Degree of PhD at the University of Warwick

Permanent WRAP URL:

<http://wrap.warwick.ac.uk/90897>

Copyright and reuse:

This thesis is made available online and is protected by original copyright.

Please scroll down to view the document itself.

Please refer to the repository record for this item for information to help you to cite it.

Our policy information is available from the repository home page.

For more information, please contact the WRAP Team at: wrap@warwick.ac.uk

Advanced Materials Prepared by Ring-Opening (Co)Polymerisations of an Alkene-Functional Cyclic Carbonate

Anthony W. Thomas

Submitted for the degree of Doctor of Philosophy

THE UNIVERSITY OF
WARWICK

Department of Chemistry

September 2016

Table of Contents

Table of Contents	i
List of Figures, Schemes and Tables	viii
Figures	viii
Schemes	xvii
Tables	xx
Acknowledgements	xxi
Declaration of Authorship.....	xxii
List of Publications.....	xxiii
Abstract.....	xxiv
List of Abbreviations.....	xxv
1 Introduction.....	1
1.1 Introduction.....	2
1.2 Aliphatic polyesters and polycarbonates in biomedicine.....	2
1.3 Polymerisation techniques	5
1.3.1 Metallo-organic catalysis	5
1.3.2 Organocatalysis.....	6
1.3.3 Toxicity of organocatalysts.....	8
1.4 Functional polymers.....	9
1.4.1 Functional polyesters	10

1.4.2	Functional polycarbonates	11
1.4.3	Post-polymerisation modification of alkene-functional polycarbonates.....	15
1.4.3.1	Radical thiol-ene addition	16
1.4.3.2	Michael addition	24
1.4.3.3	Epoxidation	28
1.4.3.4	Free-radical crosslinking.....	31
1.4.3.5	Other functionalisations	35
1.5	Degradation.....	36
1.5.1	Degradation of aliphatic polyesters and polycarbonates.....	36
1.5.2	Effect of pendent functionality on degradation rate and behaviour	38
1.6	A-B-A triblock copolymers	40
1.6.1	Microphase separation and thermoplastic elastomer behaviour	40
1.6.2	Aliphatic polyester and polycarbonate-based A-B-A triblock copolymers	43
1.7	Conclusion	46
1.8	Aims and Research Objectives	46
1.8	References.....	48
2	Post-Polymerisation Modifications of an Alkene-Functional Polycarbonate.	66
2.1	Introduction.....	67
2.2	Results and discussion	72
2.2.1	Synthesis and polymerisation of 2-allyloxymethyl-2-ethyltrimethylene carbonate (AOMECE).....	72
2.2.2	Post-polymerisation modification of PAOMECE	81
2.2.3	Synthesis of a PAOMECE-based thermoresponsive polymer.....	88

2.3	Conclusions.....	96
2.4	References.....	97
3	Random Copolymers of Cyclic Carbonates and Esters with Tuneable Functional Group Density	102
3.1	Introduction.....	103
3.2	Results and Discussion	107
3.2.1	Monomer screening.....	107
3.2.2	Reactivity ratio studies.....	112
3.2.3	Degradation studies.....	124
3.2.4	Terpolymer synthesis	127
3.3	Conclusions.....	138
3.4	References.....	139
4	Microstereolithography of Resins Based on an Alkene-Functional Polycarbonate.....	143
4.1	Introduction.....	144
4.2	Results and discussion	150
4.2.1	Resin formulation.....	150
4.2.2	3D Printing.....	160
4.2.3	Synthesis and printing of materials bearing epoxide functionality	170
4.3	Conclusion	175
4.4	References.....	176
5	Copolymers of Cyclic Esters and an Alkene- Functional Carbonate for the Synthesis of Thermoplastic Elastomers.....	183

5.1	Introduction.....	184
5.2	Results and discussion	191
5.2.1	Initial experiments.....	191
5.2.2	Variation of AOMECA:VL midblock composition.....	198
5.2.3	Variation of PLLA:midblock composition	210
5.3	Conclusions.....	216
5.4	References.....	217
6	Conclusions and Future Perspectives.....	224
6.1	Conclusions.....	225
6.2	Further work.....	227
6.3	References.....	230
7	Experimental.....	231
7.1	Materials	232
7.2	General Considerations.....	233
7.2.1	NMR spectroscopy.....	233
7.2.2	Mass spectrometry	233
7.2.3	Size exclusion chromatography	234
7.2.4	FT-IR spectroscopy.....	234
7.2.5	UV light source for post-polymerisation modifications.....	234
7.2.6	Determination of lower critical solution temperatures (LCST)	235
7.2.7	Rheometry.....	235
7.2.8	Degradation studies.....	235
7.2.9	Mechanical testing	235

7.2.10	Dynamic mechanical thermal analysis (DMTA)	236
7.2.11	Thermal analysis	236
7.2.12	Microstereolithography (μ SL)	237
7.2.13	Computed tomography.....	237
7.3	Experimental protocols	238
7.3.1	Synthesis of 2-allyloxymethyl-2-ethyltrimethylene carbonate (AOMECE)	238
7.3.2	General procedure for the synthesis of poly(2-allyloxymethyl-2-ethyltrimethylene carbonate (PAOMECE) by DBU/TU-catalysed ring-opening polymerisation (ROP)	239
7.3.3	Synthesis of poly(<i>L</i> -lactide)- <i>b</i> -poly(AOMECE)- <i>b</i> -poly(<i>L</i> -lactide) (PLLA- <i>b</i> -PAOMECE- <i>b</i> -PLLA)	240
7.3.4	Synthesis of PAOMECE- <i>b</i> -PEG- <i>b</i> -PAOMECE	241
7.3.5	General procedure for synthesis of P(AOMECE- <i>co</i> -VL) by organocatalysed ring-opening copolymerisation	242
7.3.6	General procedure for the synthesis of PAOMECE by TBD-catalysed ROP	243
7.3.7	Post-polymerisation functionalisation of PAOMECE with 1-dodecanethiol (DDT)	244
7.3.8	Post-polymerisation functionalisation of PAOMECE with 3-mercaptopropionic acid (3-MPA)	245
7.3.9	Post-polymerisation functionalisation of PAOMECE with benzyl mercaptan (BnSH)	245
7.3.10	Post-polymerisation functionalisation of PAOMECE with 1-thioglycerol.....	246
7.3.11	General procedure for synthesis of thiol-functional poly(ethylene glycol) monomethyl ether (MeO-PEG-SH)	246

7.3.12	General procedure for functionalisation of PAOMEC with thiol-functional PEG monomethyl ether.....	247
7.3.13	Organocatalysed ring-opening copolymerisation of 5-methyl-5-allyloxycarbonyl-1,3-dioxan-2-one (MAC) with δ -valerolactone (VL)	249
7.3.14	Synthesis of poly(δ -valerolactone) (PVL) by organocatalysed ring-opening polymerisation.....	249
7.3.15	Synthesis of 3-ethyl-3-hydroxymethyloxetane	250
7.3.16	Synthesis of 2-(bromomethyl)-2-ethyl-1,3-propanediol	251
7.3.17	Synthesis of 5-(bromomethyl)-5-ethyl-2,2-dimethyl-1,3-dioxane.....	251
7.3.18	Synthesis of 5-ethyl-2,2-dimethyl-5-(propoxymethyl)-1,3-dioxane	252
7.3.19	Synthesis of 2-ethyl-2-(propoxymethyl)propane-1,3-diol	253
7.3.20	Synthesis of 2-propyloxymethyl-2-ethyltrimethylene carbonate (POMEC)....	254
7.3.21	General procedure for the synthesis of poly(2-propyloxymethyl-2-ethyltrimethylene carbonate) (PPOMEC) by organocatalysed ROP.....	255
7.3.22	General procedure for the synthesis of P(AOMEC- <i>co</i> -POMEC) by organocatalysed ROP	255
7.3.23	Synthesis of P(AOMEC- <i>co</i> -POMEC- <i>co</i> -VL) by organocatalysed ROP	256
7.3.24	Procedure for H ₂ O-initiated ROP of AOMEC.....	257
7.3.25	Synthesis of poly(2-allyloxymethyl-2-ethyltrimethylene carbonate)- <i>co</i> -(2-(oxiranyloxy)methyl-2-ethyltrimethylene carbonate) (P(AOMEC- <i>co</i> -OOMEC))..	258
7.3.26	General procedure for 3D printing of structures by radical thiol-ene addition	259
7.3.27	General procedure for the synthesis of PLLA- <i>b</i> -P(AOMEC- <i>co</i> -VL)- <i>b</i> -PLLA triblock copolymers.....	260

7.3.28	One-pot synthesis of PLLA- <i>b</i> -PAOMEC- <i>b</i> -PLLA triblock copolymer	261
7.3.29	One-pot synthesis of PLLA- <i>b</i> -PVL- <i>b</i> -PLLA triblock copolymer	262
7.4	References.....	264
A	Appendix – Supplementary Information.....	265
A.1	Supplementary ¹ H NMR spectra.....	266
A.2	Supplementary ¹³ C NMR spectra.....	269
A.3	Supplementary size exclusion chromatograms	275
A.4	Differential scanning calorimetry (DSC) thermograms for PLLA- <i>b</i> -P(AOMEC- <i>co</i> -VL)- <i>b</i> -PLLA triblock copolymers	277
A.5	Dynamic mechanical thermal analysis data for PLLA- <i>b</i> -P(AOMEC- <i>co</i> -VL)- <i>b</i> -PLLA triblock copolymers.....	280

List of Figures, Schemes and Tables

Figures

- Figure 1.1. Structures of poly(lactic acid) (PLA), poly(lactic acid-*co*-glycolide) (PLGA), poly(ϵ -caprolactone) (PCL) and poly(trimethylene carbonate) (PTMC).....3
- Figure 1.2. Structures of 1,8-diazabicyclo[5.4.0]undec-7-ene (DBU), 1-(3,5-bis(trifluoromethyl)-phenyl)-3-cyclohexylthiourea (thiourea), and 1,5,7-triazabicyclo[4.4.0]dec-5-ene (TBD) catalysts.7
- Figure 1.3. From left to right, general structures of functional dilactones (DL), caprolactone monomers bearing functionality at the alpha, gamma and epsilon positions (*f*CL), and *O*-carboxyanhydrides (OCA)..... 10
- Figure 1.4. Cyclic carbonates bearing pendent alkene-terminated functionality..... 15
- Figure 1.5. Top: Structure of P(LA-*co*-MAC-*g*-Folic acid). Bottom: Microscope images of thin polymer films showing effect of folic acid conjugation on adhesion and proliferation of Vero cells. Left to right: PLA, P(LA-*co*-MAC), P(LA-*co*-MAC-*g*-Folic acid)..... 18
- Figure 1.6. Different mechanisms of polymer hydrolysis. Fading colour for bulk erosion indicates loss of volume throughout polymer, as opposed to a loss of material primarily on the surface of the material for surface erosion.37
- Figure 1.7. Structures of hydroxyl-functional poly(2-hydroxyl trimethylene carbonate) and benzyl-functional poly(2-benzyloxy trimethylene carbonate).39
- Figure 2.1. Structure of P(MEO₂MA-*co*-OEGMA₄₇₅) copolymers and LCST values for varying copolymer compositions.69
- Figure 2.2. ¹H NMR spectrum of 2-allyloxymethyl-2-ethyltrimethylene carbonate (AOMECA) post-distillation (400 MHz, 293 K, CDCl₃). 72
- Figure 2.3. ¹H NMR spectrum of AOMECA polymerisation taken at 62% monomer conversion. [M]₀: [I]₀ = 30, initiated from benzyl alcohol, using a catalyst system of 1 mol% DBU and 5 mol% TU (400 MHz, 293 K, CDCl₃; * = CHCl₃)..... 74
- Figure 2.4. ¹H NMR spectrum of DP 42 PAOMECA initiated from 1,4-butanediol, using a catalyst system of 5 mol% DBU and 5 mol% TU (400 MHz, 293 K, CDCl₃; * = CHCl₃, ** = residual hexane from precipitation). 75
- Figure 2.5. Plot of number-average molecular weight (*M*_n) and dispersity (*D*_M) against % monomer conversion for the homopolymerisation of AOMECA. Conditions: [AOMECA] = 2.0 M in CDCl₃, [M]₀: [I]₀ = 50 using 1,4-butanediol as initiator, 5 mol% DBU and 5 mol% TU as catalysts..... 76

Figure 2.6. Plot of number-average molecular weight (M_n) and dispersity (D_M) against initial monomer-to-initiator concentration ratio, $[M]_0:[I]_0$ for the homopolymerisation of AOMEAC. Conditions: $[AOMEAC] = 2.0$ M in $CDCl_3$, 1,4-butanediol used as initiator, 5 mol% DBU and 5 mol% TU used as catalysts.	76
Figure 2.7. SEC chromatograms of polymers initiated from pentaerythritol dibenzyl ether (PDE), with $[M]_0:[I]_0$ ranging from 12 to 290 to give polymers with DPs of 11 to 232, and D_M values ranging from 1.17 to 1.04. Samples measured against polystyrene standards using $CHCl_3$ as eluent.....	77
Figure 2.8. Mono- and bifunctional alcohol initiators used for the polymerisation of AOMEAC. 1 = Benzyl alcohol; 2 = 1,4-butanediol; 3 = 1,4-benzenedimethanol; 4 = Pentaerythritol dibenzyl ether (PDE).	78
Figure 2.9. 1H NMR spectrum of PAOMEAC ₁₃ -PEG ₆₂ -PAOMEAC ₁₃ triblock copolymer synthesised using a catalyst system of 5 mol% DBU and 5 mol% TU (400 MHz, 293 K, $CDCl_3$; * = $CHCl_3$).	79
Figure 2.10. Size exclusion chromatograms of PEG prior to chain growth ($M_n = 2,000$ g mol ⁻¹ , $D_M = 1.04$) and PAOMEAC-PEG-PAOMEAC triblock ($M_n = 13,300$ g mol ⁻¹ , $D_M = 1.07$). Samples measured against polystyrene standards using $CHCl_3$ as eluent....	79
Figure 2.11. 1H NMR spectrum of PLA ₉₃ -PAOMEAC ₈₀ -PLA ₉₃ triblock copolymer synthesised using a catalyst system of 1 mol% DBU (400 MHz, 293 K, $CDCl_3$; * = $CHCl_3$; ** = residual hexane from precipitation).	80
Figure 2.12. Size exclusion chromatograms of PAOMEAC prior to chain extension ($M_n = 15,800$ g mol ⁻¹ , $D_M = 1.13$) and PLLA-PAOMEAC-PLLA triblock copolymer ($M_n = 30,100$ g mol ⁻¹ , $D_M = 1.12$). Samples measured against polystyrene standards using $CHCl_3$ as eluent.	80
Figure 2.13. Size exclusion chromatograms of PAOMEAC initiated from 1,4-benzenedimethanol using TBD as bifunctional catalyst, with $[M]_0:[I]_0$ ranging from 10 to 125 to give polymers with DPs of 9 to 98, and D_M values ranging from 1.20 to 1.11. Samples measured against polystyrene standards using $CHCl_3$ as eluent.	81
Figure 2.14. 1H NMR spectrum of DP 24 PAOMEAC functionalised with 1-dodecanethiol. Note the absence of alkene resonances at <i>ca.</i> $\delta = 5.8$ and 5.15 ppm, which indicates that complete functionalisation has taken place. (400 MHz, 293 K, $CDCl_3$; * = $CHCl_3$).	82
Figure 2.15. Size exclusion chromatograms of DP 24 PAOMEAC initiated from pentaerythritol dibenzyl ether ($M_n = 5,200$ g mol ⁻¹ , $D_M = 1.11$) and DP 24 PAOMEAC following post-polymerisation functionalisation with 1-dodecanethiol ($M_n = 10,600$ g mol ⁻¹ , $D_M = 1.13$). Samples measured against polystyrene standards using $CHCl_3$ as eluent.	83
Figure 2.16. MALDI-ToF MS of PAOMEAC (DP 20), measured in reflectron mode (top), and MALDI-ToF MS of PAOMEAC post-functionalisation with 1-dodecanethiol, measured in linear mode (bottom).	84

Figure 2.17. Size exclusion chromatograms showing effect on dispersity of varying exposure time to UV light during functionalisation of PAOMEC with 2 eq. of 3-mercaptopropionic acid per alkene group. No clear effect on dispersity can be observed, with $D_M = ca. 1.20$ for all samples. Samples measured against poly(methyl methacrylate) standards using DMF as eluent.	85
Figure 2.18. Size exclusion chromatograms showing effect on dispersity of varying thiol equivalents for functionalisation of PAOMEC with 3-mercaptopropionic acid. Samples measured against poly(methyl methacrylate) standards using DMF as eluent.	86
Figure 2.19. Graphical representation of dispersity (D_M) from SEC to show effect of varying thiol equivalents for functionalisation of PAOMEC with 3-mercaptopropionic acid.	86
Figure 2.20. 1H NMR spectrum of MeO-PEG ₅₅₀ -SH (400 MHz, 293 K, CDCl ₃ ; * = CHCl ₃ ; ** = residual CH ₂ Cl ₂ from washing).....	89
Figure 2.21. SEC trace of MeO-PEG ₅₅₀ -SH. $M_n = 1,150 \text{ g mol}^{-1}$, $D_M = 1.08$). Sample measured against polystyrene standards using CHCl ₃ as eluent.....	89
Figure 2.22. 1H NMR spectrum of PAOMEC-g-PEG ₅₅₀ -OMe (400 MHz, 293 K, CDCl ₃ ; * = H ₂ O).	91
Figure 2.23. SEC traces of PAOMEC ($M_n = 17,700 \text{ g mol}^{-1}$, $D_M = 1.13$) and PAOMEC-g-PEG ₅₅₀ -OMe ($M_n = 67,800 \text{ g mol}^{-1}$, $D_M = 1.17$). Samples measured against polystyrene standards using CHCl ₃ as eluent.	91
Figure 2.24. Plots of transmittance as a function of temperature for PAOMEC-g-PEG ₅₅₀ -OMe over heating and cooling cycles, indicating low polymer hysteresis...92	92
Figure 2.25. Plots of transmittance as a function of temperature for PAOMEC-g-PEG-OMe with various PEG molecular weights measured during heating cycles.....93	93
Figure 2.26. 1H NMR spectrum of PAOMEC-g-PEG _{210/550} -SH showing relative integrals for AOMEC region and PEG repeat units, highlighted in orange and blue respectively. (400 MHz, 293 K, CDCl ₃).....94	94
Figure 2.27. Plots of transmittance as a function of temperature for PAOMEC-g-PEG-OMe with varying average PEG molecular weights prepared by simultaneous grafting of two separate PEG-thiol precursors to PAOMEC, measured during heating cycles. Note that the noise observed for PAOMEC-g-PEG _{210/550} is the result of a fault developed by the UV-visible spectrometer used.....94	94
Figure 2.28. Plot of polymer LCST against average number of PEG repeat units for PAOMEC-g-PEG-OMe.95	95
Figure 3.1. Plot of monomer conversion against time for the copolymerisation of MAC and VL. Conditions: Overall monomer concentration ($[M]$) = 1.0 M in CDCl ₃ , $[MAC]_0:[VL]_0:[I]_0 = 10:10:1$ using benzyl alcohol as initiator, 1 mol% DBU and 5 mol% TU as catalysts..... 109	109

Figure 3.2. ¹ H NMR spectrum of AOMECE/VL copolymerisation taken at 62% AOMECE/28% VL conversion. [AOMECE] ₀ : [VL] ₀ : [BnOH] ₀ = 10:10:1, using a catalyst system of 5 mol% DBU and 5 mol% TU (400 MHz, 293 K, CDCl ₃ ; * = CHCl ₃). .. 110	110
Figure 3.3. Plot of monomer conversion against time for the copolymerisation of AOMECE and VL. Conditions: [M] = 2.0 M in CDCl ₃ , [AOMECE] ₀ : [VL] ₀ : [I] ₀ = 10:10:1 using BnOH as initiator, 5 mol% DBU and 5 mol% TU as catalysts..... 111	111
Figure 3.4. ¹ H NMR spectrum of P(AOMECE _{8-co} -VL ₄) initiated from BnOH (400 MHz, 293 K; * = CDCl ₃ , ** = residual hexane from precipitation, *** = H ₂ O)..... 112	112
Figure 3.5. Size exclusion chromatogram of P(AOMECE _{8-co} -VL ₄) initiated from BnOH (<i>M</i> _n = 2,200 g mol ⁻¹ , <i>D</i> _M = 1.13), measured against polystyrene standards using CHCl ₃ as eluent. Unimodal distribution indicates the synthesis of a single copolymer species. 112	112
Figure 3.6. Plot showing comparison of monomer conversion against time for the copolymerisation of AOMECE with VL using two different catalyst systems. [AOMECE] ₀ : [VL] ₀ : [I] ₀ = 20:80:1, using BDM as initiator, and 5 mol% DBU/5 mol% TU (top x-axis) or 1 mol% TBD (bottom x-axis) as catalysts. 116	116
Figure 3.7. Plot of AOMECE incorporation in the copolymer against AOMECE fraction in the monomer feed, as determined by ¹ H NMR spectroscopy (400 MHz, 293 K, CDCl ₃). This data was subjected to nonlinear least-squares regression analysis to determine the reactivity ratios of AOMECE and VL..... 117	117
Figure 3.8. Expanded carbonyl carbon regions of stacked ¹³ C NMR spectra for polymers 1-5 (AOMECE:VL ratios of 100:0, 89:11, 61:39, 35:65 and 0:100 respectively), showing the change in intensity for the different carbonyl carbon environments with changing copolymer composition (125 MHz, 298 K, CDCl ₃). .. 119	119
Figure 3.9. Deconvoluted and expanded carbonyl carbon regions in ¹³ C NMR spectrum of polymer 3 (AOMECE:VL composition 61:39), with proposed assignments for individual resonances (V = VL, C = AOMECE, observed carbon denoted with *) (125 MHz, 293 K, CDCl ₃). 120	120
Figure 3.10. Plot of decrease in % molecular weight against time for PAOMECE ₈₈ determined by SEC, charting the degradation of the sample in 5M KOH solution. 126	126
Figure 3.11. Selected size exclusion chromatograms showing the molecular weight distribution of PAOMECE recovered at different time points. Note the non-linear degradation behaviour, demonstrating the unreliability of the degradation method used. 126	126
Figure 3.12. ¹ H NMR spectrum of POMECE post-distillation (400 MHz, 293 K, CDCl ₃ , * = CHCl ₃). 129	129
Figure 3.13. ¹ H NMR spectrum of POMECE polymerisation taken at 67% monomer conversion. [POMECE] ₀ : [I] ₀ = 30, initiated from BDM, using a dual catalyst system of DBU (5 mol%) and TU (5 mol%) (400 MHz, 293 K, CDCl ₃ ; * = CHCl ₃). 130	130

Figure 3.14. ^1H NMR spectrum of PPOMEC ₂₃ initiated from BDM, using a catalyst system of 5 mol% DBU and 5 mol% TU (400 MHz, 293 K, CDCl ₃ ; * = CHCl ₃). .	130
Figure 3.15. Size exclusion chromatogram of PPOMEC ₂₃ homopolymer initiated from BDM ($M_n = 5,100 \text{ g mol}^{-1}$, $D_M = 1.14$). Sample measured against polystyrene standards using CHCl ₃ as eluent.	131
Figure 3.16. ^1H NMR spectrum of POMEC/AOMEC copolymerisation taken at 69% monomer conversion. [POMEC] ₀ : [AOMEC] ₀ : [I] ₀ = 62.5:62.5:1 initiated from BDM, using a dual catalyst system of DBU (5 mol%) and TU (5 mol%) (400 MHz, 293 K, CDCl ₃ ; * = CHCl ₃).....	132
Figure 3.17. Expanded pendent ether-methylene regions of stacked ^1H NMR spectra for the copolymerisation of POMEC with AOMEC at different conversions, demonstrating the roughly equal rate of polymerisation of each monomer.....	133
Figure 3.18. ^1H NMR spectrum of P(POMEC _{49-co} -AOMEC ₅₁) initiated from BDM (400 MHz, 293 K; * = CDCl ₃ , ** = residual hexane from precipitation).....	134
Figure 3.19. Stacked ^{13}C NMR spectra of PAOMEC (bottom), PPOMEC (middle) and P(POMEC-co-AOMEC) (top), with deconvoluted and expanded carbonyl carbon regions illustrating the presence of minor block-like homopolymer and major random copolymer resonances in P(POMEC-co-AOMEC) copolymer (125 MHz, 298 K, CDCl ₃).....	135
Figure 3.20. ^1H NMR spectrum of P(POMEC _{10-co} -AOMEC _{11-co} -VL ₄₂) initiated from BDM (400 MHz, 293 K; * = CDCl ₃ , ** = acetone, *** = <i>n</i> -hexane).	136
Figure 3.21. Size exclusion chromatogram of P(POMEC _{10-co} -AOMEC _{11-co} -VL ₄₂) copolymer initiated from BDM ($M_n = 10,800 \text{ g mol}^{-1}$, $D_M = 1.17$). Sample measured against polystyrene standards using CHCl ₃ as eluent.	137
Figure 4.1. Schematic representation of 3D printing by SLA. 1) A target object is scanned and digitally mapped by techniques such as microCT. 2) A digital CAD model is rendered and cut into 2D slices. 3) A digital photomask is rendered for each layer. 4) Using either a scanning laser or a digital mirror device, each layer is then projected sequentially onto a photopolymer, typically using a UV light source to cure the liquid resin. The structure is built upon a moveable build platform, which is moved by the layer height between each projection. The set-up depicted in this figure uses a digital mirror device and a top-down build approach, with the Z-stage moving down into a resin bath between layers.	145
Figure 4.2. ^1H NMR spectrum of DP40 PAOMEC initiated from water, using 1 mol% TBD as catalyst (400 MHz, 293 K; * = CHCl ₃ , ** = H ₂ O, c' = chain end unit)....	151
Figure 4.3. Size exclusion chromatograms of PAOMEC initiated from water, using 1 mol% TBD ($M_n = 8,200 \text{ g mol}^{-1}$, $D_M = 1.37$) and 5 mol% TBD ($M_n = 21,000 \text{ g mol}^{-1}$, $D_M = 1.83$) as catalyst. Samples measured against polystyrene standards using CHCl ₃ as eluent.....	152

Figure 4.4. Size exclusion chromatograms of PAOMEC initiated from H ₂ O, with M_n = 1,500, 2,200 and 3,300 g mol ⁻¹ , and D_M values of 2.43, 1.33 and 1.29 respectively. Samples measured against polystyrene standards using CHCl ₃ as eluent.	154
Figure 4.5. Plot of viscosity (mPa s ⁻¹) against ascending and descending shear rate (s ⁻¹) for PAOMEC homopolymers initiated from water with M_n = 3,300, 2,200, and 1,500 g mol ⁻¹	156
Figure 4.6. Plot of viscosity (mPa s ⁻¹) against ascending and descending shear rate (s ⁻¹) for PAOMEC homopolymer (M_n = 2,200 g mol ⁻¹) and resin formulations containing PAOMEC, tetrathiol crosslinker (RSH) and 5, 10 and 20 wt% propylene carbonate (PC) as viscosity modifier.	157
Figure 4.7. Plot of stress (MPa) against strain (%) for photocured resin samples, displaying elastic deformation until failure.	159
Figure 4.8. Plot of stress (MPa) against strain (%) for cyclic extension tests of photocured resin samples, displaying no deformation or loss of modulus over 10 cycles.	160
Figure 4.9. Photographs of resin formulations cured by exposure to rectangular projections of purple light. All samples pictured were exposed for 30 s, using photoinitiator/inhibitor loadings of (A) 0.5/0.25 wt%, (B) 1.0/0.25 wt%, (C) 2.0/0.25 wt% and (D) 0.5/0 wt%.	161
Figure 4.10. Schematic and photographic representation of μ SL setup. A = purple light engine with peak output at 415 nm; B = digital mirror device for mask projection; C = focussing optics; D = 45° mirror; E = transparent silicone resin tray; F = build platform mounted on a motion stage moveable along the Z-axis; G = computer system for control of exposure times and build platform movement.	163
Figure 4.11. Exposure pattern progression used for the building of 1 mm-high walls. Each 100 μ m resin layer was exposed to all 5 projections sequentially, with the pattern progressing every 5 seconds.	165
Figure 4.12. Photograph of 1 mm-high walls produced by μ SL using exposure times of (left to right) 35, 40, 45, 50 and 55 seconds.	165
Figure 4.13. Photographs of (10,3)-a mathematical network produced by μ SL of PAOMEC-based resin, displaying good feature fidelity and interconnected pores running through structure, with structure placed on a 5 pence piece in lower photographs to illustrate scale.	167
Figure 4.14. Micro-CT images of (10,3)-a mathematical network produced by μ SL of PAOMEC-based resin. Top left: image of complete structure viewed along a single axis. Top right: image of interior structure, showing the presence of interconnected pores in a single plane. Bottom: rectangular cutaway of structure, showing the porous nature of the construct through all three axes.	168

Figure 4.15. FT-IR spectra of PAOMEC and crosslinked PAOMEC-based resin, with key absorptions and absences highlighted.	169
Figure 4.16. ¹ H NMR spectrum of P(AOMEC ₅ - <i>co</i> -OOMECS ₅) synthesised by partial epoxidation of PAOMEC ₁₀ with mCPBA (400 MHz, 293 K, CDCl ₃ ; * = CHCl ₃). 171	171
Figure 4.17. Size exclusion chromatogram of P(AOMEC ₅ - <i>co</i> -OOMECS ₅), with $M_n = 2,700 \text{ g mol}^{-1}$ and $D_M = 1.31$. Sample measured against polystyrene standards using CHCl ₃ as eluent.	171
Figure 4.18. FT-IR spectra of PAOMEC and P(AOMEC- <i>co</i> -OOMECS), with oxirane C-O-C stretch highlighted.	172
Figure 4.19. Photographs of a 400 μm -thick baseplate bearing 100 μm -high lines, produced by μSL of P(AOMEC- <i>co</i> -OOMECS)-based resin. Exposure times for lines (left to right): 115, 125, 135, 145 and 155 seconds.	173
Figure 4.20. FT-IR spectra of P(AOMEC- <i>co</i> -OOMECS) and cured P(AOMEC- <i>co</i> -OOMECS)-based resin, indicating that the epoxide group remains unaffected by the thiol-ene crosslinking reaction.	174
Figure 5.1. Schematic representation of a multiblock thermoplastic elastomer with semi-crystalline hard domains. (I) Polymer in relaxed state and (II) under uniaxial tensile stress. Upon removal of stress, configuration I is regained.	186
Figure 5.2. Examples of aliphatic polymers prepared by ROP and employed as amorphous segments of A-B-A triblock and multiblock copolymers.	187
Figure 5.3. ¹ H NMR spectrum of P(AOMEC ₁₆ - <i>co</i> -VL ₁₁) initiated from BDM (400 MHz, 293 K; * = CHCl ₃).	192
Figure 5.4. Stacked ¹ H NMR spectra of PLLA- <i>b</i> -P(AOMEC- <i>co</i> -VL)- <i>b</i> -PLLA triblock copolymers, showing the change in intensity of the PLLA methine proton ($\delta = 5.16 \text{ ppm}$) with varying PLLA block incorporation (400 MHz, 293 K, CDCl ₃).	194
Figure 5.5. Size exclusion chromatograms for P(AOMEC ₁₆ - <i>co</i> -VL ₁₁) macroinitiator and PLLA- <i>b</i> -P(AOMEC- <i>co</i> -VL)- <i>b</i> -PLLA triblock copolymers with different PLLA block incorporations. $M_n = 5,500 - 9,900 \text{ g mol}^{-1}$, $D_M \leq 1.16$ for all samples. Samples measured against polystyrene standards using CHCl ₃ as eluent.	195
Figure 5.6. ¹ H NMR spectrum of PLLA- <i>b</i> -P(AOMEC- <i>co</i> -VL)- <i>b</i> -PLLA triblock copolymer (56 mol% PLLA) initiated from P(AOMEC ₄₅ - <i>co</i> -VL ₅₃), using 0.5 mol% DBU as polymerisation catalyst (400 MHz, 293 K, CDCl ₃ ; * = CHCl ₃).	197
Figure 5.7. Size exclusion chromatogram of P(AOMEC ₄₅ - <i>co</i> -VL ₅₃) macroinitiator (DP 98, $M_n = 15,000 \text{ g mol}^{-1}$, $D_M = 1.17$) and corresponding PLLA- <i>b</i> -P(AOMEC- <i>co</i> -VL)- <i>b</i> -PLLA triblock copolymer (56 mol% PLLA, $M_n = 38,800 \text{ g mol}^{-1}$, $D_M = 1.09$). Samples measured against polystyrene standards with CHCl ₃ as eluent.	197
Figure 5.8. Example plots of stress (MPa) against strain (%) for triblock copolymers based on DP 27 and DP 98 macroinitiators up to 50% strain. Full extension data for ABA triblock based on DP 98 macroinitiator is shown in Figure 5.15 (P 209).	198

Figure 5.9. Stacked ^1H NMR spectra of PLLA- <i>b</i> -P(AOMECEC- <i>co</i> -VL)- <i>b</i> -PLLA triblock copolymers, showing the change in intensity of the PAOMECEC and PVL methylene resonances with varying AOMECEC:VL midblock composition (400 MHz, 293 K, CDCl_3).....	200
Figure 5.10. Size exclusion chromatograms of PLLA- <i>b</i> -P(AOMECEC- <i>co</i> -VL)- <i>b</i> -PLLA triblock copolymers with varying AOMECEC:VL midblock composition. $M_n = 22,900 - 49,200 \text{ g mol}^{-1}$, $D_M \leq 1.18$ for all polymers. Samples measured against polystyrene standards using CHCl_3 as eluent.	200
Figure 5.11. Expanded DSC thermograms of PLLA- <i>b</i> -P(AOMECEC- <i>co</i> -VL)- <i>b</i> -PLLA triblock copolymers showing the change in soft block T_g with varying AOMECEC:VL midblock composition.....	202
Figure 5.12. Expanded DSC thermograms of PLLA- <i>b</i> -P(AOMECEC- <i>co</i> -VL)- <i>b</i> -PLLA triblock copolymers showing the change in hard block T_g with varying AOMECEC:VL midblock composition. Tangent lines included to highlight the change in gradient of each thermogram.	203
Figure 5.13. Graphical representation of changing glass transition temperatures of PLLA- <i>b</i> -P(AOMECEC- <i>co</i> -VL)- <i>b</i> -PLLA triblock copolymers with varying AOMECEC:VL midblock composition.....	205
Figure 5.14. Plot of elastic and loss moduli of PLLA- <i>b</i> -P(AOMECEC- <i>co</i> -VL)- <i>b</i> -PLLA triblock copolymers (MPa) against AOMECEC midblock content (%), determined by dynamic mechanical thermal analysis using a heating rate of $2 \text{ }^\circ\text{C min}^{-1}$ and an oscillation rate of 0.5 Hz.	205
Figure 5.15. Example plots of stress (MPa) against strain (%) for PLLA- <i>b</i> -P(AOMECEC- <i>co</i> -VL)- <i>b</i> -PLLA triblock copolymers with varying AOMECEC:VL midblock composition.	207
Figure 5.16. Initial stress (MPa) vs strain (%) curves for PLLA- <i>b</i> -P(AOMECEC- <i>co</i> -VL)- <i>b</i> -PLLA triblock copolymers with varying AOMECEC:VL midblock composition, highlighting the difference in stiffness between materials.....	208
Figure 5.17. Plots of stress (MPa) against strain (%) for PLLA- <i>b</i> -P(AOMECEC- <i>co</i> -VL)- <i>b</i> -PLLA triblock copolymers under repeated application of 200% strain, using an elongation rate of 5 mm min^{-1}	209
Figure 5.18. Size exclusion chromatograms of PLLA- <i>b</i> -P(AOMECEC- <i>co</i> -VL)- <i>b</i> -PLLA triblock copolymers with varying PLLA:midblock composition. $M_n = 25,700 - 55,600 \text{ g mol}^{-1}$, $D_M \leq 1.18$ for all polymers. Samples measured against polystyrene standards using CHCl_3 as eluent.	211
Figure 5.19. Example plots of stress (MPa) against strain (%) for PLLA- <i>b</i> -P(AOMECEC- <i>co</i> -VL)- <i>b</i> -PLLA triblock copolymers with varying PLLA:midblock composition.	214

Figure 5.20. Plot of stress (MPa) against strain (%) for PLLA-*b*-P(AOMEC-*co*-VL)-*b*-PLLA triblock copolymers with varying PLLA:midblock composition under single application and removal of 200% strain, using an elongation rate of 5 mm min⁻¹..215

Schemes

Scheme 1.1. Coordination-insertion mechanism for ROP of cyclic monomers.	5
Scheme 1.2. Mechanism of intermolecular transesterification using PLA as an example polymer. Individual polymer chains and components have been coloured for clarity.....	6
Scheme 1.3. Mechanism of bifunctional initiation, where E is the electrophilic species and B is the Brønsted base, using δ -valerolactone as an example monomer.....	8
Scheme 1.4. Multistep synthesis of 3-(<i>S</i>)-[(benzyloxycarbonyl)methyl]-1,4-dioxane-2,5-dione (BMD).....	11
Scheme 1.5. Synthesis of 5-methyl-5-allyloxycarbonyl-1,3-dioxan-2-one (MAC). .	14
Scheme 1.6. Post-polymerisation modification of PMAC with mercaptans <i>via</i> radical thiol-ene addition.	16
Scheme 1.7. Synthesis of PMAC- <i>g</i> -(ADPC- <i>co</i> -Mal-DOX), with DOX functionality highlighted.	20
Scheme 1.8. Reaction scheme for the synthesis of a photocured 3D-printed scaffold.	24
Scheme 1.9. Functionalisation of P(CL- <i>co</i> -AC) with mercaptans <i>via</i> Michael-type addition.....	25
Scheme 1.10. Orthogonal modification of alkene-functional copolymer by sequential Michael and thiol-ene addition.....	27
Scheme 1.11. Epoxidation of PMAC and subsequent functionalisation with PEI for the formation of polycarbonate/DNA polyplexes.	29
Scheme 1.12. Epoxidation of PATMC and subsequent ROP of ATMC, using epoxide functionality as initiator.	31
Scheme 1.13. Crosslinking of P(LLA- <i>co</i> -CL- <i>co</i> -MAC) with UV and no additional crosslinker.	34
Scheme 1.14. <i>In situ</i> synthesis of aldehyde-functional polycarbonate and functionalisation with <i>O</i> -(carboxymethyl)hydroxylamine.....	35
Scheme 1.15. Hydrolysis of aliphatic polyesters (top) and polycarbonates (bottom).	37
Scheme 1.16. ROP of TMC using a bifunctional initiator to generate a telechelic macroinitiator, followed by chain extension with <i>L</i> -lactide to generate an A-B-A triblock copolymer.	44
Scheme 2.1. Synthesis of MAC <i>via</i> allylation of bis-MPA, followed by ring-closure of the resulting 1,3-diol.	70

Scheme 2.2. Synthesis of 2-allyloxymethyl-2-ethyltrimethylene carbonate (AOMECE) <i>via</i> ring-closure of trimethylolpropane allyl ether diol (TMAD).....	72
Scheme 2.3. Synthesis of PAOMECE <i>via</i> organocatalyzed ring-opening polymerisation, using a dual DBU/thiourea catalyst system. ROH = mono- or bifunctional alcohol initiator.....	73
Scheme 2.4. Post-polymerisation functionalisation of PAOMECE with 1-dodecanethiol.....	82
Scheme 2.5. Synthesis of monofunctional PEG-thiol.....	88
Scheme 2.6. Grafting of MeO-PEG-SH onto PAOMECE.....	90
Scheme 3.1. Synthesis of P(MACE-co-VL) <i>via</i> ring opening polymerisation, using a dual catalyst system of DBU/thiourea and benzyl alcohol as initiator.	108
Scheme 3.2. General reaction scheme for the synthesis of P(AOMECE-co-VL) <i>via</i> ring-opening polymerisation, using DBU (5 mol%) and TU (5 mol%) as polymerisation catalysts. HO-R-OH = 1,4-butanediol (BDO), pentaerythritol dibenzyl ether (PDE) or 1,4-benzenedimethanol (BDM).....	110
Scheme 3.3. Synthetic procedure for the production of the alkyl ether-functional monomer, 2-propyloxymethyl-2-ethyltrimethylene carbonate (POMECE).....	128
Scheme 3.4. Synthesis of PPOMECE <i>via</i> ring opening polymerisation, using a dual catalyst system of DBU/thiourea and 1,4-benzenedimethanol as initiator.	129
Scheme 3.5. Synthesis of P(POMECE-co-AOMECE-co-VL) <i>via</i> ring opening polymerisation, using a dual catalyst system of DBU/thiourea and 1,4-benzenedimethanol as initiator.....	136
Scheme 4.1. Synthesis of PAOMECE <i>via</i> TBD-catalysed ROP, using water as the initiating species.....	151
Scheme 4.2. Mechanism of nucleophilic attack of AOMECE by water followed by subsequent decarboxylation of the intermediate carbonic acid-functional species, to yield a bifunctional alcohol initiator.	153
Scheme 4.3. Synthesis of 3D crosslinked networks by radical thiol-ene addition, using Irgacure 819 as photoinitiator, propylene carbonate as viscosity modifier, and purple light with a peak output at 415 nm to initiate crosslinking.....	164
Scheme 4.4. Synthesis of polymer bearing both alkene and epoxide pendent functionalities (P(AOMECE-co-OOMECE)) by post-polymerisation modification of PAOMECE.....	170
Scheme 5.1. General reaction scheme for the synthesis of P(AOMECE-co-VL) macroinitiators <i>via</i> ring-opening polymerisation, using DBU (5 mol%) and TU (5 mol%) as polymerisation catalysts and 1,4-benzenedimethanol (BDM) as initiator.	192

Scheme 5.2. General reaction scheme for the synthesis of PLLA-*b*-P(AOMECA-co-VL)-*b*-PLLA triblock copolymers *via* ring-opening polymerisation using DBU (0.5 mol%) as polymerisation catalyst. 193

Tables

Table 1.1 – Mechanical properties of aliphatic polyesters and carbonates commonly used in biomedicine.....	4
Table 1.2. Cyclic carbonates bearing a small selection of available functionalities..	12
Table 2.1. Polymers of AOMECEC initiated from different mono- and bifunctional alcohol initiators.....	78
Table 2.2. Photoinitiated radical thiol-ene post-polymerisation modification of PAOMECEC	87
Table 3.1. Homo- and copolymers of AOMECEC and VL prepared by ring-opening polymerisation.....	118
Table 3.2. Dyad and triad fractions of VL sequences in P(AOMECEC-co-VL) copolymers as determined by integration of relevant resonances using ¹³ C NMR spectroscopy.....	122
Table 3.3. Dyad and triad fractions of AOMECEC sequences in P(AOMECEC-co-VL) copolymers as determined by integration of relevant resonances using ¹³ C NMR spectroscopy.....	122
Table 3.4. Number-average sequence lengths for VL and AOMECEC calculated from dyad and triad fractions, using equations 7-10.....	123
Table 3.5. Degrees of randomness for P(AOMECEC-co-VL) copolymers calculated from dyad and triad fractions using equation 11.	123
Table 5.1. Composition of triblock copolymers prepared from macroinitiators with varying AOMECEC:VL ratios.....	199
Table 5.2. Glass transition temperatures of PLLA- <i>b</i> -P(AOMECEC-co-VL)- <i>b</i> -PLLA triblock copolymers with varying AOMECEC:VL midblock composition.....	203
Table 5.3. Mechanical properties of PLLA- <i>b</i> -P(AOMECEC-co-VL)- <i>b</i> -PLLA triblock copolymers with varying AOMECEC:VL midblock composition.....	207
Table 5.4. Composition of triblock copolymers with PLLA:midblock ratios.	211
Table 5.5. Glass transition temperatures of PLLA- <i>b</i> -P(AOMECEC-co-VL)- <i>b</i> -PLLA triblock copolymers with varying PLLA:midblock composition.	213
Table 5.6. Mechanical properties of PLLA- <i>b</i> -P(AOMECEC-co-VL)- <i>b</i> -PLLA triblock copolymers with varying PLLA:midblock composition.....	214

Acknowledgements

Firstly, I would like to thank Prof. Andrew Dove for giving me the opportunity to undertake a PhD in his group, and for his continual guidance (and occasional kicks up the backside) over the course of the last four years. The Universities of Warwick and Queensland are also gratefully acknowledged for funding my research.

The work that has gone into the preparation of this thesis is probably best described as a labour of... well, labour! No man is an island, and I couldn't have achieved this work without the help and support of my friends and colleagues in the Dove and O'Reilly groups. The experiences we've shared have made me both a better chemist and a better person, and my genuine thanks go to all those who I've worked with past and present. Special mentions go to Craig, Ed, Anaïs, Becky, and the dream team of Annette and Guillaume – whether it was advice, a sympathetic ear over a tea/pint, or twerking to awful, awful music in the lab, you guys went a long way to making it all worthwhile. Additional thanks also go to my marvellous team of proof-readers (Anaïs, Becky, Chiara, Ed, and Guillaume), who have undoubtedly saved me from considerable embarrassment and made this thesis vaguely readable.

Outside of the university, I'm forever thankful for the faith and support of my teachers, friends, and family. Thank you to my parents for their constant love and support, and for giving me the confidence to achieve more in my life to date than I would ever have believed possible. Finally, my thanks and love go to my long-suffering and significantly better half, Naomi, who has (for reasons unknown) stood by me through thick and thin. I promise I'll be a bit less boring now that I've submitted, and I can't wait to find out what our PhD-free future holds in store for us.

Declaration of Authorship

This thesis is submitted to the University of Warwick in support of my application for the degree of Doctor of Philosophy. It has been composed by myself and has not been submitted in any previous application for any degree. The work presented (including data generated and data analysis) was carried out by the author except in the cases outlined below:

- Non-linear least squares regression analysis in Chapter 3 was performed by Dr Yan Kang (University of Warwick).
- Differential scanning calorimetry data in Chapter 4 was performed by Dr Ruairí Brannigan and Marianne Rolph (University of Warwick).
- MicroCT images were obtained by Edward Cant (University of Warwick). Dr Simon Leigh (University of Warwick) is gratefully acknowledged for providing permission to use the X-ray CT scanner.
- Quantitative ^{13}C NMR spectra were obtained by Dr Ivan Prokes and Rob Perry (University of Warwick).

List of Publications

Synthesis of aliphatic polycarbonates with a tuneable thermal response, Thomas, A.W.; Kuroishi, P. K.; Madrigal, M. M. P.; Whittaker, A. K.; Dove, A. P.; *submitted (Polym. Chem.) (Chapter 2)*.

Synthesis of degradable poly(ϵ -caprolactone)-based graft copolymers via a “grafting-from” approach, Bexis, P.; Thomas, A. W.; Bell, C. A.; Dove, A. P. *Polym. Chem.* **2016**, *7*, 7126.

Postpolymerisation Modifications of Alkene-Functional Polycarbonates for the Development of Advanced Biomaterials, Thomas, A. W.; Dove, A. P. *Macromol. Biosci.* **2016**, *16*, 1762 (Chapter 1).

Core functionalization of semi-crystalline polymeric cylindrical nanoparticles using photo-initiated thiol–ene radical reactions, Sun, L; Pitto-Barry, A.; Thomas, A. W.; Inam, M.; Doncom, K.; Dove, A. P.; O'Reilly, R. K. *Polym. Chem.* **2016**, *7*, 2337.

Highly Polarized Alkenes as Organocatalysts for the Polymerization of Lactones and Trimethylene Carbonate, Naumann, S.; Thomas, A. W.; Dove, A. P. *ACS Macro Lett.* **2016**, *5*, 134.

N-Heterocyclic Olefins as Organocatalysts for Polymerization: Preparation of Well-Defined Poly(propylene oxide), Naumann, S.; Thomas, A. W.; Dove, A. P. *Angew Chem. Int. Ed.* **2015**, *54*, 9550.

Abstract

This thesis describes the synthesis of functional materials based on homo- and copolymers of an alkene-functional cyclic carbonate, 2-allyloxymethyl-2-ethyltrimethylene carbonate (AOMECE), prepared *via* organocatalysed ring-opening polymerisations (ROP).

Chapter 1 provides a general introduction to the main concepts which are applied throughout this thesis, and surveys the reported applications of alkene-functional polycarbonates prepared by ROP in the published literature.

Chapter 2 details the synthesis of poly(2-allyloxymethyl-2-ethyltrimethylene carbonate) (PAOMECE) *via* organocatalysed ROP, and subsequent post-polymerisation modifications of this material through radical thiol-ene addition chemistry. In addition, the grafting of poly(ethylene glycol) (PEG) to the polycarbonate backbone to generate thermoresponsive materials is described.

Chapter 3 describes the synthesis of statistical copolymers of AOMECE and δ -valerolactone (VL), and the synthesis of terpolymers of AOMECE, VL and an alkyl-functional carbonate, 2-propyloxymethyl-2-ethyltrimethylene carbonate (POMECE) in order to provide materials with independently modifiable functional group density and ester:carbonate composition.

Chapter 4 explores the use of thiol-ene addition chemistry to generate PAOMECE-based porous 3D structures *via* microstereolithography. The partial epoxidation of the pendent alkene groups of PAOMECE is also described, and initial results detailing the fabrication of epoxide-functional 3D constructs are presented.

Chapter 5 details the use of homo- and copolymers of AOMECE and VL as macroinitiators for the ROP of *L*-lactide (LLA) in order to generate A-B-A triblock copolymers with thermoplastic elastomer character. In addition, this chapter describes the simple modification of the mechanical properties and elastomeric behaviour of these materials through variation of the midblock composition, and also by changing the ratio of hard to soft block segments.

Chapter 6 provides a general summary of Chapters 2-5, and explores opportunities for further work that may be productively undertaken based on the results presented in this thesis.

Chapter 7 lists experimental protocols and spectroscopic data for the materials presented in this thesis.

List of Abbreviations

$[M]_0:[I]_0$	Monomer:iniator ratio
1,3-DTC	1,3-Dimethyl trimethylene carbonate
2,2-DTC	2,2-Dimethyl trimethylene carbonate
3-MPA	3-Mercaptopropionic acid
<i>a</i>	Size of monomer
AC	(Meth)Acryloyl carbonate
ACL	Anterior cruciate ligament
ADPC	12-Acryloyloxy dodecyl phosphorylcholine
AHA	α -Hydroxy acid
AIBN	Azobis(isobutyronitrile)
AOMEC	2-Allyloxymethyl-2-ethyltrimethylene carbonate
ATMC	5-Allyloxy-1,3-dioxan-2-one
BDM	1,4-Benzenedimethanol
BDO	1,4-Butanediol
BHEAA	<i>N,N</i> -Bis(2-hydroxyethyl)-9-anthracene-methanamine
BHECA	<i>N,N</i> -Bis(2-hydroxyethyl) cinnamamide
BHT	Butylated hydroxytoluene
bis-MPA	2,2'-Bis(hydroxymethyl) propionic acid

BMD	3-(<i>S</i>)-[(Benzyloxycarbonyl)methyl]-1,4-dioxane-2,5-dione
BnSH	Benzyl mercaptan
BSA	Bovine serum albumen
BTMC	2-Benzyloxy trimethylene carbonate
CAD	Computer-aided design
CC	Cytochrome C
CDSA	Crystallisation-driven self-assembly
CL	ϵ -Caprolactone
CT	Computerised tomography
CuAAC	Copper-catalysed azide-alkyne cycloaddition
d	Doublet
DBU	1,8-Diazabicyclo[5.4.0]undec-7-ene
DCTB	Trans-2-[3-(4-tertbutylphenyl)-2-methyl-2-propylidene]malonitrile
dd	Doublet of doublets
DDT	1-Dodecanethiol
DL	ϵ -Decalactone
DLP	Direct light projection
DLs	Cyclic dilactones
D_M	Dispersity

DMAP	4-Dimethylaminopyridine
DMD	Digital mirror device
DMF	Dimethylformamide
DMPA	2,2-Dimethoxy-2-phenylacetophenone
DMTA	Dynamic mechanical thermal analysis
DNA	Deoxyribonucleic acid
DOPA	3,4-Dihydroxyphenylalanine
DOPA-thiol	<i>N</i> -(3,4-Dihydroxyphenetyl)-4-mercaptobutanamide
DOX	Doxorubicin
DP	Degree of polymerisation
DPC	Diphenyl carbonate
DSC	Differential scanning calorimetry
<i>E</i>	Young's modulus
<i>E'</i>	Storage modulus
<i>E''</i>	Loss modulus
eq.	Equivalents
ESI	Electrospray Ionisation
<i>F</i>	Molar fraction
<i>f</i> CL	Functionalised ϵ -caprolactone

F_{stretch}	Stretching force
FT-IR	Fourier transform-infrared spectroscopy
F_{VV}	Copolymer dyad sequence fraction (for two adjacent V units)
h	Hextet
HDI	Hexamethylene diisocyanate
J	Proton coupling constant
k_{B}	Boltzmann constant
k_{init}	Rate of initiation
k_{prop}	Rate of propagation
KRSR	Lysine-arginine-serine-arginine peptide
k_{x}	Rate of reaction
LCST	Lower critical solution temperature
LDA	Lithium diisopropyl amide
LiTFSI	Lithium bis(trifluoromethanesulfonimide)
LLA	<i>L</i> -Lactide
L_{V}	Average sequence length (of monomer V)
m	Multiplet
MAC	5-Methyl-5-allyloxycarbonyl-1,3-dioxan-2-one
MALDI-ToF	Matrix-assisted laser desorption ionisation time-of-flight

Mal-DOX	6-Maleimidocaproyl-doxorubicin
MC	5-Methyl-5-cinnamoyloxymethyl-1,3-dioxan-2-one
<i>m</i> CPBA	3-Chloroperoxybenzoic acid
MeO-PEG-OH	Poly(ethylene glycol) monomethyl ether
MeO-PEG-SH	Thiol-terminated poly(ethylene glycol) monomethyl ether
MEW	Melt electrospinning writing
micro-CT	Micro computerised tomography
M_n	Number-average molecular weight
mPEG	Methoxy-poly(ethylene glycol)
MRI	Magnetic resonance imaging
MS	Mass spectrometry
MTC-Et	5-Methyl-5-ethyloxycarbonyl-1,3-dioxane-2-one
MTT	3-(4,5-Dimethylthiazol-2-yl)-2,5-diphenyltetrazolium bromide
M_w	Weight-average molecular weight
N	Total degree of polymerisation
n_A	Degree of polymerisation (of monomer A)
NMR	Nuclear magnetic resonance
NVP	<i>N</i> -Vinyl-2-pyrrolidone
OCA	<i>O</i> -Carboxyanhydride

OEGMA	Oligo(ethylene glycol) methyl ether methacrylate
OOMECC	2-(Oxiranyloxy)methyl-2-ethyl trimethylene carbonate
P3HB	Poly(3-hydroxybutyrate)
P4HB	Poly(4-hydroxybutyrate)
PBS	Phosphate buffered saline
PC	Propylene carbonate
PDE	Pentaerythritol dibenzyl ether
PDLA	Poly(<i>D</i> -lactide)
PDLLA	Poly(<i>D,L</i> -lactide)
PDMS	Poly(dimethylsiloxane)
PDXO	Poly(1,5-dioxepan-2-one)
PEG	Poly(ethylene glycol)
PEI	Polyethyleneimine
PGA	Poly(glycolide)
PGS	Poly(glycerol sebacate)
PHTMC	Poly(2-hydroxyl trimethylene carbonate)
PLA	Poly(lactic acid)
PLGA	Poly(lactide- <i>co</i> -glycolide)
PMOC	Poly(5-methyl-5-oxoethyloxycarbonyl-1,3-dioxan-2-one)

PMVL	Methyl-substituted poly(valerolactone)
POMEC	2-Propyloxymethyl-2-ethyltrimethylene carbonate
PPF	Poly(propylene fumarate)
PTFE	Poly(tetrafluoroethylene)
<i>p</i> TSA	<i>para</i> -Toluenesulfonic acid
<i>R</i>	Degree of randomness
<i>r</i> ₁	Reactivity ratio (of monomer 1)
RDRP	Reversible-deactivation radical polymerisation
RGD	Arginylglycylaspartic acid tripeptide
RGDC	Arginine-glycine-aspartic acid-cysteine peptide
RI	Refractive index
ROP	Ring-opening polymerisation
<i>s</i>	Singlet
SEC	Size exclusion chromatography
SLA	Stereolithography
SPAAC	Strain-promoted azide-alkyne cycloaddition
<i>t</i>	Triplet
<i>T</i>	Temperature
TBD	1,5,7-Triazabicyclo[4.4.0]dec-5-ene

TBDMS	<i>tert</i> -Butyldemethylsilyl
T_g	Glass transition temperature
TGA	Thermogravimetric analysis
THF	Tetrahydrofuran
THPA	Tetrahydropyran acrylate
TMAD	Trimethylolpropane allyl ether diol
TMC	Trimethylene carbonate
TPE	Thermoplastic elastomer
TU	1-(3,5-Bis(trifluoromethyl)-phenyl)-3-cyclohexylthiourea
UTS	Ultimate tensile strength
UV	Ultra-violet
VL	δ -Valerolactone
VS	Vinyl sulfone
Z	Number of nearest-neighbour monomers
δ	Chemical shift
ΔG_{mix}	Gibbs free energy of mixing
ΔH_{mix}	Enthalpy of mixing
ΔS_{mix}	Entropy of mixing
ϵ_{AB}	Interaction energy (between monomers A and B)

ϵ_b	Strain at break
λ	Wavelength
μSL	Microstereolithography
ϕ_A	Volume fraction
χ	Flory-Huggins interaction parameter

1 Introduction

1.1 Introduction

The research presented in this thesis is focussed on the preparation of materials based on an aliphatic polycarbonate bearing pendent functionality, for potential applications in the field of biomedicine. The following chapter is designed to serve as an overview of previous published research relevant to the work presented in subsequent chapters. The use of common commercially available aliphatic polyesters and polycarbonates in biomedicine will first be evaluated, followed by an appraisal of polymerisation techniques that are commonly employed for their preparation. The development of more exotic functional polyesters and polycarbonates, and their modification post-polymerisation will then be discussed, along with the degradation behaviour of these materials. Finally, the use of copolymers of cyclic esters and carbonates for the preparation of thermoplastic elastomers will be reviewed.

1.2 Aliphatic polyesters and polycarbonates in biomedicine

In recent years, the development of biocompatible, biodegradable polymers has provided a raft of new materials with applications in the biomedical field, including drug delivery vehicles and support structures for hard and soft tissues.¹⁻⁴ As polymerisation techniques have improved and become more versatile, the number of materials available for biomedical application has increased dramatically. The increase in the number of these materials has enabled the development of materials which are not only biocompatible and non-toxic, but also degradable at a rate concordant with the rate of new tissue growth, possessing tuneable mechanical properties and with the ability to promote tissue regeneration through the incorporation of biologically active molecules.⁴⁻⁸

One class of polymers that has shown particular promise as biomedical materials is aliphatic polyesters, the most widely studied of which are homo- and copolymers of α -hydroxy acids, in particular poly(lactic acid) and poly(lactide) (PLA), poly(lactide-*co*-glycolide) (PLGA), and poly(ϵ -caprolactone) (PCL), the structures of which are shown in Figure 1.1.⁹⁻¹⁹ The success of these materials results from the control that can be achieved over their degradation times and mechanical properties, the low toxicity of both the polymers and their degradation products, and the fact that these degradation products are often either excreted or resorbed *via* metabolic pathways – for example, PLA is hydrolysed to lactic acid, which is removed in the Krebs cycle.²⁰⁻²³ The low cost and ready availability of the starting materials also makes these polymers attractive options for larger-scale syntheses. However, these materials have limited application in tissue engineering as a consequence of their rigidity compared to soft tissues. As an example, isotactic poly(*L*-lactic acid) (PLLA) and poly(*D*-lactic acid) (PDLA) have elastic moduli in the region of 1,200-3,000 MPa dependent on molecular weight, while that of myocardium is below 1 MPa.^{24,25}

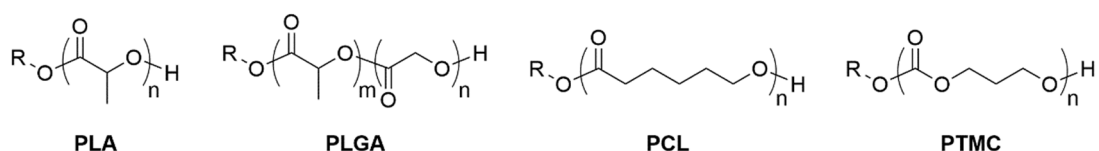


Figure 1.1. Structures of poly(lactic acid) (PLA), poly(lactic acid-*co*-glycolide) (PLGA), poly(ϵ -caprolactone) (PCL) and poly(trimethylene carbonate) (PTMC).

Advances in polymerisation techniques and the development of new functional monomers have resulted in an increasing interest in the use of aliphatic polycarbonates for biomedical applications in recent years.²⁶⁻²⁸ To date, the only aliphatic polycarbonate which has been widely studied and ratified for use in biomedical implants is poly(trimethylene carbonate) (PTMC, Figure 1.1), however these materials

offer an interesting alternative to polyesters as a result of their mechanical properties, degradation behaviour, and relative ease of incorporating functionality in the polymer backbone.²⁹⁻³¹ Aliphatic polycarbonates can possess much lower elastic moduli than polyesters (*e.g.* 3 MPa for PTMC, Table 1.1) and as such, by copolymerising cyclic esters with cyclic carbonates, it is possible to drastically reduce the rigidity of a polymer with respect to polyester homopolymers.²⁵ For example, whilst PCL possesses an elastic modulus of *ca.* 400 MPa, Bat *et al.* were able to demonstrate that copolymerisation of ϵ -caprolactone with trimethylene carbonate could reduce the elastic modulus to as low as 2.7 MPa for polymers with molecular weights of up to 113,500 g mol⁻¹.³²

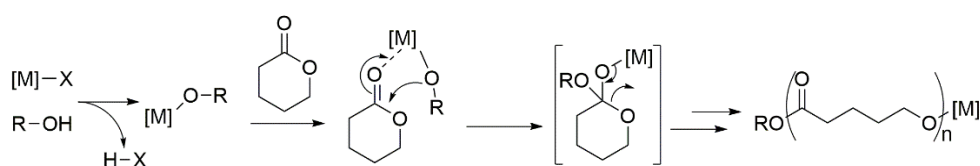
Table 1.1 – Mechanical properties of aliphatic polyesters and carbonates commonly used in biomedicine.²⁵

Polymer	Molecular Weight (g mol ⁻¹)	Tensile Strength (MPa)	Young's Modulus (MPa)	Elongation (Yield %)	Elongation (Break %)
PLLA	50,000	28	1,200	3.7	6.0
PLLA	100,000	50	2,700	2.6	3.3
PDLA	107,000	29	1,900	4.0	5.6
PCL	44,000	16	400	7.0	80
PTMC	48,000	0.5	3	20	160

1.3 Polymerisation techniques

1.3.1 Metallo-organic catalysis

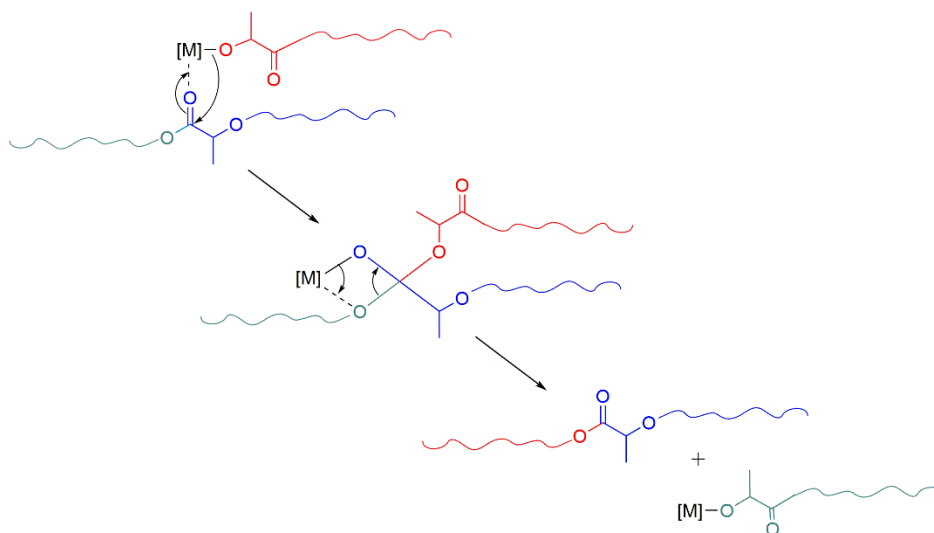
Aliphatic polyesters and polycarbonates are generally produced by the ring-opening polymerisation (ROP) of cyclic lactone and carbonate monomers. The ROP of these monomers is most commonly achieved through the use of metallo-organic catalysts such as tin(II) bis-2-ethylhexanoate (stannous octanoate).³³⁻³⁶ Metallo-organic complexes, particularly those based on metal alkoxides, have been shown to be excellent catalysts for ring-opening polymerisations, generating very fast rates and high turnover numbers, and usually proceed by a coordination-insertion mechanism.³⁷⁻³⁹ The mechanism for the reaction involves the metallo-organic catalyst activating an alcohol initiator to form the metal alkoxide. The metal centre activates the monomer by coordination to the carbonyl oxygen, followed by nucleophilic attack of the carbonyl by the alkoxide moiety. Once insertion has occurred, the catalyst forms a metal alkoxide with the alcohol of the chain end, thus propagating the reaction (Scheme 1.1).⁴⁰



Scheme 1.1. Coordination-insertion mechanism for ROP of cyclic monomers.⁴⁰

However, there are some disadvantages to using metallo-organic catalysts. The catalysts are typically highly sensitive, and the coordination-insertion mechanism often leads to both inter- and intramolecular transesterification reactions.⁴⁰ The former involves the catalyst coordinating to a carbonyl in the growing polymer chain instead of the carbonyl of the monomer, resulting in chain-transfer and a broadening of the

dispersity of the polymer (Scheme 1.2). Intramolecular transesterifications proceed in a similar manner, but with the catalyst and carbonyl being part of the same polymer chain, leading to the formation of cyclic by-products.



Scheme 1.2. Mechanism of intermolecular transesterification using PLA as an example polymer. Individual polymer chains and components have been coloured for clarity.⁴⁰

In addition, the necessary removal of potentially toxic metal catalyst residues to reach safe levels post-polymerisation, particularly for biomedical applications, can be time consuming and expensive. These factors have driven efforts to develop alternative strategies for the catalysis of ROP.⁴¹

1.3.2 Organocatalysis

The use of organocatalysis for ring-opening polymerisations is a relatively new development. Whilst the metal-catalysed ROP of lactide was first reported in 1932 by Carothers,⁴² the first documented use of an organic catalyst for ROP was the polymerisation of lactide using 4-dimethylaminopyridine (DMAP) in 2001 by Nederberg *et al.*⁴³ The use of organocatalysis brings several advantages over the use of metallo-organic complexes. Organocatalysts are generally less air and water

sensitive than their metallo-organic counterparts, they are generally synthesised from cheaper and more readily available starting materials, have simpler methods of preparation and are comparatively environmentally benign.⁴⁴ As a result, a considerable amount of research has been conducted in this field with a wide range of diverse organic catalysts (including those based on pyridine, phosphines, phosphazenes, diphenyl phosphoric acid, sulfonic acids, *N*-heterocyclic carbenes and *N*-heterocyclic olefins) shown to be active for the polymerisation of cyclic lactones and carbonates.^{40,41,45-52}

“Superbase” catalysts based on amidine and guanidine substructures have been widely applied to the ROP of cyclic monomers.^{47,53-56} In 2006 Lohmeijer and co-workers first described the use of guanidine catalyst 1,5,7-triazabicyclo[4.4.0]dec-5-ene (TBD) and the amidine catalyst 1,8-diazabicyclo[5.4.0]undec-7-ene (DBU) (Figure 1.2) for the organocatalytic ring-opening of cyclic esters. Both catalysts showed excellent activity for the polymerisation of lactide, with > 98% conversion achieved in 2 h for a monomer to initiator ratio ($[M]_0:[I]_0$) of 500 using 1 mol% DBU, and as little as 1 minute using 0.1 mol% of the more basic TBD under similar conditions. Dispersities (D_M) of < 1.1 were reported for both catalysts, although it should be noted that the high activity of TBD led to a significant degree of transesterification at extended reaction times.⁵³

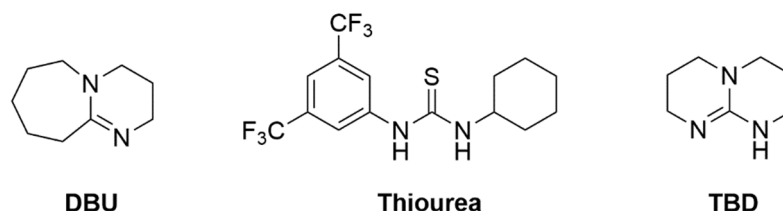
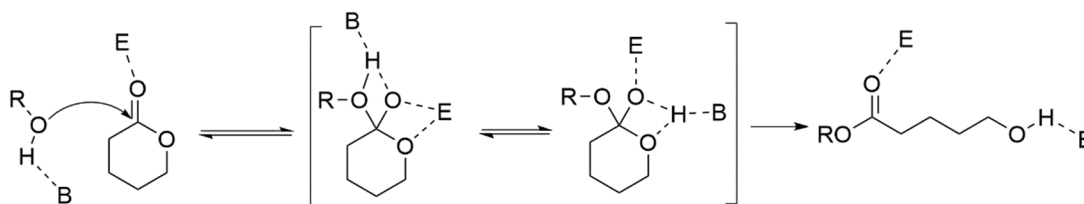


Figure 1.2. Structures of 1,8-diazabicyclo[5.4.0]undec-7-ene (DBU), 1-(3,5-bis(trifluoromethyl)phenyl)-3-cyclohexylthiourea (thiourea), and 1,5,7-triazabicyclo[4.4.0]dec-5-ene (TBD) catalysts.

Whilst active for the polymerisation of lactide, it has been shown that DBU alone is not active for the polymerisation of δ -valerolactone (VL) or ϵ -caprolactone (CL). However, the inclusion of a thiourea-based co-catalyst (such as 1-(3,5-bis(trifluoromethyl)-phenyl)-3-cyclohexylthiourea, Figure 1.2) results in these polymerisations proceeding *via* a bifunctional catalyst system. DBU acts as a Brønsted base and forms a hydrogen-bond with the initiating alcohol, thus activating it by enhancing its nucleophilicity, whilst an electrophile (the thiourea) simultaneously activates the carbonyl of the monomer unit through hydrogen bond donation (Scheme 1.3). In contrast, TBD can simultaneously hydrogen bond to both the initiating alcohol and the carbonyl moiety of the monomer, and can therefore function as a bifunctional catalyst without requiring the use of a co-catalyst.^{53,57}



Scheme 1.3. Mechanism of bifunctional initiation, where E is the electrophilic species and B is the Brønsted base, using δ -valerolactone as an example monomer.⁴⁰

1.3.3 Toxicity of organocatalysts

Nachtergaeel and co-workers have assessed the cytotoxicity of a wide selection of organocatalysts used for the polymerisation of cyclic lactones and carbonates. Performing colourimetric assays using 3-(4,5-dimethylthiazol-2-yl)-2,5-diphenyltetrazolium bromide (MTT) on two different cell lines, the authors demonstrated that in general these organocatalysts displayed remarkably low levels of cytotoxicity, with DBU and TBD catalysts showing 100% cell viability at concentrations of over 110 μ M. This represents a significant advantage over certain

commercially-employed metallo-organic catalysts such as dibutyltinbis(2-ethylhexanoate), which resulted in > 90% cell death at concentrations of as little as 5 μM . However, it was noted that the functional thiourea catalyst tested did exhibit considerable cytotoxicity, with cell death exceeding 50% at concentrations of *ca.* 10 μM . Whilst the authors recommend subjecting the thiourea catalyst to rigorous toxicity studies before validating its use for biomedical and green chemistry applications, its toxicity still represents an improvement on dibutyltinbis(2-ethylhexanoate), particularly considering that the catalyst concentrations assessed in the study are far higher than likely residual levels in polymers.⁵⁸

1.4 Functional polymers

The ability to incorporate chemical functionalities in polymers that can promote specific and favourable cell behaviour is highly desirable for applications in targeted therapeutics and tissue engineering.^{59,60} As such, there is an increasing interest in polymers bearing pendent functionality, both for physical and chemical modification of materials post-polymerisation, and for the attachment of biologically active molecules. Traditionally, functionality has been incorporated in polyesters and polycarbonates by ROP of a cyclic monomer bearing the desired functionality, however the number of different functionalities available is limited by this approach due to the incompatibility of certain functional groups (such as alcohols and carboxylic acids) with ROP. By modification of relatively simple pendent moieties post-polymerisation, the challenges associated with limited monomer compatibility can be circumvented to achieve functional polymers which would not otherwise be available.^{61,62}

1.4.1 Functional polyesters

Several examples of functional polymers based on polyesters have been reported in the literature, and are generally produced by ROP of one of three classes of monomers: (i) cyclic dilactones (DLs) based on the 1,4-dioxane-2,5-dione substructure produced by dimerisation of pre-prepared functional α -hydroxyacids (AHAs),⁶³⁻⁶⁶ (ii) seven-membered lactone monomers produced by anionic activation of ϵ -caprolactone using lithium diisopropyl amide (LDA), followed by addition of the functional reagent to the resulting lithium carbanion to generate a functional caprolactone monomer (*f*CL),⁶⁷⁻⁷² and; (iii) *O*-carboxyanhydrides (OCAs), prepared by the ring-closure of functional AHAs using diphosgene (Figure 1.3).⁷³⁻⁷⁶

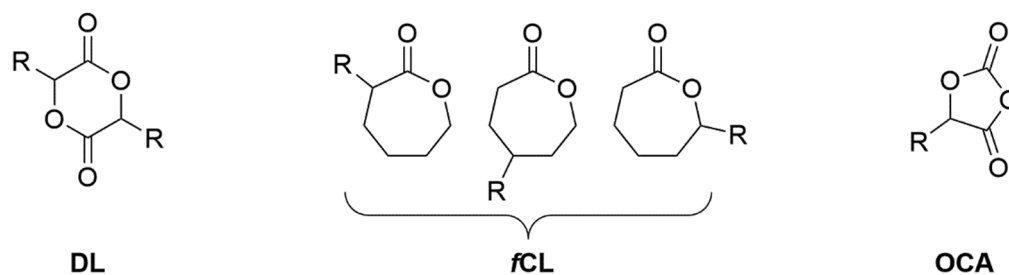
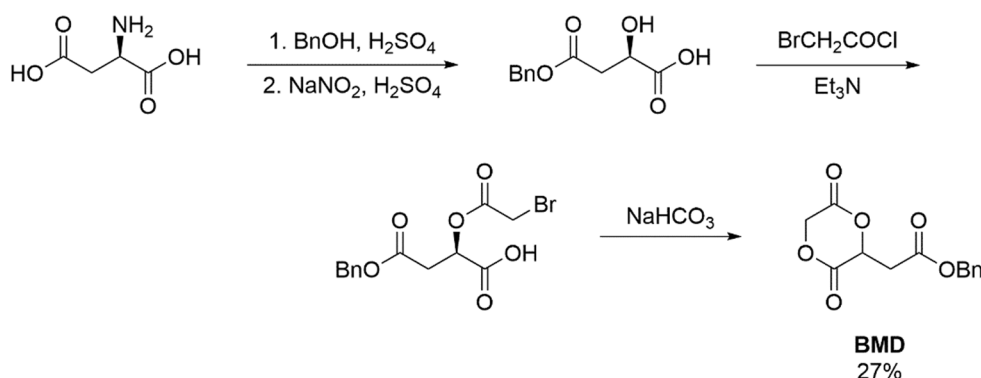


Figure 1.3. From left to right, general structures of functional dilactones (DL), caprolactone monomers bearing functionality at the alpha, gamma and epsilon positions (*f*CL), and *O*-carboxyanhydrides (OCA).

There are several thorough review articles covering the large library of functional polyesters prepared by ROP of these monomers, including benzyl-protected carboxylic acids and ethers, acetal-protected alcohols, poly(ethylene glycol) (PEG) side-chains, alkene, allyl, and carboxybenzyl-protected amine groups. Post-polymerisation modification of these materials has further broadened the range of available polyesters to include those bearing free hydroxyl-bearing groups.^{59,66,77-79}

However, whilst these classes of monomer offer routes to a broad range of functional degradable polymers, they are not without their drawbacks. Syntheses typically

involve several complex and time-consuming synthetic steps, coupled with low overall yields (typically up to 40% for DLs, with some examples yielding as little as 10%).^{66,78} For example, the synthesis of the functional DL 3-(*S*)-[(benzyloxycarbonyl)methyl]-1,4-dioxane-2,5-dione (BMD) is achieved through β -carboxylic acid protection of aspartic acid with benzyl alcohol, followed by diazotisation with sodium nitrite. The resulting intermediate is then coupled to bromoacetyl chloride in the presence of triethylamine (Et_3N) to form the required AHA precursor, which is subsequently cyclised using sodium hydrogen carbonate (NaHCO_3) to produce BMD in only 27% overall yield (Scheme 1.4).⁶⁴ As a result of these difficulties, the viability of functional polyesters for practical applications is limited.



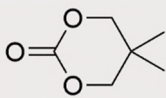
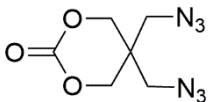
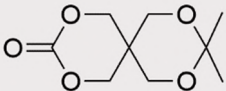
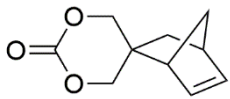
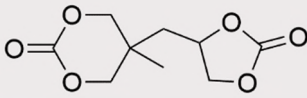
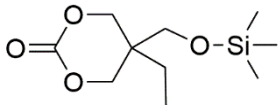
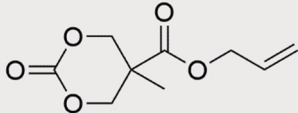
Scheme 1.4. Multistep synthesis of 3-(*S*)-[(benzyloxycarbonyl)methyl]-1,4-dioxane-2,5-dione (BMD).⁶⁴

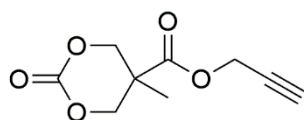
1.4.2 Functional polycarbonates

Although less common than functional polyesters, functional aliphatic polycarbonates have received considerable attention in recent years as they can offer a relatively simple route to degradable polymers bearing pendent functionality. Their synthesis can be achieved either through the synthetically challenging copolymerisation of epoxides with CO_2 , or by the ring-opening polymerisation of cyclic carbonate monomers prepared by the ring-closure of 1,3-diols (typically through the use of

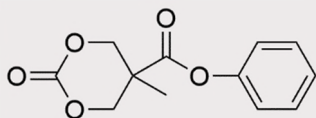
phosgene derivatives), with the latter of these methodologies being more prevalent as a result of the comparative ease of synthesis.^{27,28,31} As with the case for functional polyesters, several recent comprehensive review articles may be found in the literature detailing the various functionalities available using this approach, a selection of which are shown in Table 1.2.^{30,31,80-83}

Table 1.2. Cyclic carbonates bearing a small selection of available functionalities.^{30,82,83}

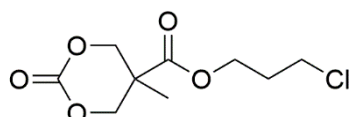
Functional group	Year	Authors
	1997	Ariga, T., Takata, T. and Endo, T. ⁸⁴
	1998	Cai, J., Zhu, K. J. and Yang, S. L. ⁸⁵
	1999	Vandenberg, E. J., and Tian, D. A. ⁸⁶
	1991	Kühling, S., Keul, H., Höcker, H., Buysch, H. J., Schön, N., and Leitz, E. ⁸⁷
	2005	Endo, T., Kakimoto, K., Ochiai, B., and Nagai, D. ⁸⁸
	1991	Kühling, S.; Keul, H.; Höcker, H.; Buysch, H. J., Schön, N. ⁸⁹
	2003	Mullen, B. D., Tang, C. N., and Storey, R. F. ⁹⁰



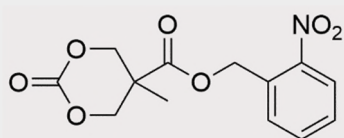
2008 Pratt, R. C., Nederberg, F., Waymouth, R. M., and Hedrick, J. L.⁹¹



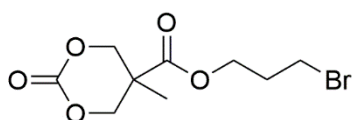
2009 Seow, W. Y., and Yang, Y. Y. J.⁹²



2008 Pratt, R. C., Nederberg, F., Waymouth, R. M., and Hedrick, J. L.⁹¹

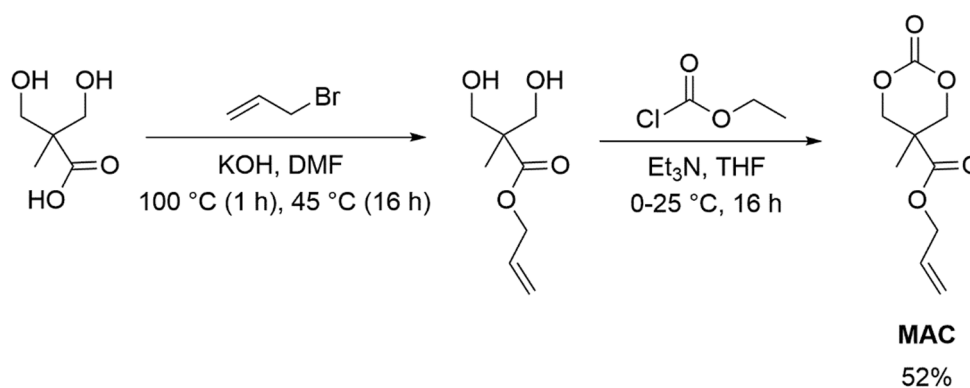


2008 Xie, Z. G., Hu, X. L., Chen, X. S., Sun, J., Shi, Q., and Jing, X. B.⁹³



2010 Sanders, D. P., Fukushima, K., Coady, D. J., Nelson, A., Fujiwara, M., Yasumoto, M., and Hedrick, J. L.⁹⁴

In contrast to functional ester monomers, the synthesis of cyclic carbonate monomers bearing pendent functionality is relatively simple to achieve, with higher yields (up to *ca.* 80%) and fewer synthetic steps. For example, the synthesis of the allyl-functional cyclic carbonate 5-methyl-5-allyloxycarbonyl-1,3-dioxan-2-one (MAC) can be achieved in only two steps from the commercially available 2,2'-bis(hydroxymethyl) propionic acid (bis-MPA) precursor (Scheme 1.5), with an overall yield of 52% (*c.f.* four synthetic steps and 27% overall yield for the benzyl-functional dilactone BMD).^{31,95}



Scheme 1.5. Synthesis of 5-methyl-5-allyloxycarbonyl-1,3-dioxan-2-one (MAC).⁹⁵

Functional carbonates have been copolymerised with non-functional cyclic esters and TMC as a method of incorporating functionality and conferring favourable mechanical properties on materials. Carbonates bearing non-reactive pendent groups such as methyl groups or alkyl chains are generally employed to tailor mechanical properties and degradation rates, or are copolymerised with carbonates bearing reactive functionalities in order to tailor the percentage of reactive groups present in a material.^{96,97} Carbonates bearing reactive functionalities such as aryl, allyl, halide and azide moieties provide a route for modification of a material's properties post-polymerisation.⁹⁸⁻¹⁰¹

Whilst the number of pendent functionalities compatible with ROP is not limited to the relatively simple functionalities listed above,^{88,102} post-polymerisation modification of materials bearing even these simple functionalities can be employed to produce materials bearing a much wider range of functional groups. As a small selection of potential modifications, benzyl-functional polymers may be deprotected by hydrolysis to yield alcohol and carboxylic acid functional groups (which may then be further modified themselves *e.g.* by esterification),¹⁰³⁻¹⁰⁵ pendent halide functionalities may undergo reaction with nucleophiles,^{101,106,107} alkene groups can be modified to provide a wide range of additional functionalities through Michael

addition or radical thiol-ene coupling reactions,¹⁰⁸⁻¹¹⁰ and alkyne and azide-functional polymers may be modified through copper or strain-promoted azide-alkyne click chemistry (CuAAC and SPAAC).^{100,111,112} Incorporation of multiple functionalities or sequential modification can be used to generate materials bearing multiple functionalities that would normally be incompatible with ROP.^{113,114}

1.4.3 Post-polymerisation modification of alkene-functional polycarbonates

One of the most versatile groups for post-polymerisation modification is the alkene functionality. These materials have proved useful as no protection or deprotection steps are needed to yield the functional polymer. In addition, the versatility of the alkene group allows a wide range of modifications to be performed, for example through Michael addition, radical thiol-ene addition, and epoxidation reactions. The broad range of techniques that can be used to modify alkene-functional polycarbonates is particularly useful, as if one method of introducing additional functionality is unsuitable under certain conditions, a more amenable method of modification may be used to confer similar functionality. The following subsections present an in-depth review of practical applications of polymers prepared from cyclic carbonates bearing alkene-terminated pendent functionalities (Figure 1.4).

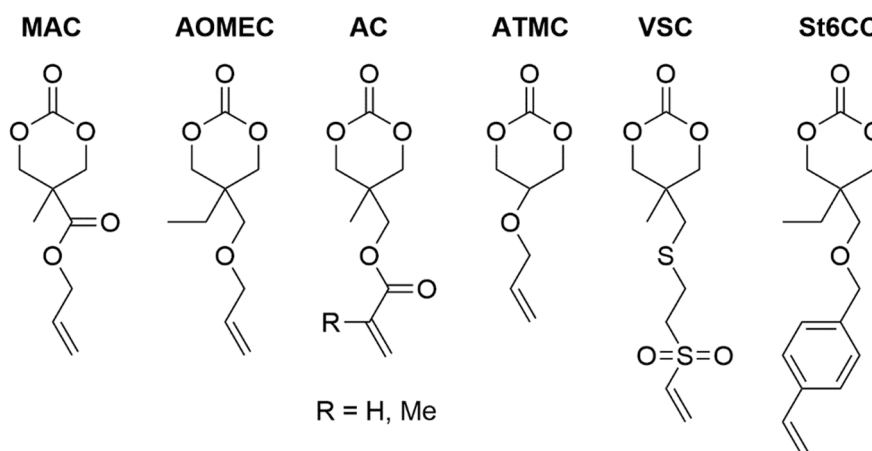
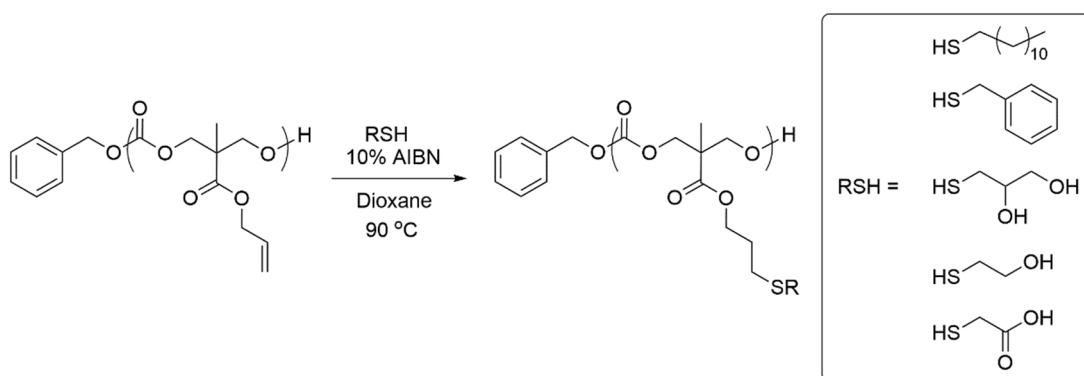


Figure 1.4. Cyclic carbonates bearing pendent alkene-terminated functionality.

1.4.3.1 Radical thiol-ene addition

1.4.3.1.1 Conjugation of additional functionality

The most widely studied method of modifying alkene-functional polycarbonates is by the conjugation of thiol-bearing compounds to the polymer through thermally or photochemically-initiated radical thiol-ene addition reactions. Using this method, a wide range of different chemical functionalities have been conferred onto alkene-functional polymers. For instance, thermally-initiated radical thiol-ene chemistry has been utilised by Tempelaar *et al.* to attach several different thiols to a PMAC backbone. Using PMAC as the alkene-functional polycarbonate platform, azobis(isobutyronitrile) (AIBN) as a radical initiator and two equivalents of thiol per alkene group to avoid unwanted crosslinking, 1-dodecanethiol, benzyl mercaptan, 1-thioglycerol, mercaptoethanol and mercaptoacetic acid were all successfully attached to the polymer backbone with near quantitative conversion of the allyl groups (Scheme 1.6). In addition to introducing new functionality to the polymer, thermal analysis demonstrated that changing the pendent groups had a marked effect on physical properties, with the glass transition temperature (T_g) of the materials ranging from -33 °C for mercaptoacetic acid up to -5.1 °C for benzyl mercaptan.¹⁰⁹



Scheme 1.6. Post-polymerisation modification of PMAC with mercaptans *via* radical thiol-ene addition.¹⁰⁹

Olsén *et al.* have shown that the thiol-ene reaction can be applied to polymers of the allyloxy-functional monomer, 2-allyloxymethyl-2-ethyltrimethylene carbonate (AOMECE). PAOMECE was functionalised by means of photoinitiated radical thiol-ene addition, using five equivalents of dodecanethiol per allyl group and benzophenone as a photoinitiator. The functionalisation was shown to proceed with good control, with a linear relation between conversion of allyl groups and increasing polymer molecular weight, with the structural integrity of the final polymer maintained.¹¹⁵

In a recent paper, Olofsson and co-workers used thiol-ene addition chemistry to prepare self-healing gel materials with catechol functionality. To achieve this, the researchers first synthesised *N*-(3,4-dihydroxyphenetyl)-4-mercaptobutanamide (DOPA-thiol), a synthetic alternative to naturally occurring 3,4-dihydroxyphenylalanine (DOPA), an amino acid which has attracted considerable interest as a result of its interesting adhesive properties. PMAC was then functionalised with DOPA-thiol using UV light to trigger a photoinitiated radical thiol-ene addition, generating polycarbonates with pendent catechol groups. Gels were formed by addition of Fe^{3+} , as a result of the high affinity of the catechol functionality for these ions. Increasing pH resulted in a higher degree of complexation of Fe^{3+} ions with the catechol group, ranging from monocomplexes at pH 5, to *bis* and *tris* complexes at higher pH. A solution of catechol-functional polymer with $\text{FeCl}_3 \cdot 6\text{H}_2\text{O}$ (catechol: Fe^{3+} ratio of 3:1) was prepared in a solution of 2 M NaOH in methanol, resulting in the production of free-standing gels. Application of strain to the gels resulted in a drop in elastic modulus and viscosity, and a consequent loss in gel properties. However, when the strain was removed, the gel-like character of the material was fully regained. The reliability of this self-healing property was

demonstrated by repeated application and removal of strain, with the complete reformation of the gel shown to occur in under 6 seconds after each test.¹¹⁶

The thiol-ene reaction has also been utilised for the direct conjugation of biologically active molecules. In 2008, Hu *et al.* synthesised P(LA-*co*-MAC) copolymers conjugated with folic acid. The synthesis of the material was achieved by first activating folic acid with *N*-hydroxysuccinimide and reacting this activated species with 2-aminoethanethiol to yield thiol-functional folic acid, which was then grafted onto the P(LA-*co*-MAC) copolymer *via* radical thiol-ene addition. The cytotoxicity and cell affinity of the material was assessed using Vero cells. Following incubation for 48 h, folic acid-grafted polymers showed greater cell adhesion and proliferation than both PLA and P(LA-*co*-MAC) films (Figure 1.5), indicating that these materials have improved interaction between the polymer and cells, thus potentially limiting foreign body reactions typically associated with polymeric soft tissue implants.^{95,117}

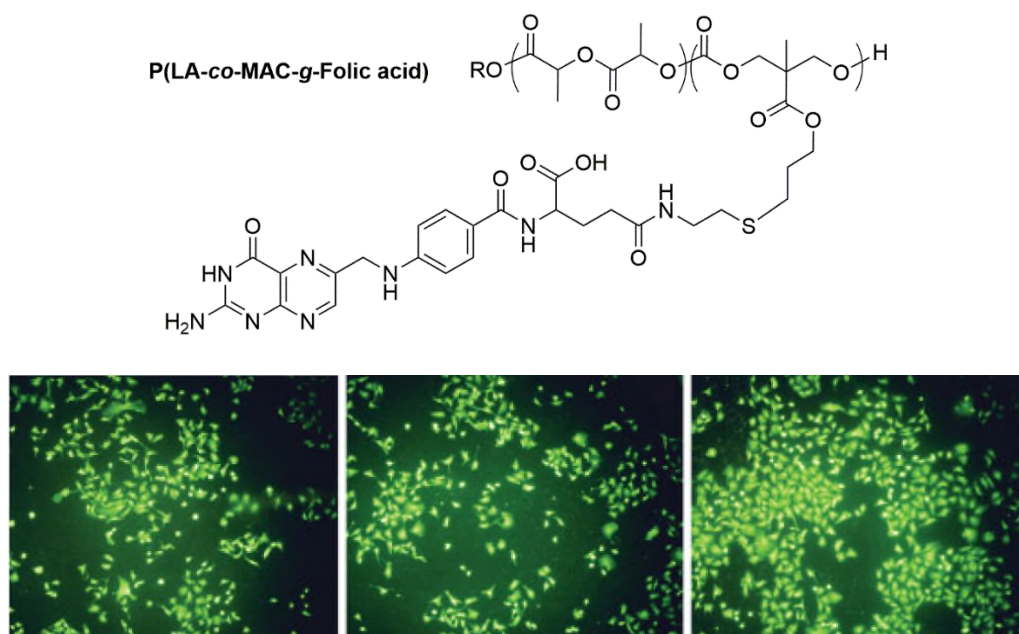


Figure 1.5. Top: Structure of P(LA-*co*-MAC-*g*-Folic acid). Bottom: Microscope images of thin polymer films showing effect of folic acid conjugation on adhesion and proliferation of Vero cells. Left to right: PLA, P(LA-*co*-MAC), P(LA-*co*-MAC-*g*-Folic acid).¹¹⁷

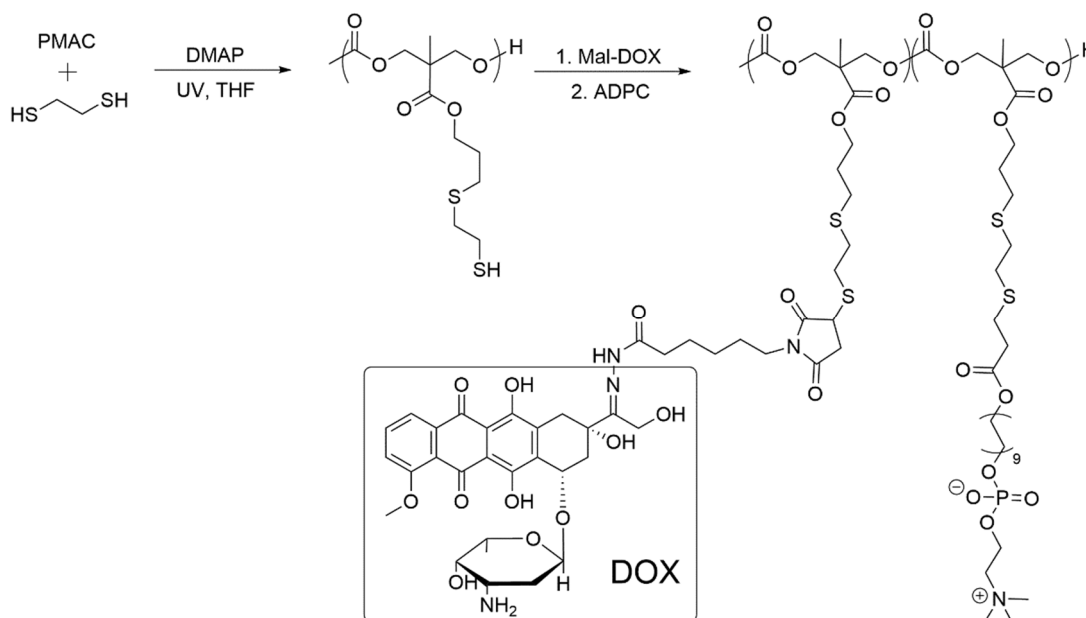
1.4.3.1.2 Functional micelles

Yue *et al.* demonstrated the versatility of post-polymerisation modification of MAC *via* radical thiol-ene addition in micelles. Micelles prepared from methoxy-poly(ethylene glycol)-*b*-poly(*L*-lactide-*co*-2-methyl-2-allyloxycarbonyl-propylene carbonate) (mPEG-*b*-P(LA-*co*-MAC)) were successfully functionalised with 3-mercaptopropionic acid, 2-(Boc-amino)ethanethiol, and 3-mercapto-1,2-propanediol. Following on from previous work by the same research group demonstrating the non-cytotoxic nature of the mPEG-*b*-P(LA-*co*-MAC) micelles,¹¹⁷ the cytocompatibility of the micelles functionalised with thiol groups was tested *via* colourimetric assay using MTT and an L929 cell line. For each of the functionalised polymers, the cell survival rate exceeded 80% following incubation for 24 h at micelle concentrations of up to 500 µg/mL, indicating that the mercaptan-functionalised micelles were potentially safe enough to be used as drug delivery carriers.¹¹⁸

Recently, our group reported the synthesis of functional cylindrical micelles prepared by the crystallisation-driven self-assembly (CDSA) of triblock copolymers consisting of tetrahydropyran acrylate (THPA), MAC and *L*-lactide. Following CDSA, the cylinders were successfully functionalised with both benzyl mercaptan and the more bulky 6-(ferrocenyl)hexanethiol through the use of photoinitiated radical thiol-ene addition chemistry without disturbing the self-assembled structure, thus demonstrating the possibility of loading cargo into pre-assembled cylindrical micelles using this method.¹¹⁹

Wang *et al.* have described the synthesis of a pH-sensitive micellar prodrug through the grafting of 12-acryloyloxy dodecyl phosphorylcholine (ADPC) and 6-maleimidocaproyl-doxorubicin (Mal-DOX) to PMAC using photoinitiated radical thiol-ene chemistry. This grafting was achieved by first functionalising PMAC with

1,2-ethanedithiol and isolating the thiol-functional polymer. Mal-DOX (0.2 equivalents per thiol group) and ADPC (one equivalent per thiol group) were then added sequentially to generate PMAC-*g*-(ADPC-*co*-Mal-DOX) (Scheme 1.7), which self-assembled into spherical micelles with phosphorylcholine shells in water. The anti-cancer agent doxorubicin was connected to the prodrug *via* hydrazone bonds, which while stable under normal physiological pH (7.4), are readily cleaved under acidic conditions, such as those found in the extracellular matrix of tumours (pH *ca.* 5.0).¹²⁰ The researchers were able to demonstrate that in phosphate buffered saline solution (PBS, pH 7.4), DOX release over 48 h was less than 10%, whilst in pH 5.0 conditions more than 30% of the drug was released in 24 h. They were also able to show that the polymeric prodrug could be successfully internalised by HepG2 and HeLa cancer cells, with subsequent cleavage of the hydrazone linkages to release DOX, demonstrating the potential of the material for targeted drug delivery.¹²¹



Scheme 1.7. Synthesis of PMAC-*g*-(ADPC-*co*-Mal-DOX), with DOX functionality highlighted.¹²¹

Kuang *et al.* have demonstrated the formation of micelles bearing adenine and thymine nucleobase functionality. The micelles were formed by first grafting 3-mercapto-1,2-propanediol to mPEG-*b*-P(LA-*co*-MAC) copolymers *via* photoinitiated radical thiol-ene chemistry to introduce diol functionality in the polymer. Following the radical thiol-ene addition, the diol-functionality was further modified with 1-(carboxymethyl)thymine by means of dicyclohexylcarbodiimide coupling, thus introducing thymine functionality to the material. Nanoparticles were then prepared by dissolution of the thymine-functional amphiphilic polymer and 1-bromohexadecane-functionalised adenine in THF, followed by dispersion into water. Thymine and adenine are complementary base pairs, and as such the formed nanoparticles displayed enhanced stability and a much reduced critical aggregation concentration as a result of the hydrogen bonding between the base pairs. An MTT assay using an L929 cell line demonstrated that the nanoparticles displayed no obvious toxicity up to concentrations of 1 mg/mL, and drug release studies using DOX as a model demonstrated that the rate of drug release was reduced and became more controlled with increasing adenine concentration.¹²²

1.4.3.1.3 Cross-linking

Radical thiol-ene addition has also been employed for the crosslinking of functional polymers. Stevens *et al.* have exploited the thiol-ene reaction for the formation of nanosponges, through crosslinking copolymers consisting of MAC and the non-functional carbonate 5-methyl-5-ethyloxycarbonyl-1,3-dioxane-2-one (MTC-Et) using dithiolethyleneoxide as crosslinker. By varying the incorporation of MAC from 5 to 20%, nanosponges could be prepared with diameters ranging from 150-220 nm.¹²³

Truong *et al.* prepared hydrogels with tuneable properties including equilibrium water content, mechanical strength and degradation time by crosslinking PMAC with a range

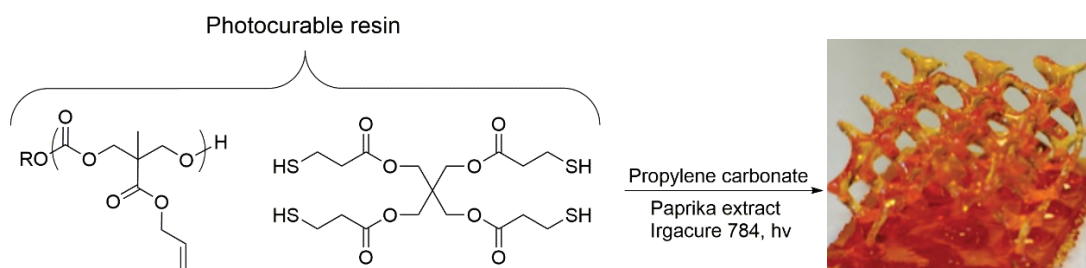
of PEG-thiols. These PEG-thiols were prepared by esterification with 3-mercaptopropionic acid by heating to reflux under Dean-Stark conditions in the presence of sulphuric acid as catalyst, yielding mono-, bi- and tri-functional PEG-thiols. PMAC was then partially grafted with a methoxy-terminated PEG-monothiol by means of photoinitiated radical thiol-ene chemistry to yield a water soluble polymer with free pendent allyl groups. This polymer was then crosslinked under ambient conditions in water, using di- and trithiol-functional PEGs in the presence of a water-soluble photoinitiator (2-hydroxy-4'-(2-hydroxyethoxy)-2-methylpropio-phenone, Irgacure-2959) to yield hydrogels with a range of crosslinking densities and molecular weights. Longer dithiol crosslinkers were found to produce materials with lower crosslinking densities, leading to lower mechanical strength, higher equilibrium water content (associated with larger pore sizes in the crosslinked network), faster water uptake, and faster degradation of the hydrogels. The trithiol-crosslinked hydrogels displayed an unexpectedly low crosslinking density, however these materials still displayed a low equilibrium water content and extended degradation times, attributed to the greater hydrophobicity of the crosslinked network. It was also shown that changing temperature affected the swelling ability of the hydrogels, with materials possessing a lower equilibrium water content undergoing more pronounced changes in water retention. This thermoresponsive change in the degree of swelling in the polymers makes these materials promising candidates for drug delivery applications with drug release triggered by changing temperature.¹²⁴

Stevens and co-workers utilised similar chemistry for the formation of hydrogels from PMAC with tuneable swelling, mechanical properties and drug release rates by changing the length of the ethylene glycol-based dithiol crosslinker and incorporating non-covalently bound polyglycidol as a filler. Hydrogels synthesised using

dithiolethyleneoxide as crosslinker exhibited greater mechanical strength and compressive moduli than those crosslinked using 1.5 kDa dithiol-PEG. However, both polymers were significantly stronger than their equivalent gels incorporating polyglycidol, with the compressive modulus of the materials decreasing from *ca.* 130 kPa to below 10 kPa. Polymers containing the longer crosslinker were shown to possess much greater swelling potential both in water and simulated gastric fluid (*ca.* 180%, compared to *ca.* 20% for dithiolethyleneoxide-linked hydrogels), with incorporation of the hydrophilic polyglycidol filler slightly increasing the efficiency of water uptake for each material. Following loading of the hydrogels with the anti-cancer drug Paclitaxel (> 98% loading efficiency for each gel), controlled release was demonstrated for all four materials, with dithiolethyleneoxide-linked materials releasing as little as 7.2% and polyglycidol-filled 1.5 kDa dithiol-PEG releasing as much as 29.9% of the Paclitaxel after 7 days in PBS solution, demonstrating that the rate of controlled release can be fine-tuned simply by changing the length of the crosslinker conjugated to the polycarbonate using radical thiol-ene chemistry.¹²⁵

Barker *et al.* have utilised photoinitiated radical thiol-ene chemistry to produce 3D-printed structures based on polycarbonates *via* microstereolithography, as an alternative to potentially toxic acrylate-based printing systems. A photocurable resin was produced by mixing low molecular weight PMAC, tetrakis(3-mercaptopropionate) (a 4-arm thiol crosslinker), propylene carbonate (as a viscosity modifier) and the titanium-based photoradical generator Irgacure 784 in the absence of light. By exposure of sequential 2D layers of resin at 100 μm thickness, a partial 3D-printed construct of a porous (10,3)-a mathematical network was successfully produced with overall dimensions of $11.50 \times 8.00 \times 5.50$ mm (Scheme 1.8). The proliferation and viability of intervertebral disc cells on the cured resin was assessed

relative to standard polystyrene tissue culture plates. Following incubation over 7 days, proliferation and cell morphology was shown to be equivalent for the cured resin and polystyrene standards, demonstrating the non-cytotoxic nature of the photocured material.¹²⁶

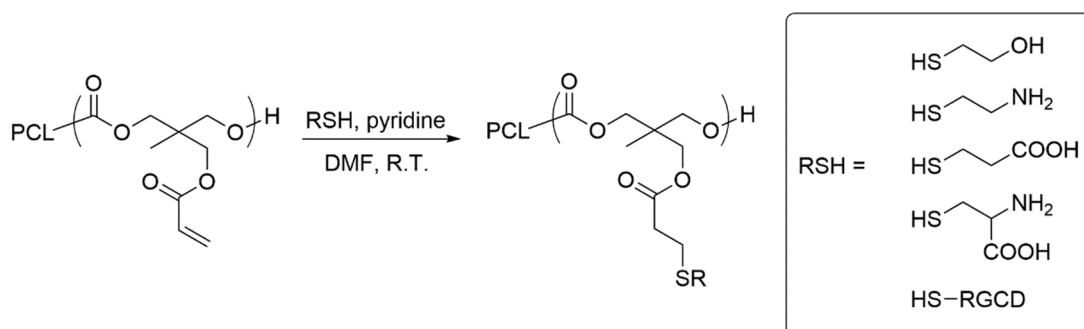


Scheme 1.8. Reaction scheme for the synthesis of a photocured 3D-printed scaffold.¹²⁶

1.4.3.2 Michael addition

As with radical thiol-ene addition, Michael addition reactions can be used to confer additional functionality to alkene-functional polycarbonates by addition of mercaptans to the alkene moiety. Chen *et al.* have demonstrated that a wide range of different functionalities can be conferred on polycarbonates bearing pendent acryloyl groups. Copolymers of acryloyl or methacryloyl carbonate (AC) with CL or LLA were prepared by ring-opening polymerisation. P(CL-*co*-AC) and P(LA-*co*-AC) were then modified with a wide range of thiol-containing compounds, including 2-mercaptoethanol, 2-mercaptoethylamine hydrochloride, 3-mercaptopropanoic acid, *L*-cysteine, and arginine-glycine-aspartic acid-cysteine (RGDC) peptide (Scheme 1.9). Using pyridine as catalyst to activate the thiol functionality, and a ten molar excess of thiol relative to AC groups, the copolymers were successfully endowed with functionalities including hydroxyl, amino, carboxyl, amino acid, and peptide groups. Attachment of RGDC was also shown to improve cell adhesion and proliferation to

thin films of the material relative to non-functionalised P(CL-*co*-AC), and comparable to the tissue culture plastic control.¹¹⁰



Scheme 1.9. Functionalisation of P(CL-*co*-AC) with mercaptans *via* Michael-type addition.¹¹⁰

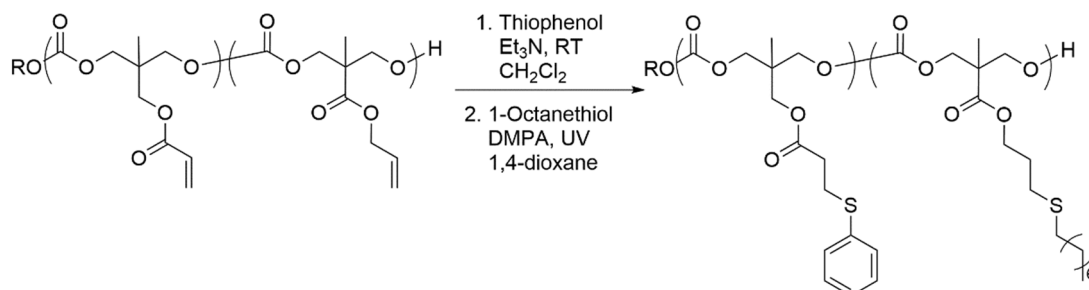
Li and co-workers have utilised the Michael addition of thiol-containing compounds to prepare biodegradable polymersomes with ionisable membranes for pH-responsive drug delivery applications. Diblock copolymers of mPEG-*b*-P(TMC-*co*-AC) were functionalised with carboxylic acid and amine functionality through Michael addition of 3-mercaptopropionic acid and cysteamine hydrochloride respectively. Polymersomes were prepared by direct dispersion of the acrylate, carboxylic acid and amine-functional polymers in phosphate buffer solution, with MTT assays using MCF-7 and HeLa cells demonstrating the non-toxicity of the polymersomes. The polymersomes were then loaded with fluorescence-labelled bovine serum albumen (BSA) and cytochrome C (CC). The ionisable carboxylic acid and amine-functional polymers demonstrated exceptional loading efficiencies (up to 92 and 98% respectively for BSA, and up to 81 and 83% for CC), particularly when compared to the acrylate-functional polymer (up to 51% for BSA, 19% for CC). The carboxylic acid and amine-functional polymers were also shown to undergo drug release in a pH-dependent manner, with significantly increased CC release at pH 5.4 compared to pH 7.4 – the carboxylic acid-functional polymer demonstrated 13.9% CC release after

24 h at pH 7.4 compared to 88% at pH 5.4, with the amine-functional polymer releasing 36.9 and 95.9% at pH 7.4 and 5.4 respectively. The pH-responsive nature of the carboxylic acid and amine-functional polymers is attributed to weakened interactions between the protein and the charged polymersome membrane at acidic pH. In comparison, a relatively small change in release was observed for the acrylate-functional polymer (< 20% change at different pH), as expected in the absence of an ionisable polymersome membrane.¹²⁷

Michael addition was employed by Yu *et al.* to prepare injectable hydrogels based on acrylate-functional carbonates. Water soluble PAC-*b*-PEG-*b*-PAC copolymers were prepared and functionalised with biocompatible and bioadhesive thiolated glycol chitosan through rapid mixing of aqueous solutions of each component, resulting in *in situ* Michael addition. Gels were formed in as little as 1.1 minutes, with storage moduli ranging from 0.1 to 4.3 kPa and solid concentrations of as little as 1.5-4.5%, depending on the degree of substitution of the glycol chitosan. The ability to form hydrogels with glycol chitosan is advantageous as (unlike the more commonly employed PEG and dextran-based hydrogels) this material has been shown to be enzymatically degradable using lysozyme.¹²⁸

A 2014 paper by Uysal *et al.* demonstrated that the different mechanisms of Michael addition and radical thiol-ene addition can be exploited for orthogonal modification of copolymers containing two different allyl functionalities. P(MAC-*co*-AC) copolymers were produced, bearing pendent groups of acrylate present on AC, and the less-activated allyl-terminated ester functionality of MAC. Initial functionalisation was performed through addition of 2-mercaptoethanol to the pendent acrylate groups through Michael addition, using triethylamine as catalyst and stirring in dichloromethane at room temperature for 2 h. Under these conditions, quantitative

conversion of the acrylate to the hydroxyl functionality was achieved, with the alkene groups of the MAC repeat units remaining unmodified as determined by ^1H NMR spectroscopy. Upon irradiation with UV light in the presence of a photoinitiator, *N*-acetyl-*L*-cysteine methyl ester was successfully added to these remaining alkene groups, demonstrating the possibility of simply introducing multiple functionalities onto polymers bearing pendent alkene functionality. The researchers were also able to show that the acrylate groups could be selectively functionalised with cysteine through Michael addition, followed by subsequent addition of mercaptoethanol to the MAC-alkene groups, demonstrating the orthogonality of the reaction. The versatility of this method was further demonstrated by extending the reaction to include 1-octanethiol and thiophenol (although the latter was found to be incompatible with radical thiol-ene addition due to the rapid formation of diphenyl sulphide) (Scheme 1.10), generating a small library of selectively-functionalised materials.¹²⁹



Scheme 1.10. Orthogonal modification of alkene-functional copolymer by sequential Michael and thiol-ene addition.¹²⁹

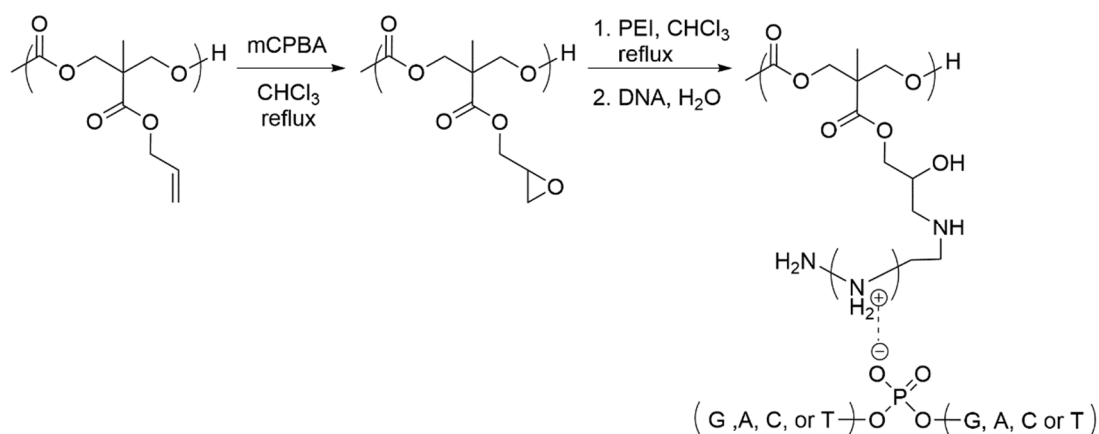
Michael addition has also been demonstrated for polymers bearing pendent vinyl sulfone (VS) functionality. Wang and coworkers prepared copolymers of the VS-carbonate with CL, LLA and TMC. As a consequence of the highly activated nature of the VS functionality, the authors were able to quantitatively functionalise these copolymers with 2-mercaptoethanol, cystamine, cysteine, thiolated glycol chitosan,

RGDC, and thiolated PEG in the absence of catalyst, simply by stirring the thiol-functional reagents with the VS-functional polymer in DMF at room temperature for 24 h. Cell culture studies showed that cell adhesion could be readily modified by changing the functionality of the polymers, with the VS and RGDC-functional polymers displaying excellent cell adhesion and proliferation, whilst polymers bearing anti-fouling functionality (PEG and glycol chitosan) showed greatly diminished cell adhesion and subsequent growth, thus demonstrating the versatility of VS-functional polycarbonates for applications in biomedical engineering.¹³⁰

1.4.3.3 Epoxidation

Several researchers have reported the epoxidation of pendent allyl groups in polycarbonates, providing an alternative method of functionalising polycarbonates through nucleophilic addition to the epoxide functionality.¹³¹⁻¹³³ A 2009 paper by Wang *et al.* described the synthesis of PMAC grafted with polyethyleneimine (PEI) as biodegradable polycations for potential application as gene delivery vehicles. To this end, the pendent allyl groups of PMAC were first epoxidised by refluxing the polycarbonate with a four molar excess of mCPBA in CHCl_3 over 12 h, followed by purification of the polymer by precipitation into methanol. A ten molar excess of PEI was then added to the isolated epoxidised polymer in CHCl_3 and the solution heated to reflux, in order to facilitate the covalent grafting of PEI to the epoxide *via* the free amino functionality. Following neutralisation, dialysis and lyophilisation of the product, purified PMAC-g-PEI was achieved. MTT assays of PMAC grafted with PEI423 and PEI800 demonstrated reduced cytotoxicity relative to free PEI at concentrations up to 0.3 mg/mL, attributed to the ability of the PMAC backbone to shield and reduce the charge density of PEI. PMAC-g-PEI was then complexed to deoxyribonucleic acid (DNA) by way of electrostatic interactions between anionic

nucleic acids and the cationic polymer species (Scheme 1.11). The transfection ability of these polyplexes was assessed by green fluorescence protein assay, using pEGFP-C1 as a fluorescent reporter gene, and by Luciferase assay, using PGL-3 as a reporter gene. Crucially, the synthesised polyplexes all showed transfection capabilities at least as good as free PEI, and significantly higher in the case of PMAC-g-PEI1800/DNA, highlighting the potential of these materials as potential gene delivery vectors.¹³⁴

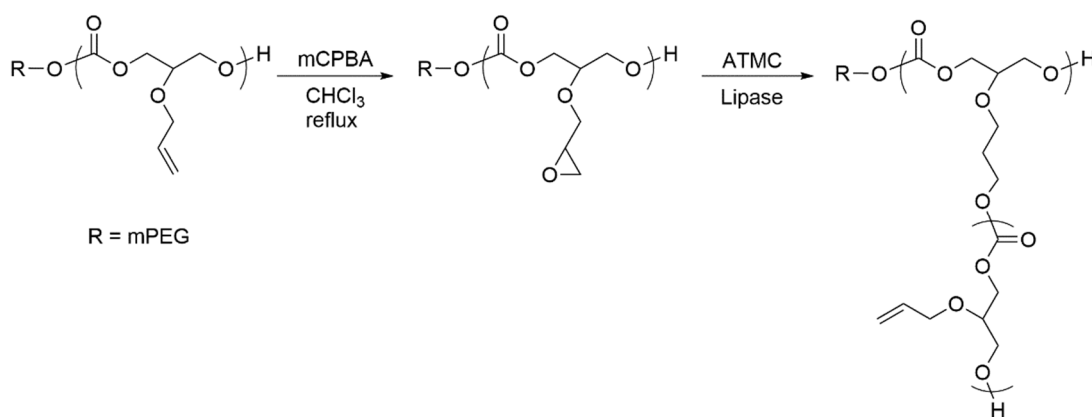


Scheme 1.11. Epoxidation of PMAC and subsequent functionalisation with PEI for the formation of polycarbonate/DNA polyplexes.¹³⁴

Incorporation of a non-functional carbonate such as 2,2-dimethyl trimethylene carbonate (2,2-DTC) can allow the grafting density of a material to be reduced. In a follow-up study, He *et al.* introduced PEI into a copolymer of P(MAC-*co*-DTC) using a similar synthetic method. The reduced grafting density resulted in reduced cytotoxicity relative to PMAC-g-PEI, with higher DTC incorporation in the material resulting in increased hydrophobicity and a greater reduction in charge density, thus preventing combination with cell surfaces. The incorporation of the non-functional comonomer was also shown to result in higher gene transfection efficiency relative to both free PEI and PMAC-g-PEI/DNA polyplexes.¹³⁵

Stevens *et al.* have utilised the epoxidation of pendent allyl groups for the crosslinking of PMAC using an ethylene oxide-based diamine. Following full epoxidation of the allyl groups in P(MAC-*co*-MTC-Et) using 1.2 equivalents of mCPBA, copolymers containing 5, 10 and 20% of epoxidised PMAC were functionalised with four equivalents of diaminoethyleneoxide to produce nanosponges with sizes ranging from 160 to 230 nm. The size of these nanoparticles is comparable to those formed using thiol-ene chemistry in the same study, thus demonstrating the potential of using epoxide-amine chemistry as an alternative to thiol-ene chemistry in situations where the latter method may be unsuitable.¹²³

A 2013 paper by Jiang and co-workers demonstrated the potential of grafting polycarbonates from allyl-functional carbonates through the use of epoxides. Amphiphilic block copolymers consisting of methoxy-poly(ethylene glycol)-*b*-poly(5-allyloxy-1,3-dioxan-2-one) (mPEG-*b*-PATMC) were synthesised, and the pendent allyl groups of the PATMC block were epoxidised using mCPBA in CHCl₃. Following epoxidation, additional ATMC was grafted from the epoxidised polymer precursor using temperatures of 140 °C and lipase as a polymerisation catalyst, resulting in quantitative functionalisation of the pendent epoxide groups (Scheme 1.12). Micelles of mPEG-*b*-PATMC and mPEG-*b*-PATMC-*g*-PATMC were prepared and loaded with the anti-cancer drug doxorubicin (DOX). The grafted polymer demonstrated greater drug loading capacity and encapsulation efficiency, along with more sustained drug release behaviour *in vitro* when compared to the linear diblock copolymer, indicating the potential of these grafted polymers as drug delivery vehicles.¹³⁶



Scheme 1.12. Epoxidation of PATMC and subsequent ROP of ATMC, using epoxide functionality as initiator.¹³⁶

A second paper by the same research group investigated the conjugation of DOX to mPEG-*b*-P(ATMC-*co*-DTC). Following epoxidation of the pendent allyl groups with an excess of mCPBA, the epoxidised polymer was functionalised with hydrazine monohydrate by heating to reflux in methanol for 2 h, and the resultant solution dialysed and dried under reduced pressure to yield mPEG-*b*-P(ATMC-*co*-DTC)-*g*-hydrazine. Addition of DOX-hydrochloride to the hydrazine-grafted polymers in dimethylformamide containing 2% triethylamine yielded the micellar mPEG-*b*-P(ATMC-*co*-DTC)-*g*-DOX prodrug. DOX release from this prodrug was shown to be pH-dependent, as a result of the sensitivity of the hydrazone linkage to acidic environments. Efficient delivery of DOX into the nuclei of cells was demonstrated, with the prodrug showing effective but slightly reduced cytotoxicity against HeLa cells compared to free DOX.¹³⁷

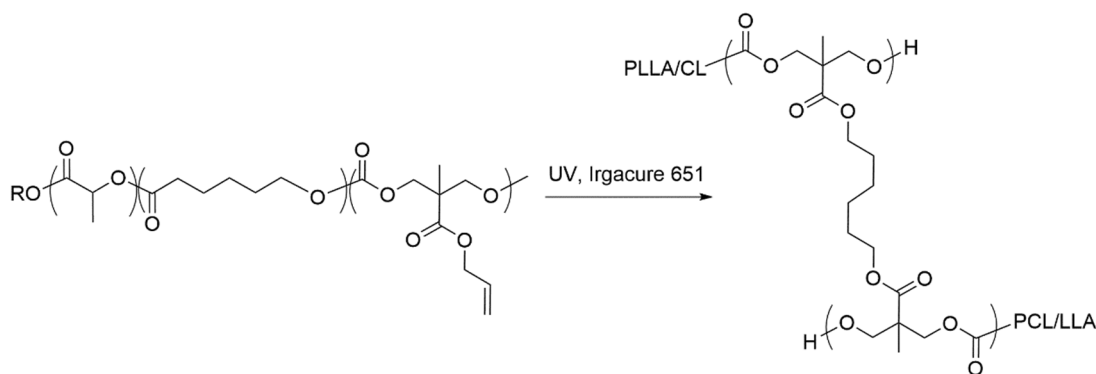
1.4.3.4 Free-radical crosslinking

The ability of alkene-functional polycarbonates to undergo photoinitiated radical crosslinking in the absence of additional crosslinkers has also been demonstrated and utilised for practical applications. Several groups have exploited this methodology to

produce core-crosslinked micelles through micellisation of block copolymers, followed by crosslinking the allyl groups present on the pendent functionality. Polycarbonates which have been used for this purpose include PMAC, PAC, and a cinnamate-functional carbonate, 5-methyl-5-cinnamoyloxymethyl-1,3-dioxan-2-one (MC).¹³⁸⁻¹⁴¹ Research by Hu and co-workers and separately by Danquah *et al.* has shown that such core-crosslinked micelles possess improved properties, such as increased thermal stability and reduced aggregation, and greater resistance to water dilation and organic solvents in comparison to non-crosslinked micelles.^{134,139}

Chen *et al.* have used the direct crosslinking method to generate fibrous materials with properties similar to human anterior cruciate ligament (ACL) tissue. To achieve this, P(LLA-*co*-AC) copolymers were first synthesised and deposited into aligned fibres using electrospinning. A wave-like “crimp” pattern (typical of ACL tissue) was induced in the fibres by immersion in PBS, and the material crosslinked by exposure to UV light for 10 minutes. Crosslinking the fibres resulted in an increase in elastic modulus of the dry fibres from 86 MPa to 222 MPa. Non-crosslinked P(LLA-*co*-AC) fibres were shown to be subject to a loss in elastic modulus and an increase in gauge length (the length of each crimp in the fibres) with repeated strain and relaxation cycles. The hydrated crosslinked fibres showed improved results for each of these characteristics, with only a slight loss in elastic modulus from *ca.* 40 to 30 MPa and an increase in gauge length of only 5% over ten extension-relaxation cycles, compared to a decrease from 40 to 10 MPa in elastic modulus and an increase in gauge length of over 20% for non-crosslinked fibres. Good cell viability for the crosslinked materials was also demonstrated, with no difference in fibroblast attachment and proliferation between crosslinked and non-crosslinked fibres.¹⁴²

A subsequent paper by the same research group demonstrated that the crosslinking reaction could be employed to crosslink fibres deposited by melt electrospinning writing (MEW), a method of 3D-printing. Biomaterials previously prepared by MEW have been limited to thermoplastics with relatively low melting points such as PCL, however these materials have been shown to undergo undesirable mechanical creep (a gradual change in the dimensions of the constructed material) and display reduced moduli upon hydration. To overcome these problems, the researchers prepared scaffolds by depositing low melting point P(LLA-*co*-CL-*co*-AC) fibres containing a thermally stable photoinitiator (2,2-dimethoxy-2-phenylacetophenone, Irgacure 651) with MEW, and subsequently crosslinked the fibres with UV light (Scheme 1.13). As with their previous research, Chen *et al.* showed that the crosslinked fibres had significantly improved mechanical properties compared to non-crosslinked fibres, with the crosslinked hydrated fibres possessing elastic moduli of 370 MPa compared to about 40 MPa for the non-crosslinked materials. This high modulus was retained even after 10,000 strain-relaxation cycles, with the samples remaining intact after 200,000 cycles. In contrast, the average modulus for the non-crosslinked samples was significantly reduced due to shearing of the fibres in the material – four of the six non-crosslinked samples tested underwent complete mechanical failure after as few as 2,500 cycles, demonstrating the potential of the post-processing crosslinking of polyester-*co*-carbonate fibres for developing improved materials for soft tissue scaffolds.¹⁴³

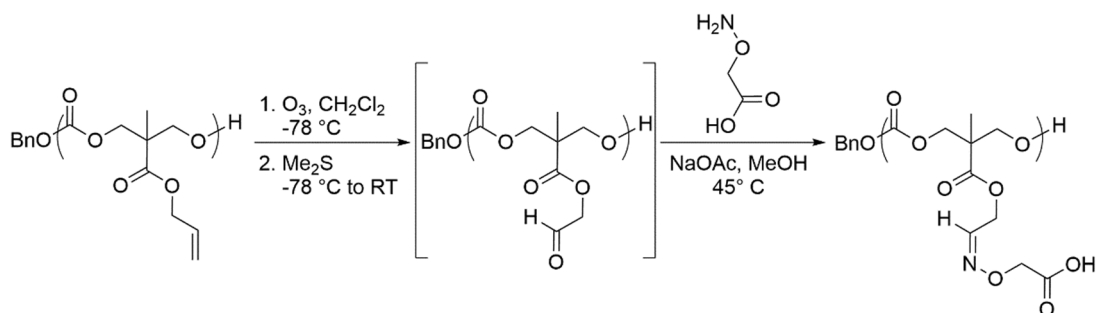


Scheme 1.13. Crosslinking of P(LLA-*co*-CL-*co*-MAC) with UV and no additional crosslinker.¹⁴³

Mindemark *et al.* have recently used the crosslinking reaction to form polycarbonate-based polymer electrolytes for potential application in thin-film solid-state lithium battery cells. Using PAOMEC as their allyl-functional carbonate, electrolyte films were prepared by first mixing PAOMEC (a viscous liquid at room temperature) with lithium bis(trifluoromethanesulfonimide) (LiTFSI) and DMPA as photoinitiator in acetonitrile, followed by evaporation of the solvent. This prepolymer was then loaded into Teflon moulds and exposed to UV light to induce crosslinking. The residual solvent was then removed under reduced pressure to yield thin, mechanically stable polymer films doped with Li⁺ ions, with Li⁺ shown to coordinate to both the carbonyl and ether oxygen atoms of the polymer. The ionic conductivity of the polymer electrolytes was found to reach a maximum at 22-32 wt% LiTFSI concentration, comparable to that for PTMC-based electrolytes (18-26 wt%). Crucially, the PAOMEC-based electrolytes displayed an improved ionic conductivity (relative to PTMC-based systems) of up to an order of magnitude at low temperatures, with this improved performance attributed to the plasticising effect of the pendent allyl ether side groups. The authors also assembled functional thin-film batteries using a Li metal anode and a V₂O₅ cathode with the polymer as the electrolyte, confirming the ability of crosslinked PAOMEC to shuttle Li⁺ between the electrodes.¹⁴⁴

1.4.3.5 Other functionalisations

While less common, several other methods of modifying allkene-functional carbonates have been reported in the literature. Heo *et al.* have prepared aldehyde-functional polymers from PMAC and subsequently modified these materials. Aldehyde functionality was conferred upon the polycarbonate backbone through ozonolysis of the pendent allyl groups present on PMAC, followed by reductive work up to yield poly(5-methyl-5-oxoethyl-oxycarbonyl-1,3-dioxan-2-one) (PMOC). As a consequence of the limited solubility of the formed PMOC, further functionalisations were performed through *in situ* generation of the aldehyde and immediate reaction with aminoxy-functional *O*-benzylhydroxylamine and *O*-(carboxymethyl)hydroxylamine to produce an organic-soluble polycarbonate bearing pendent benzyl functionality and a water-soluble polymer bearing carboxylic acid functionality (Scheme 1.14). The authors also demonstrated that by partial ozonolysis, a P(MAC-*co*-MOC) copolymer could be produced, and by performing an aldehyde-aminoxy addition of *O*-benzylhydroxylamine and a consecutive radical thiol-ene addition of ethyl-2-mercaptoacetate, polymers could be produced bearing orthogonal benzyl and ester functionalities.¹⁴⁵



Scheme 1.14. *In situ* synthesis of aldehyde-functional polycarbonate and functionalisation with *O*-(carboxymethyl)hydroxylamine.¹⁴⁵

Research by Miyagawa and co-workers has described the synthesis of a polycarbonate bearing pendent styrene functionality. The authors first described the temperature-dependent reversible ring-opening polymerisation of the carbonate using potassium *tert*-butoxide as catalyst. The polycarbonate was then crosslinked by free-radical polymerisation of the pendent styrene moiety with additional styrene, using benzoyl peroxide as the radical initiator. Following successful crosslinking of the material, the polymer was then subsequently de-crosslinked by depolymerisation of the polycarbonate chain, yielding linear polystyrene bearing pendent cyclic carbonyl functionality, and thus demonstrating the chemical recyclability of the carbonate group.¹⁴⁶

1.5 Degradation

1.5.1 Degradation of aliphatic polyesters and polycarbonates

In aqueous media, aliphatic polyesters and polycarbonates undergo hydrolytic degradation. Unsubstituted polycarbonates such as PTMC have been shown to degrade at much slower rates than commercially available polyester biomaterials such as PLA, PLGA and PCL,^{29,147} with the hydrophobic nature of PTMC resulting in the material undergoing surface erosion.¹⁴⁸ Surface erosion occurs when the rate of hydrolysis at the surface of a material exceeds the rate of diffusion of the degradation medium into the material. In the case of PLA, PLGA and PCL, the rate of diffusion into the polymer is greater than that of hydrolysis, and so the materials undergo bulk degradation (Figure 1.6).¹⁴⁹⁻¹⁵¹ Surface erosion is a desirable property in scaffold design and some drug delivery applications, as it results in linear and more predictable drug release rates and changes in mechanical properties.¹⁵²

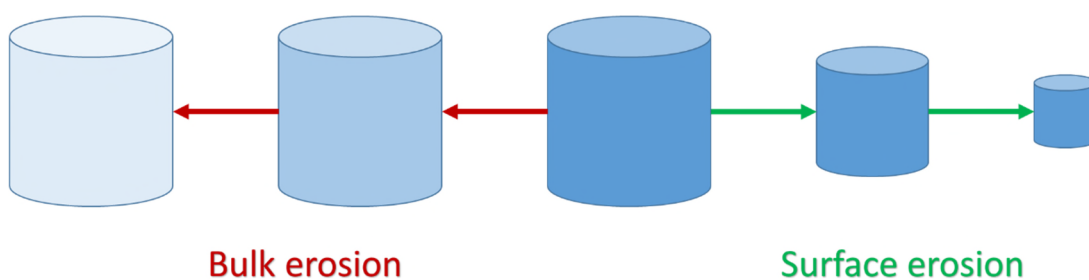
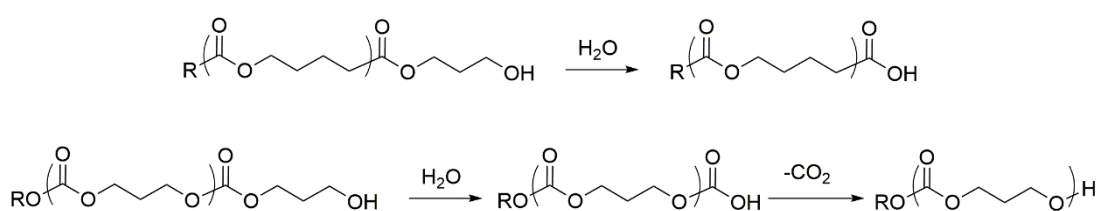


Figure 1.6. Different mechanisms of polymer hydrolysis. Fading colour for bulk erosion indicates loss of volume throughout polymer, as opposed to a loss of material primarily on the surface of the material for surface erosion.

In addition, the degradation of polyesters can be autocatalysed by the formation of acidic end groups as a product of hydrolysis, resulting in a lowering of the local pH and accelerated degradation (Scheme 1.15).¹⁵³ The formation of carboxylic acids *in vivo* is potentially problematic, as changes in local pH can stimulate an inflammatory response, particularly if the degrading material is trapped in a confined area.¹⁵² The degradation of polycarbonates does not result in the formation of acids, as the terminal carbonic acid moiety degrades further to yield CO₂ and a hydroxyl-terminated polymer (Scheme 1.15).¹⁴⁷



Scheme 1.15. Hydrolysis of aliphatic polyesters (top) and polycarbonates (bottom).¹⁴⁷

The use of copolymers can allow the degradation rate of a material to be readily modified by varying the incorporation of relatively hydrophilic and hydrophobic repeat units. The most common example of this is in the hydrolytic degradation of PLGA. Increasing the incorporation of lactide repeat units in PLGA decreases the rate of hydrolysis of the material, as the presence of methyl side groups on poly(lactide)

renders it more hydrophobic than poly(glycolide) (PGA).¹⁵⁴⁻¹⁵⁶ Copolymers can also be used to modify degradation rates by disrupting the semi-crystalline regions of polymers. For example, incorporation of *D*-lactide into PLLA has been shown to increase degradation rates by disrupting the semi-crystalline nature of isotactic PLLA, thus enabling easier diffusion of water into the material.¹⁵⁷⁻¹⁵⁹

The degradation of copolymers produced from esters and carbonates are of particular interest as the prolonged degradation times and surface-eroding nature of hydrophobic polycarbonates can provide degradation behaviour to biomaterials which would otherwise not be available. Incorporation of TMC into PGA and PLGA has been shown to prolong the degradation times of these polymers both *in vitro* and *in vivo*,^{103,160-162} whilst incorporation of TMC into PCL, PDLA and PLLA results in a decreased degradation time *in vivo* as a consequence of disrupting the semi-crystalline regions of the materials, combined with the higher rate of enzymatic hydrolysis of PTMC.^{96,163-165} For both *in vitro* and *in vivo* degradations, the incorporation of TMC can also confer increased surface degradation character to these polyesters.¹⁶⁶⁻¹⁶⁹

1.5.2 Effect of pendent functionality on degradation rate and behaviour

The incorporation of carbonates bearing pendent functionality allows for the degradation profiles of polyesters to be modified even further. In general, the presence of hydrophobic functionalities such as alkyl and benzyl groups leads to extended degradation times, whilst hydrophilic groups lead to reduced degradation times.³⁰ For instance, the glycerol-derived hydroxyl-functional polycarbonate poly(2-hydroxyl trimethylene carbonate) (PHTMC) was shown to have a much faster degradation rate in comparison to PTMC, with PHTMC undergoing complete degradation over the course of one month in PBS solution (no weight loss was observed for PTMC under the same conditions).¹⁷⁰ The increased degradation rate was attributed to the increased

hydrophilicity of the polymer, combined with an autocatalysed degradation effect as a result of the pendent hydroxyl groups. In contrast, poly(2-benzyloxy trimethylene carbonate) (PBTMC), a benzyl-protected analogue of PHTMC (Figure 1.7), has been shown to be highly hydrophobic, with minimal mass loss (< 2%) observed over a 65 day period.¹⁷¹

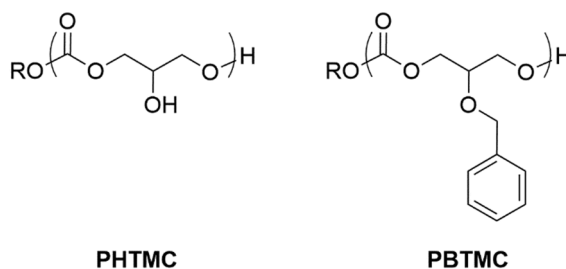


Figure 1.7. Structures of hydroxyl-functional poly(2-hydroxyl trimethylene carbonate) and benzyl-functional poly(2-benzyloxy trimethylene carbonate).^{170,171}

Copolymers bearing pendent functionality allow the degradation rates of polyester and carbonate materials to be broadened even further. Whilst the copolymerisation of TMC with DLLA has been shown to prolong the *in vitro* degradation time of PDLLA, Xu *et al.* have successfully demonstrated that the incorporation of a bis(hydroxy)-functional carbonate into PDLLA results in a markedly reduced degradation time, with complete *in vitro* degradation observed in as little as 2 days.¹⁰³ Similarly, copolymers of *L*-lactide with 10 mol% of a glycerol-based carbonate were shown to undergo 35% mass loss in as little as 7 days, compared to 60 weeks for PLLA containing 10% TMC under similar conditions.^{163,172} In contrast, PCL has been shown to degrade more slowly when copolymerised with the dimethyl-functional carbonate 1,3-dimethyl trimethylene carbonate (1,3-DTC) due to the high frequency of methyl groups distributed along the polymer backbone increasing the hydrophobicity of the copolymer.⁹⁷ In addition, the benzyl-functional BTMC monomer has been copolymerised with PGA to produce materials with longer degradation times than

PGA incorporating non-functional TMC repeat units, owing to the greater hydrophobicity of the PBTMC moiety.¹⁷¹

It should be noted that the effect of the hydrophobic moiety can be offset by the effect of disrupting the crystallinity of some polymers. For instance, copolymers of PDLLA or PCL with 2,2-DTC degrade slightly more quickly than copolymers containing TMC, despite the hydrophobicity conferred by the pendent methyl groups, likely owing to the increased disruption of the short semi-crystalline regions in the materials.^{173,174} Through careful consideration of the effects of different functionalities on degradation hydrolysis, it is possible to prepare materials with very specific degradation rates and behaviours.

1.6 A-B-A triblock copolymers

Whilst it is clear that the vast library of cyclic ester and carbonate monomers can provide homopolymers and statistical copolymers with a wide range of different properties, the synthesis of A-B-A-type triblock copolymers can broaden the range of available physical and mechanical properties still further. In particular, these can provide materials with thermoplastic elastomer character, presenting both the elasticity associated with rubbers and the mechanical robustness associated with thermoplastics.¹⁷⁵

1.6.1 Microphase separation and thermoplastic elastomer behaviour

Thermoplastic elastomer character arises from the phase separation behaviour of the materials. Different polymers will undergo phase separation when mixed, resulting from the chemical incompatibility of the monomer units. Even small differences in chemical functionality can lead to phase separation – for example, polystyrene and deuterated polystyrene have been shown to undergo phase separation at sufficiently

high molecular weights.¹⁷⁶ To explain this phenomenon, the thermodynamics of mixing must be considered. For two separate polymers to be miscible, the Gibbs free energy of mixing (ΔG_{mix}) must be favourable;¹⁷⁷

$$\Delta G_{\text{mix}} = \Delta H_{\text{mix}} - T\Delta S_{\text{mix}} < 0 \quad \text{Equation 1.1}$$

Where ΔH_{mix} represents the enthalpy of mixing, T represents the temperature, and ΔS_{mix} represents the entropy of mixing. As disorder naturally increases on mixing, ΔS_{mix} is always positive, however the enthalpy of mixing is also usually positive. As such, miscibility is only favoured when the gain in entropy exceeds the enthalpic contribution;^{177,178}

$$\Delta H_{\text{mix}} < T\Delta S_{\text{mix}} \quad \text{Equation 1.2}$$

Each of these terms can be expressed as follows;^{177,179}

$$\Delta S_{\text{mix}} = -k_B[n_A \ln\Phi_A + n_B \ln\Phi_B] \quad \text{Equation 1.3}$$

$$\Delta H_{\text{mix}} = k_B T \chi_{AB} N \Phi_A \Phi_B \quad \text{Equation 1.4}$$

Where k_B is the Boltzmann constant, χ is the Flory-Huggins interaction parameter, n_A and n_B represent the degree of polymerisation of each monomer, N is the total degree of polymerisation, and Φ_A and Φ_B represent the volume fraction of each polymer. As both the entropic and enthalpic term are dependent on the volume fraction of the polymer, the relative contribution of the enthalpic term is mostly dependent on the degree of polymerisation and the Flory-Huggins interaction parameter, which describes the free energy cost per monomer for contact between A and B monomers.¹⁸⁰

In turn, χ can be expressed as follows;¹⁸¹

$$\chi_{AB} = (Z/k_B T)[\epsilon_{AB} - (1/2)(\epsilon_{AA} + \epsilon_{BB})] \quad \text{Equation 1.5}$$

where Z is the number of nearest-neighbour monomers to a change in copolymer configuration (*i.e.* the repeat unit at which a switch from A to B domains occurs and *vice versa*), and ϵ_{AB} , ϵ_{AA} and ϵ_{BB} are the interaction energies between monomers, per monomer. In the absence of strong favourable interactions (such as hydrogen bonding) between the A and B domains, the interaction energies arising from the repulsion between A and B repeat units will be higher than those between A and A or B and B repeat units, resulting in a small, positive value for χ_{AB} . Therefore, given a sufficiently high degree of polymerisation, the value of ΔH_{mix} will exceed that of $T\Delta S_{\text{mix}}$ resulting in phase separation of the two polymer domains. It should be noted that as χ_{AB} is inversely related to temperature, mixing of the two phases typically becomes more favourable at higher temperatures.¹⁸¹

In the case of immiscible polymer blends, macrophase separation (such as that seen in immiscible solvents) will occur. However, the presence of covalent linkages between immiscible domains in block copolymers results in separation on a much smaller scale, termed microphase separation (although this term also includes phase separation on the nano- and mesoscopic scales). It is this microphase separation that gives rise to the elastomeric nature of A-B-A-type block copolymers by preserving the elasticity of the rubbery domains. The thermodynamic forces which drive phase separation dictate that the polymer chains should be in an extended configuration to ensure that the A and B segments of the polymer are at as great a distance from each other as possible. However, as there are fewer possible configurations for extended polymer chains to adopt, this leads to a decrease in entropy and is unfavoured.¹⁸² As the material is stretched and the polymer chains are extended, the entropic force grows to counteract the decreasing entropy, tending to move the chains back towards their coiled configuration and limiting the degree of phase separation.¹⁸³ The entropic force law

($F = T\Delta S$) is approximately Hookean, therefore for polymer chain blocks extended to a distance R from the equilibrium state, the elastic free energy giving rise to the entropic force can be expressed as;¹⁸¹

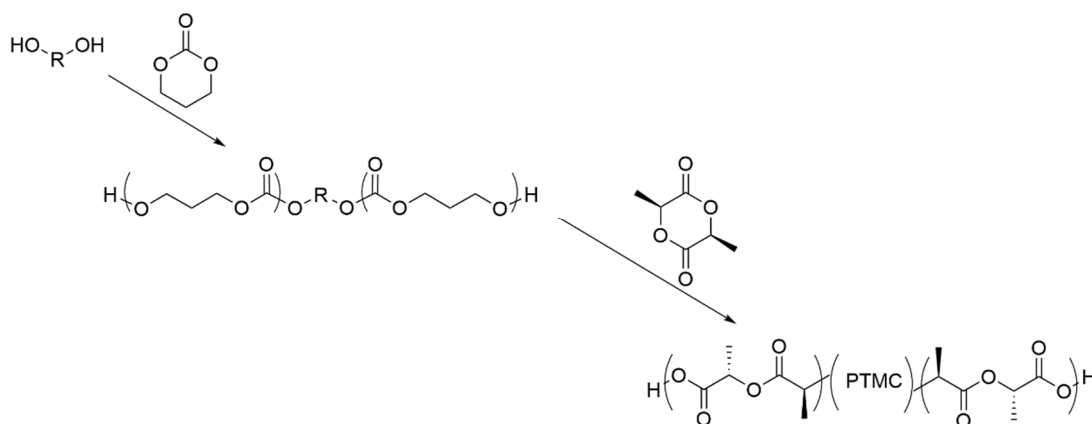
$$F_{\text{stretch}} = 3k_B TR^2/(2Na^2) \quad \text{Equation 1.6}$$

where N and a represent the number and size of the monomers respectively.

It is important to note that only A-B-A, (A-B)_n and (AB)_x star structures are capable of forming hard block domains that will physically crosslink to provide robust network structures (*e.g.* through hydrogen bonding, crystallisation or hydrophobic interactions). A-B diblock copolymers are incapable of forming these network structures, as only one end of the soft block component is covalently linked to a hard block domain.¹⁸⁴

1.6.2 Aliphatic polyester and polycarbonate-based A-B-A triblock copolymers

Microphase separation between covalently linked block copolymers has been widely applied in polymer science to generate materials with thermoplastic elastomer character, perhaps the most well-known of which are styrene-based block copolymers such as poly(styrene-*b*-butadiene-*b*-styrene), where the glassy, hard polystyrene domains provide mechanical strength, and the rubbery polybutadiene contributes elasticity.¹⁸⁵⁻¹⁸⁷ In recent years, there has been considerable focus on developing degradable analogues of these styrenic thermoplastic elastomers for biomedical applications.¹⁸⁸⁻¹⁹⁴ Triblocks comprising cyclic esters and carbonates have been prepared by sequential ROP, typically by first synthesising a central soft block to generate a telechelic macroinitiator, followed by chain extension with a second monomer to generate the hard domains (Scheme 1.16).¹⁸⁹



Scheme 1.16. ROP of TMC using a bifunctional initiator to generate a telechelic macroinitiator, followed by chain extension with *L*-lactide to generate an A-B-A triblock copolymer.¹⁸⁹

For several reasons, the majority of these studies have focussed on the use of semi-crystalline PLLA as the hard domain – the monomer is cheap and readily available, whilst the polymer has proven biocompatibility and can be physically crosslinked *via* crystallisation to provide the mechanical robustness required for thermoplastic elastomers.¹⁹⁵⁻¹⁹⁸ A variety of more flexible polymers immiscible with PLLA have been used as soft domains to confer elasticity on and improve the ductility of polylactide, most commonly PCL.¹⁹⁹⁻²⁰¹ Other amorphous polyesters with low glass transition temperatures including poly(1,5-dioxepan-2-one) (PDXO),^{202,203} poly(menthane) (PMI),²⁰⁴⁻²⁰⁶ poly(ϵ -decalactone) (PDL)²⁰⁷⁻²⁰⁹ and alkyl-substituted polyvalerolactones^{210,211} have also been studied as the soft domains in lactide-based A-B-A triblock copolymers, in order to provide materials with a broader range of properties. PTMC has also been applied for this purpose, generating A-B-A copolymers containing an aliphatic polycarbonate mid-block.²¹²⁻²¹⁴ PLLA-*b*-PTMC-*b*-PLLA triblock copolymers have been shown to be less tough but more flexible than triblock copolymers possessing a PCL mid-block, a property attributed to the completely amorphous nature of PTMC in comparison to semi-crystalline PCL.²¹⁵

These properties can be broadened further still by the use of statistical copolymers as the central soft block.²¹⁵⁻²²⁰ For example, Schneiderman and co-workers have prepared lactide-based triblock copolymers with mid-blocks consisting of PDL homopolymers and statistical copolymers of P(CL-*co*-DL). Through this, the researchers were able to prepare a library of materials with different mechanical properties, ranging from ultimate tensile strength (UTS) and strain at break values of 0.24 MPa and 218% for low molecular weight PLLA-*b*-PDL-*b*-PLLA containing 30% lactide, up to UTS and strain values of 18 MPa and 1200% for high molecular weight PLLA-*b*-P(CL-*co*-DL)-*b*-PLLA containing a similar percentage of lactide.^{208,220}

Separately, Widjaja *et al.* have shown that varying the ratio of CL:TMC in a statistical mid-block of the two had a marked effect on the properties of PLLA-*b*-P(CL-*co*-TMC)-*b*-PLLA triblock copolymers, with mid-blocks containing a ratio of 75:25 CL:TMC providing materials with UTS of 12 MPa and strains of over 1000% at break, whilst those containing 50:50 CL:TMC possessed UTS and strain values of *ca.* 4 MPa and 500% respectively. However, lower amounts of semi-crystalline CL in the 50:50 copolymer did result in materials with significantly improved elasticity when strained to 300%.²¹⁵

Despite the potential advantages associated with incorporating modifiable pendent functionality in these materials, to date functionality in lactide-based A-B-A triblock copolymers prepared by ROP appears to be limited to alkyl groups, such as those present in mid-block polymers such as PMI and PDL.^{204,210,221} Amorphous aliphatic polycarbonate central blocks meanwhile are limited to non-functional PTMC only. There are limited examples of degradable A-B-A triblocks bearing pendent functionality on the hard segments,^{192,194,222} however in lactide-based materials functionality must be incorporated on the mid-block to avoid disruption of the semi-

crystalline nature of the PLLA segments, which would have a deleterious effect on the mechanical properties of such a material.

1.7 Conclusion

In conclusion, functional aliphatic polyesters and polycarbonates produced by the ROP of their respective monomers possess great potential for the development of advanced biomedical polymers. This potential results from their ease of synthesis and the wide array of different functionalities available, providing a method of producing materials with highly specific degradation rates and mechanical properties, which can be targeted depending on the desired application.

However, to the best of our knowledge, there have been no reports to date of A-B-A triblock copolymers consisting solely of aliphatic polyesters and polycarbonates bearing pendent functionality on the central soft segment. Elastomeric materials bearing pendent functionalities present an attractive proposition, as these would enable the facile modification of thermoplastic elastomers post-polymerisation. Scaffolds designed using these materials could have readily tuneable physical and mechanical properties, variable degradation rates, and could even facilitate the attachment of therapeutic compounds, including those designed to promote tissue regeneration.

1.8 Aims and Research Objectives

The purpose of the work presented in this thesis is to develop new materials with potential applications in the field of biomedicine, either for drug delivery or as materials to form the basis of soft tissue scaffolds. To be applied in this manner, these materials would have to be degradable and biocompatible, and have tuneable physical and mechanical properties. There are two major ways in which these properties can be

varied; firstly, by post-polymerisation modification of polymers bearing pendent functional groups, and secondly, by copolymerisation of two or more monomers to synthesise random or block copolymers. However, to date, the use of polymers bearing pendent functionality in biomedicine is generally limited by the need for complex, multi-step syntheses. The individual chapters in this thesis aim to explore the modification of an alkene-functional polycarbonate prepared in one step from a low cost commercial precursor, both through post-polymerisation modifications and through the synthesis of random and block copolymers. The objectives of this work are therefore as follows;

Firstly, to introduce additional functionality to the polymer through post-polymerisation modification of the alkene group. It is envisioned that this will be achieved through photoinitiated radical thiol-ene addition chemistry.

Secondly, to prepare stimuli responsive materials with potential applications in drug delivery, specifically by grafting a hydrophilic polymer to the hydrophobic polycarbonate backbone to generate a thermoresponsive material.

Thirdly, to prepare random copolymers of the alkene-functional polycarbonate and a non-functional co-monomer, with a view to controlling the degradation rate and functional group density of the materials.

Fourthly, to prepare materials with potential application as tissue scaffolds through post-polymerisation modification of the polycarbonate. This may be achieved through photoinitiated crosslinking of the polymer, for example using a dithiol-crosslinker, with precise structures fabricated using a stereolithographic process.

Finally, to prepare materials with thermoplastic elastomer character and tuneable mechanical properties, specifically by synthesising ABA-type triblock copolymers

with the central soft block consisting of random copolymers of the alkene-functional carbonate and a cyclic ester. Through this method, it is envisioned that the mechanical properties may be modified either by variation of the ester:carbonate composition of the soft block, or by variation of the ABA composition of the polymer.

1.9 References

- (1) Hutmacher, D. W. *Biomaterials* **2000**, *21*, 2529.
- (2) Kohane, D. S.; Langer, R. *Pediatr. Res.* **2008**, *63*, 487.
- (3) Tateishi, T.; Guoping, C.; Ushida, T.; Murata, T.; Mizuno, S. In *Tissue Engineering and Biodegradable Equivalents*; 1 ed.; Lewandrowski, K.-U. Wise, D. L.; Trantolo, D. J.; Gresser, J. D.; Yaszemski, M. J.; Altobelli, D. E., Ed.; Marcel Dekker: New York, 2002, p 99.
- (4) Ulery, B. D.; Nair, L. S.; Laurencin, C. T. *J. Polym. Sci. Part B Polym. Phys.* **2011**, *49*, 832.
- (5) Dhandayuthapani, B.; Yoshida, Y.; Maekawa, T.; Kumar, D. S. *Int. J. Polym. Sci.* **2011**.
- (6) Bressan, E.; Favero, V.; Gardin, C.; Ferroni, L.; Iacobellis, L.; Favero, L.; Vindigni, V.; Berengo, M.; Sivolella, S.; Zavan, B. *Polymers* **2011**, *3*, 509.
- (7) O'Brien, F. J. *Mater. Today* **2011**, *14*, 88.
- (8) Martina, M.; Hutmacher, D. W. *Polym. Int.* **2007**, *56*, 145.
- (9) Gupta, A. P.; Kumar, V. *Eur. Polym. J.* **2007**, *43*, 4053.

- (10) Sisson, A. L.; Schroeter, M.; Lendlein, A. In *Handbook of Biodegradable Polymers*; Lendlein, A.; Sisson, A. L., Ed.; Wiley-VCH: Weinheim, 2011, p 1.
- (11) Gentile, P.; Chiono, V.; Carmagnola, I.; Hatton, P. V. *Int. J. Mol. Sci.* **2014**, *15*, 3640.
- (12) Jain, R. A. *Biomaterials* **2000**, *21*, 2475.
- (13) Makadia, H. K.; Siegel, S. J. *Polymers* **2011**, *3*, 1377.
- (14) Bendix, D. *Polym. Degrad. Stab.* **1998**, *59*, 129.
- (15) Davachi, S. M.; Kaffashi, B. *Polym. Plast. Technol. Eng.* **2015**, *54*, 944.
- (16) Jagur-Grodzinski, J. *Polymer. Adv. Tech.* **2006**, *17*, 395.
- (17) Dash, T. K.; Konkimalla, V. B. *J. Control. Release* **2012**, *158*, 15.
- (18) Woodruff, M. A.; Hutmacher, D. W. *Prog. Polym. Sci.* **2010**, *35*, 1217.
- (19) Nair, L. S.; Laurencin, C. T. *Prog. Polym. Sci.* **2007**, *32*, 762.
- (20) Laine, P.; Kontio, R.; Lindqvist, C.; Suuronen, R. *Int. J. Oral Maxillofac. Surg.* **2004**, *33*, 240.
- (21) Gunatillake, P.; Mayadunne, R.; Adhikari, R. *Biotechnol. Annu. Rev. Vol 12* **2006**, *12*, 301.
- (22) Anderson, J. M.; Shive, M. S. *Adv. Drug Deliv. Rev.* **2012**, *64*, 72.
- (23) Bezwada, R. S.; Jamiolkowski, D. D.; Lee, I. Y.; Agarwal, V.; Persivale, J.; Trenkabethin, S.; Ernetta, M.; Suryadevara, J.; Yang, A.; Liu, S. *Biomaterials* **1995**, *16*, 1141.

- (24) Nagueh, S. F.; Shah, G.; Wu, Y. M.; Torre-Amione, G.; King, N. M. P.; Lahmers, S.; Witt, C. C.; Becker, K.; Labeit, S.; Granzier, H. L. *Circulation* **2004**, *110*, 155.
- (25) Domb, A. J.; Kumar, N.; Sheskin, T.; Bentolila, A.; Slager, J.; Teomim, D. In *Polymeric Biomaterials*; 2 ed.; Dumitriu, S., Ed.; CRC Press: Boca Raton, 2001.
- (26) Xu, J.; Feng, E.; Song, J. *J. Appl. Polym. Sci.* **2014**, *131*.
- (27) Keul, H. In *Handbook of Ring-Opening Polymerization*; Dubois, P.; Coulembier, O.; Raquez, J.-M., Ed.; Wiley-VCH Verlag GmbH & Co. KGaA: New York, 2009, p 307.
- (28) Rokicki, G. *Prog. Polym. Sci.* **2000**, *25*, 259.
- (29) Artham, T.; Doble, M. *Macromol. Biosci.* **2008**, *8*, 14.
- (30) Feng, J.; Zhuo, R.-X.; Zhang, X.-Z. *Prog. Polym. Sci.* **2012**, *37*, 211.
- (31) Tempelaar, S.; Mespouille, L.; Coulembier, O.; Dubois, P.; Dove, A. P. *Chem. Soc. Rev.* **2013**, *42*, 1312.
- (32) Bat, E.; Plantinga, J. A.; Harmsen, M. C.; van Luyn, M. J. A.; Zhang, Z.; Grijpma, D. W.; Feijen, J. *Biomacromolecules* **2008**, *9*, 3208.
- (33) Gupta, B.; Revagade, N.; Hilborn, J. *Prog. Polym. Sci.* **2007**, *32*, 455.
- (34) Sodergard, A.; Stolt, M. In *Poly(lactic acid): Synthesis, Structures, Properties, Processing, and Applications*; 1 ed.; Auras, R. A., Lim, L. T., Selke, S. E. M., Tsuji, H., Eds.; Wiley: Hoboken, 2010, p 27.

- (35) Kowalski, A.; Duda, A.; Penczek, S. *Macromol. Rapid Commun.* **1998**, *19*, 567.
- (36) Kowalski, A.; Duda, A.; Penczek, S. *Macromolecules* **2000**, *33*, 7359.
- (37) Coates, G. W.; Jeske, R. C. In *Handbook of Green Chemistry, Volume 1: Homogeneous Catalysis*; 1 ed.; Crabtree, R. H., Ed.; Wiley: Weinheim, 2009, p 343.
- (38) Dubois, P.; Jacobs, C.; Jerome, R.; Teyssie, P. *Macromolecules* **1991**, *24*, 2266.
- (39) Paul, S.; Zhu, Y.; Romain, C.; Brooks, R.; Saini, P. K.; Williams, C. K. *Chem. Commun.* **2015**, *51*, 6459.
- (40) Kiesewetter, M. K.; Shin, E. J.; Hedrick, J. L.; Waymouth, R. M. *Macromolecules* **2010**, *43*, 2093.
- (41) Kamber, N. E.; Jeong, W.; Waymouth, R. M.; Pratt, R. C.; Lohmeijer, B. G.; Hedrick, J. L. *Chem. Rev.* **2007**, *107*, 5813.
- (42) Carothers, W. H.; Dorough, G. L.; van Natta, F. J. *J. Am. Chem. Soc.* **1932**, *52*, 761.
- (43) Nederberg, F.; Connor, E. F.; Moller, M.; Glauser, T.; Hedrick, J. L. *Angew. Chem. Int. Ed.* **2001**, *40*, 2712.
- (44) MacMillan, D. W. C. *Nature* **2008**, *455*, 304.
- (45) Dove, A. P. *ACS Macro Lett.* **2012**, *1*, 1409.
- (46) Zhang, L.; Nederberg, F.; Pratt, R. C.; Waymouth, R. M.; Hedrick, J. L.; Wade, C. G. *Macromolecules* **2007**, *40*, 4154.

- (47) Mespouille, L.; Coulembier, O.; Kawalec, M.; Dove, A. P.; Dubois, P. *Prog. Polym. Sci.* **2014**, *39*, 1144.
- (48) Naumann, S.; Thomas, A. W.; Dove, A. P. *Angew. Chem. Int. Ed.* **2015**, *54*, 9550.
- (49) Naumann, S.; Thomas, A. W.; Dove, A. P. *ACS Macro Lett.* **2016**, *5*, 134.
- (50) Raynaud, J.; Ottou, W. N.; Gnanou, Y.; Taton, D. *Chem. Commun.* **2010**, *46*, 3203.
- (51) Naumann, S.; Dove, A. P. *Polym. Int.* **2016**, *65*, 16.
- (52) Todd, R.; Rubio, G.; Hall, D. J.; Tempelaar, S.; Dove, A. P. *Chem. Sci.* **2013**, *4*, 1092.
- (53) Lohmeijer, B. G. G.; Pratt, R. C.; Leibfarth, F.; Logan, J. W.; Long, D. A.; Dove, A. P.; Nederberg, F.; Choi, J.; Wade, C.; Waymouth, R. M.; Hedrick, J. L. *Macromolecules* **2006**, *39*, 8574.
- (54) Olsen, P.; Odelius, K.; Keul, H.; Albertsson, A.-C. *Macromolecules* **2015**, *48*, 1703.
- (55) Pratt, R. C.; Lohmeijer, B. G. G.; Long, D. A.; Waymouth, R. M.; Hedrick, J. L. *J. Am. Chem. Soc.* **2006**, *128*, 4556.
- (56) Misaka, H.; Kakuchi, R.; Zhang, C.; Sakai, R.; Satoh, T.; Kakuchi, T. *Macromolecules* **2009**, *42*, 5091.
- (57) Fu, X.; Tan, C.-H. *Chem. Commun.* **2011**, *47*, 8210.
- (58) Nachtergaele, A.; Coulembier, O.; Dubois, P.; Helvenstein, M.; Duez, P.; Blankert, B.; Mespouille, L. *Biomacromolecules* **2015**, *16*, 507.

- (59) Albertsson, A. C.; Varma, I. K. *Biomacromolecules* **2003**, *4*, 1466.
- (60) Tian, H.; Tang, Z.; Zhuang, X.; Chen, X.; Jing, X. *Prog. Polym. Sci.* **2012**, *37*, 237.
- (61) Heiny, M.; Wurth, J. J.; Shastri, V. P. In *Natural and Synthetic Biomedical Polymers*; 1 ed.; Kumbar, S. G., Laurencin, C. T., Deng, M., Eds.; Elsevier: San Diego, 2014, p 167.
- (62) Günay, K. A.; Theato, P.; Klok, H.-A. In *Functional Polymers by Post-Polymerization Modification: Concepts, Guidelines, and Applications*; 1 ed.; Theato, P., Klok, H.-A., Eds.; Wiley-VCH: Weinheim, 2013, p 1.
- (63) Zou, J.; Hew, C. C.; Themistou, E.; Li, Y. K.; Chen, C. K.; Alexandridis, P.; Cheng, C. *Adv. Mater.* **2011**, *23*, 4274.
- (64) Kimura, Y.; Shirotani, K.; Yamane, H.; Kitao, T. *Macromolecules* **1988**, *21*, 3338.
- (65) Yamaoka, T.; Hotta, Y.; Kobayashi, K.; Kimura, Y. *Int. J. Biol. Macromolec.* **1999**, *25*, 265.
- (66) Yu, Y.; Zou, J.; Cheng, C. *Polym. Chem.* **2014**, *5*, 5854.
- (67) Darcos, V.; El Habnoui, S.; Nottelet, B.; El Ghzaoui, A.; Coudane, J. *Polym. Chem.* **2010**, *1*, 280.
- (68) Falamarzian, A.; Lavasanifar, A. *Macromol. Biosci.* **2010**, *10*, 648.
- (69) Lenoir, S.; Riva, R.; Lou, X.; Detrembleur, C.; Jerome, R.; Lecomte, P. *Macromolecules* **2004**, *37*, 4055.
- (70) Mahmud, A.; Xiong, X. B.; Lavasanifar, A. *Macromolecules* **2006**, *39*, 9419.

- (71) Massoumi, B.; Abdollahi, M.; Fathi, M.; Entezami, A. A.; Hamidi, S. *J. Polym. Res.* **2013**, *20*.
- (72) Riva, R.; Schmeits, P.; Stoffelbach, F.; Jerome, C.; Jerome, R.; Lecomte, P. *Chem. Commun.* **2005**, 5334.
- (73) Buchard, A.; Carbery, D. R.; Davidson, M. G.; Ivanova, P. K.; Jeffery, B. J.; Kociok-Koehn, G. I.; Lowe, J. P. *Angew. Chem. Int. Ed.* **2014**, *53*, 13858.
- (74) du Boullay, O. T.; Bonduelle, C.; Martin-Vaca, B.; Bourissou, D. *Chem. Commun.* **2008**, 1786.
- (75) du Boullay, O. T.; Marchal, E.; Martin-Vaca, B.; Cossio, F. P.; Bourissou, D. *J. Am. Chem. Soc.* **2006**, *128*, 16442.
- (76) Pounder, R. J.; Fox, D. J.; Barker, I. A.; Bennison, M. J.; Dove, A. P. *Polym. Chem.* **2011**, *2*, 2204.
- (77) Jerome, C.; Lecomte, P. *Adv. Drug Deliv. Rev.* **2008**, *60*, 1056.
- (78) Pounder, R. J.; Dove, A. P. *Polym. Chem.* **2010**, *1*, 260.
- (79) Rainbolt, E. A.; Washington, K. E.; Biewer, M. C.; Stefan, M. C. *Polym. Chem.* **2015**, *6*, 2369.
- (80) Chen, W.; Meng, F.; Cheng, R.; Deng, C.; Feijen, J.; Zhong, Z. *J. Control. Release* **2014**, *190*, 398.
- (81) Fukushima, K. *Biomater. Sci.* **2016**, *4*, 9.
- (82) Guillaume, S. M.; Mespouille, L. *J. Appl. Polym. Sci.* **2014**, *131*.

- (83) Rokicki, G.; Parzuchowski, P. G. In *Polymer Science: A Comprehensive Reference*; 1 ed.; Matyjaszewski, K., and Möller, M., Ed.; Elsevier: Oxford, 2012; Vol. 4, p 247.
- (84) Ariga, T.; Takata, T.; Endo, T. *Macromolecules* **1997**, *30*, 737.
- (85) Cai, J.; K. Zhu, K. J.; Yang, S. L. *Polymer* **1998**, *39*, 4409.
- (86) Vandenberg, E. J.; Tian, D. *Macromolecules* **1999**, *32*, 3613.
- (87) Kühling, S.; Keul, H.; Hoecker, H.; Buysch, H. J.; Schön, N.; Leitz, E. *Macromolecules* **1991**, *24*, 4229.
- (88) Endo, T.; Kakimoto, K.; Ochiai, B.; Nagai, D. *Macromolecules* **2005**, *38*, 8177.
- (89) Kühling, S.; Keul, H.; Höcker, H.; Buysch, H. J.; Schön, N. *Macromol. Chem. Phys.* **1991**, *192*, 1193.
- (90) Mullen, B. D.; Tang, C. N.; Storey, R. F. *Polym. Prepr., ACS Div. Polym. Chem.* **2003**, *44*, 767.
- (91) Pratt, R. C.; Nederberg, F.; Waymouth, R. M.; Hedrick, J. L. *Chem. Commun.* **2008**, *1*, 114.
- (92) Seow, W. Y.; Yang, Y. Y. *J. Control. Release* **2009**, *139*, 40.
- (93) Xie, Z. G.; Hu, X. L.; Chen, X. S.; Sun, J.; Shi, Q.; Jing, X. B. *Biomacromolecules* **2008**, *9*, 376.
- (94) Sanders, D. P.; Fukushima, K.; Coady, D. J.; Nelson, A.; Fujiwara, M.; Yasumoto, M.; Hedrick, J. L. *J. Am. Chem. Soc.*, **2010**, *132*, 14724.

- (95) Hu, X.; Chen, X.; Xie, Z.; Liu, S.; Jing, X. *J. Polym. Sci. A: Polym. Chem.* **2007**, *45*, 5518.
- (96) Yang, L.; Li, J.; Meng, S.; Jin, Y.; Zhang, J.; Li, M.; Guo, J.; Gu, Z. *Polymer* **2014**, *55*, 5111.
- (97) Yasuda, H.; Aludin, M. S.; Kitamura, N.; Tanabe, M.; Sirahama, H. *Macromolecules* **1999**, *32*, 6047.
- (98) Al-Azemi, T. F.; Harmon, J. P.; Bisht, K. S. *Biomacromolecules* **2000**, *1*, 493.
- (99) Hansell, C. F.; O'Reilly, R. K. *ACS Macro Lett.* **2012**, *1*, 896.
- (100) Xu, J.; Prifti, F.; Song, J. *Macromolecules* **2011**, *44*, 2660.
- (101) Nederberg, F.; Zhang, Y.; Tan, J. P. K.; Xu, K. J.; Wang, H. Y.; Yang, C.; Gao, S. J.; Guo, X. D.; Fukushima, K.; Li, L. J.; Hedrick, J. L.; Yang, Y. Y. *Nat. Chem.* **2011**, *3*, 409.
- (102) Aguirre-Chagala, Y. E.; Santos, J. L.; Aguilar-Castillo, B. A.; Herrera-Alonso, M. *ACS Macro Lett.* **2014**, *3*, 353.
- (103) Xu, J.; Liu, Z. L.; Zhuo, R. X. *J. Appl. Polym. Sci.* **2006**, *101*, 1988.
- (104) Lu, J.; Shoichet, M. S. *Macromolecules* **2010**, *43*, 4943.
- (105) Shi, M.; Wosnick, J. H.; Ho, K.; Keating, A.; Shoichet, M. S. *Angew. Chem. Int. Ed.* **2007**, *46*, 6126.
- (106) Engler, A. C.; Tan, J. P. K.; Ong, Z. Y.; Coady, D. J.; Ng, V. W. L.; Yang, Y. Y.; Hedrick, J. L. *Biomacromolecules* **2013**, *14*, 4331.
- (107) Ono, R. J.; Liu, S. Q.; Venkataraman, S.; Chin, W.; Yang, Y. Y.; Hedrick, J. L. *Macromolecules* **2014**, *47*, 7725.

- (108) Onbulak, S.; Tempelaar, S.; Pounder, R. J.; Gok, O.; Sanyal, R.; Dove, A. P.; Sanyal, A. *Macromolecules* **2012**, *45*, 1715.
- (109) Tempelaar, S.; Mespouille, L.; Dubois, P.; Dove, A. P. *Macromolecules* **2011**, *44*, 2084.
- (110) Chen, W.; Yang, H.; Wang, R.; Cheng, R.; Meng, F.; Wei, W.; Zhong, Z. *Macromolecules* **2010**, *43*, 201.
- (111) Shi, Y.; Wang, X.; Graff, R. W.; Phillip, W. A.; Gao, H. *J. Polym. Sci. A: Polym. Chem.* **2015**, *53*, 239.
- (112) Tempelaar, S.; Barker, I. A.; Truong, V. X.; Hall, D. J.; Mespouille, L.; Dubois, P.; Dove, A. P. *Polym. Chem.* **2013**, *4*, 174.
- (113) Voo, Z. X.; Khan, M.; Narayanan, K.; Seah, D.; Hedrick, J. L.; Yang, Y. Y. *Macromolecules* **2015**, *48*, 1055.
- (114) Williams, R. J.; Barker, I. A.; O'Reilly, R. K.; Dove, A. P. *ACS Macro Lett.* **2012**, *1*, 1285.
- (115) Olsen, P.; Odelius, K.; Albertsson, A.-C. *Macromolecules* **2014**, *47*, 6189.
- (116) Olofsson, K.; Malkoch, M.; Hult, A. *J. Polym. Sci. A: Polym. Chem.* **2016**.
- (117) Hu, X.; Chen, X.; Liu, S.; Shi, Q.; Jing, X. *J. Polym. Sci. A: Polym. Chem.* **2008**, *46*, 1852.
- (118) Yue, J.; Li, X.; Mo, G.; Wang, R.; Huang, Y.; Jing, X. *Macromolecules* **2010**, *43*, 9645.
- (119) Sun, L.; Pitto-Barry, A.; Thomas, A. W.; Inam, M.; Doncom, K.; Dove, A. P.; O'Reilly, R. K. *Polym. Chem.* **2016**, *7*, 2337.

- (120) Griffiths, J.R.; *Br. J. Cancer* **1991**, *64*, 425
- (121) Wang, H.; Wang, Y.; Chen, Y.; Jin, Q.; Ji, J. *Polym. Chem.* **2014**, *5*, 854.
- (122) Kuang, H.; Wu, S.; Xie, Z.; Meng, F.; Jing, X.; Huang, Y. *Biomacromolecules* **2012**, *13*, 3004.
- (123) Stevens, D. M.; Tempelaar, S.; Dove, A. P.; Harth, E. *ACS Macro Lett.* **2012**, *1*, 915.
- (124) Truong, V. X.; Barker, I. A.; Tan, M.; Mespouille, L.; Dubois, P.; Dove, A. P. *J. Mater. Chem. B* **2013**, *1*, 221.
- (125) Stevens, D. M.; Rahalkar, A.; Spears, B.; Gilmore, K.; Douglas, E.; Muthukumar, M.; Harth, E. *Polym. Chem.* **2015**, *6*, 1096.
- (126) Barker, I. A.; Ablett, M. P.; Gilbert, H. T. J.; Leigh, S. J.; Covington, J. A.; Hoyland, J. A.; Richardson, S. M.; Dove, A. P. *Biomater. Sci.* **2014**, *2*, 472.
- (127) S. Li, F. Meng, Z. Wang, Y. Zhong, M. Zheng, H. Liu, *Eur. J. Pharm. Biopharm.*, **2012**, *82*, 103.
- (128) Yu, Y.; Deng, C.; Meng, F.; Shi, Q.; Feijen, J.; Zhong, Z. *J. Biomed. Mater. Res. A* **2011**, *99A*, 316.
- (129) Uysal, B. B.; Gunay, U. S.; Hizal, G.; Tunca, U. *J. Polym. Sci. A: Polym. Chem.* **2014**, *52*, 1581.
- (130) Wang, R.; Chen, W.; Meng, F.; Cheng, R.; Deng, C.; Feijen, J.; Zhong, Z. *Macromolecules* **2011**, *44*, 6009.
- (131) Liu, G.; He, F.; Wang, Y. P.; Feng, J.; Zhuo, R. X. *Chin. Chem. Lett.* **2006**, *17*, 137.

- (132) Mullen, B. D.; Tang, C. N.; Storey, R. F. *J. Polym. Sci. A: Polym. Chem.* **2003**, *41*, 1978.
- (133) He, F.; Wang, Y.-P.; Liu, G.; Jia, H.-L.; Feng, J.; Zhuo, R.-X. *Polymer* **2008**, *49*, 1185.
- (134) Wang, C.-F.; Lin, Y.-X.; Jiang, T.; He, F.; Zhuo, R.-X. *Biomaterials* **2009**, *30*, 4824.
- (135) He, F.; Wang, C.-F.; Jiang, T.; Han, B.; Zhuo, R.-X. *Biomacromolecules* **2010**, *11*, 3028.
- (136) Jiang, T.; Li, Y.-M.; Lv, Y.; Cheng, Y.-J.; He, F.; Zhuo, R.-X. *Colloids Surf., B* **2013**, *111*, 542.
- (137) Jiang, T.; Li, Y.; Lv, Y.; Cheng, Y.; He, F.; Zhuo, R. *J. Mater. Sci. Mater. Med.* **2014**, *25*, 131.
- (138) Hu, X.; Chen, X.; Cheng, H.; Jing, X. *J. Polym. Sci. A: Polym. Chem.* **2009**, *47*, 161.
- (139) Danquah, M.; Fujiwara, T.; Mahato, R. I. *J. Polym. Sci. A: Polym. Chem.* **2013**, *51*, 347.
- (140) Yang, R.; Meng, F.; Ma, S.; Huang, F.; Liu, H.; Zhong, Z. *Biomacromolecules* **2011**, *12*, 3047.
- (141) Wu, Y.; Chen, W.; Meng, F.; Wang, Z.; Cheng, R.; Deng, C.; Liu, H.; Zhong, Z. *J. Control. Release* **2012**, *164*, 338.
- (142) Chen, F.; Hayami, J. W. S.; Amsden, B. G. *Biomacromolecules* **2014**, *15*, 1593.

- (143) Chen, F.; Hochleitner, G.; Woodfield, T.; Groll, J.; Dalton, P. D.; Amsden, B. *G. Biomacromolecules* **2016**, *17*, 208.
- (144) Mindemark, J.; Imholt, L.; Montero, J.; Brandell, D. *J. Polym. Sci. Part A: Polym. Chem.* **2016**.
- (145) Heo, G. S.; Cho, S.; Wooley, K. L. *Polym. Chem.* **2014**, *5*, 3555.
- (146) Miyagawa, T.; Shimizu, M.; Sanda, F.; Endo, T. *Macromolecules* **2005**, *38*, 7944.
- (147) Zhu, K. J.; Hendren, R. W.; Jensen, K.; Pitt, C. G. *Macromolecules* **1991**, *24*, 1736.
- (148) Pego, A. P.; Van Luyn, M. J. A.; Brouwer, L. A.; van Wachem, P. B.; Poot, A. A.; Grijpma, D. W.; Feijen, J. *J. Biomed. Mater. Res. A* **2003**, *67A*, 1044.
- (149) Pitt, C. G.; Zhong-wei, G. *J. Control. Release* **1987**, *4*, 283.
- (150) Gopferich, A. *Macromolecules* **1997**, *30*, 2598.
- (151) Uhrich, K. E.; Cannizzaro, S. M.; Langer, R. S.; Shakesheff, K. M. *Chem. Rev.* **1999**, *99*, 3181.
- (152) Lyu, S. P.; Untereker, D. *Int. J. Mol. Sci.* **2009**, *10*, 4033.
- (153) Gopferich, A. *Biomaterials* **1996**, *17*, 103.
- (154) Therin, M.; Christel, P.; Li, S. M.; Garreau, H.; Vert, M. *Biomaterials* **1992**, *13*, 594.
- (155) Vert, M.; Li, S.; Garreau, H. *J. Control. Release* **1991**, *16*, 15.
- (156) Wu, X. S.; Wang, N. *J. Biomater. Sci. Polym. Ed.* **2001**, *12*, 21.

- (157) Cai, H.; Dave, V.; Gross, R. A.; McCarthy, S. P. *J. Polym. Sci. Part B Polym. Phys.* **1996**, *34*, 2701.
- (158) MacDonald, R. T.; McCarthy, S. P.; Gross, R. A. *Macromolecules* **1996**, *29*, 7356.
- (159) Tokiwa, Y.; Calabia, B. P. *Appl. Microbiol. Biotechnol.* **2006**, *72*, 244.
- (160) Buchholz, B. *J. Mater. Sci. Mater. Med.* **1993**, *4*, 381.
- (161) Dong, J.; Liao, L.; Ma, Y.; Shi, L.; Wang, G.; Fan, Z.; Li, S.; Lu, Z. *Polym. Degrad. Stab.* **2014**, *103*, 26.
- (162) Jie, C.; Zhu, K. J.; Yang, S. L. *Polym. Int.* **1996**, *41*, 369.
- (163) Grijpma, D. W.; Pennings, A. J. *Macromol. Chem. Phys.* **1994**, *195*, 1633.
- (164) Pego, A. P.; Poot, A. A.; Grijpma, D. W.; Feijen, J. *J. Control. Release* **2003**, *87*, 69.
- (165) Sodergard, A.; Stolt, M. *Prog. Polym. Sci.* **2002**, *27*, 1123.
- (166) Ajiro, H.; Takahashi, Y.; Akashi, M.; Fujiwara, T. *Polymer* **2014**, *55*, 3591.
- (167) Bat, E.; van Kooten, T. G.; Harmsen, M. C.; Plantinga, J. A.; van Luyn, M. J. A.; Feijen, J.; Grijpma, D. W. *Macromol. Biosci.* **2013**, *13*, 573.
- (168) Diaz-Celorio, E.; Franco, L.; Rodriguez-Galan, A.; Puiggali, J. *Polym. Degrad. Stab.* **2013**, *98*, 133.
- (169) Yuan, Y.; Jin, X.; Fan, Z.; Li, S.; Lu, Z. *J. Mater. Sci. Mater. Med.* **2015**, *26*.
- (170) Acemoglu, M.; Bantle, S.; Mindt, T.; Nimmerfall, F. *Macromolecules* **1995**, *28*, 3030.

- (171) Cheng, S. X.; Miao, Z. M.; Wang, L. S.; Zhuo, R. X. *Macromol. Rapid Commun.* **2003**, *24*, 1066.
- (172) Ray, W. C.; Grinstaff, M. W. *Macromolecules* **2003**, *36*, 3557.
- (173) Nakayama, Y.; Yasuda, H.; Yamamoto, K.; Tsutsumi, C.; Jerome, R.; Lecomte, P. *React. Funct. Polym.* **2005**, *63*, 95.
- (174) Peng, H.; Ling, J.; Liu, J.; Zhu, N.; Ni, X.; Shen, Z. *Polym. Degrad. Stab.* **2010**, *95*, 643.
- (175) Hamley, I. W. In *Developments in Block Copolymer Science and Technology*; 1 ed.; Hamley, I. W., Ed.; John Wiley & Sons: Chichester, 2004, p 1.
- (176) Jones, R. A. L.; Richards, R. W. In *Polymers at Surfaces and Interfaces*; 1 ed.; Cambridge University Press: Cambridge, 1999, p 127.
- (177) Eisele, U. In *Introduction to Polymer Physics*; 1 ed.; Springer-Verlag: Heidelberg, 1990, p 158.
- (178) Hamley, I. W. *The Physics of Block Copolymers*; Oxford University Press: Oxford, 1998.
- (179) Sperling, L. H. In *Introduction to Physical Polymer Science*; 4 ed.; John Wiley & Sons: Hoboken, 2006, p 145.
- (180) Tadros, T. In *Encyclopedia of Colloid and Interface Science*; 1 ed.; Tadros, T., Ed.; Springer-Verlag: Heidelberg, 2013, p 523.
- (181) Bates, F. S.; Fredrickson, G. H. *Phys. Today* **1999**, *52*, 32.
- (182) Ravve, A. In *Principles of Polymer Chemistry*; 3 ed.; Springer: 2012, p 17.
- (183) Verlinde, E. J. *High Energy Phys.* **2011**.

- (184) McGrath, J. E. In *Block Copolymers: Science and Technology*; Meier, D. J., Ed.; Harwood Academic Press: Chur, 1983; Vol. 3, p 1.
- (185) Adhikari, R.; Michler, G. H. *Prog. Polym. Sci.* **2004**, *29*, 949.
- (186) Honeker, C. C.; Thomas, E. L. *Chem. Mater.* **1996**, *8*, 1702.
- (187) Coessens, V.; Pintauer, T.; Matyjaszewski, K. *Prog. Polym. Sci.* **2001**, *26*, 337.
- (188) Ding, K.; John, A.; Shin, J.; Lee, Y.; Quinn, T.; Tolman, W. B.; Hillmyer, M. A. *Biomacromolecules* **2015**, *16*, 2537.
- (189) Guillaume, S. M. *Eur. Polym. J.* **2013**, *49*, 768.
- (190) Holmberg, A. L.; Reno, K. H.; Wool, R. P.; Epps, T. H., III *Soft Matter* **2014**, *10*, 7405.
- (191) Kricheldorf, H. R.; Stricker, A. *Macromol. Chem. Phys.* **1999**, *200*, 1726.
- (192) Sun, H.; Meng, F.; Dias, A. A.; Hendriks, M.; Feijen, J.; Zhong, Z. *Biomacromolecules* **2011**, *12*, 1937.
- (193) Wilson, J. A.; Hopkins, S. A.; Wright, P. M.; Dove, A. P. *Biomacromolecules* **2015**, *16*, 3191.
- (194) Brannigan, R. P.; Walder, A.; Dove, A. P. *J. Polym. Sci. A: Polym. Chem.* **2014**, *52*, 2279.
- (195) Lendlein, A.; Langer, R. *Science* **2002**, *296*, 1673.
- (196) Frick, E. M.; Zalusky, A. S.; Hillmyer, M. A. *Biomacromolecules* **2003**, *4*, 216.
- (197) Gramlich, W. M. *Macromol. Chem. Phys.* **2015**, *216*, 145.

- (198) MacDonald, J. P.; Parker, M. P.; Greenland, B. W.; Hermida-Merino, D.; Hamley, I. W.; Shaver, M. P. *Polym. Chem.* **2015**, *6*, 1445.
- (199) Kong, J. F.; Lipik, V.; Abadie, M. J. M.; Deen, G. R.; Venkatraman, S. S. *Polym. Int.* **2012**, *61*, 43.
- (200) Lipik, V. T.; Kong, J. F.; Chattopadhyay, S.; Widjaja, L. K.; Liow, S. S.; Venkatraman, S. S.; Abadie, M. J. M. *Acta Biomater.* **2010**, *6*, 4261.
- (201) Qian, H. T.; Bei, J. Z.; Wang, S. G. *Polym. Degrad. Stab.* **2000**, *68*, 423.
- (202) Arias, V.; Olsén, P.; Odelius, K.; Höglund, A.; Albertsson, A. C. *Polym. Degrad. Stab.* **2016**.
- (203) Ryner, M.; Albertsson, A. C. *Biomacromolecules* **2002**, *3*, 601.
- (204) Hillmyer, M. A.; Tolman, W. B. *Acc. Chem. Res.* **2014**, *47*, 2390.
- (205) Wanamaker, C. L.; O'Leary, L. E.; Lynd, N. A.; Hillmyer, M. A.; Tolman, W. B. *Biomacromolecules* **2007**, *8*, 3634.
- (206) Wanamaker, C. L.; Tolman, W. B.; Hillmyer, M. A. *Biomacromolecules* **2009**, *10*, 443.
- (207) Lin, J.-O.; Chen, W.; Shen, Z.; Ling, J. *Macromolecules* **2013**, *46*, 7769.
- (208) Martello, M. T.; Schneiderman, D. K.; Hillmyer, M. A. *ACS Sustain. Chem. Eng.* **2014**, *2*, 2519.
- (209) Olsen, P.; Borke, T.; Odelius, K.; Albertsson, A.-C. *Biomacromolecules* **2013**, *14*, 2883.
- (210) Schneiderman, D. K.; Hillmyer, M. A. *Macromolecules* **2016**, *49*, 2419.

- (211) Xiong, M.; Schneiderman, D. K.; Bates, F. S.; Hillmyer, M. A.; Zhang, K. *Proc. Natl. Acad. Sci. U.S.A.* **2014**, *111*, 8357.
- (212) Guerin, W.; Helou, M.; Carpentier, J.-F.; Slawinski, M.; Brusson, J.-M.; Guillaume, S. M. *Polym. Chem.* **2013**, *4*, 1095.
- (213) Tyson, T.; Finne-Wistrand, A.; Albertsson, A.-C. *Biomacromolecules* **2009**, *10*, 149.
- (214) Zhang, Z.; Grijpma, D. W.; Feijen, J. *Macromol. Chem. Phys.* **2004**, *205*, 867.
- (215) Widjaja, L. K.; Kong, J. F.; Chattopadhyay, S.; Lipik, V. T.; Liow, S. S.; Abadie, M. J. M.; Venkatraman, S. S. *J. Mech. Behav. Biomed. Mater.* **2012**, *6*, 80.
- (216) Andronova, N.; Albertsson, A. C. *Biomacromolecules* **2006**, *7*, 1489.
- (217) Huang, Y.; Chang, R.; Han, L.; Shan, G.; Bao, Y.; Pan, P. *ACS Sustain. Chem. Eng.* **2016**, *4*, 121.
- (218) Kricheldorf, H. R.; Rost, S. *Macromolecules* **2005**, *38*, 8220.
- (219) Widjaja, L. K.; Kong, J. F.; Chattopadhyay, S.; Lipik, V. T.; Liow, S. S.; Abadie, M. J. M.; Venkatraman, S. S. *J. Biomed. Mater. Res. A* **2011**, *99A*, 38.
- (220) Schneiderman, D. K.; Hill, E. M.; Martello, M. T.; Hillmyer, M. A. *Polym. Chem.* **2015**, *6*, 3641.
- (221) Martello, M. T.; Hillmyer, M. A. *Macromolecules* **2011**, *44*, 8537.
- (222) Dhamaniya, S.; Das, D.; Satapathy, B. K.; Jacob, J. *Polymer* **2012**, *53*, 4662.

2 Post-Polymerisation Modifications of an Alkene-Functional Polycarbonate

2.1 Introduction

The use of aliphatic polycarbonates for biomedical applications has long been the subject of considerable interest, as a consequence of their low toxicity, biocompatibility and biodegradability.¹⁻³ In particular, recent research has focussed on the ability to vary the pendent groups on the polymer backbone, thereby providing fine control over the physical properties of the polymer and potentially allowing the addition of biologically-active compounds to these materials. Polycarbonates can be synthesised by the copolymerisation of CO₂ with epoxides, and also by ring-opening polymerisation (ROP) of cyclic carbonate monomers.³⁻⁸ Given that epoxide/CO₂ copolymerisation requires the use of air-sensitive coordination compounds and can result in the production of five-membered cyclic carbonate byproducts and unwanted ether linkages, the relatively facile synthesis and ROP of cyclic carbonate monomers as a method of producing polycarbonates has led to a greater number of studies, most recently using organic catalysts and mild reaction conditions.⁹⁻¹¹

The synthesis of cyclic carbonate monomers is commonly achieved by the ring-closing of the corresponding 1,3-diols. Functionality can be incorporated into polymers by the inclusion of a functional group in the cyclic monomer, which is then polymerised by ROP.¹² However, the availability of materials produced using this method is limited by the incompatibility of some functional groups with ROP. An alternative route to functionalised polycarbonates is to synthesise relatively simple polymers and modify them post-polymerisation, thus avoiding the problem of monomer incompatibility.^{13,14} A wide range of polycarbonates bearing functionalities including alkene,¹⁵ alkyne,¹⁶ azide,¹⁷ carbamate¹⁸ and benzyl groups,¹⁹ amongst others,^{12,20,21} have all been modified post-polymerisation to incorporate new pendent groups onto the polymer backbone. Sequential post-polymerisation modifications to

introduce a range of functionalities onto a single polymer have also been performed, further demonstrating the power of post-polymerisation modification in the production of functional materials.^{22,23}

Polycarbonates bearing pendent alkene groups are of interest as they provide a facile method of further functionalising the polymer. For example, radical thiol-ene reactions have been applied to a wide range of polymers, using both thermally and photochemically-initiated systems, as described by Hoyle *et al.* and Campos *et al.*, amongst others.²⁴⁻²⁶ Photoinitiated reactions in particular have been shown to proceed with good control in short timeframes, with almost quantitative yields using only mild reaction conditions. The ability to functionalise polycarbonates with thiols is of particular relevance to the biomedical field, as this provides a method for the attachment of proteins and peptides to a polymer support *via* cysteine residues in these molecules.^{27,28} The biological function of these materials can be easily modified by varying the type of protein or peptide attached, or by varying the distribution of these molecules along the polymer backbone.

The ability to functionalise a polycarbonate post-polymerisation also opens up the possibility of generating a thermoresponsive polymer. It has been shown that varying the proportion of hydrophobic and hydrophilic components of a polymer can affect its lower critical solution temperature (LCST), below which the polymer and water phases are completely miscible, and above which they are immiscible.²⁹⁻³¹ However, the addition of hydrophilic groups to a hydrophobic polymer (either through synthesis of block copolymers or grafting to the hydrophobic polymer repeat unit) can drastically change the miscibility of the polymer in water, and introduce an LCST. Work by Lutz *et al.* demonstrated that by varying the number of pendent ethylene glycol repeat units in poly(oligo(ethylene glycol) methyl ether methacrylate)

(POEGMA), fine control could be achieved over the LCST of the polymer, with values ranging from 26 to 90 °C. Further work demonstrated that by copolymerising POEGMAs possessing different numbers of ethylene glycol repeat units, the LCST of the polymers could be further tailored (Figure 2.1).^{32,33}

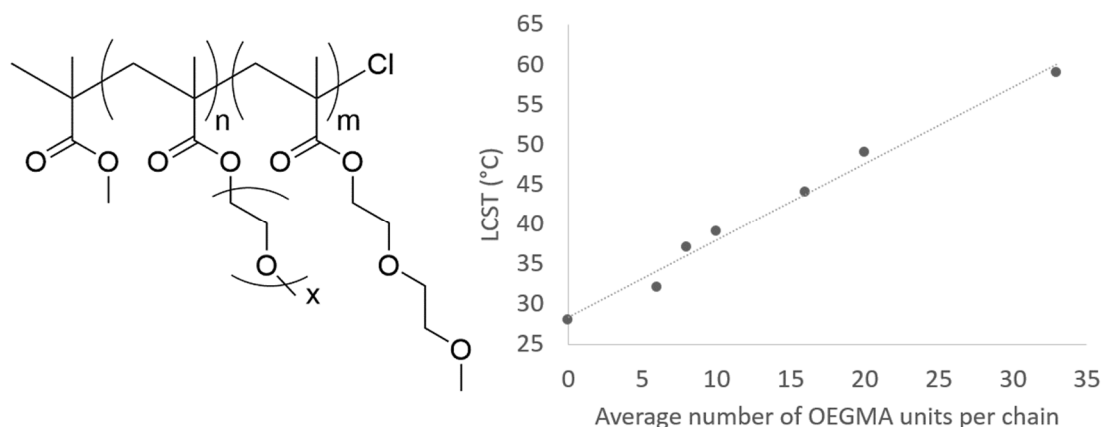
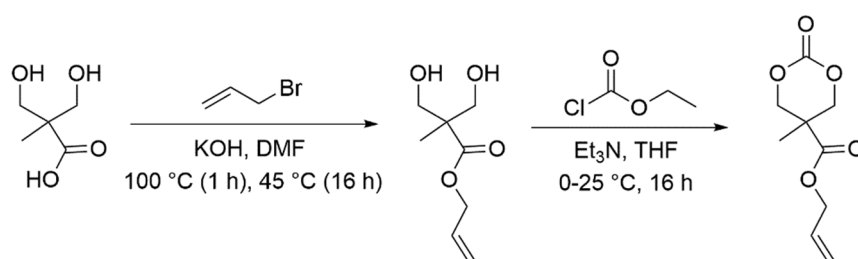


Figure 2.1. Structure of P(MEO₂MA-co-OEGMA₄₇₅) copolymers and LCST values for varying copolymer compositions.³³

Thermoresponsive polycarbonates possessing pendent PEG chains have also been prepared by ROP, both through the ring-opening of PEG-bearing monomers and the post-polymerisation modification of functional polymers.^{23,34-37} Of particular relevance to the research in this chapter, Truong *et al.* have demonstrated the possibility of grafting poly(ethylene glycol) (PEG) to an alkene-functional polycarbonate backbone by radical thiol-ene addition of PEG to the polycarbonate, although the LCST of this material was not investigated.³⁸

Whilst there are several examples of alkene-functional polycarbonates reported in the literature, the synthesis of their cyclic carbonate precursors generally involves several steps and can be time consuming. Of the monomers which have been subjected to post-polymerisation modification, the synthesis of 5-methyl-5-allyloxycarbonyl-1,3-dioxan-2-one (MAC) reported by Hu *et al.* is the most simple described to date.³⁹⁻⁴⁶

The MAC monomer must be prepared in two steps from 2,2'-bis(hydroxymethyl) propionic acid (bis-MPA). The first step involves the time-consuming addition of allyl bromide to bis-MPA, with the resulting alkene-functional diol requiring extensive purification prior to ring closure with ethyl chloroformate (Scheme 2.1). The carbonate is then ring-opened using either metal-based or organic catalysts to yield the alkene-functional polymer.



Scheme 2.1. Synthesis of MAC *via* allylation of bis-MPA, followed by ring-closure of the resulting 1,3-diol.

A more simple route to comparable materials is therefore attractive. In this chapter, the one-step preparation of an allyl-functional carbonate monomer (2-allyloxymethyl-2-ethyltrimethylene carbonate, AOMECE) and its subsequent organocatalysed ring-opening polymerisation are described. The resulting polymer is then modified post-polymerisation with various functionalities *via* photoinitiated radical thiol-ene coupling reactions. Throughout, good control is maintained over the molecular weight and dispersity of the polymer. In addition, the polymer is functionalised with PEG in order to generate a thermoresponsive polycarbonate, and the LCST of the polymer is then modified by changing the molecular weight of the pendent PEG chains.

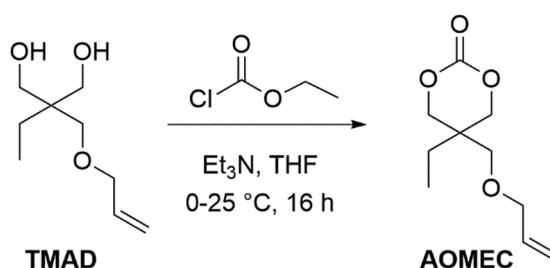
It should be noted that during the course of this research, a paper was published by Olsén *et al.* describing the preparation of AOMECE by ring-closing depolymerisation, and the subsequent ring-opening polymerisation of the monomer using an

organocatalyst.⁴⁷ An example of post-polymerisation modification by photoinitiated radical thiol-ene addition of a thiol to the polymer backbone was also given. However, the work described in this chapter demonstrates the use of a different organocatalyst system for polymerisation, with higher molecular weights and narrower dispersities achieved. In addition, the post-polymerisation of the polymer is expanded to include a range of different thiol functionalities, along with the grafting of a hydrophilic polymer in order to induce thermoresponsive behaviour.

2.2 Results and discussion

2.2.1 Synthesis and polymerisation of 2-allyloxymethyl-2-ethyltrimethylene carbonate (AOMEC)

The allyl-functional carbonate monomer, 2-allyloxymethyl-2-ethyltrimethylene carbonate (AOMEC) was prepared in only one step from a cheap and commercially available precursor, trimethylolpropane allyl ether diol (TMAD). The synthesis of the AOMEC monomer was carried out by the ring closure of TMAD by carbonylation using ethyl chloroformate, as previously reported by He *et al.* (Scheme 2.2).⁴⁸ Purification of the crude liquid monomer was performed by vacuum distillation, with the pure AOMEC recovered in 73% yield (Figure 2.2).



Scheme 2.2. Synthesis of 2-allyloxymethyl-2-ethyltrimethylene carbonate (AOMEC) *via* ring-closure of trimethylolpropane allyl ether diol (TMAD).

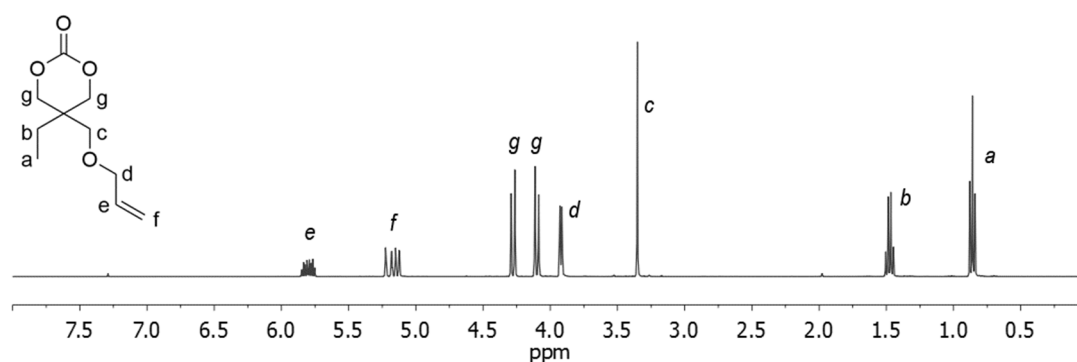
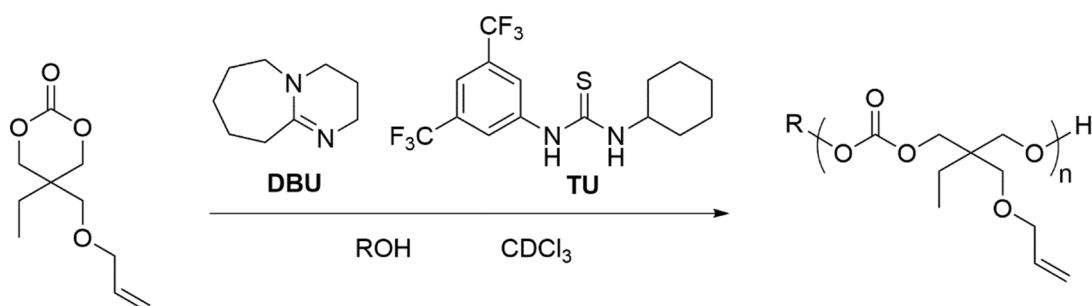


Figure 2.2. ¹H NMR spectrum of 2-allyloxymethyl-2-ethyltrimethylene carbonate (AOMEC) post-distillation (400 MHz, 293 K, CDCl₃).

Initial polymerisation studies were performed in CDCl_3 at $25\text{ }^\circ\text{C}$ with initial monomer to initiator ratio ($[\text{M}]_0:[\text{I}]_0$) = 30, using a bifunctional organocatalytic system of 1,8-diazabicyclo[5.4.0]undec-7-ene (DBU, 1 mol%) and 1-(3,5-bis(trifluoromethyl)-phenyl)-3-cyclohexylthiourea (TU, 5 mol%), with benzyl alcohol used as initiator (Scheme 2.3). This dual catalyst system was selected as it has previously been shown to have good activity for the ROP of cyclic carbonates whilst still maintaining control over the polymerisation.^{49,50} Monomer conversion for all polymerisations was monitored by ^1H NMR spectroscopy, specifically the change in integral of the methylene signals on the pendent ether group of both the carbonate and polymer (at $\delta = 3.27$ and 3.19 ppm respectively (Figure 2.3), with number-average molecular weight (M_n) determined by measuring the integral of the CH_2 resonance of the benzyl alcohol against either the integral of the methylene on the ether group (at $\delta = 3.19$ ppm), or the integral of the alkene CH resonance ($\delta = 5.79$ ppm). At 1.0 M AOMEC concentration, the polymerisation proceeded with a linear increase in monomer conversion up to 66% after 45 h, at which point the polymerisation rate decreased rapidly, with no further discernible increase in molecular weight observed by ^1H NMR spectroscopy.



Scheme 2.3. Synthesis of PAOMEC *via* organocatalyzed ring-opening polymerisation, using a dual DBU/thiourea catalyst system. ROH = mono- or bifunctional alcohol initiator.

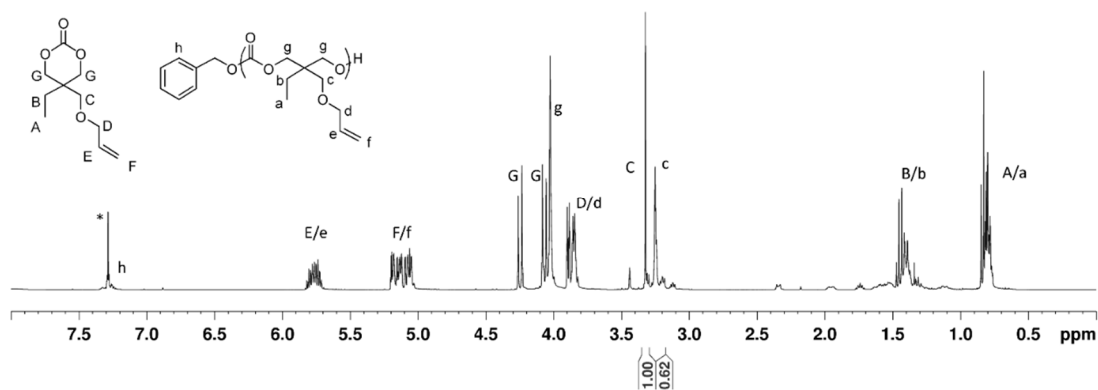


Figure 2.3. ^1H NMR spectrum of AOMECE polymerisation taken at 62% monomer conversion. $[\text{M}]_0:[\text{I}]_0 = 30$, initiated from benzyl alcohol, using a catalyst system of 1 mol% DBU and 5 mol% TU (400 MHz, 293 K, CDCl_3 ; * = CHCl_3).

By comparison, the homopolymerisation of MAC under the same conditions proceeds to *ca.* 80% monomer conversion in just 40 minutes, before rapid retardation of the polymerisation to equilibrium at *ca.* 90% monomer conversion.⁴⁹ The reduced polymerisation rate of AOMECE with respect to MAC is likely the result of both steric and electronic factors - the increased steric bulk of the pendent ethyl group may have some inhibiting effect on nucleophilic attack by the initiating alcohol species or propagating polymer chains at the α -carbon, whilst the pendent ether group of AOMECE should be less electron-withdrawing than the ester group of MAC, resulting in the α -carbon being less susceptible to nucleophilic attack by the propagating alcohol species.

In order to increase the polymerisation rate, the concentration of the reaction mixture was increased to 2 M and the catalyst loading increased to 5 mol% DBU and 5 mol% TU. Under these conditions, the $[\text{M}]_0:[\text{I}]_0 = 30$ polymerisation achieved 82% conversion in only 150 minutes, at which point the polymerisation rate was rapidly retarded. The polymerisation was quenched by addition of acidic Amberlyst 15 ion exchange resin, with purification of the polymer performed by repeated precipitations

into cold *n*-hexane. ^1H NMR spectroscopy and size exclusion chromatography (SEC) analysis demonstrated that the polymerisation proceeds with good control, with the observed molecular weight closely matching the theoretical value, and the polymer possessing narrow dispersity (Theoretical $M_n = 5,000 \text{ g mol}^{-1}$, observed $M_n = 5,000 \text{ g mol}^{-1}$, $D_M = 1.08$) (Figure 2.4). The polymerisation study was extended across a range of degrees of polymerisation (DPs), with a linear correlation observed for both M_n against $[\text{M}]_0:[\text{I}]_0$, and M_n against monomer conversion, both characteristic of a living polymerisation (Figure 2.5 and 2.6). Across the range of molecular weights and conversions, excellent control was maintained over the polymerisation of the monomer, with dispersities ranging from 1.04 for a DP 230 polymer to 1.17 for DP 10 (Figure 2.7).

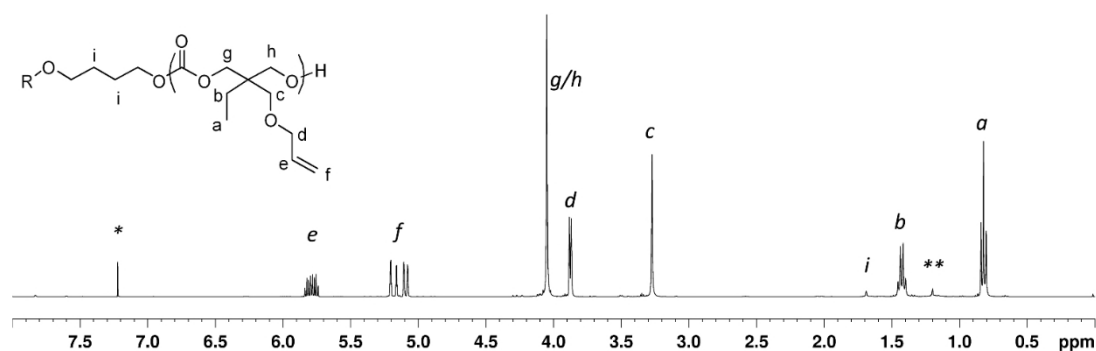


Figure 2.4. ^1H NMR spectrum of DP 42 PAOMEC initiated from 1,4-butanediol, using a catalyst system of 5 mol% DBU and 5 mol% TU (400 MHz, 293 K, CDCl_3 ; * = CHCl_3 , ** = residual hexane from precipitation).

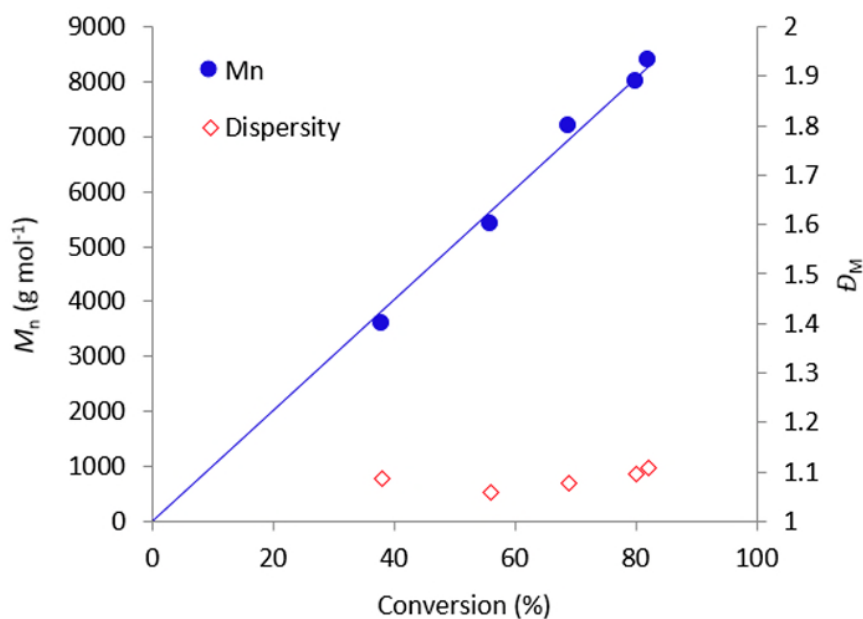


Figure 2.5. Plot of number-average molecular weight (M_n) and dispersity (D_M) against % monomer conversion for the homopolymerisation of AOMECE. Conditions: [AOMECE] = 2.0 M in $CDCl_3$, $[M]_0:[I]_0 = 50$ using 1,4-butanediol as initiator, 5 mol% DBU and 5 mol% TU as catalysts.

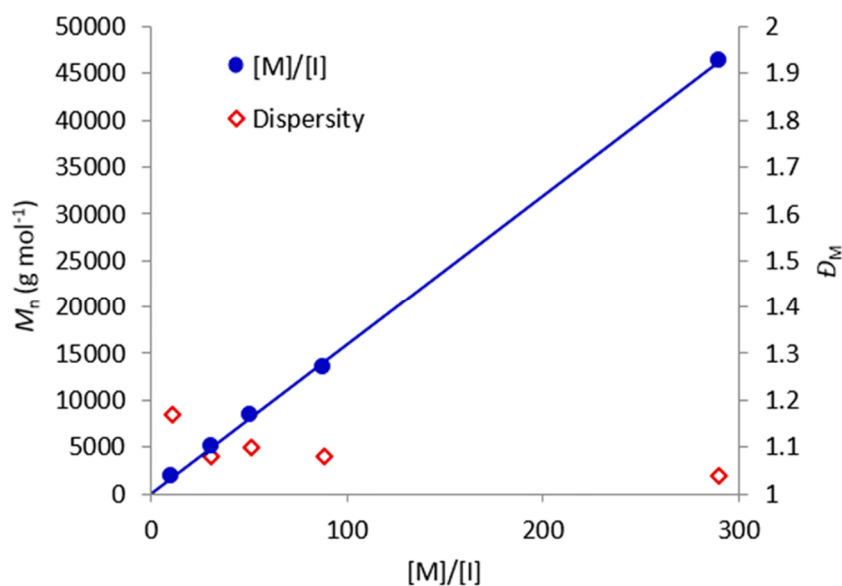


Figure 2.6. Plot of number-average molecular weight (M_n) and dispersity (D_M) against initial monomer-to-initiator concentration ratio, $[M]_0:[I]_0$ for the homopolymerisation of AOMECE. Conditions: [AOMECE] = 2.0 M in $CDCl_3$, 1,4-butanediol used as initiator, 5 mol% DBU and 5 mol% TU used as catalysts.

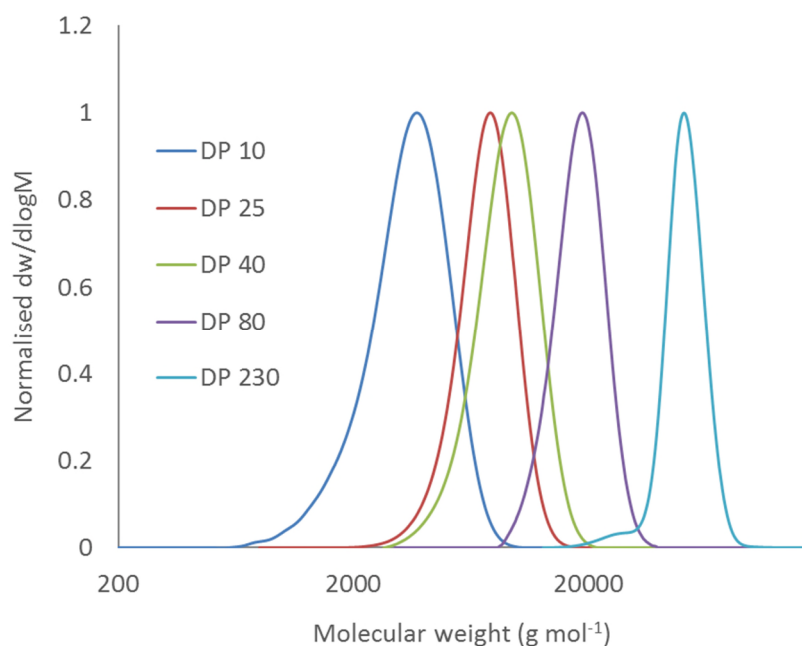


Figure 2.7. SEC chromatograms of polymers initiated from pentaerythritol dibenzyl ether (PDE), with $[M]_0:[I]_0$ ranging from 12 to 290 to give polymers with DPs of 11 to 232, and D_M values ranging from 1.17 to 1.04. Samples measured against polystyrene standards using CHCl_3 as eluent.

Various mono- and bifunctional alcohols were demonstrated to be effective initiators for the polymerisation of AOMECE, including 1,4-butanediol, 1,4-benzenedimethanol and pentaerythritol dibenzyl ether (PDE) (Figure 2.8). In each case, the polymerisation of AOMECE proceeds with excellent control, producing polymers with narrow dispersities and predictable molecular weights as determined with ^1H NMR spectroscopy, by integration of resonances from the initiating species against the methylene resonance on the pendent ether of the polymer (Table 2.1). Polymerisation was also initiated from a bifunctional poly(ethylene glycol) (PEG) macroinitiator ($M_n = 2,000 \text{ g mol}^{-1}$, $D_M = 1.04$). The reaction proceeds with good control, resulting in a $\text{PAOMECE}_{13}\text{-}b\text{-PEG}_{62}\text{-}b\text{-PAOMECE}_{13}$ triblock copolymer with narrow dispersity ($M_n = 9,200 \text{ g mol}^{-1}$, $D_M = 1.07$), further demonstrating the initiator versatility of the monomer (Figure 2.9 and 2.10).

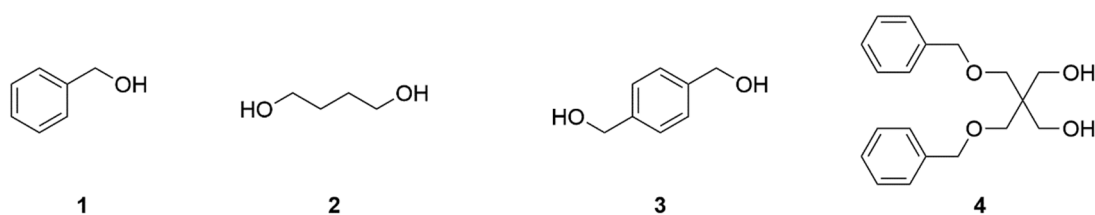


Figure 2.8. Mono- and bifunctional alcohol initiators used for the polymerisation of AOMECE. 1 = Benzyl alcohol; 2 = 1,4-butanediol; 3 = 1,4-benzenedimethanol; 4 = Pentaerythritol dibenzyl ether (PDE).

Table 2.1. Polymers of AOMECE initiated from different mono- and bifunctional alcohol initiators^a

Initiator	$[M]_0:[I]_0^b$	Conversion (%) ^b	Time (h)	Theor. M_n (g mol^{-1}) ^c	DP^b	M_n (g mol^{-1}) ^b	\bar{D}_M^d
1	25	80	3	4,000	21	4,200	1.10
2	20	84	3	3,400	17	3,400	1.16
3	62.5	82	6	10,200	49	9,800	1.09
4	12	86	1.5	2,000	11	2,200	1.17
4	25	87	3	4,400	22	4,400	1.09
4	50	82	6	8,200	40	8,000	1.14
4	100	77	10	15,400	77	15,400	1.13
4	290	80	24	46,400	232	46,400	1.04

^a Polymerisations performed in CDCl_3 at 25 °C, $[\text{AOMECE}] = 2.0 \text{ M}$, using 5 mol% DBU and 5 mol% TU. ^b $[M]_0:[I]_0$, monomer conversion, degree of polymerisation and number average molecular weight determined by $^1\text{H NMR}$ spectroscopy. ^c Theoretical M_n calculated from $[M]_0:[I]_0 \times$ monomer conversion \times molecular weight of AOMECE ($200.23 \text{ g mol}^{-1}$). ^d Determined by SEC analysis against polystyrene standards, using CHCl_3 as eluent.

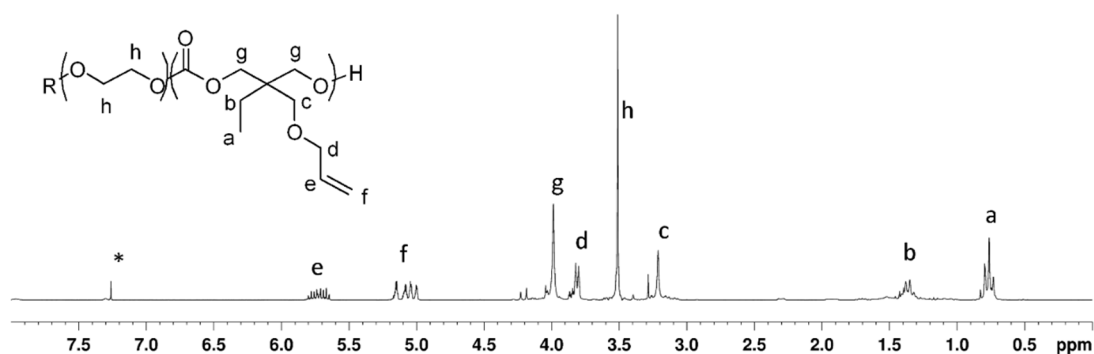


Figure 2.9. ^1H NMR spectrum of PAOMECE₁₃-PEG₆₂-PAOMECE₁₃ triblock copolymer synthesised using a catalyst system of 5 mol% DBU and 5 mol% TU (400 MHz, 293 K, CDCl_3 ; * = CHCl_3).

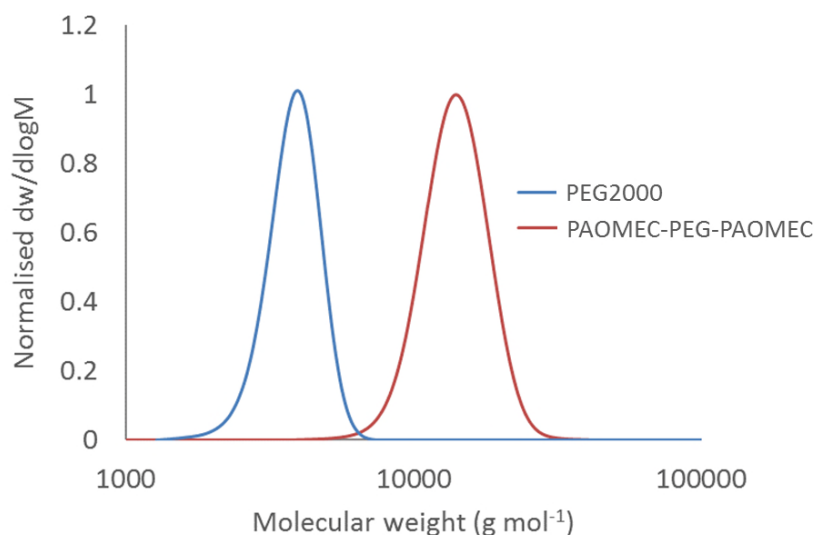


Figure 2.10. Size exclusion chromatograms of PEG prior to chain growth ($M_n = 2,000 \text{ g mol}^{-1}$, $\mathcal{D}_M = 1.04$) and PAOMECE-PEG-PAOMECE triblock ($M_n = 13,300 \text{ g mol}^{-1}$, $\mathcal{D}_M = 1.07$). Samples measured against polystyrene standards using CHCl_3 as eluent.

Triblock copolymers were also synthesised using PAOMECE as a macroinitiator. A DP 80 sample of PAOMECE initiated from PDE was isolated, purified and dried. The DBU-catalysed ring-opening polymerisation of *L*-lactide (LLA) using this PAOMECE macroinitiator was then performed, yielding a PLLA₉₃-*b*-PAOMECE₈₀-*b*-PLLA₉₃ triblock copolymer with $M_n = 29,400 \text{ g mol}^{-1}$ (Figure 2.11). Analysis by SEC

demonstrated that the polymer possessed a narrow dispersity ($D_M = 1.12$), which indicates that the polymerisation of LLA proceeded with good control (Figure 2.12).

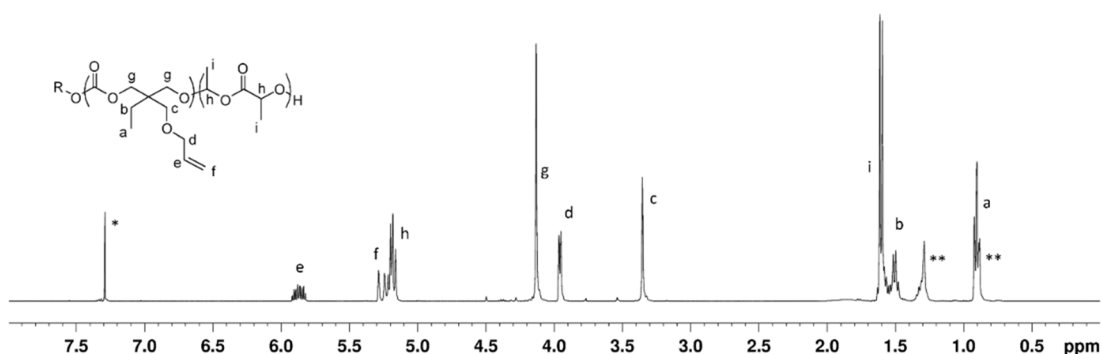


Figure 2.11. ^1H NMR spectrum of $\text{PLA}_{93}\text{-PAOMECE}_{80}\text{-PLA}_{93}$ triblock copolymer synthesised using a catalyst system of 1 mol% DBU (400 MHz, 293 K, CDCl_3 ; * = CHCl_3 ; ** = residual hexane from precipitation).

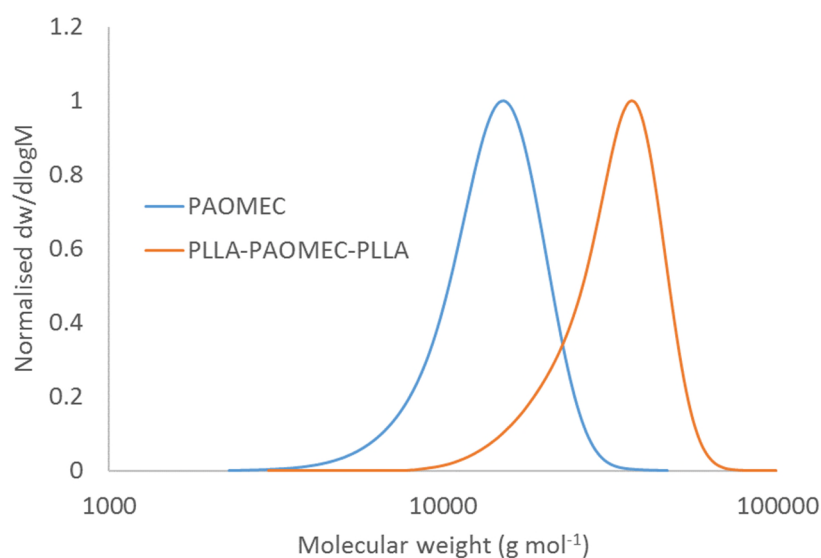


Figure 2.12. Size exclusion chromatograms of PAOMECE prior to chain extension ($M_n = 15,800 \text{ g mol}^{-1}$, $D_M = 1.13$) and PLLA-PAOMECE-PLLA triblock copolymer ($M_n = 30,100 \text{ g mol}^{-1}$, $D_M = 1.12$). Samples measured against polystyrene standards using CHCl_3 as eluent.

The activity of organocatalysts which can be applied to the homopolymerisation of MAC is limited by the potential for the pendent ester functionality to undergo transesterification, thus generating branched polymers.¹² However, the absence of

ester functionality in AOMEC enables the application of less selective catalyst systems to the polymerisation of this monomer. To this end, triazabicyclodecene (TBD) was also applied as a bifunctional catalyst for the polymerisation of AOMEC across a range of monomer to initiator ratios. Applying a catalyst concentration of 1 mol%, the polymerisations were considerably faster than those catalysed by the dual DBU/TU system, with polymerisations up to DP 100 reaching 80% monomer conversion in under 1 h. Polymerisations catalysed by the bifunctional TBD catalyst remain well-controlled, with dispersities not exceeding 1.20 (Figure 2.13).

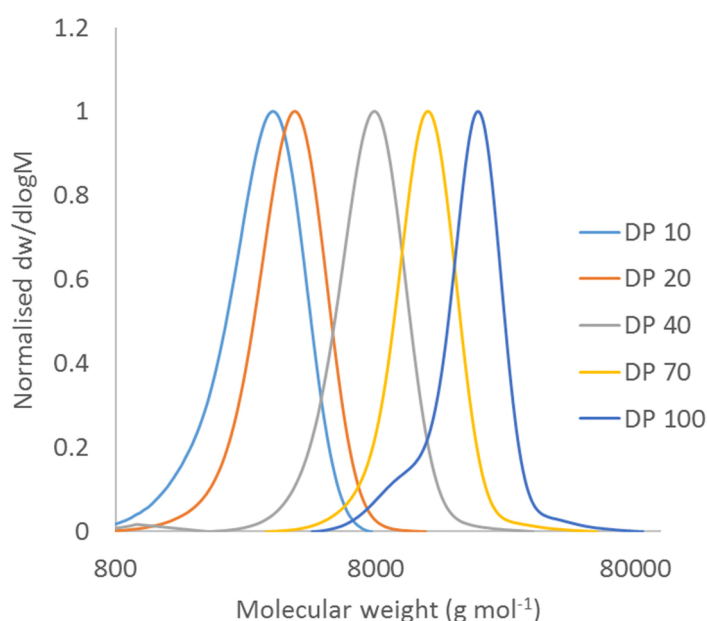
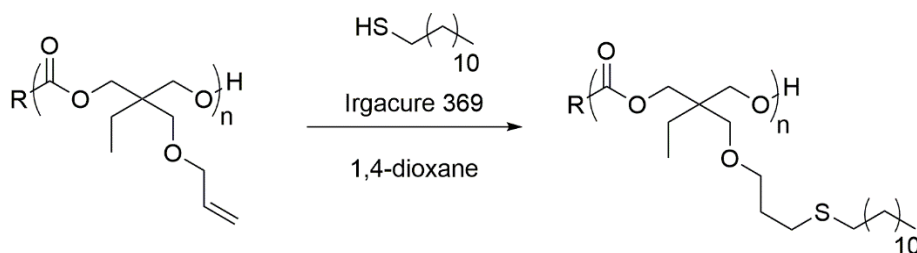


Figure 2.13. Size exclusion chromatograms of PAOMEC initiated from 1,4-benzenedimethanol using TBD as bifunctional catalyst, with $[M]_0:[I]_0$ ranging from 10 to 125 to give polymers with DPs of 9 to 98, and \bar{D}_M values ranging from 1.20 to 1.11. Samples measured against polystyrene standards using CHCl_3 as eluent.

2.2.2 Post-polymerisation modification of PAOMEC

PAOMEC was functionalised with a selection of thiols containing a range of functional groups, with varying degrees of success. The photoinitiated radical addition

of thiols to the pendent alkene groups of the polymer was first attempted using 2 equivalents of 1-dodecanethiol to alkene groups on the polymer backbone ([PAOMEC] = 0.01 M), with 1,4-dioxane as solvent and 2-benzyl-2-dimethylamino-1-(4-morpholinophenyl)-butanone-1 (Irgacure 369) as a radical initiator (Scheme 2.4).



Scheme 2.4. Post-polymerisation functionalisation of PAOMEC with 1-dodecanethiol.

After exposure to UV light for 2 hours, the reaction had reached completion (> 99.9% reduction in intensity of polymer alkene resonances observed by ^1H NMR spectroscopy at $\delta = 5.84$ and 5.18 ppm (Figure 2.14)), with the molecular weight of the polymer observed to increase by SEC with no broadening of dispersity observed ($D_M = 1.10$, Figure 2.15). Thioglycerol was also added on to the polymer backbone using the same conditions, again without degradation of the polymer and retention of narrow dispersity ($D_M = 1.09$), and with complete functionalisation observed by ^1H NMR spectroscopy.

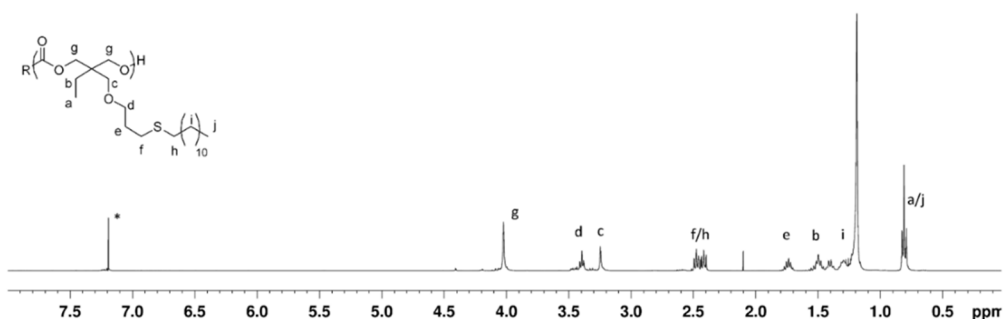


Figure 2.14. ^1H NMR spectrum of DP 24 PAOMEC functionalised with 1-dodecanethiol. Note the absence of alkene resonances at *ca.* $\delta = 5.8$ and 5.15 ppm, which indicates that complete functionalisation has taken place. (400 MHz, 293 K, CDCl_3 ; * = CHCl_3).

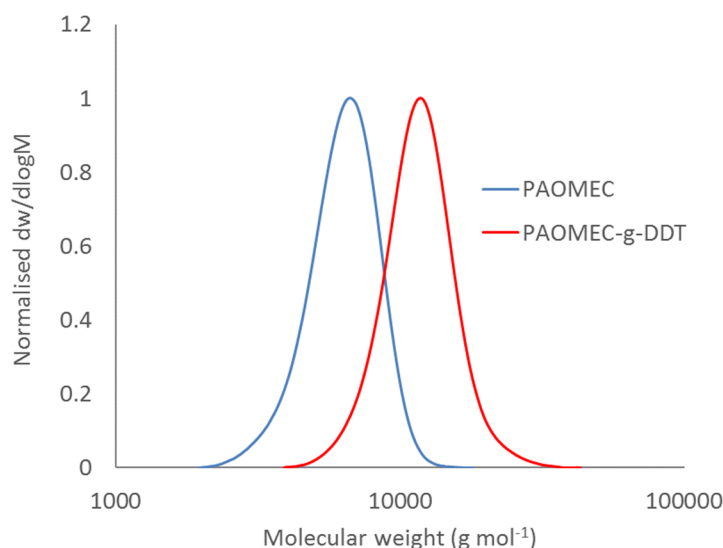


Figure 2.15. Size exclusion chromatograms of DP 24 PAOMECE initiated from pentaerythritol dibenzyl ether ($M_n = 5,200 \text{ g mol}^{-1}$, $\mathcal{D}_M = 1.11$) and DP 24 PAOMECE following post-polymerisation functionalisation with 1-dodecanethiol ($M_n = 10,600 \text{ g mol}^{-1}$, $\mathcal{D}_M = 1.13$). Samples measured against polystyrene standards using CHCl_3 as eluent.

MALDI-ToF mass spectrometry was performed on both a DP 20 sample of PAOMECE, and a sample of the same polymer post-functionalisation with 1-dodecanethiol. The distribution plot for the unfunctionalised polymer shows a spacing of 200 m/z between signals, equivalent to one AOMECE unit (Figure 2.16, top). The peak at m/z 2916 represents a DP 14 polymer chain initiated from 1,4-butanediol and carrying a charged sodium ion. The distribution for the functionalised PAOMECE has a spacing of 402 m/z between signals, with the peak appearing at m/z 5751 representative of the equivalent 1-dodecanethiol-functionalised DP 14 polymer chain (Figure 2.16, bottom). The absence of significant signals between distributions for the functionalised polymer further suggests that near-quantitative functionalisation takes place.

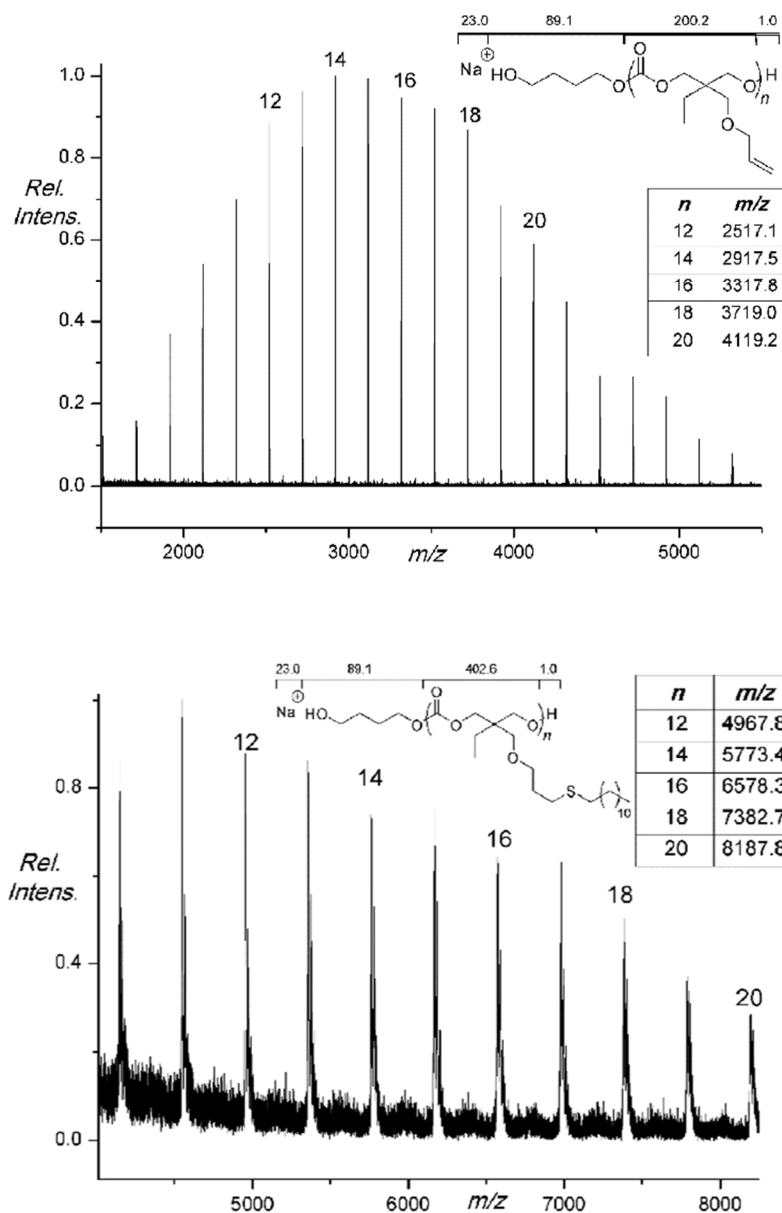


Figure 2.16. MALDI-ToF MS of PAOMECS (DP 20), measured in reflectron mode (top), and MALDI-ToF MS of PAOMECS post-functionalisation with 1-dodecanethiol, measured in linear mode (bottom).

The thiol-ene reaction was also undertaken with benzyl mercaptan (BnSH) and 3-mercaptopropionic acid (3-MPA) in order to broaden the range of pendent functionalities on the polymer to include those not compatible with ROP. However, a broadening of dispersity was observed for both of these reactions (D_M BnSH = 1.54, 3-MPA = 1.23) under the conditions described above, possibly as a result of the electron-withdrawing groups on these thiols reducing the reactivity of the radical, thus

making the radical addition less efficient and allowing cross-linking between the allyl groups on the polymer backbone to become competitive. To overcome the problem of unwanted crosslinking, the equivalents of thiol to pendent alkene groups on the polymer backbone and the exposure time to UV were varied. While varying the exposure time had no discernible effect on the degree of crosslinking taking place during the reaction (Figure 2.17), it did reveal that the radical addition was complete in as little as 10 minutes. Koo and co-workers have previously reported that increasing the concentration of thiol relative to alkene groups can reduce the number of side-reactions which occur in radical thiol-ene additions,⁵¹ and indeed increasing the thiol concentration was found to greatly improve the efficiency of PAOMEC functionalisation (Figure 2.18 and 2.19). Using 10 equivalents of thiol and 30 minutes of exposure time, BnSH and 3-MPA-functionalised polymers with narrow dispersities were successfully produced (Table 2.2).

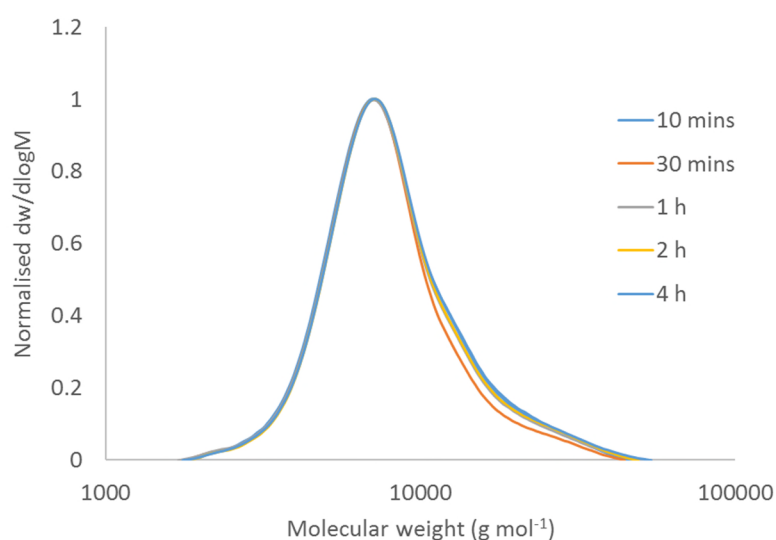


Figure 2.17. Size exclusion chromatograms showing effect on dispersity of varying exposure time to UV light during functionalisation of PAOMEC with 2 eq. of 3-mercaptopropionic acid per alkene group. No clear effect on dispersity can be observed, with $\bar{D}_M = ca. 1.20$ for all samples. Samples measured against poly(methyl methacrylate) standards using DMF as eluent.

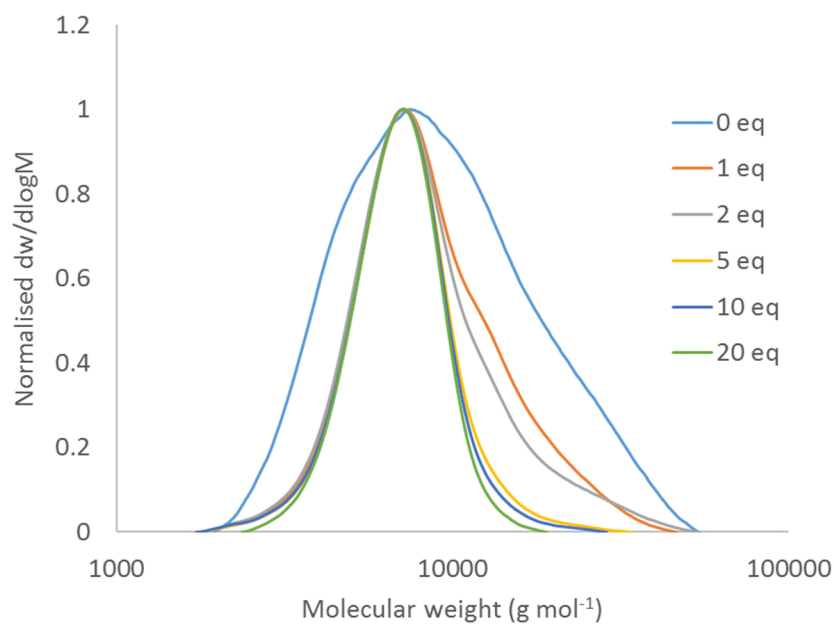


Figure 2.18. Size exclusion chromatograms showing effect on dispersity of varying thiol equivalents for functionalisation of PAOMECC with 3-mercaptopropionic acid. Samples measured against poly(methyl methacrylate) standards using DMF as eluent.

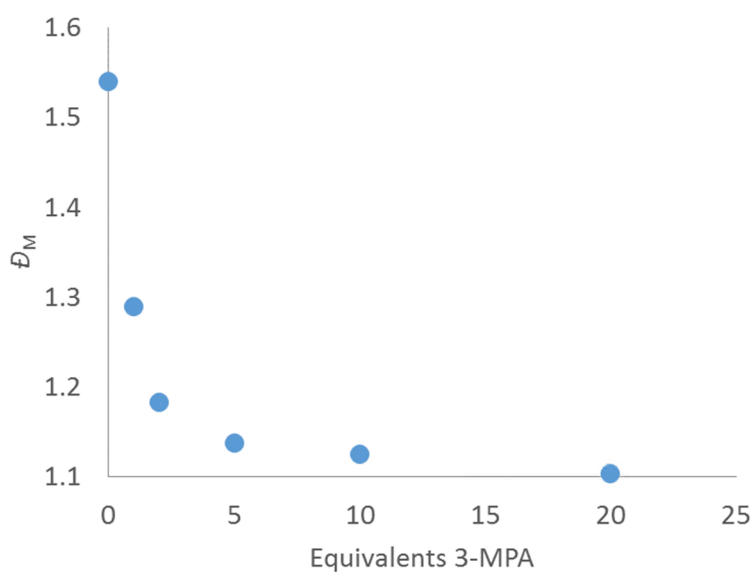


Figure 2.19. Graphical representation of dispersity (D_M) from SEC to show effect of varying thiol equivalents for functionalisation of PAOMECC with 3-mercaptopropionic acid.

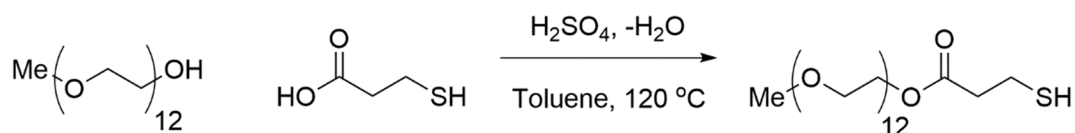
Table 2.2. Photoinitiated radical thiol-ene post-polymerisation modification of PAOMECE^a

Polymer	Thiol	Thiol Equivalents	M_n (g mol ⁻¹) ^b	\bar{D}_M
PAOMECE ₁₉	-	-	3,800	1.09 ^c
PAOMECE ₂₄	-	-	4,800	1.11 ^c / 1.14 ^d
PAOMECE ₇₉	-	-	15,800	1.13 ^c / 1.12 ^d
PAOMECE ₂₄	1-Dodecanethiol	2	9,000	1.13 ^c
PAOMECE ₇₉	1-Dodecanethiol	2	30,000	1.12 ^c
PAOMECE ₁₉	3-Mercaptopropionic acid	10	6,000	1.12 ^d
PAOMECE ₇₉	3-Mercaptopropionic acid	10	24,800	1.10 ^d
PAOMECE ₂₄	1-Thioglycerol	2	7,600	1.12 ^d
PAOMECE ₇₉	1-Thioglycerol	10	21,900	1.10 ^d
PAOMECE ₁₉	Benzyl mercaptan	10	5,800	1.18 ^d
PAOMECE ₇₉	Benzyl mercaptan	10	25,600	1.16 ^d

^a [PAOMECE] = 0.01 M in 1,4-dioxane, 20 mol% Irgacure 369, exposure to UV light ($\lambda = 365$ nm) for 30 minutes. ^b Determined by ¹H NMR spectroscopy. ^c Determined by SEC against polystyrene standards using CHCl₃ as eluent. ^d Determined by SEC against poly(methyl methacrylate) standards using DMF as eluent.

2.2.3 Synthesis of a PAOMECC-based thermoresponsive polymer

In an initial experiment, poly(ethylene glycol) monomethyl ether (MeO-PEG-OH) ($M_n = 550 \text{ g mol}^{-1}$) was selected as a hydrophilic polymer to graft onto PAOMECC. A monofunctional polymer was selected in order to avoid the PEG acting as a crosslinker between PAOMECC chains. This MeO-PEG₅₅₀-OH was then esterified with 3-mercaptopropionic acid in order to generate a thiol-terminated PEG (MeO-PEG₅₅₀-SH) (Scheme 2.5, Figure 2.20). The crude product was dissolved in CH₂Cl₂ and washed with NaHCO₃. After drying over MgSO₄ and removal of the solvent under reduced pressure, the product was recovered as a pale yellow oil in 73% yield. SEC analysis of the MeO-PEG₅₅₀-SH revealed a secondary peak at roughly twice the molecular weight of the main peak (Figure 2.21) – this is likely indicative of the presence of a small amount of disulfide-linked PEG chains in the polymer. Given that the functionalisation of the PAOMECC was to be carried out with a large excess of the thiol, it was deemed unnecessary to remove this minor disulphide impurity from the PEG-thiol.



Scheme 2.5. Synthesis of monofunctional PEG-thiol.

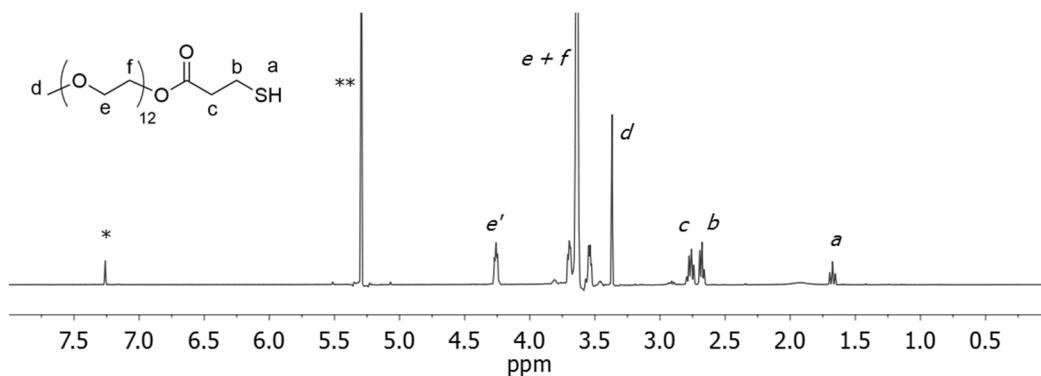


Figure 2.20. ^1H NMR spectrum of MeO-PEG₅₅₀-SH (400 MHz, 293 K, CDCl_3 ; * = CHCl_3 ; ** = residual CH_2Cl_2 from washing).

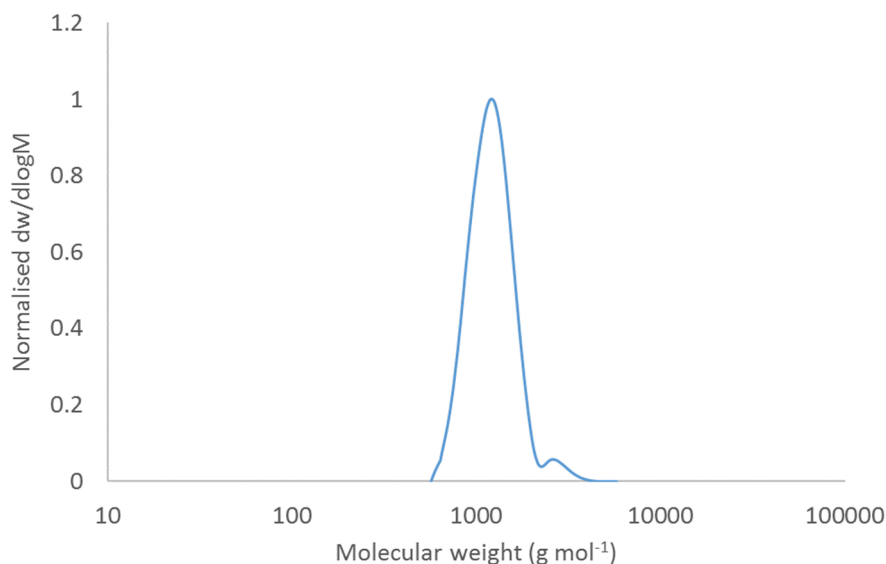
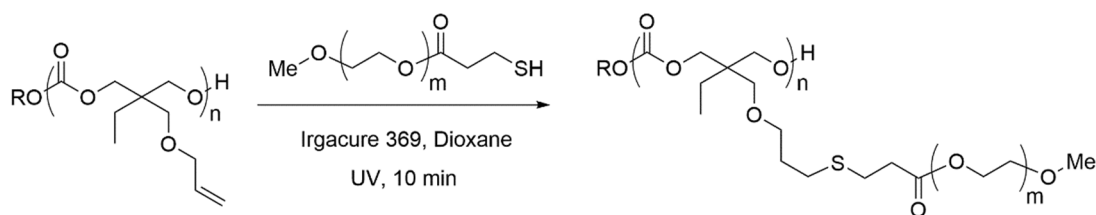


Figure 2.21. SEC trace of MeO-PEG₅₅₀-SH. $M_n = 1,150 \text{ g mol}^{-1}$, $D_M = 1.08$). Sample measured against polystyrene standards using CHCl_3 as eluent.

Having successfully synthesised the monofunctional PEG-thiol precursor, the material was grafted onto DP 82 PAOMECS by means of photoinitiated radical thiol-ene addition. The same conditions were employed for the grafting as were used for the previous modification of the polymer with small molecules ($[\text{PAOMECS}] = 0.01 \text{ M}$), 1,4-dioxane as solvent and 2-benzyl-2-dimethylamino-1-(4-morpholinophenyl)-butanone-1 (Irgacure 369) as a radical initiator), and using 5 equivalents of PEG-thiol to alkene groups on the PAOMECS backbone (Scheme 2.6).



Scheme 2.6. Grafting of MeO-PEG-SH onto PAOMEC.

After 10 minutes of exposure to UV light, the reaction mixture was dialysed against water (molecular weight cut-off = 3,500 g mol⁻¹) in order to remove unreacted MeO-PEG₅₅₀-SH and disulphide-linked PEG impurities from the product. Analysis of the recovered purified product by ¹H NMR spectroscopy and SEC revealed that the reaction was successful, with > 99.9% reduction in intensity of polymer alkene resonances at $\delta = 5.84$ and 5.18 ppm, and the appearance of resonances corresponding to MeO-PEG-SH, in particular the large resonance at $\delta = 3.58$ which corresponds to the methylene resonances of the PEG repeat units (Figure 2.22). Comparison of the integrals for the PEG resonances and the methyl resonance of the PAOMEC backbone indicates an average of 11.5 ethylene glycol repeat units grafted onto each alkene functional group, corresponding closely to the average number of ethylene glycol repeat units present in the MeO-PEG₅₅₀-SH precursor (11.8). The slight discrepancy is suggested to be the result of a small amount of crosslinking occurring during functionalisation, as indicated by the slight increase in polymer dispersity (PAOMEC $D_M = 1.13$, PAOMEC-*g*-PEG₅₅₀-OMe $D_M = 1.17$, Figure 2.23).

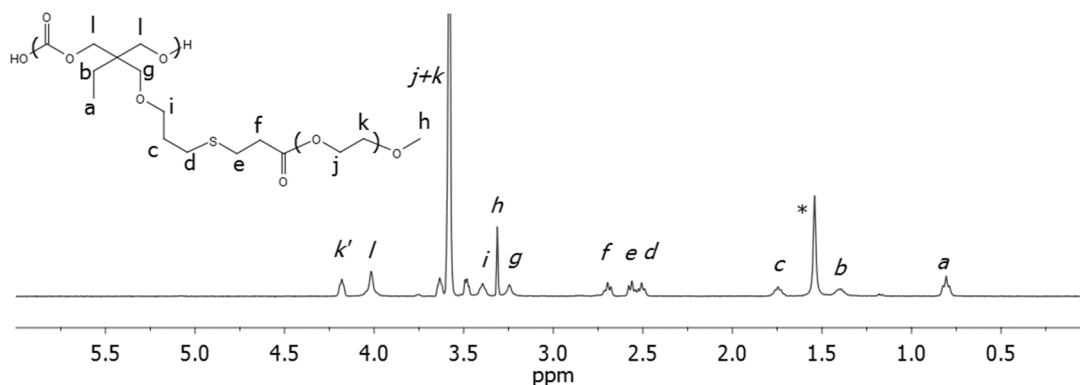


Figure 2.22. ^1H NMR spectrum of PAOMECS-g-PEG₅₅₀-OMe (400 MHz, 293 K, CDCl_3 ; * = H_2O).

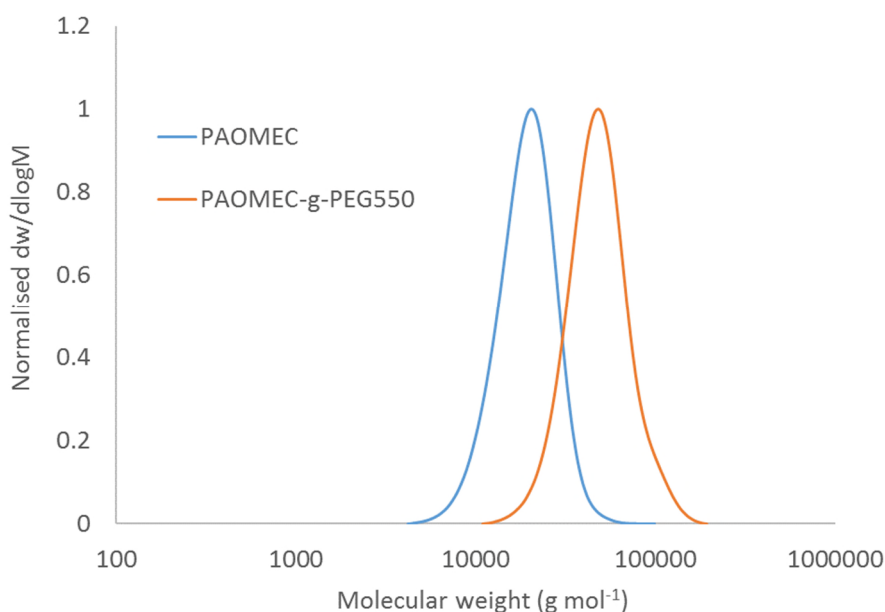


Figure 2.23. SEC traces of PAOMECS ($M_n = 17,700 \text{ g mol}^{-1}$, $D_M = 1.13$) and PAOMECS-g-PEG₅₅₀-OMe ($M_n = 67,800 \text{ g mol}^{-1}$, $D_M = 1.17$). Samples measured against polystyrene standards using CHCl_3 as eluent.

A solution of PAOMECS-g-PEG₅₅₀-OMe in water (3mg/mL) was prepared for measurement of the polymer LCST by turbidimetry, using UV-Vis spectrometry to determine the cloud point of the sample (measured at 50% transmittance), scanning across a temperature range of 7 to 80 °C. Using a detection wavelength of 550 nm, the cloud point of the solution was determined to be 76 °C upon both heating and cooling, indicating a very low degree of hysteresis. This low level of hysteresis, combined with

the sharp change in transmittance, indicates that the polymer undergoes rapid dehydration and rehydration above and below the LCST respectively (Figure 2.24).

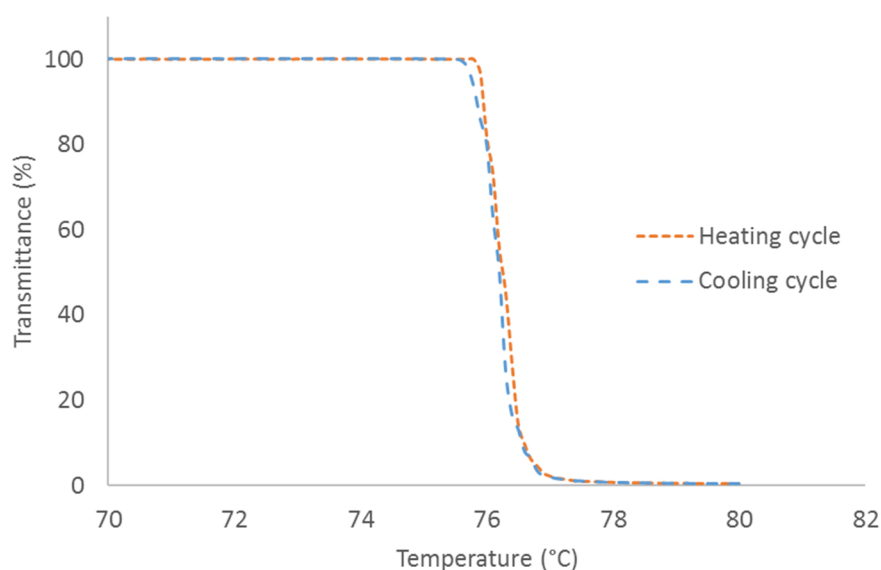


Figure 2.24. Plots of transmittance as a function of temperature for PAOMECE-g-PEG₅₅₀-OMe over heating and cooling cycles, indicating low polymer hysteresis.

The effect of changing the length of the grafted PEG branches on the LCST of the polymer was investigated. It was thought that shorter PEG branches would reduce the LCST due to the reduced hydrophilic content of the polymer, thus lowering the degree of interaction between the polymer and the solvent, and consequently reducing the temperature at which the material would become immiscible in water. As such, two additional MeO-PEG precursors ($M_n = 210$ and 350 g mol^{-1}) were esterified with 3-MPA, and the resulting PEG-thiols subsequently grafted onto PAOMECE using the same reaction conditions employed in the grafting of MeO-PEG₅₅₀-SH. After recovery and dialysis of the crude products, LCST measurements were taken which revealed a marked effect on the LCST of the polymers. For PAOMECE-g-PEG₃₅₀-OMe, the LCST was reduced to $46 \text{ }^\circ\text{C}$, while for PAOMECE-g-PEG₂₁₀-OMe the LCST was reduced still further to $13 \text{ }^\circ\text{C}$ (Figure 2.25).

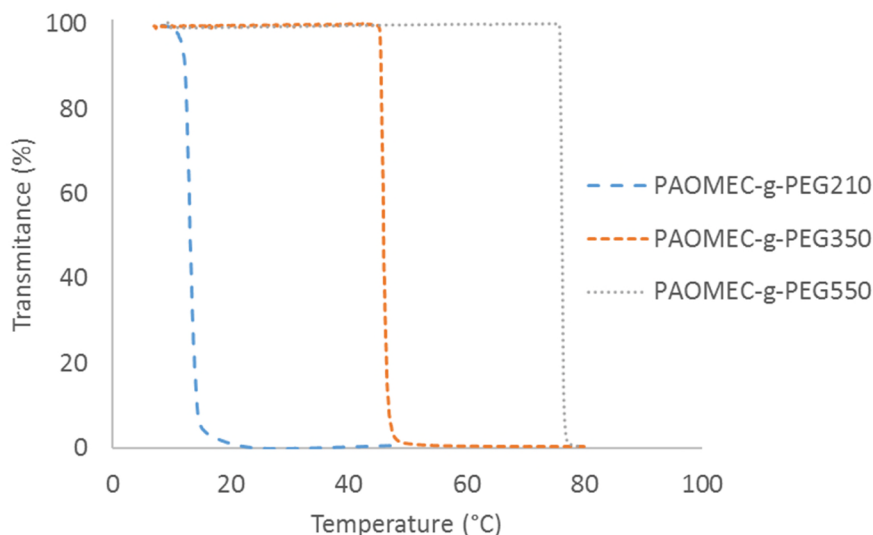


Figure 2.25. Plots of transmittance as a function of temperature for PAOMECE-g-PEG-OMe with various PEG molecular weights measured during heating cycles.

Having successfully demonstrated that the LCST of the polymer could be varied by changing the length of the grafted PEG chains, an attempt was made to tune the LCST of the polymer by simultaneously grafting two different PEG-thiol chain lengths to the same PAOMECE backbone. To this end, experiments were performed using the same grafting conditions previously employed, but with 2.5 equivalents of MeO-PEG₅₅₀-SH, and 2.5 equivalents of either MeO-PEG₂₁₀-SH or MeO-PEG₃₅₀-SH. For the MeO-PEG_{210/550}-SH grafted polymer, ¹H NMR spectroscopic analysis confirmed that the average PEG M_n was 372 g mol⁻¹ (expected M_n for a true 50/50 graft ratio = 380 g mol⁻¹) (Figure 2.26), while for the MeO-PEG_{350/550}-SH grafted polymer the average PEG M_n was found to be 436 g mol⁻¹ (expected M_n = 450 g mol⁻¹). The LCST of these polymers was found to be 60 and 65 °C respectively, closely matching the trend displayed by PAOMECE grafted with only single PEG chain lengths (Figure 2.27 and 2.28).

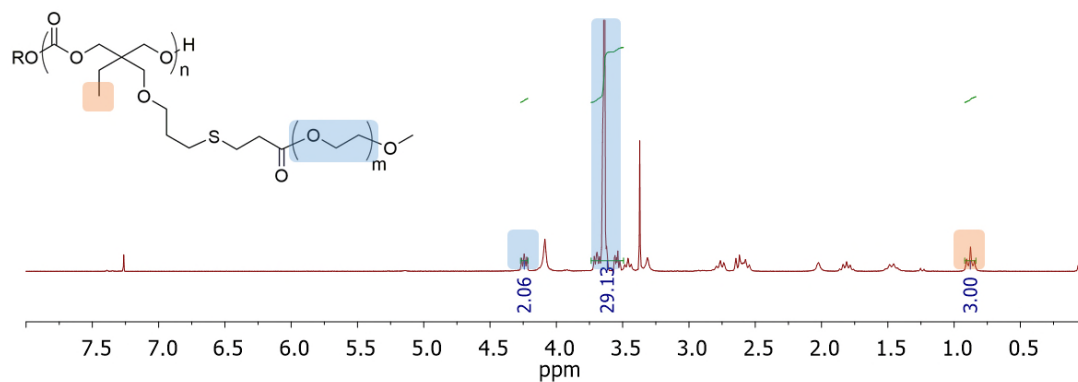


Figure 2.26. ^1H NMR spectrum of PAOMEC-*g*-PEG_{210/550}-SH showing relative integrals for AOMEC region and PEG repeat units, highlighted in orange and blue respectively. (400 MHz, 293 K, CDCl_3).

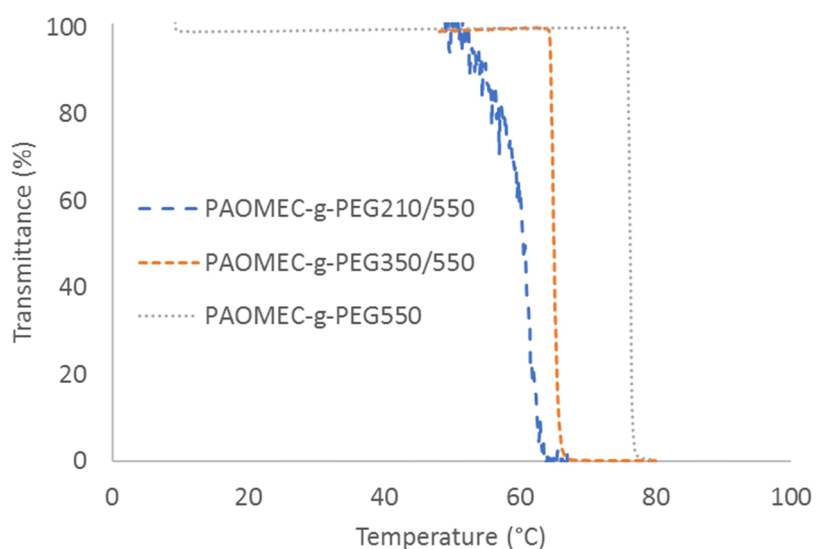


Figure 2.27. Plots of transmittance as a function of temperature for PAOMEC-*g*-PEG-OMe with varying average PEG molecular weights prepared by simultaneous grafting of two separate PEG-thiol precursors to PAOMEC, measured during heating cycles. Note that the noise observed for PAOMEC-*g*-PEG_{210/550} is the result of a fault developed by the UV-visible spectrometer used.

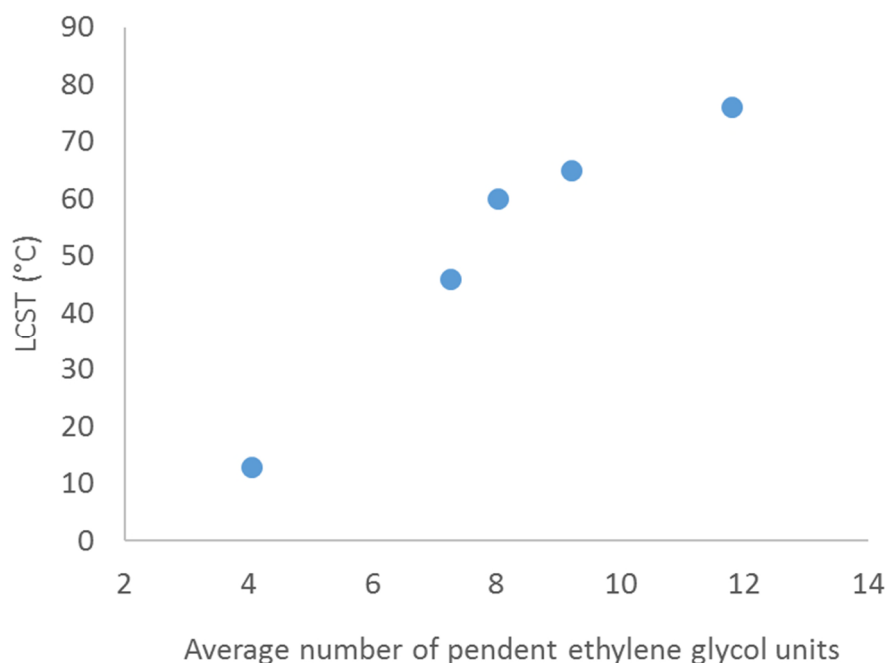


Figure 2.28. Plot of polymer LCST against average number of PEG repeat units for PAOMECE-g-PEG-OMe.

The phase transition temperature ranges (ΔT) observed for these polymers are slightly broader than those for PAOMECE grafted with only uniform chain-length PEG, particularly for PAOMECE-g-PEG_{210/550}-OMe which shows a ΔT of 11.2 °C (in comparison to 2 °C for PAOMECE-g-PEG₅₅₀-OMe and 2.7 °C for PAOMECE-g-PEG_{350/550}-OMe). This range in phase transition temperature has previously been described for POEGMA copolymers prepared by ATRP, and has been ascribed to slight differences in the composition of different chains (given that the distribution of OEGMA with different pendent chain lengths would not be uniform for all polymers).²⁸ A similar effect may be seen here, with uneven grafting of the different PEG chains across the PAOMECE backbone, thus accounting for the broadening of ΔT seen for these polymers. The effect may be more pronounced for PAOMECE-g-PEG_{210/550}-SH due to the larger discrepancy in the molecular weight of the pendent PEG chains.

2.3 Conclusions

The synthesis and polymerisation of AOMECE and the subsequent post-polymerisation modification of the polymer provides a route to a range of polycarbonates bearing various pendent functionalities in just three steps, significantly reducing the time and expense required for the synthesis of this versatile class of materials. The application of AOMECE as a monomer for ring-opening polymerisation has been demonstrated to proceed with excellent control achieved over the molecular weight and dispersities of the polymers. The pendent alkene functionality on the monomer provides a route to post-polymerisation modification of the material, and this has been shown to occur without degradation of the polymer or significant increase in dispersity using photoinitiated radical thiol-ene coupling chemistry. A range of functional thiols were successfully added to the polymer backbone, thus providing a potential route to further modification of the material. The facile synthesis of the monomer and absence of base-sensitive functionalities in the pendent group makes AOMECE an exciting and valuable alternative to previously researched alkene-functional carbonate monomers. The ability to generate a thermoresponsive polycarbonate by grafting hydrophilic PEG to the polymer backbone was also demonstrated, as was the ability to tune the LCST of the polymer by simply varying the molecular weight of the pendent PEG chains.

2.4 References

- (1) Feng, J.; Zhuo, R.-X.; Zhang, X.-Z. *Prog. Polym. Sci.* **2012**, *37*, 211.
- (2) Xu, J.; Feng, E.; Song, J. *J. Appl. Polym. Sci.* **2014**, *131*.
- (3) Rokicki, G. *Prog. Polym. Sci.* **2000**, *25*, 259.
- (4) Keul, H. In *Handbook of Polymer Chemistry*; Wiley-VCH Verlag GmbH & Co. KGaA: New York, 2009, p 307.
- (5) Lu, X. B.; Shi, L.; Wang, Y. M.; Zhang, R.; Zhang, Y. J.; Peng, X. J.; Zhang, Z. C.; Li, B. *J. Am. Chem. Soc.* **2006**, *128*, 1664.
- (6) Tempelaar, S.; Barker, I. A.; Truong, V. X.; Hall, D. J.; Mespouille, L.; Dubois, P.; Dove, A. P. *Polym. Chem.* **2013**, *4*, 174.
- (7) Venkataraman, S.; Veronica, N.; Voo, Z. X.; Hedrick, J. L.; Yang, Y. Y. *Polym. Chem.* **2013**, *4*, 2945.
- (8) Wang, X. L.; Zhuo, R. X.; Liu, L. J.; He, F.; Liu, G. *J. Polym. Sci. A: Polym. Chem.* **2002**, *40*, 70.
- (9) Kiesewetter, M. K.; Shin, E. J.; Hedrick, J. L.; Waymouth, R. M. *Macromolecules* **2010**, *43*, 2093.
- (10) MacMillan, D. W. C. *Nature* **2008**, *455*, 304.
- (11) Nederberg, F.; Connor, E. F.; Moller, M.; Glauser, T.; Hedrick, J. L. *Angew. Chem. Int. Ed.* **2001**, *40*, 2712.
- (12) Tempelaar, S.; Mespouille, L.; Coulembier, O.; Dubois, P.; Dove, A. P. *Chem. Soc. Rev.* **2013**, *42*, 1312.

- (13) Elised Aguirre-Chagala, Y.; Santos, J. L.; Herrera-Najera, R.; Herrera-Alonso, M. *Macromolecules* **2013**, *46*, 5871.
- (14) Nederberg, F.; Trang, V.; Pratt, R. C.; Mason, A. F.; Frank, C. W.; Waymouth, R. M.; Hedrick, J. L. *Biomacromolecules* **2007**, *8*, 3294.
- (15) Hansell, C. F.; O'Reilly, R. K. *ACS Macro Lett.* **2012**, *1*, 896.
- (16) Nandivada, H.; Jiang, X.; Lahann, J. *Adv. Mater.* **2007**, *19*, 2197.
- (17) Xu, J.; Prifti, F.; Song, J. *Macromolecules* **2011**, *44*, 2660.
- (18) Hu, X.; Chen, X.; Xie, Z.; Cheng, H.; Jing, X. *J. Polym. Sci. A: Polym. Chem.* **2008**, *46*, 7022.
- (19) Al-Azemi, T. F.; Harmon, J. P.; Bisht, K. S. *Biomacromolecules* **2000**, *1*, 493.
- (20) Rokicki, G.; Parzuchowski, P. G. In *Polymer Science: A Comprehensive Reference*; 1 ed.; Matyjaszewski, K., and Möller, M., Ed.; Elsevier: Oxford, 2012; Vol. 4, p 247.
- (21) Chen, W.; Meng, F.; Cheng, R.; Deng, C.; Feijen, J.; Zhong, Z. *J. Control. Release* **2014**, *190*, 398.
- (22) Li, M.; De, P.; Li, H.; Sumerlin, B. S. *Polym. Chem.* **2010**, *1*, 854.
- (23) Williams, R. J.; Barker, I. A.; O'Reilly, R. K.; Dove, A. P. *ACS Macro Lett.* **2012**, *1*, 1285.
- (24) Campos, L. M.; Killops, K. L.; Sakai, R.; Paulusse, J. M. J.; Damiron, D.; Drockenmuller, E.; Messmore, B. W.; Hawker, C. J. *Macromolecules* **2008**, *41*, 7063.
- (25) Justynska, J.; Hordyjewicz, Z.; Schlaad, H. *Polymer* **2005**, *46*, 12057.

- (26) Kade, M. J.; Burke, D. J.; Hawker, C. J. *J. Polym. Sci. A: Polym. Chem.* **2010**, *48*, 743.
- (27) Hoyle, C. E.; Bowman, C. N. *Angew. Chem. Int. Ed.* **2010**, *49*, 1540.
- (28) Kim, Y. G.; Ho, S. O.; Gassman, N. R.; Korlann, Y.; Landorf, E. V.; Collart, F. R.; Weiss, S. *Bioconjugate Chem.* **2008**, *19*, 786.
- (29) Alarcon, C. D. H.; Pennadam, S.; Alexander, C. *Chem. Soc. Rev.* **2005**, *34*, 276.
- (30) Klouda, L.; Mikos, A. G. *Eur. J. Pharm. Biopharm.* **2008**, *68*, 34.
- (31) Ward, M. A.; Georgiou, T. K. *Polymers* **2011**, *3*, 1215.
- (32) Lutz, J.-F. *J. Polym. Sci. A: Polym. Chem.* **2008**, *46*, 3459.
- (33) Lutz, J. F.; Hoth, A. *Macromolecules* **2006**, *39*, 893.
- (34) Engler, A. C.; Chan, J. M. W.; Coady, D. J.; O'Brien, J. M.; Sardon, H.; Nelson, A.; Sanders, D. P.; Yang, Y. Y.; Hedrick, J. L. *Macromolecules* **2013**, *46*, 1283.
- (35) Kim, S. H.; Tan, J. P. K.; Fukushima, K.; Nederberg, F.; Yang, Y. Y.; Waymouth, R. M.; Hedrick, J. L. *Biomaterials* **2011**, *32*, 5505.
- (36) Yu, L.; Zheng, Z.; Liu, Y.; Li, Z.; Wang, X. L. *RSC Adv.* **2015**, *5*, 64832.
- (37) Zhang, X. J.; Chen, F. J.; Zhong, Z. L.; Zhuo, R. X. *Macromol. Rapid Commun.* **2010**, *31*, 2155.
- (38) Truong, V. X.; Barker, I. A.; Tan, M.; Mespouille, L.; Dubois, P.; Dove, A. P. *J. Mater. Chem. B* **2013**, *1*, 221.

- (39) Chen, W.; Yang, H.; Wang, R.; Cheng, R.; Meng, F.; Wei, W.; Zhong, Z. *Macromolecules* **2010**, *43*, 201.
- (40) Chen, X. H.; McCarthy, S. P.; Gross, R. A. *Macromolecules* **1997**, *30*, 3470.
- (41) He, F.; Wang, Y.-P.; Liu, G.; Jia, H.-L.; Feng, J.; Zhuo, R.-X. *Polymer* **2008**, *49*, 1185.
- (42) Hu, X.; Chen, X.; Cheng, H.; Jing, X. *J. Polym. Sci. A: Polym. Chem.* **2009**, *47*, 161.
- (43) Miyagawa, T.; Shimizu, M.; Sanda, F.; Endo, T. *Macromolecules* **2005**, *38*, 7944.
- (44) Murayama, M.; Sanda, F.; Endo, T. *Macromolecules* **1998**, *31*, 919.
- (45) Onbulak, S.; Tempelaar, S.; Pounder, R. J.; Gok, O.; Sanyal, R.; Dove, A. P.; Sanyal, A. *Macromolecules* **2012**, *45*, 1715.
- (46) Wang, R.; Chen, W.; Meng, F.; Cheng, R.; Deng, C.; Feijen, J.; Zhong, Z. *Macromolecules* **2011**, *44*, 6009.
- (47) Olsen, P.; Odelius, K.; Albertsson, A.-C. *Macromolecules* **2014**, *47*, 6189.
- (48) He, Y.; Keul, H.; Moeller, M. *React. Funct. Polym.* **2011**, *71*, 175.
- (49) Tempelaar, S.; Mespouille, L.; Dubois, P.; Dove, A. P. *Macromolecules* **2011**, *44*, 2084.
- (50) Lohmeijer, B. G. G.; Pratt, R. C.; Leibfarth, F.; Logan, J. W.; Long, D. A.; Dove, A. P.; Nederberg, F.; Choi, J.; Wade, C.; Waymouth, R. M.; Hedrick, J. L. *Macromolecules* **2006**, *39*, 8574.

- (51) Koo, S. P. S.; Stamenovic, M. M.; Prasath, R. A.; Inglis, A. J.; Du Prez, F. E.; Barner-Kowollik, C.; Van Camp, W.; Junkers, T. *J. Polym. Sci. A: Polym. Chem.* **2010**, *48*, 1699.

3 Random Copolymers of Cyclic Carbonates and Esters with Tuneable Functional Group Density

3.1 Introduction

Homopolymers and copolymers of cyclic esters such as lactide, glycolide and ϵ -caprolactone have been widely studied for applications in biomedicine (*e.g.* as tissue regeneration scaffolds and drug delivery vehicles), as a result of the control that can be achieved over their degradation time and mechanical properties, combined with their biocompatibility and the fact that their degradation products are often resorbed *via* metabolic pathways.¹⁻⁵ However, the use of polyesters for soft tissue engineering applications is limited in scope for several reasons. The materials have high elastic moduli in comparison to soft tissues,^{6,7} and the hydrolytic degradation of aliphatic polyesters can result in the generation of carboxylic acid-terminated degradation products, causing a lowering of the local pH *in vivo* and subsequently triggering an inflammatory immune response.⁸⁻¹⁰ In addition, the use of aliphatic polyesters for drug delivery applications is limited by the fact that the materials typically undergo bulk degradation, where the rate of ingress of the degradation medium exceeds the rate of degradation, resulting in a burst-release of the active ingredient.^{11,12} Furthermore, incorporation of functionality into aliphatic polyesters is synthetically challenging, limiting the possibilities for post-polymerisation modification of these materials (*e.g.* for altering mechanical properties, degradation rates or incorporating biologically active molecules on the polymer).¹³⁻¹⁵

One method of mitigating these limitations is to copolymerise cyclic esters with cyclic carbonates bearing pendent functionality. Incorporating pendent functionality in the polymer allows the physical and chemical properties of the material to be readily modified post-polymerisation. The synthesis of polycarbonates bearing pendent functionality is relatively simple in comparison to the synthesis of functional polyesters, and a wide range of cyclic carbonate monomers bearing a variety of

different functionalities have been synthesised and polymerised.¹⁶⁻¹⁹ Aliphatic polycarbonates generally possess lower elastic moduli than their polyester counterparts,^{6,20} and polycarbonate hydrolysis has been shown to not result in the generation of acidic degradation products, as the carbonic acid end-group decomposes to yield hydroxyl-terminated degradation products and CO₂.²¹ Consequently, biomedical implants prepared from aliphatic polycarbonates have been shown to result in reduced soft tissue inflammation in comparison to those prepared from polyesters.²²⁻

24

Aliphatic polycarbonates are also more resistant to hydrolysis and undergo slower degradation *in vitro* than analogous polyesters, under both standard and accelerated conditions.^{20,25,26} This resistance to *in vitro* hydrolysis can be beneficial for applications *in vivo*, where extra-cellular enzymes have been shown to catalyse the hydrolysis of polycarbonates. As the enzymes are too large to penetrate the polymer matrix, the degradation of the polycarbonates is accelerated only at the surface of the material. Consequently, under enzyme-catalysed degradation conditions, polycarbonates degrade primarily *via* a surface erosion mechanism, where the rate of hydrolysis at the surface of the material exceeds that of the bulk.^{20,27-29} Surface erosion is a desirable property for tissue scaffolds and some drug delivery applications, as the materials undergo linear and predictable changes in mechanical properties and drug release rates as they degrade.¹⁰

Random (statistical) copolymers of cyclic esters and carbonates have been used as a method of tailoring the mechanical properties and degradation rates of polyesters and polycarbonates.³⁰⁻³⁴ Furthermore, copolymers with a random distribution of functionality along the polymer backbone are desirable for several applications in biomedicine. For example, in the case of polymers bearing functionalities promoting

tissue growth, an even distribution of such functionality may promote greater cell adhesion and tissue regeneration, in contrast to areas of high and low functionalisation density.³⁷ Materials functionalised with lignin or the tripeptide arginylglycylaspartic acid (RGD) are known to promote cell adhesion and proliferation, with increasing bioactive molecule content resulting in increased cell adhesion.³⁵⁻³⁷ However, it has been demonstrated that cell proliferation is highly dependent on cell migration, and consequently the functionalisation density of materials. Too low a concentration of bioactive groups results in cells not being able to adhere to the surface of the material, whilst too high a concentration results in cells becoming adhered too firmly and remaining stuck in place, resulting in insufficient cell migration to facilitate tissue regeneration.³⁵⁻⁴⁰

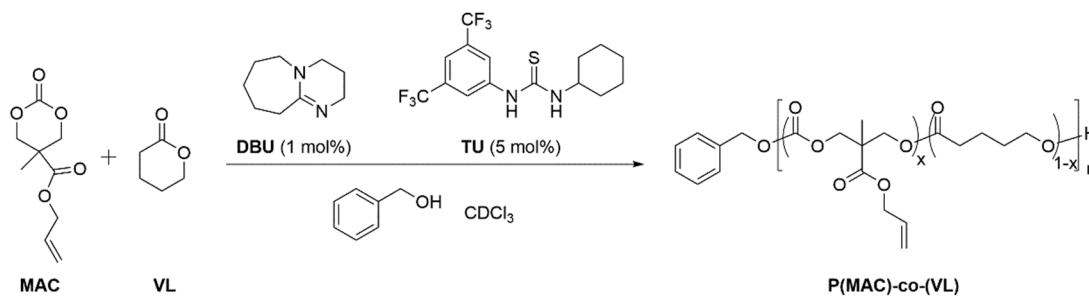
The ability to tune the functionalisation density of a material is therefore advantageous, and can be achieved through the copolymerisation of functional and non-functional monomers.^{17,41-43} However, achieving materials which possess both ideal functionalisation density and degradation rate or mechanical properties is challenging, as modifying one property generally has an adverse effect on the others.^{25,44,45} One potential solution is to only partially modify a material during post-polymerisation modification, however this is not always a suitable option – as demonstrated in Chapter 2 of this thesis, partial functionalisation of poly(2-allyloxymethyl-2-ethyltrimethylene carbonate) (PAOMEC) using photoinitiated radical thiol-ene addition chemistry can result in unwanted cross-linking. An alternative strategy may be to incorporate an additional non-functional monomer into a material as a replacement for a portion of the functional monomers, forming a terpolymer.

The following chapter details the synthesis of random copolymers of a non-functional cyclic ester (δ -valerolactone, VL) and a functional cyclic carbonate (2-allyloxymethyl-2-ethyltrimethylene carbonate, AOMEC) by ring-opening polymerisation (ROP). The synthesis of a series of random copolymers with different ester:carbonate compositions is described, and the degree of randomness of these polymers is investigated with quantitative ^{13}C NMR spectroscopy. In addition, the synthesis of a carbonate monomer bearing alkyl ether functionality, 2-propyloxymethyl-2-ethyltrimethylene carbonate (POMEC) as a non-modifiable analogue of AOMEC is reported. The homopolymerisation of POMEC and its copolymerisation with AOMEC to modify the density of alkene groups in the polycarbonate is reported. Further, the copolymerisation of POMEC with AOMEC and VL to form a terpolymer is demonstrated, enabling the synthesis of materials with tuneable carbonate:ester composition and independently modifiable pendent alkene functional group density.

3.2 Results and Discussion

3.2.1 Monomer screening

5-Methyl-5-allyloxycarbonyl-1,3-dioxan-2-one (MAC) and δ -valerolactone (VL) were initially chosen as potential monomers for the synthesis of poly(ester-*co*-carbonate) copolymers bearing pendent functionality. MAC was selected as the functional carbonate component as a result of its ease of synthesis, its well-controlled polymerisation using organocatalysis, and its previously demonstrated facile post-polymerisation modification *via* radical thiol-ene addition.⁴⁶ The ester component of the copolymer was selected based on two criteria; firstly, the monomer was desired to be cheap and readily available, and secondly it must have a similar polymerisation rate to that of the carbonate monomer under similar conditions, as too high or low a polymerisation rate would result in block-like rather than random copolymers. Lohmeijer *et al.* have previously reported the polymerisation rates of L-lactide (LLA), δ -valerolactone and ϵ -caprolactone (CL) using a dual organocatalyst system of 1,8-diazabicyclo[5.4.0]undec-7-ene (DBU) and 1-(3,5-bis(trifluoromethyl)-phenyl)-3-cyclohexylthiourea (TU), a system which has also been applied to the polymerisation of MAC.⁴⁷ Of these cyclic ester monomers, VL was shown to polymerise at a rate in the same order of magnitude as that of MAC using a similar catalyst system, whilst CL possesses a much lower polymerisation rate and LLA possesses a much higher polymerisation rate than MAC.



Scheme 3.1. Synthesis of P(MAC-*co*-VL) via ring opening polymerisation, using a dual catalyst system of DBU/thiourea and benzyl alcohol as initiator.

An initial copolymerisation of MAC and VL was carried out using an overall monomer concentration of 1 M in CDCl₃. DBU and TU were used as organocatalysts in loadings of 1 and 5 mol% respectively (relative to overall monomer concentration). Benzyl alcohol was employed as an initiator, targeting a [MAC]₀:[VL]₀:[I]₀ ratio of 10:10:1 (Scheme 3.1). It immediately became apparent that the polymerisation of MAC proceeds much faster than that of VL - at 40 minutes, conversion of MAC and VL were found to be 78% and 13% respectively for a reaction with degree of polymerisation (DP) of 20 (Figure 3.1). Beyond this point, the polymerisation of MAC retards significantly while the polymerisation of VL continues at a similar rate. This results in copolymers with block-like character rather than a random distribution of each monomer throughout the polymer. In addition, the slow polymerisation rate of VL under the catalyst conditions used renders the copolymer synthesis impractical. Whilst the polymerisation rate could be increased through use of higher catalyst loadings, higher loadings of DBU have been shown to induce significant transesterification in the ROP of MAC.⁴⁶ As a result, this co-monomer system was deemed unsuitable for the synthesis of random copolymers, and an alternative carbonate monomer was sought.

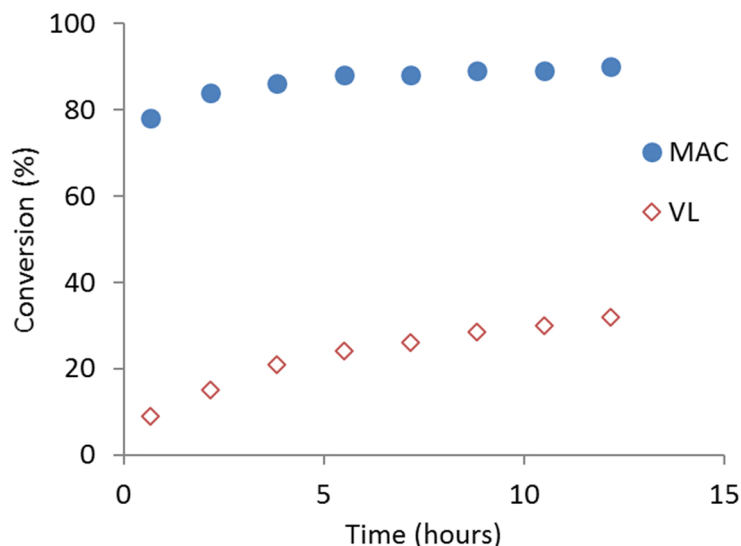


Figure 3.1. Plot of monomer conversion against time for the copolymerisation of MAC and VL. Conditions: Overall monomer concentration ($[M]$) = 1.0 M in $CDCl_3$, $[MAC]_0:[VL]_0:[I]_0 = 10:10:1$ using benzyl alcohol as initiator, 1 mol% DBU and 5 mol% TU as catalysts.

2-Allyloxymethyl-2-ethyltrimethylene carbonate (AOMEC) was considered as an alternative functional carbonate monomer. As described in Chapter 2 of this thesis, the homopolymerisation of AOMEC proceeds at a much lower rate than that of MAC under similar catalyst conditions. For $[M]_0:[I]_0 = 20$ and using a dual catalyst system of DBU (1 mol%) and TU (5 mol%), AOMEC requires 45 h to achieve 66% conversion, whilst MAC requires as little as 40 minutes to achieve 80% conversion. Whilst the homopolymerisation rate of AOMEC is still greater than that of VL, it was hypothesised that the copolymerisation of AOMEC with VL would be more likely to provide a material with random character in comparison to MAC. In addition, the polymerisation of AOMEC has been demonstrated to be resistant to transesterification using catalyst loadings of up to 5 mol% DBU (Chapter 2). As a result, higher catalyst loadings could be employed for the copolymerisation of AOMEC and VL, thus reducing the reaction time.

The difference in polymerisation rates is much reduced compared to the copolymerisation of MAC with VL. At 13% VL conversion, AOMECE had achieved only *ca.* 33% conversion (*c.f.* 78% conversion for MAC) (Figure 3.3). The polymerisation of AOMECE became severely retarded at *ca.* 80% monomer conversion, therefore the reaction was quenched at this point by addition of acidic Amberlyst A15 resin. Purification was performed by repeated precipitation into cold hexane, followed by passing the polymer through a silica plug. Methylene chloride was first used as eluent to remove residual TU and monomer, followed by ethyl acetate for collection of the copolymer. The final copolymer was observed to have an AOMECE:VL composition of *ca.* 67:33 (overall DP = 12, with number-average molecular weight (M_n) = 2,000 g mol⁻¹ (determined by ¹H NMR spectroscopy, Figure 3.4). A unimodal trace was obtained from size exclusion chromatography (SEC) with dispersity (D_M) = 1.13, which indicates that the copolymerisation of the two monomers is both successful and well-controlled (Figure 3.5).

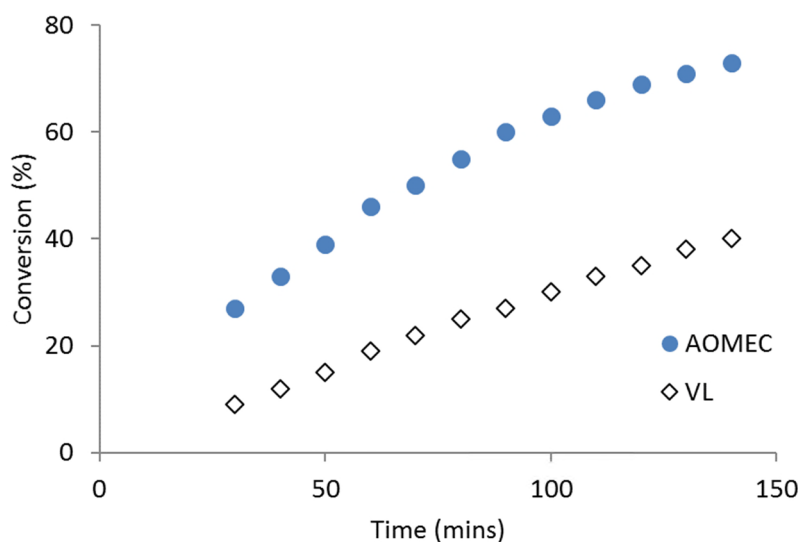


Figure 3.3. Plot of monomer conversion against time for the copolymerisation of AOMECE and VL. Conditions: $[M] = 2.0$ M in $CDCl_3$, $[AOMECE]_0:[VL]_0:[I]_0 = 10:10:1$ using $BnOH$ as initiator, 5 mol% DBU and 5 mol% TU as catalysts.

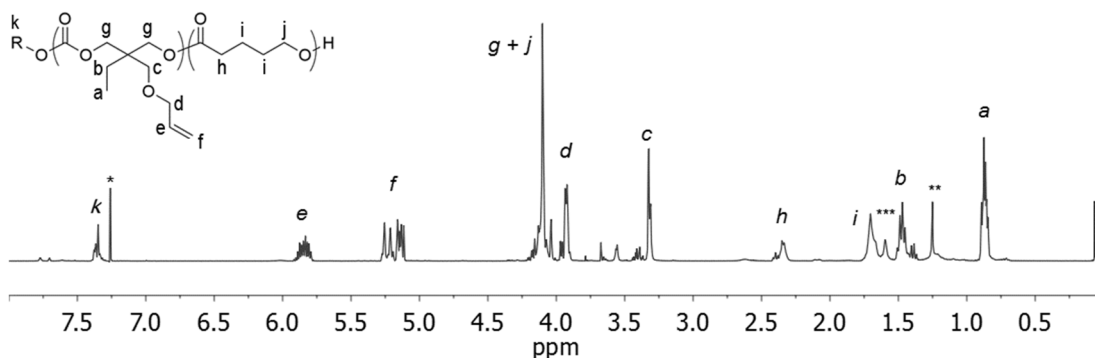


Figure 3.4. ^1H NMR spectrum of P(AOME c_8 -*co*-VL $_4$) initiated from BnOH (400 MHz, 293 K; * = CDCl_3 , ** = residual hexane from precipitation, *** = H_2O).

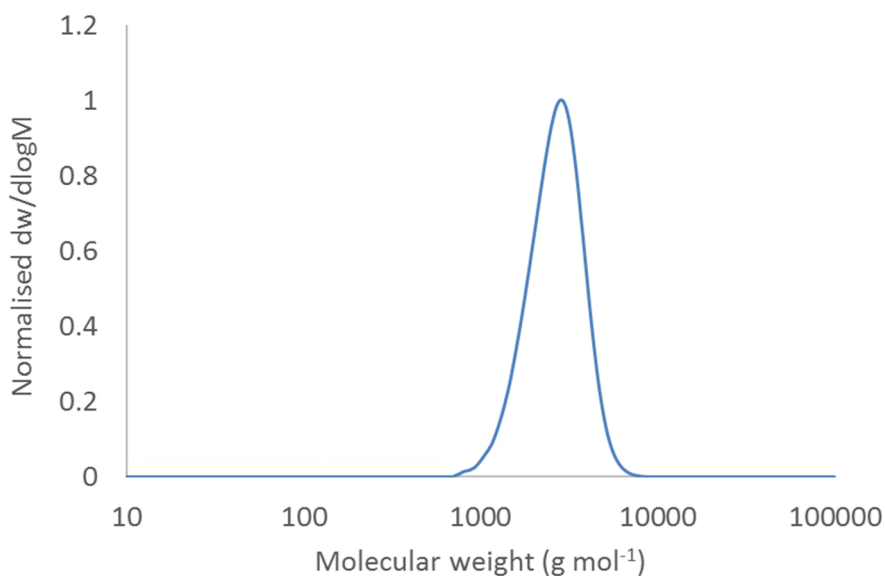


Figure 3.5. Size exclusion chromatogram of P(AOME c_8 -*co*-VL $_4$) initiated from BnOH ($M_n = 2,200 \text{ g mol}^{-1}$, $\mathcal{D}_M = 1.13$), measured against polystyrene standards using CHCl_3 as eluent. Unimodal distribution indicates the synthesis of a single copolymer species.

3.2.2 Reactivity ratio studies

Given that AOME c polymerises at a greater rate than VL, it appeared unlikely that truly random copolymers were being formed. In order to investigate the degree of randomness of the AOME c /VL copolymerisation, a reactivity ratio study was undertaken. The reactivity ratios of a copolymerisation determine the likelihood of

each monomer reacting with either a second unit of itself or its co-monomer, and consequently provide information about the distribution of each monomer throughout the copolymer. For the copolymerisation of AOMECE and VL, four possible reactions can occur at the reactive chain end,^{48,49}



where k_x is the rate of reaction. The reactivity ratios of AOMECE (r_1) and VL (r_2) are defined as follows,^{48,49}

$$r_1 = \frac{k_1}{k_2} \quad \text{Equation 3.5}$$

$$r_2 = \frac{k_3}{k_4} \quad \text{Equation 3.6}$$

As such, large values of r indicate a preference for a monomer to react with additional monomer units of the same type, whilst small values of r indicate a tendency for a monomer to react with its co-monomer. Therefore, the values of r can give an indication of the copolymer sequences that are likely to be obtained from a copolymerisation. For systems where $r_1 = r_2 \gg 1$, the two monomers will react exclusively with monomers of their own type, leading to the formation of two homopolymers. For a system where $r_1 = r_2 > 1$ a block copolymer will form, as while each monomer will preferentially homopolymerise, occasionally the other monomer will insert into the polymer chain, and a block segment of this monomer will then

polymerise. For a perfectly random copolymerisation (ideal copolymerisation), $r_1 = r_2 \approx 1$, as the chance of each monomer reacting is equal. Random copolymers may also be formed in copolymerisations where the product of $r_1 r_2 \approx 1$, whilst alternating copolymers tend to form in systems where $r_1 = r_2 \ll 1$, as the chance of each monomer homopolymerising is small. For systems where $r_1 > 1 > r_2$, the first monomer is consumed more rapidly in the initial stages of the copolymerisation, with units of the second monomer being incorporated more into the polymer as the first monomer is depleted, leading to composition drift and the formation of a gradient copolymer.⁴⁹

In order to determine the reactivity ratios of the monomers in the system, polymerisations were performed across a range of monomer feed ratios and limited to low conversions. For each reaction, the monomer fraction in the feed was plotted against the monomer fraction in the copolymer, measured by the relative integrals of monomer and polymer resonances determined by ¹H NMR spectroscopy. Monomer conversion was restricted to < 10%, as the consumption of one monomer can potentially drastically alter the rate of consumption of its co-monomer, however this effect is limited at low conversions. Reactivity ratios can then be calculated using nonlinear least squares regression analysis, as described by van Herk *et al.*^{50,51}

The initial reactivity ratio experiments were performed using the DBU/TU catalyst system. However, it soon became apparent that this system would not be suitable for studying the reactivity ratios of this copolymerisation, as a consequence of the methylene resonances of VL at *ca.* $\delta = 2.25$ ppm overlapping slightly with DBU resonances at $\delta = 2.30$ ppm in the ¹H NMR spectrum. As a consequence of the low monomer conversions at which the ¹H NMR spectra must be taken for the calculation of reactivity ratios, any form of overlap between peaks can greatly alter the integrals of the relevant resonances and consequently affect the reactivity ratio values obtained.

In order to circumvent this problem, triazabicyclodecene (TBD) was considered as a bifunctional catalyst for the reactivity ratio study. This catalyst possesses an advantage over the DBU/TU system in that none of its ^1H NMR resonances overlap with those of AOMEK, VL or their polymers. However, it is possible that changing the catalyst system could also change the reactivity ratios as a result of differences in the strength of hydrogen bonding between the catalyst and the carbonyl groups of the monomers.

Therefore, prior to reactivity ratio determination, the conversion of AOMEK and VL was monitored for copolymerisations using two different feed ratios (20:80 and 50:50), firstly using the dual DBU/TU system (5 mol% DBU and 5 mol% TU relative to monomer concentration) and secondly using the bifunctional TBD catalyst (1 mol% catalyst loading) in order to determine the effect of changing the catalyst system on copolymerisation rates. For each feed ratio, the results indicated that whilst the conversion of both monomers was much greater using the TBD catalyst system, any difference in relative monomer conversion rates between the two catalyst systems was negligible (Figure 3.6). The reactivity ratio study was therefore performed using the bifunctional TBD catalyst.

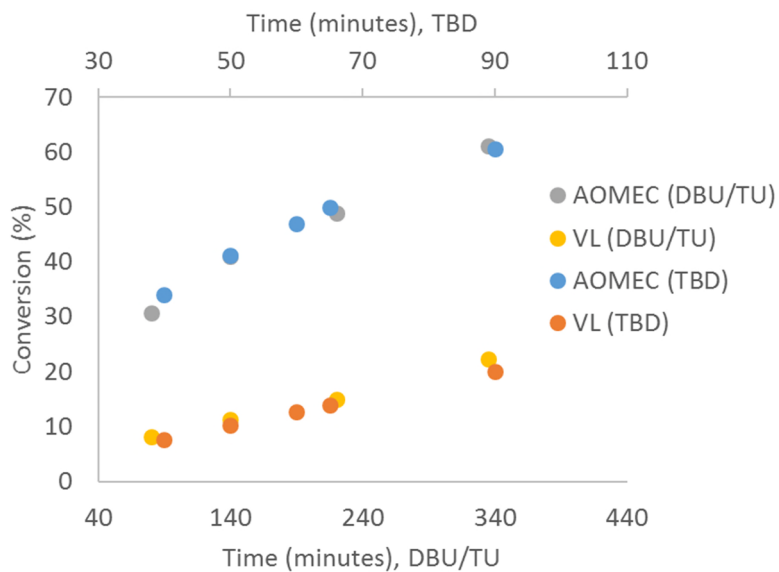


Figure 3.6. Plot showing comparison of monomer conversion against time for the copolymerisation of AOMEc with VL using two different catalyst systems. [AOMEc]₀: [VL]₀: [I]₀ = 20:80:1, using BDM as initiator, and 5 mol% DBU/5 mol% TU (top x-axis) or 1 mol% TBD (bottom x-axis) as catalysts.

As a consequence of the high activity of TBD,⁴⁷ the catalyst loading was reduced from 1 mol% to 0.1 mol% relative to monomer concentration in order to allow ¹H NMR spectra to be obtained below 10% monomer conversion. Polymerisations were performed across a range of nine monomer feed ratios (from AOMEc:VL = 10:90 to 90:10), with each data point taken in triplicate (Figure 3.7).

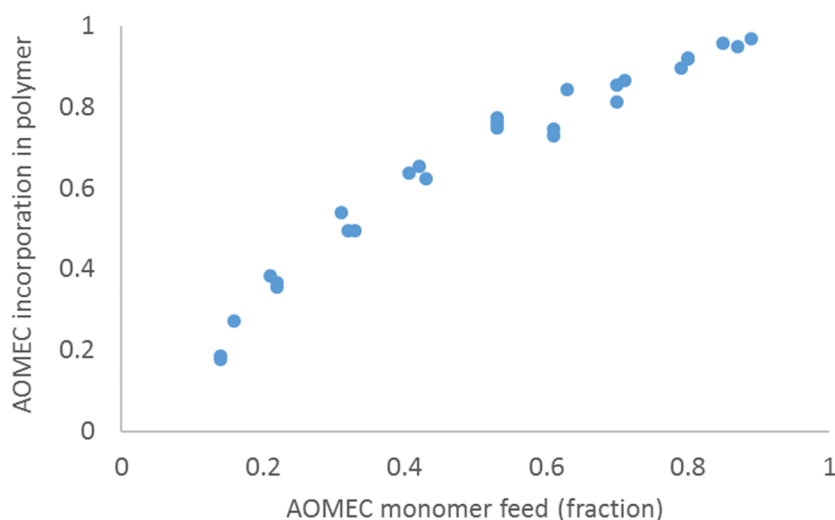


Figure 3.7. Plot of AOMEC incorporation in the copolymer against AOMEC fraction in the monomer feed, as determined by ^1H NMR spectroscopy (400 MHz, 293 K, CDCl_3). This data was subjected to nonlinear least-squares regression analysis to determine the reactivity ratios of AOMEC and VL.

After applying nonlinear least-squares regression analysis, the reactivity ratios were determined to be $r_1 = 2.707 \pm 0.100$ and $r_2 = 0.529 \pm 0.020$ for AOMEC and VL respectively. Given that $r_1 > 1 > r_2$, the copolymerisation of AOMEC with VL leads to the formation of gradient copolymers rather than truly random copolymers.

To compensate for the effect of composition drift, the information gleaned from the reactivity ratio studies was used to target specific copolymer compositions with random monomer distributions. By adjusting the monomer feed ratios to compensate for the higher rate of AOMEC conversion, and limiting the conversion of AOMEC to $< 80\%$, it was postulated that the effect of composition drift could be largely limited, resulting in the synthesis of copolymers with predictable AOMEC:VL compositions and near-random monomer distribution. For example, from the reactivity ratio data, to achieve a copolymer with 50% AOMEC incorporation would require a monomer feed of *ca.* 30% AOMEC and 70% VL. By quenching the reaction at 80% AOMEC incorporation, block-like VL regions can be avoided.

To this end, a series of copolymerisations were performed targeting AOMECE:VL compositions of 80:20, 50:50 and 20:80 and overall $[M]_0:[I]_0 = 100$, using AOMECE:VL monomer feeds of 62:38, 31:69 and 16:84 respectively. 1,4-Benzenedimethanol (BDM) was used as a bifunctional alcohol initiator, with DBU (5 mol%) and TU (5 mol%) employed as the dual organocatalyst system. Conversion was monitored by ^1H NMR spectroscopy, and the reactions were quenched by addition of acidic Amberlyst A15 ion exchange resin upon reaching 80% AOMECE conversion. Following purification, the copolymers were analysed by ^1H and ^{13}C NMR spectroscopy, yielding copolymers with AOMECE:VL compositions of 89:11, 61:39 and 35:65, with overall DPs ranging from 76 to 81 and dispersities ranging from 1.09 to 1.17 (Table 3.1).

Table 3.1. Homo- and copolymers of AOMECE and VL prepared by ring-opening polymerisation.^a

Polymer	Polymer composition ^b	M_n (g mol ⁻¹) ^b	D_M ^c	AOMECE:VL ^b
1	PAOMECE ₈₈	17,600	1.15	100:0
2	P(AOMECE _{72-<i>co</i>} -VL ₉)	15,300	1.12	89:11
3	P(AOMECE _{47-<i>co</i>} -VL ₃₁)	12,500	1.14	61:39
4	P(AOMECE _{26-<i>co</i>} -VL ₅₀)	10,200	1.17	35:65
5	PVL ₇₈	7,800	1.09	0:100

^a Polymerisations performed in CHCl_3 at 25 °C, $[M] = 2.0$ M, using BDM as initiator and 5 mol% DBU/5 mol% TU as catalysts. ^b Polymer composition and number-average molecular weight determined by ^1H NMR spectroscopy. ^c Determined by SEC analysis in CHCl_3 .

Quantitative ^{13}C NMR spectroscopy was performed on the copolymers, along with samples of PAOMEC and PVL homopolymers. Using this technique, through detailed analysis of the carbonyl regions for the AOMEC and VL repeat units (Figure 3.8), information on the local monomer sequences in the copolymers can be obtained.

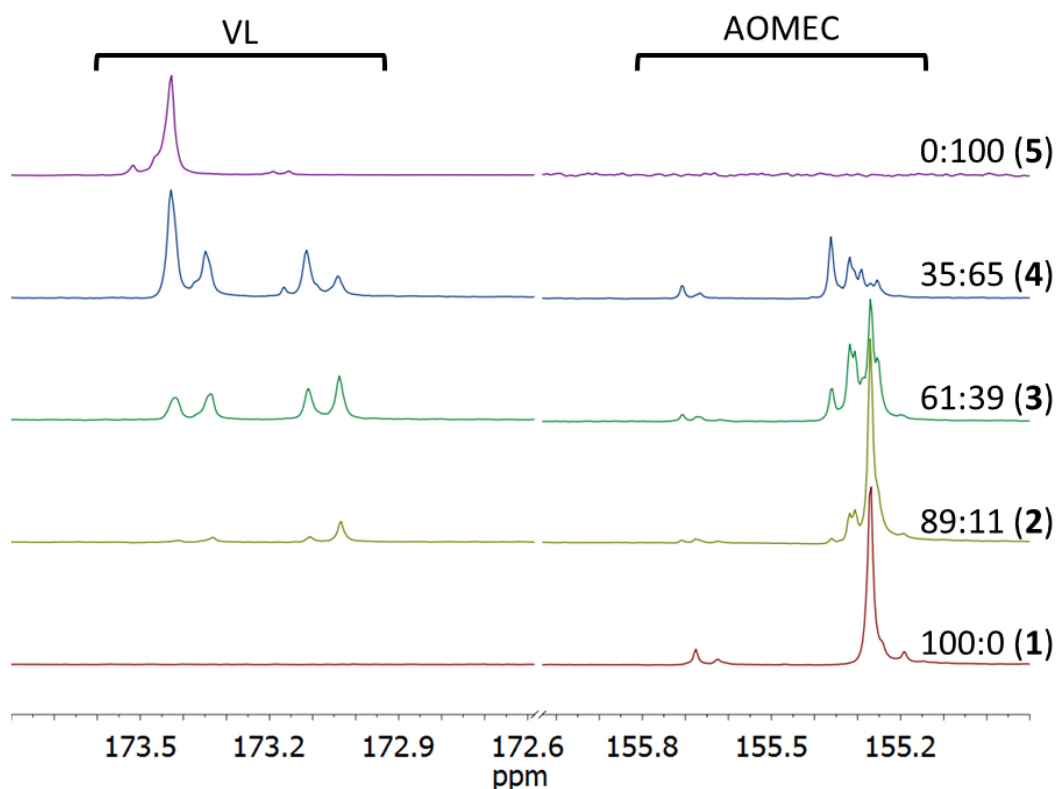


Figure 3.8. Expanded carbonyl carbon regions of stacked ^{13}C NMR spectra for polymers **1-5** (AOMEC:VL ratios of 100:0, 89:11, 61:39, 35:65 and 0:100 respectively), showing the change in intensity for the different carbonyl carbon environments with changing copolymer composition (125 MHz, 298 K, CDCl_3).

The ^{13}C NMR spectra were deconvoluted prior to measurement of resonance integrals in order to accurately determine the degree of randomness of the copolymers. Taking the ^{13}C NMR spectrum of 61:39 copolymer (**3**) as an example (Figure 3.9), measurement of the integrals for the VL resonances indicates that approximately 80% of the VL units are affected by AOMEC, as evidenced by an upfield shift of carbonyl resonances from $\delta = 173.4$ ppm to $\delta = 173.3$, 173.1 or 173.0 ppm. This gives

information about the sequencing of the copolymers up to triad level and possibly further. For VL repeat units, the greater the number of AOMECS in the surrounding environment, the greater the magnitude of the upfield shift for the VL carbonyl carbon in the ^{13}C NMR spectrum.

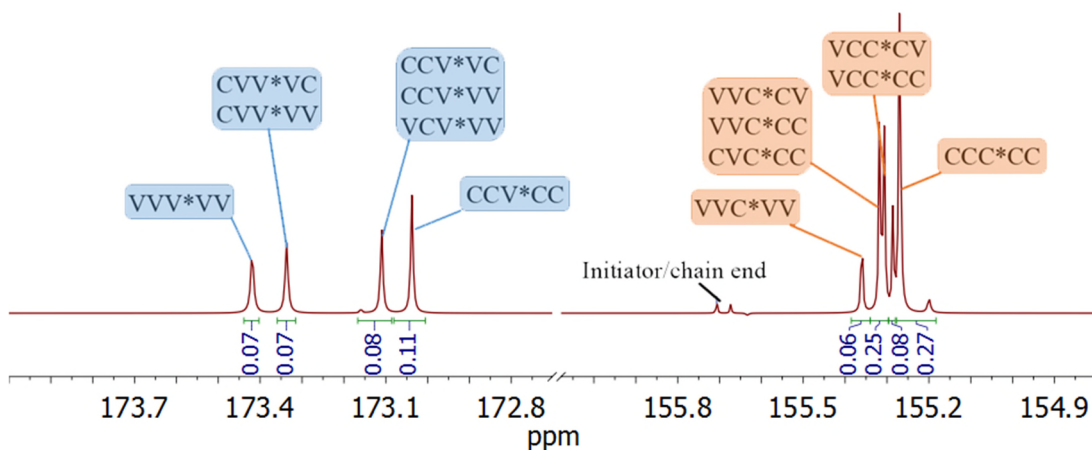


Figure 3.9. Deconvoluted and expanded carbonyl carbon regions in ^{13}C NMR spectrum of polymer **3** (AOMECS:VL composition 61:39), with proposed assignments for individual resonances (V = VL, C = AOMECS, observed carbon denoted with *) (125 MHz, 293 K, CDCl_3).

From the above ^{13}C NMR spectrum (Figure 3.9), it is proposed that the furthest downfield shift ($\delta = 173.4$ ppm) represents VL units bordered by VL units, which are in turn bordered by additional VL units (VVV*VV). This assignment is confirmed by the ^{13}C NMR spectrum for the PVL homopolymer (**5**), which displays only a major resonance at $\delta = 173.4$ ppm for the VL carbonyl, and minor additional peaks at $\delta = 173.5$, 173.1 and 173.1 ppm (corresponding to chain-end carbonyls and carbonyls lying adjacent to the initiating species). The highest upfield shift ($\delta = 173.0$ ppm) likely represents VL units surrounded entirely by AOMECS units (CCV*CC). This assignment is corroborated by the gradual increase in the intensity of this resonance in relation to the other VL carbonyl resonances, as total VL concentration decreases. The

likelihood of a lone VL unit being bordered by blocky AOMECS sections would be expected to increase in such circumstances.

The intermediate resonances are more difficult to assign, but may represent VL units bordered on one side by AOMECS and by VL on the other, or by two VL units which are in turn bordered by AOMECS units or vice versa, or a combination of these arrangements with the resonances overlapping. A similar case is proposed for the AOMECS resonances, with increasing VL influence generating a greater downfield chemical shift for the AOMECS carbonyl resonances from $\delta = 155.2$ ppm to $\delta = 155.3$, 155.3 and 155.4 ppm. The possible configurations are illustrated for clarity in Figure 3.9.

The integration of the individual carbonyl carbon resonances from ^{13}C NMR spectroscopy enables the calculation of the average sequence length of PAOMECS and PVL in each copolymer. The number-average lengths of each monomer can be calculated by both dyad (*i.e.* two-monomer sequence) and triad (*i.e.* three-monomer sequence) analysis using the following equations;⁵²

$$L_V = (F_{VV} + F_{VC}/2)/(F_{VC}/2) \quad \text{Equation 3.7}$$

$$L_C = (F_{CC} + F_{CV}/2)/(F_{CV}/2) \quad \text{Equation 3.8}$$

$$L_V = (F_{VVV} + F_{VVC} + F_{CVC})/(F_{VVC} + F_{CVC}/2) \quad \text{Equation 3.9}$$

$$L_C = (F_{CCC} + F_{CCV} + F_{VCV})/(F_{CCV} + F_{VCV}/2) \quad \text{Equation 3.10}$$

where L_V and L_C are the number-average lengths of PVL and PAOMECS in the copolymers, and $F_{XY/XYZ}$ denotes the fraction of each dyad or triad sequence in the copolymers. The fraction of each dyad and triad sequence and calculated L_V and L_C values are given in Table 3.2-3.4.

Table 3.2. Dyad and triad fractions of VL sequences in P(AOME*C-co*-VL) copolymers as determined by integration of relevant resonances using ^{13}C NMR spectroscopy.

Polymer	Dyad fractions		Triad fractions		
	F_{VV}	F_{VC}	F_{VVV}	F_{VVC}	F_{CVC}
2	0.0066	0.0912	0.0066	0.0347	0.0565
3	0.0675	0.267	0.0675	0.1584	0.1086
4	0.2895	0.3477	0.2895	0.2822	0.0655

Table 3.3. Dyad and triad fractions of AOME*C* sequences in P(AOME*C-co*-VL) copolymers as determined by integration of relevant resonances using ^{13}C NMR spectroscopy.

Polymer	Dyad fractions		Triad fractions		
	F_{CC}	F_{CV}	F_{CCC}	F_{CCV}	F_{VCV}
2	0.6064	0.2959	0.6064	0.1983	0.0976
3	0.2699	0.3957	0.2699	0.3957	0.0586
4	0.0757	0.1963	0.0757	0.168	0.1066

Table 3.4. Number-average sequence lengths for VL and AOMEK calculated from dyad and triad fractions, using equations 7-10.

Polymer	Average sequence length (VL)		Average sequence length (AOMEK)	
	L_V Dyad	L_V Triad	L_C Dyad	L_C Triad
2	1.14	1.32	5.10	4.59
3	1.51	1.78	2.36	2.82
4	2.67	3.08	1.77	1.84

For a copolymer to be described as truly random, the monomer distribution throughout the polymer must obey Bernoullian statistics.⁵³ The degree of randomness (R) of the copolymers can be calculated using the following equation;^{49,54}

$$R = 1/L_V + 1/L_C \quad \text{Equation 3.11}$$

Table 3.5. Degrees of randomness for P(AOMEK-co-VL) copolymers calculated from dyad and triad fractions using equation 11.

Polymer	R (dyad)	R (triad)
2	1.07	0.97
3	1.09	0.92
4	0.94	0.87

The values of R calculated for the copolymers range from 1.00 to 1.05 for dyad fractions, and 0.87 to 0.93 for triad fractions (Table 3.5). For truly random copolymers, $R = 1$. For systems where $R > 1$, the copolymer tends towards an alternating microstructure, whilst for systems where $R < 1$, the copolymer tends towards block-like character.⁴⁹ As such, the R values calculated from both dyad and triad integration indicate that each of the copolymers possesses a high degree of random monomer distribution. The small discrepancy in R values between dyad and triad analysis likely arises from the error associated with integration of the AOMECE carbonyl carbon resonances in the ¹³C NMR spectra as a result of overlap between the peaks, although this has been mitigated as much as possible by deconvolution of the resonances. However, both dyad and triad analysis are strongly indicative of each of the copolymers possessing a high degree of randomness.

3.2.3 Degradation studies

A degradation study was devised with the aim of comparing the degradability of different copolymer compositions. An initial test degradation was performed using samples of PAOMECE homopolymer with DP 88. Typical degradation studies reported in the literature are carried out by first preparing uniformly-sized samples through either compression-moulding or extrusion. The samples are then submerged in the degradation medium, with the mass of the samples monitored periodically throughout the degradation process. This is achieved simply by removing the sample from the degradation medium, drying and weighing the sample, and re-submerging the same sample in the degradation medium until the next monitoring point.^{25,26,44} However, at room temperature the PAOMECE exists as a viscous liquid. As such, compression moulding and sample recovery for accurate mass reading was not possible, therefore an alternative approach was devised using sacrificial degradation samples. As such,

multiple PAOMEC samples of equal weight (50 mg) were submerged in 5 M aqueous KOH solution (10 ml) in disposable glass scintillation vials. The vials were sealed and incubated at 37 °C with constant gentle agitation. Samples were taken at regular intervals and washed with CHCl₃ in order to recover the polymer and degradation products. The recovered samples were then analysed by SEC to monitor the relative change in polymer molecular weight over time.

Aqueous 5 M KOH solution was selected as the degradation medium as aliphatic polycarbonates have been shown to undergo accelerated hydrolysis under strongly basic conditions, as a consequence of the electropositive nature of the carbonyl carbon atom being susceptible to nucleophilic attack by hydroxide ions.^{20,26} In contrast to polyesters, polycarbonates are much more resistant to hydrolysis under strongly acidic conditions, whilst both classes of materials have been shown to require several months or even years to degrade under mild conditions (*e.g.* in phosphate-buffered saline (PBS) solution).²⁰ The relative resistance of polycarbonates to acid-catalysed hydrolysis (in comparison to polyesters) has been attributed to the lower electronegativity of the carbonate carbonyl oxygen in carbonate linkages. This results from the additional inductive effect of the additional oxygen atom serving to draw electron density away from the carbonyl oxygen, thereby making it less susceptible to protonation under acidic conditions.^{20,26}

Whilst analysis of the polymer determined that PAOMEC was degradable, there were large variations in the observed molecular weight of the polymer between samples, with the degradation appearing not to proceed linearly. By way of example, the weight-average molecular weight (M_w) of the sample was observed to be as low as 33% of the initial M_w after 20 days, before reporting as 51% after 25 days, followed by 32% after 46 days and finally recovering to 58% of initial M_w after 81 days (Figure

3.10, 3.11). Consequently, upon completion of the degradability study it was deemed that the method used to monitor the degradation of the material was unreliable.

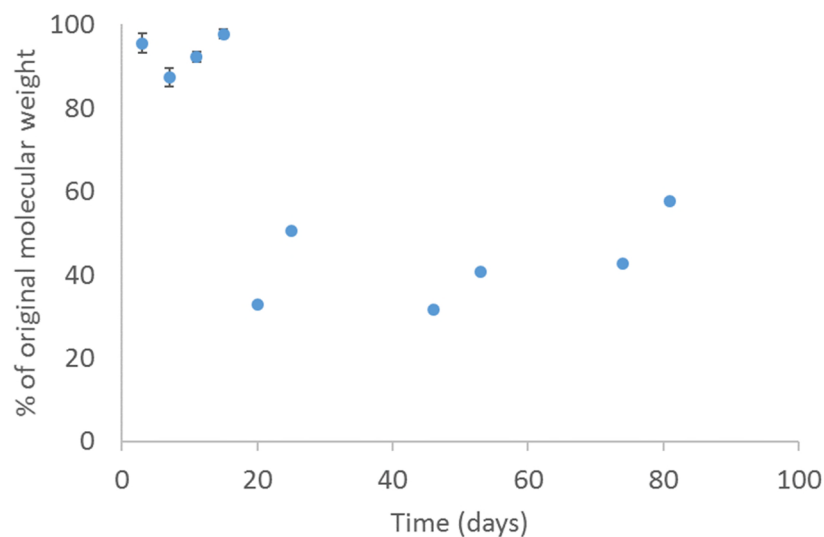


Figure 3.10. Plot of decrease in % molecular weight against time for PAOMEC₈₈ determined by SEC, charting the degradation of the sample in 5M KOH solution.

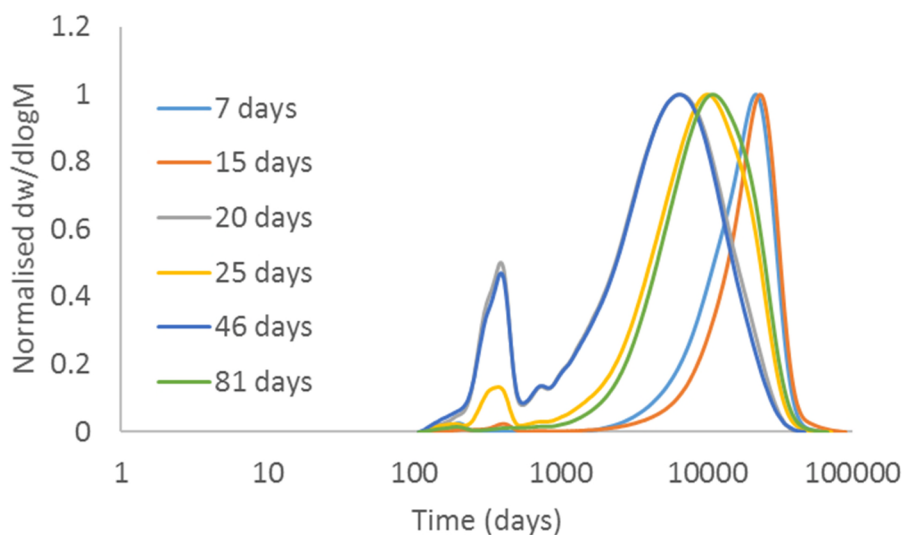


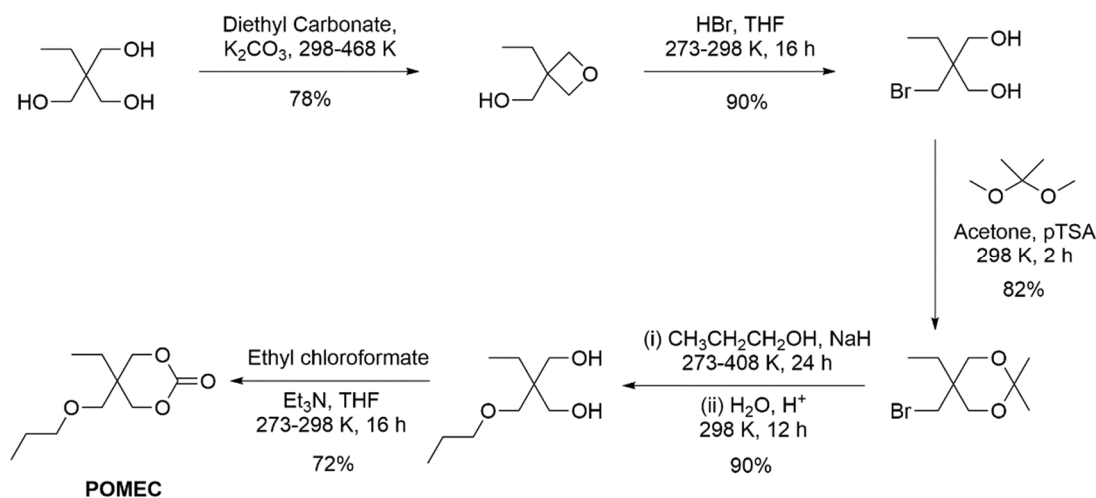
Figure 3.11. Selected size exclusion chromatograms showing the molecular weight distribution of PAOMEC recovered at different time points. Note the non-linear degradation behaviour, demonstrating the unreliability of the degradation method used.

The unexpected degradation behaviour most likely arises due errors associated with the method used. The recovery of the material into chloroform is one potential source of this error, either through variations in the relative amounts of low and high molecular weight material recovered, or by exposure of the dissolved polymer to the aqueous degradation medium at the interface of the two layers for differing lengths of time. Additionally, the presence of the aqueous degradation medium in the extracted sample may be the source of the error. The observed unpredictable degradation behaviour may then be correlated to the length of time taken for to be analysed by SEC, with the solubilisation of the polymer in CHCl₃ facilitating the ingress of the degradation medium into the polymer sample and thus accelerating degradation. As such, if the degradability of the PAOMECC and P(AOMECC-*co*-VL) samples were to be re-assessed, an alternative method of monitoring the degradation should be sought.

3.2.4 Terpolymer synthesis

While varying the composition of the AOMECC:VL copolymer allows the degree of pendent allyl functionality incorporated in the polymer to be controlled, it also inherently changes the number of carbonate linkages present in the material. In order to vary the percentage of allyl functionality in the copolymers without influencing the carbonate:ester ratio of the material, the incorporation of an additional non-functional carbonate monomer in the copolymer was considered. In order to minimise the effect on the reactivity ratio of the carbonate:ester copolymerisation, a co-monomer with a chemical structure very similar to that of AOMECC was designed, with a non-reactive alkyl ether pendent group replacing the allyl ether functionality.

The monomer was prepared in 5 steps (Scheme 3.3). First, 3-ethyl-3-hydroxymethyloxetane was synthesised by transesterification of commercially available trimethylolpropane with diethyl carbonate, followed by decarboxylation under basic conditions. The hydroxyl-functional oxetane was then ring-opened using concentrated aqueous HBr to yield 2-(bromomethyl)-2-ethyl-1,3-propanediol. The bromo-functional diol was protected using an acetal group, and etherified using 1-propanol and sodium hydride. The resulting alkyl ether-functional compound was deprotected, and the resulting diol ring closed with ethyl chloroformate. Purification was performed by vacuum distillation to generate 2-propyloxymethyl-2-ethyltrimethylene carbonate (POMEC) in 37% overall yield (Figure 3.12).



Scheme 3.3. Synthetic procedure for the production of the alkyl ether-functional monomer, 2-propyloxymethyl-2-ethyltrimethylene carbonate (POMEC).

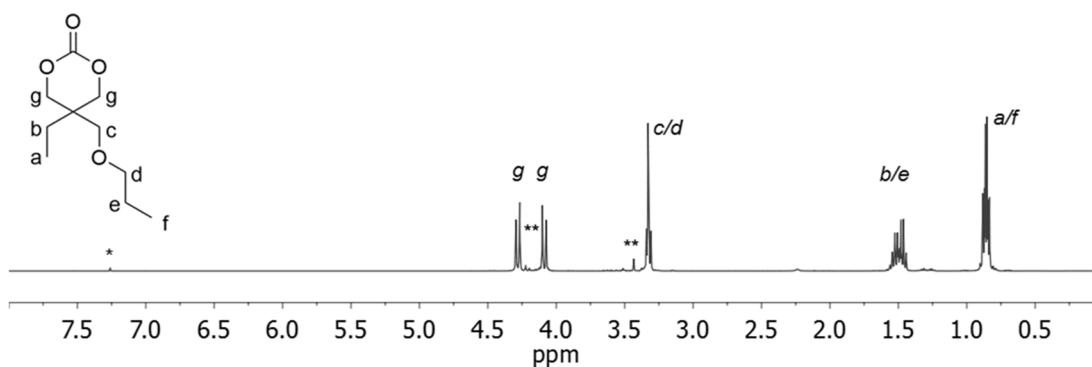
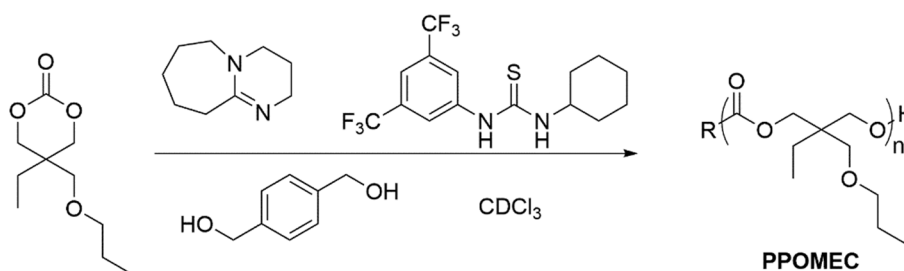


Figure 3.12. ^1H NMR spectrum of POMEC post-distillation (400 MHz, 293 K, CDCl_3 , * = CHCl_3 , ** = residual diol precursor).

An initial ROP of POMEC was performed in CDCl_3 ($[\text{POMEC}] = 2.0 \text{ M}$) using the dual DBU and TU catalyst system (5 mol% DBU and TU, relative to POMEC), and 1,4-benzenedimethanol as initiator with $[\text{M}]_0:[\text{I}]_0 = 30$ (Scheme 3.4).



Scheme 3.4. Synthesis of PPOMEC *via* ring opening polymerisation, using a dual catalyst system of DBU/thiourea and 1,4-benzenedimethanol as initiator.

Conversion was monitored by ^1H NMR spectroscopy, specifically by monitoring the change in integral for the methylene resonances at $\delta = 4.25$ and 4.09 ppm for the methylene signals at the α -position of the monomer and at $\delta = 4.05 \text{ ppm}$ for the methylene signals of the polymer backbone. As the monomer resonance at $\delta = 4.09 \text{ ppm}$ is almost completely obscured by the polymer resonance at $\delta = 4.05 \text{ ppm}$, the value of the integral at $\delta = 4.25 \text{ ppm}$ was doubled to account for the true value of the integrals of the monomer methylene resonances, and subtracted from the integral value

of the resonance at $\delta = 4.05$ ppm to account for the true value of the integrals of the polymer backbone methylene resonances (Figure 3.13).

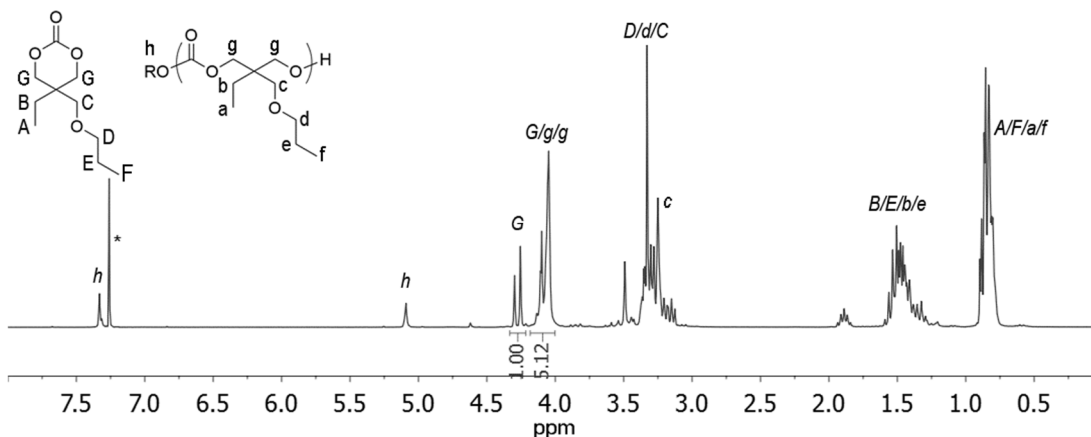


Figure 3.13. ^1H NMR spectrum of POMEc polymerisation taken at 67% monomer conversion. $[\text{POMEc}]_0: [\text{I}]_0 = 30$, initiated from BDM, using a dual catalyst system of DBU (5 mol%) and TU (5 mol%) (400 MHz, 293 K, CDCl_3 ; * = CHCl_3).

The polymerisation achieved 78% conversion in 160 minutes, at which point the reaction slowed markedly. The polymerisation was quenched by addition of acidic Amberlyst 15 ion exchange resin, and purified by repeated precipitation into cold *n*-hexane to yield the purified PPOMEc ($M_n = 4,700 \text{ g mol}^{-1}$, $D_M = 1.14$) (Figure 3.14 and 15).

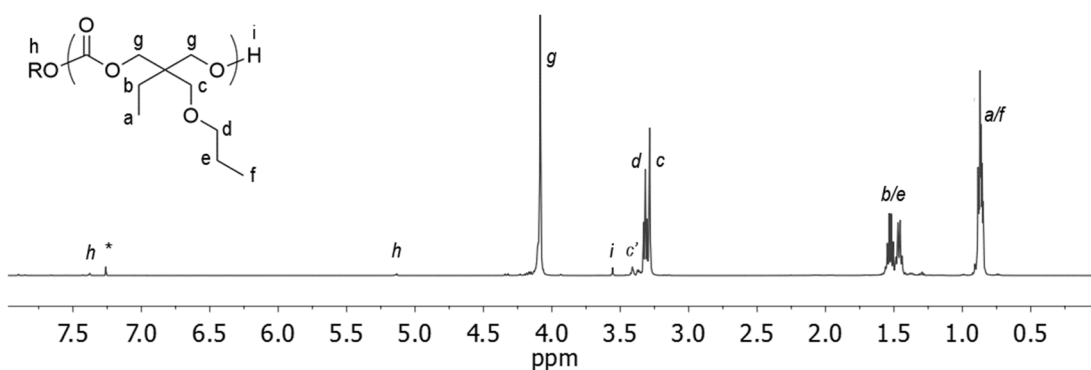


Figure 3.14. ^1H NMR spectrum of PPOMEc₂₃ initiated from BDM, using a catalyst system of 5 mol% DBU and 5 mol% TU (400 MHz, 293 K, CDCl_3 ; * = CHCl_3).

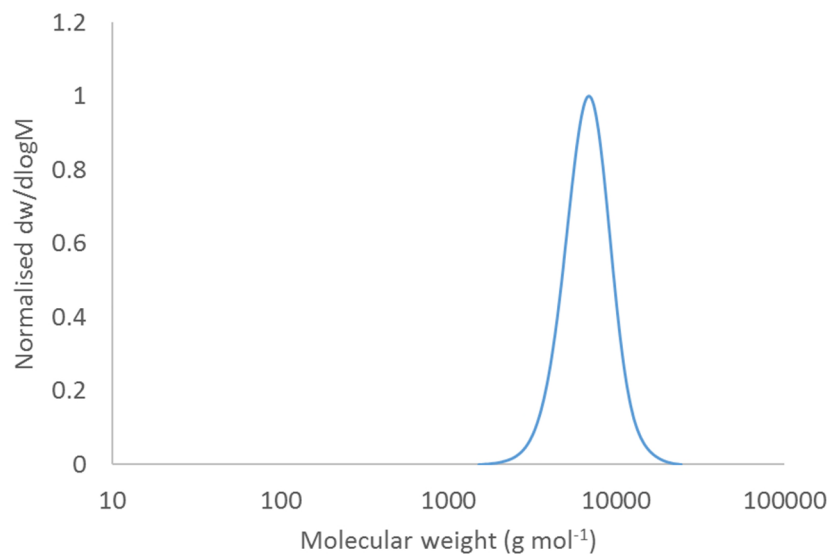


Figure 3.15. Size exclusion chromatogram of PPOMEC₂₃ homopolymer initiated from BDM ($M_n = 5,100$ g mol⁻¹, $\mathcal{D}_M = 1.14$). Sample measured against polystyrene standards using CHCl₃ as eluent.

The homopolymerisation rate of POMECC was observed to be very similar to that of AOMECC under comparable conditions, with the homopolymerisation achieving 78% monomer conversion in *ca.* 155 minutes and 79% monomer conversion in *ca.* 145 minutes respectively. As such, it was hypothesised that a copolymerisation of the two monomers would result in the formation of random copolymers with predictable compositions, without the need for adjustment of feed ratios or limitation of monomer conversion.

A copolymerisation of the two monomers was performed using an initial [AOMECC]₀: [POMECC]₀: [I]₀ ratio of 62.5:62.5:1. As the two monomers and homopolymers possess ¹H NMR spectra with multiple overlapping chemical shifts (Figure 3.16), determination of the reactivity ratios for each monomer in the copolymerisation was not possible. However, the integral of the observed resonance at $\delta = 3.26$ ppm (relating to the methylene signals between the quaternary carbon and the ether group of PAOMECC, and the methylene signals of the carbon adjacent to the

ethyl on the propyl group of PPOMEAC (4H total)) was found to be consistently twice that of the resonance at $\delta = 3.23$ ppm (corresponding to the methylene signals between the quaternary carbon and the ether group of PPOMEAC (2H total)), which indicates that both monomers polymerise at a similar rate (Figure 3.17).

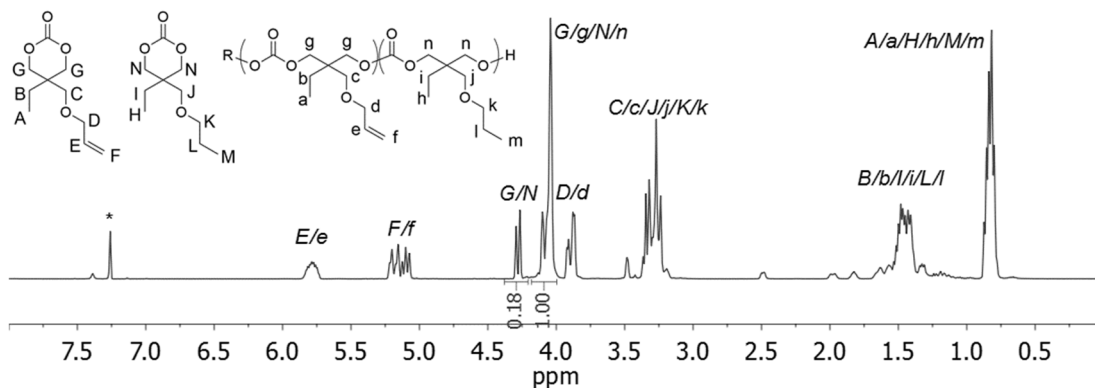


Figure 3.16. ^1H NMR spectrum of POMEAC/AOMEAC copolymerisation taken at 69% monomer conversion. $[\text{POMEAC}]_0:[\text{AOMEAC}]_0:[\text{I}]_0 = 62.5:62.5:1$ initiated from BDM , using a dual catalyst system of DBU (5 mol%) and TU (5 mol%) (400 MHz, 293 K, CDCl_3 ; * = CHCl_3).

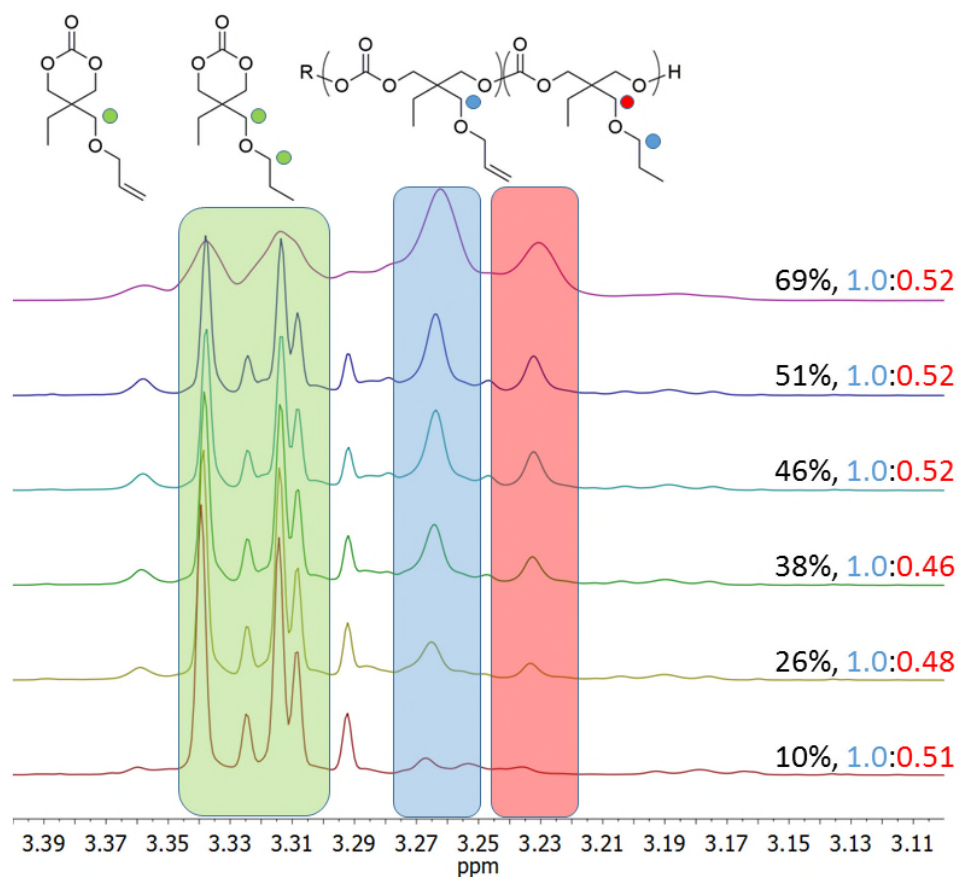


Figure 3.17. Expanded pendent ether-methylene regions of stacked ^1H NMR spectra for the copolymerisation of POMEAC with AOMEAC at different conversions, demonstrating the roughly equal rate of polymerisation of each monomer.

The final composition of the polymer was determined to be 49:51 PPOMEAC:PAOMEAC, in good agreement with the monomer feed ratio. This was determined by subtraction of the integral for the CH_2 methylene resonances of PAOMEAC at $\delta = 3.87$ ppm from the combined integrals of the CH_2 resonances of both polymers at $\delta = 3.20$ - 3.35 ppm ($M_n = 20,100$ g mol $^{-1}$, $D_M = 1.14$) (Figure 3.18).

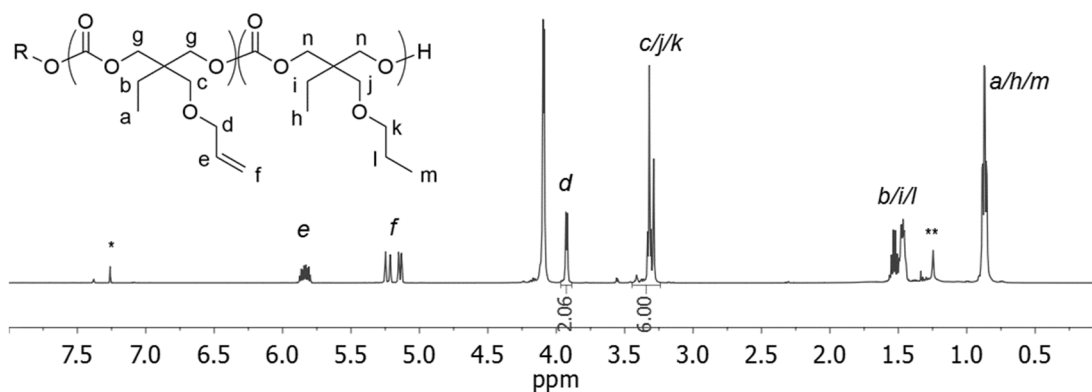


Figure 3.18. ^1H NMR spectrum of P(POMEC₄₉-*co*-AOMEC₅₁) initiated from BDM (400 MHz, 293 K; * = CDCl_3 , ** = residual hexane from precipitation).

Quantitative ^{13}C NMR spectroscopy further confirmed the composition of the copolymer. Expansion of the carbonyl carbon resonances at $\delta = 155.4\text{--}155.3$ ppm revealed three distinct resonances, corresponding to blocky sections of PPOMEC and PAOMEC at $\delta = 155.4$ and 155.3 ppm respectively, and a major peak corresponding to random monomer distribution between these block-sequence resonances. Deconvolution of the ^{13}C NMR spectrum demonstrated that the copolymer was comprised of 25.8 and 27.4% PPOMEC and PAOMEC blocks respectively, with 46.9% of the monomer repeat units being randomly distributed throughout the material. As the copolymer was shown to consist of a 49:51 ratio of POMEC:AOMEC by ^1H NMR and ^{13}C NMR spectroscopy, dyad analysis was performed on the carbonyl carbon resonances assuming a similar ratio of POMEC:AOMEC in the random sequences of the polymer. The average block lengths were found to be 3.21 and 3.30 for POMEC and AOMEC respectively, corresponding to degree of randomness (R) of 0.61. This indicates that the copolymerisation of POMEC with AOMEC using a DBU/TU organocatalyst system tends towards the generation of copolymers of short block segments, with each monomer possessing a similar reactivity ratio (*i.e.* $r_1 = r_2 > 1$).

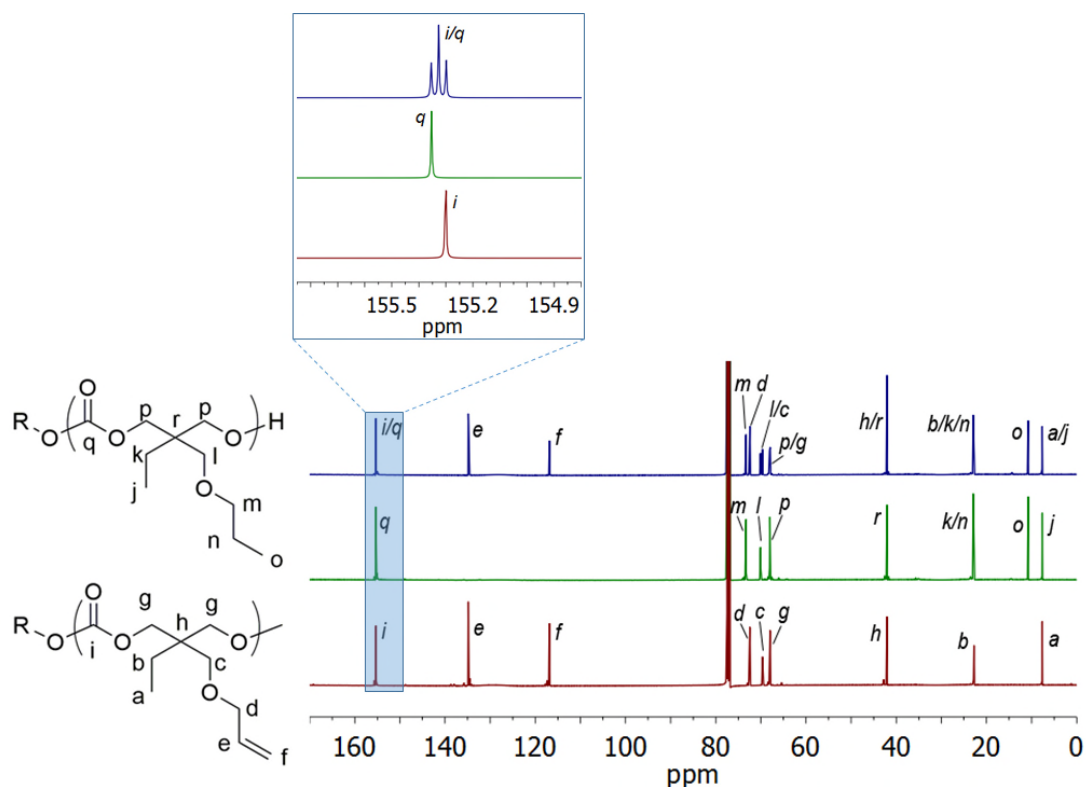
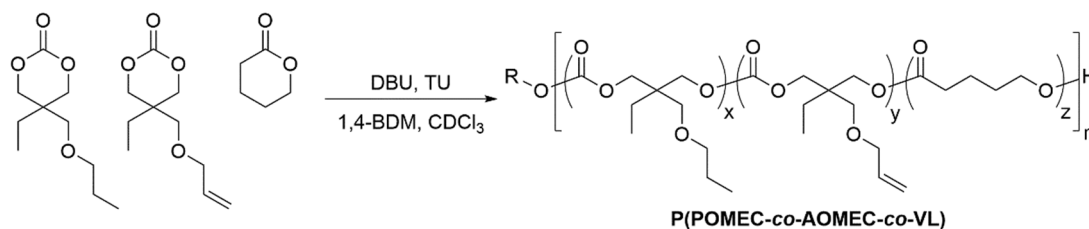


Figure 3.19. Stacked ¹³C NMR spectra of PAOMEC (bottom), PPOMEC (middle) and P(POMEC-*co*-AOMEC) (top), with deconvoluted and expanded carbonyl carbon regions illustrating the presence of minor block-like homopolymer and major random copolymer resonances in P(POMEC-*co*-AOMEC) copolymer (125 MHz, 298 K, CDCl₃).

Having demonstrated that POMEC polymerises at a similar rate as AOMEC, a terpolymer consisting of POMEC, AOMEC and VL was synthesised using the same method applied for the synthesis of P(AOMEC-*co*-VL) copolymers **2-4**. A [POMEC]:[AOMEC]:[VL]:[BDM] feed ratio of 8:8:84:1 was used in an attempt to synthesise a 3-component copolymer analogue of polymer **4**, containing a carbonate:ester ratio of 35:65 (Scheme 3.5).



Scheme 3.5. Synthesis of P(POMECCO-AOMECCO-VL) *via* ring opening polymerisation, using a dual catalyst system of DBU/thiourea and 1,4-benzenedimethanol as initiator.

^1H NMR spectroscopic analysis of the purified polymer revealed that the polymer had a PPOMECCO:PAOMECCO:PVL ratio of 16:17:67, therefore containing a total carbonate:ester ratio of 33:67 (Figure 3.20). The overall composition of the polymer was found to be P(POMECCO₁₀-*co*-AOMECCO₁₁-*co*-VL₄₂) ($M_n = 8,400 \text{ g mol}^{-1}$, $D_M = 1.17$) (Figure 3.21).

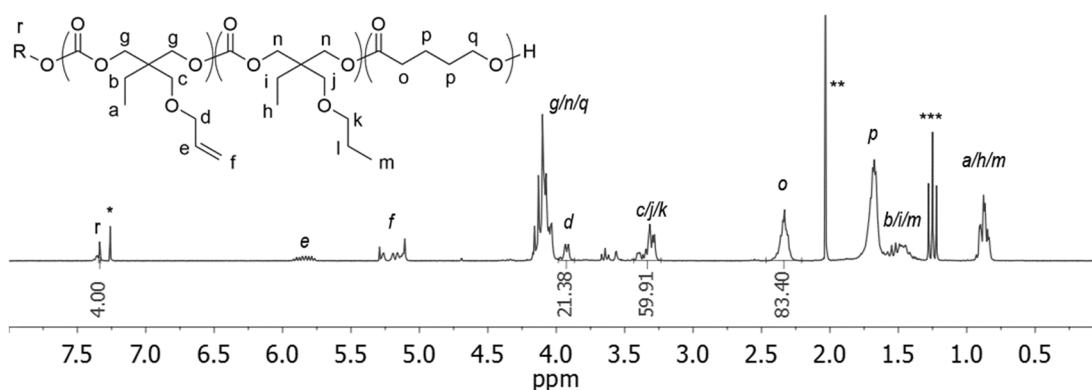


Figure 3.20. ^1H NMR spectrum of P(POMECCO₁₀-*co*-AOMECCO₁₁-*co*-VL₄₂) initiated from BDM (400 MHz, 293 K; * = CDCl_3 , ** = acetone, *** = *n*-hexane).

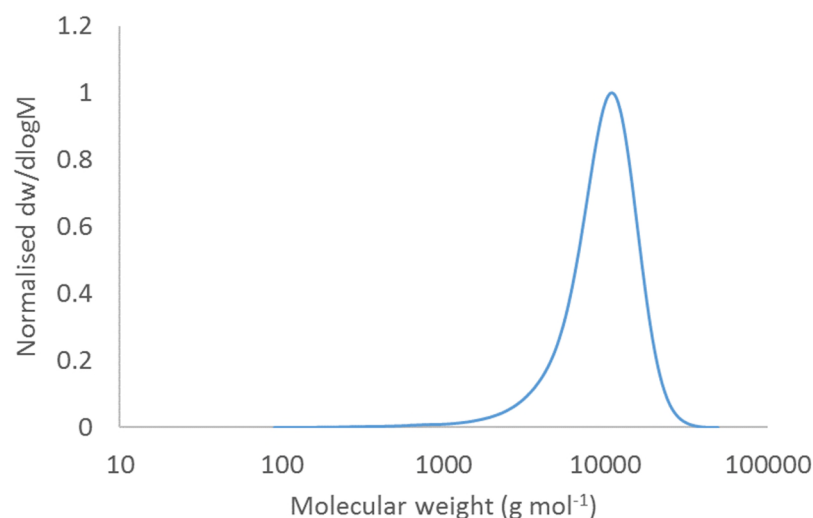


Figure 3.21. Size exclusion chromatogram of P(POMEC₁₀-*co*-AOMEC₁₁-*co*-VL₄₂) copolymer initiated from BDM ($M_n = 10,800 \text{ g mol}^{-1}$, $D_M = 1.17$). Sample measured against polystyrene standards using CHCl_3 as eluent.

The composition of the terpolymer demonstrates that the replacement of the terminal alkene functionality with the non-reactive alkyl group does not appear to have a significant effect on the reactivity ratio of the ester and carbonate. As a result, the incorporation of pendent alkene functionality and carbonate:ester composition of these terpolymers may be tuned independently.

3.3 Conclusions

Random copolymers bearing pendent alkene functionality have been synthesised *via* the organocatalysed ring-opening copolymerisation of VL and AOMECE. Despite the difference in monomer conversion rates, manipulation of monomer feed ratios and limiting the conversion of the carbonate monomer enabled the synthesis of copolymers with highly random monomer distributions. PAOMECE was subjected to hydrolysis in 5 M KOH solution and shown to be hydrolytically degradable, however the degradation was observed to proceed in a highly irregular manner, demonstrating the poor reliability of the degradation method used. In addition, POMECE was synthesised as an alkyl-ether-functional analogue of AOMECE. Replacement of AOMECE with POMECE allowed the incorporation of pendent alkene functionality in the ester:carbonate copolymers to be readily and predictably modified. This demonstrates that the functionalisation density of these materials can be readily tuned independently of carbonate:ester composition. The ability to independently modify the functionalisation density and backbone composition of polyester-carbonate random copolymers may enable the independent tuning of functionalisation density and degradation rate or mechanical properties, making these materials promising candidates for applications in the biomedical field.

3.4 References

- (1) Kohane, D. S.; Langer, R. *Pediatr. Res.* **2008**, *63*, 487.
- (2) Dhandayuthapani, B.; Yoshida, Y.; Maekawa, T.; Kumar, D. S. *Int. J. Polym. Sci.* **2011**.
- (3) Martina, M.; Hutmacher, D. W. *Polym. Int.* **2007**, *56*, 145.
- (4) Anderson, J. M.; Shive, M. S. *Adv. Drug Deliver. Rev.* **2012**, *64*, 72.
- (5) Gunatillake, P.; Mayadunne, R.; Adhikari, R. *Biotechnol. Annu. Rev. Vol 12* **2006**, *12*, 301.
- (6) Domb, A. J. K., Neeraj; Sheskin, Tzviel; Bentolila, Alfonso; Slager, Joram; Teomim, Doron In *Polymeric Biomaterials*; 2 ed.; Dumitriu, S., Ed.; CRC Press: Boca Raton, 2001.
- (7) Manavitehrani, I.; Fathi, A.; Badr, H.; Daly, S.; Shirazi, A. N.; Dehghani, F. *Polymers* **2016**, *8*.
- (8) Vert, M.; Li, S. M.; Spenlehauer, G.; Guerin, P. *J. Mater. Sci. Mater. Med.* **1992**, *3*, 432.
- (9) Woodward, S. C.; Brewer, P. S.; Moatamed, F.; Schindler, A.; Pitt, C. G. *J. Biomed. Mater. Res.* **1985**, *19*, 437.
- (10) Lyu, S. P.; Untereker, D. *Int. J. Mol. Sci.* **2009**, *10*, 4033.
- (11) Gopferich, A. *Macromolecules* **1997**, *30*, 2598.
- (12) Pitt, C. G.; Zhong-wei, G. *J. Control. Release* **1987**, *4*, 283.
- (13) Kimura, Y.; Shirotani, K.; Yamane, H.; Kitao, T. *Macromolecules* **1988**, *21*, 3338.
- (14) Pounder, R. J.; Dove, A. P. *Polym. Chem.* **2010**, *1*, 260.
- (15) Yu, Y.; Zou, J.; Cheng, C. *Polym. Chem.* **2014**, *5*, 5854.

- (16) Chen, W.; Meng, F.; Cheng, R.; Deng, C.; Feijen, J.; Zhong, Z. *J. Control. Release* **2014**, *190*, 398.
- (17) Feng, J.; Zhuo, R.-X.; Zhang, X.-Z. *Prog. Polym. Sci.* **2012**, *37*, 211.
- (18) Fukushima, K. *Biomater. Sci.* **2016**, *4*, 9.
- (19) Tempelaar, S.; Mespouille, L.; Coulembier, O.; Dubois, P.; Dove, A. P. *Chem. Soc. Rev.* **2013**, *42*, 1312.
- (20) Artham, T.; Doble, M. *Macromol. Biosci.*, **2008**, *8*, 14.
- (21) Zhu, K. J.; Hendren, R. W.; Jensen, K.; Pitt, C. G. *Macromolecules* **1991**, *24*, 1736.
- (22) Luinstra, G. A.; Borchardt, E. *Synthetic Biodegradable Polymers* **2012**, *245*, 29.
- (23) Morinaga, H.; Ochiai, B.; Endo, T. *J. Polym. Sci. A: Polym. Chem.* **2006**, *44*, 6633.
- (24) Zhu, W. X.; Huang, X.; Li, C. C.; Xiao, Y. N.; Zhang, D.; Guan, G. H. *Polym. Int.* **2011**, *60*, 1060.
- (25) Cheng, S. X.; Miao, Z. M.; Wang, L. S.; Zhuo, R. X. *Macromol. Rapid Commun.* **2003**, *24*, 1066.
- (26) Jung, J. H.; Ree, M.; Kim, H. *Catal. Today* **2006**, *115*, 283.
- (27) Zhang, Z.; Kuijjer, R.; Bulstra, S. K.; Grijpma, D. W.; Feijen, J. *Biomaterials* **2006**, *27*, 1741.
- (28) Suyama, T.; Tokiwa, Y. *Enzyme Microb. Technol.* **1997**, *20*, 122.
- (29) Tokiwa, Y.; Calabia, B. P.; Ugwu, C. U.; Aiba, S. *Int. J. Mol. Sci.* **2009**, *10*, 3722.
- (30) Diallo, A. K.; Guerin, W.; Slawinski, M.; Brusson, J. M.; Carpentier, J. F.; Guillaume, S. M. *Macromolecules* **2015**, *48*, 3247.

- (31) Pego, A. P.; Zhong, Z. Y.; Dijkstra, P. J.; Grijpma, D. W.; Feijen, J. *Macromol. Chem. Phys.* **2003**, *204*, 747.
- (32) Grijpma, D. W.; Pennings, A. J. *Macromol. Chem. Phys.* **1994**, *195*, 1633.
- (33) Pego, A. P.; Van Luyn, M. J. A.; Brouwer, L. A.; van Wachem, P. B.; Poot, A. A.; Grijpma, D. W.; Feijen, J. *J. Biomed. Mater. Res. Part A* **2003**, *67A*, 1044.
- (34) Nederberg, F.; Lohmeijer, B. G. G.; Leibfarth, F.; Pratt, R. C.; Choi, J.; Dove, A. P.; Waymouth, R. M.; Hedrick, J. L. *Biomacromolecules* **2007**, *8*, 153.
- (35) Hu, X.; Chen, X.; Xie, Z.; Cheng, H.; Jing, X. *J. Polym. Sci. A: Polym. Chem.* **2008**, *46*, 7022.
- (36) Seyednejad, H.; Ghassemi, A. H.; van Nostrum, C. F.; Vermonden, T.; Hennink, W. E. *J. Control. Release* **2011**, *152*, 168.
- (37) Griffith, L. G.; Naughton, G. *Science* **2002**, *295*, 1009.
- (38) Lutolf, M. P.; Hubbell, J. A. *Nat. Biotechnol.* **2005**, *23*, 47.
- (39) Palecek, S. P.; Loftus, J. C.; Ginsberg, M. H.; Lauffenburger, D. A.; Horwitz, A. F. *Nature* **1997**, *385*, 537.
- (40) Sagomonyants, K. B.; Gronowicz, G. In *Comprehensive Biomaterials*; Ducheyne, P., Ed.; Elsevier: Oxford, 2011, p 101.
- (41) Aguirre-Chagala, Y. E.; Santos, J. L.; Aguilar-Castillo, B. A.; Herrera-Alonso, M. *ACS Macro Lett.* **2014**, *3*, 353.
- (42) Yang, J.; Hao, Q. H.; Liu, X. Y.; Ba, C. Y.; Cao, A. *Biomacromolecules* **2004**, *5*, 209.
- (43) Xie, Z. G.; Lu, C. H.; Chen, X. S.; Chen, L.; Wang, Y.; Hu, X. L.; Shi, Q.; Jing, X. B. *J. Polym. Sci. A: Polym. Chem.* **2007**, *45*, 1737.
- (44) Xu, J.; Liu, Z. L.; Zhuo, R. X. *J. Appl. Polym. Sci.* **2006**, *101*, 1988.
- (45) Wang, L. S.; Cheng, S. X.; Zhuo, R. X. *Polym. Bull.* **2014**, *71*, 47.

- (46) Tempelaar, S.; Mespouille, L.; Dubois, P.; Dove, A. P. *Macromolecules* **2011**, *44*, 2084.
- (47) Lohmeijer, B. G. G.; Pratt, R. C.; Leibfarth, F.; Logan, J. W.; Long, D. A.; Dove, A. P.; Nederberg, F.; Choi, J.; Wade, C.; Waymouth, R. M.; Hedrick, J. L. *Macromolecules* **2006**, *39*, 8574.
- (48) Mayo, F. R.; Lewis, F. M. *J. Am. Chem. Soc.* **1944**, *66*, 1594.
- (49) Painter, P. C.; Coleman, M. M. In *Fundamentals of Polymer Science*; Painter, P. C., Coleman, M. M., Eds.; Technomic: Lancaster, PA, 1997, p 107.
- (50) Manders, B. G.; Smulders, W.; Aerdts, A. M.; van Herk, A. M. *Macromolecules* **1997**, *30*, 322.
- (51) van Herk, A. M.; Droge, T. *Macromol. Theory Simul.* **1997**, *6*, 1263.
- (52) Matsuda, H.; Asakura, T.; Miki, T. *Macromolecules* **2002**, *35*, 4664.
- (53) Painter, P. C.; Coleman, M. M. In *Fundamentals of Polymer Science*; Painter, P. C., Coleman, M. M., Eds.; Technomic: Lancaster, PA, 1997, p 1.
- (54) Newmark, R. A. *J. Polym. Sci. A: Polym. Chem.* **1980**, *18*, 559.
- (55) von Burkersroda, F.; Schedl, L.; Gopferich, A. *Biomaterials* **2002**, *23*, 4221.
- (56) Schwach-Abdellaoui, K.; Heller, J.; Gurny, R. *Macromolecules* **1999**, *32*, 301.

4 Microstereolithography of Resins Based on an Alkene-Functional Polycarbonate

4.1 Introduction

Originally developed for the rapid prototyping of new commercial and industrial products, 3D printing (also known as solid freeform fabrication or additive manufacturing) has been the subject of considerable interest in the field of biomedical engineering.¹⁻⁴ Medical imaging techniques such as magnetic resonance imaging (MRI) and computed tomography (CT) can be combined with computer-aided design (CAD) modelling to produce digital 3D representations of prosthetics and biomedical implants with patient-specific dimensions.⁵⁻⁷ The ability of 3D printing techniques to produce materials with complex and diverse geometries in short timeframes can then be harnessed to produce individual, bespoke biomedical devices based on these CAD models.⁸⁻¹¹

There are several methods of 3D printing, the oldest and most widely applied of which is stereolithography (SLA).^{1,12} SLA is favoured for the fabrication of small biomedical devices such as stents, as a result of the range of shapes and sizes that can be produced using this technique, in combination with the resolutions that can be achieved (100-150 μm).^{1,13-15} This process works by the photoinitiated crosslinking of liquid resins to form solid 3D networks, most commonly through the use of acrylate-acrylate, epoxide ring-opening, and to a lesser extent using thiol-ene and thiol-yne crosslinking chemistries.¹⁶⁻¹⁸ 3D objects are produced by first digitally slicing a CAD model into multiple 2D cross-sectional layers, the thickness of which can be tailored depending on the resolution required – thinner layers provide better resolution, however the construction of the object is more time-consuming as a consequence. The physical 3D structure is then afforded by the sequential photopolymerisation of 2D resin layers onto a moveable build platform, typically using UV light (Figure 4.1). Following the curing of each layer, the build platform with the attached cured structure is removed

from the resin along the vertical (Z) axis to allow fresh resin to flow underneath. The platform is then moved back into position at a height suitable for the next layer of resin to be cured and adhered to the structure.^{7,19}

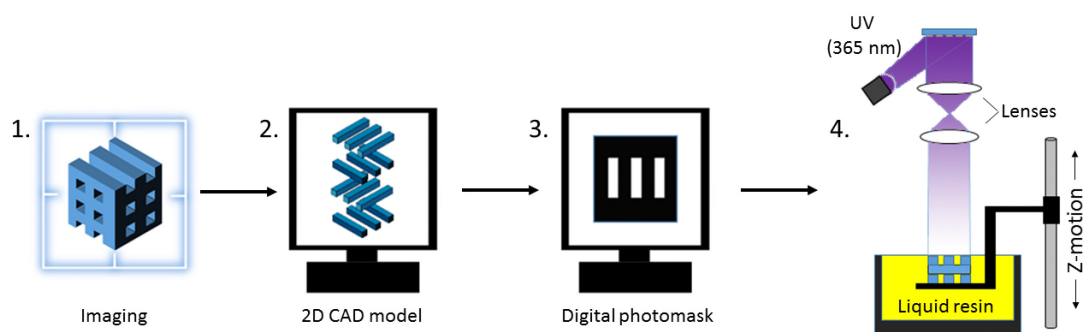


Figure 4.1. Schematic representation of 3D printing by SLA. 1) A target object is scanned and digitally mapped by techniques such as microCT. 2) A digital CAD model is rendered and cut into 2D slices. 3) A digital photomask is rendered for each layer. 4) Using either a scanning laser or a digital mirror device, each layer is then projected sequentially onto a photopolymer, typically using a UV light source to cure the liquid resin. The structure is built upon a moveable build platform, which is moved by the layer height between each projection. The set-up depicted in this figure uses a digital mirror device and a top-down build approach, with the Z-stage moving down into a resin bath between layers.

Resin curing can be achieved either by moving a single beam of light from point-to-point across each 2D cross-section (known as direct laser writing), or through a mask-based approach, where the entire 2D cross-section is cured at once by the simultaneous projection of light in desired areas across the resin (direct light projection, DLP). The latter method requires the use of a digital mirror device (DMD) such as those found in modern screen projectors. This allows the precise control of millions of micro-mirrors for the accurate projection of light in multiple areas simultaneously, and results in greatly reduced fabrication times for multiple parts in comparison to the direct laser writing method.^{1,6,20}

Microstereolithography (μ SL) is a technique which has evolved from SLA. Whilst both techniques operate using the same methods, the development of more accurate lasers for direct laser writing, and DMD projectors with greater resolutions for DLP, have resulted in significant improvements in the resolutions that can be achieved. Whilst SLA can typically achieve resolutions in the region of 150 μ m, μ SL can attain resolutions in the tens of μ m or even lower, offering a significant advantage for the fabrication of devices which require sub-100 μ m definition.^{13,21,22} The development of μ SL is of particular interest for the development of tissue regeneration scaffolds as it allows both the macro and microarchitecture of these implantable devices to be specifically tailored. The microarchitecture of 3D-printed implants has been shown to have an influence on tissue regeneration, with pore size, structure porosity and pore-interconnectivity all shown to affect cell seeding and proliferation in the materials.²³⁻

25

The main limitations of SLA/ μ SL are typically associated with the range of materials which are compatible with the process. One such limitation is that the majority of available photocurable resins require light in the ultra-violet (UV) region of the electromagnetic spectrum to initiate crosslinking.^{1,7,26} The production of UV wavelengths is energy intensive and therefore expensive, as is the equipment necessary to manipulate these wavelengths.^{27,28} However, advances in photoinitiator chemistry have enabled the preparation of resins which are curable using visible and even infra-red light.^{18,27,29-32} The ability to print using light in the visible and infra-red regions of the spectrum negates the need for specialised projection equipment, resulting in simple, low-cost SLA/ μ SL printing, and further increasing the viability of 3D printing for application at the clinical bedside.

Another limitation is that the majority of commercially available printable resins are epoxy- or acrylate-based, and generally do not exhibit good biocompatibility or biodegradability.^{6,33} As such, there has been considerable effort in recent years to develop resins which produce biodegradable and biocompatible constructs. The majority of this work has focussed on resins based on poly(propylene fumarate) (PPF), which has been shown to provide 3D constructs which are both biocompatible and biodegradable.³⁴⁻³⁸ However, crosslinked PPF possesses mechanical properties similar to trabecular bone, and whilst it has been widely applied in the development of skeletal tissue engineering constructs, these properties make it unsuitable for the fabrication of soft tissue devices.³⁶⁻³⁸ Several researchers have reported the chain-end functionalisation of hydrolytically degradable polymers (*e.g.* poly(*D,L*-lactide) (PDLLA), poly(ϵ -caprolactone) (PCL) and poly(trimethylene carbonate) (PTMC) *etc.*) with acrylate or methacrylate groups in order to generate photocrosslinkable materials.^{20,39-46} Whilst these materials possess degradable backbones and suitable mechanical properties for tissue scaffolds, they are not ideal for resin formulation. The reactivity of methacrylates is limited by the steric hindrance and stabilisation of the radical species afforded by the methyl group, whilst concerns remain over the potential cytotoxicity of unreacted acrylate groups in the cured networks.⁴⁶⁻⁴⁸

More promisingly, a small number of photocrosslinkable resins have been reported based on degradable polymers without the use of acrylates. For example, Jansen *et al.* have utilised alkene-alkene crosslinking chemistry to prepare printed materials from fumaric acid monoethyl ester-functionalised three-armed PDLLA oligomers, using *N*-vinyl-2-pyrrolidone (NVP) as a co-monomer.⁴⁹ Through this approach, cell-compatible 3D structures with mechanical properties tuneable across a wide range were successfully produced (ultimate tensile strength (UTS) = 1.3-56.0 MPa, strain at

break = 2.2-106%, Young's modulus (E) = 0.01-2.1 MPa). Heller and co-workers have developed a library of vinyl ester-based resins analogous to commercially available acrylate/methacrylate-based formulations.⁴⁸ The variety of vinyl ester monomers prepared enabled the printing of degradable materials with a range of mechanical properties (impact hardness = 10-150 MPa, E = 0.1-1.9 GPa, with biocompatibility demonstrated by both *in vitro* cell culture and *in vivo* studies. In addition, research by Barker *et al.* has shown that radical thiol-ene addition can be used to print porous structures using an alkene-functional aliphatic polycarbonate (5-methyl-5-allyloxycarbonyl-1,3-dioxan-2-one, MAC) and a multi-armed thiol crosslinker.¹⁸ Mechanical testing demonstrated that the crosslinked materials possessed an elastic modulus comparable with that of cartilaginous tissue (UTS = 3.0 MPa, strain at break = 22.6%, E = 13.1 MPa). More recently, Oesterreicher *et al.* have reported the synthesis of degradable constructs prepared by the photocrosslinking of various alkyne-functional carbonate monomers and a range of multi-armed thiols, with the curing process achieving similar rates to those of comparable acrylate-based systems. The crosslinked materials possessed storage moduli ranging from 257 to 2,346 MPa, dependent on the combination of alkyne monomer and thiol crosslinker used, and displayed similar impact strength to that of poly(lactic acid) (PLA).⁵⁰

A further challenge for the development of SLA-printable scaffolds is the ability to enhance the hydrophilicity or biological activity of the scaffolds post-fabrication.^{9,17} Post-fabrication functionalisation of constructs prepared by SLA can provide a route to materials bearing functional groups which are incompatible with the polymerisation or photocuring processes. However, despite the advantages of such an approach, very few examples have been reported. Shin and co-workers, and separately Lee *et al.*, have reported the surface modification of PPF-based materials with arginylglycylaspartic

acid (RGD) and lysine-arginine-serine-arginine (KRSR), two peptide sequences known to enhance cell adhesion and proliferation.^{51,52} This was achieved by esterification of the free hydroxyl groups of PPF with the terminal carboxylic acid functionality of RGD or KRSR, yielding materials with enhanced osteoblast adhesion and proliferation in comparison to non-functionalised scaffolds. However, with the exception of PPF-based scaffolds, post-fabrication modification of biocompatible, degradable materials prepared by μ SL/SLA has proven challenging, as a consequence of the absence of free reactive functionalities on the cured resins.¹⁹

The ability to fabricate 3D structures bearing reactive functionalities is therefore attractive. This chapter describes the formulation and subsequent 3D printing of photocurable resins based on the degradable alkene-functional polycarbonate, poly(2-allyloxymethyl-2-ethyl-trimethylene carbonate) (PAOMEK) and pentaerythritol tetrakis(3-mercaptopropionate) as a cross-linker in a 1:1 ratio of thiol to alkene groups. Using this resin formulation, a model (10,3)-a mathematical porous network was successfully printed by sequential exposure of 100 μ m-thick layers of resin to a purple light source using mask-based projection μ SL. The partial epoxidation of the pendent alkene-functional groups of PAOMEK using meta-chloroperoxybenzoic acid (mCPBA) is also described. Following resin formulation, a 400 μ m base-plate bearing 100 μ m-high walls was successfully cured, with FT-IR spectroscopy demonstrating that the printing process had no effect on the integrity of the epoxide groups. This illustrates the possibility of functionalising degradable materials prepared by μ SL post-fabrication.

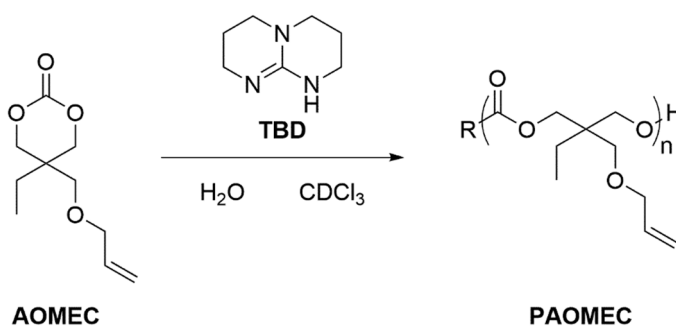
4.2 Results and discussion

4.2.1 Resin formulation

PAOMEK was selected as the alkene-functional polycarbonate component for the preparation of 3D-printed structures, owing to its ease of synthesis and amenity to photoinitiated radical thiol-ene addition, as described in Chapter 2 of this thesis. Typically, the ring-opening polymerisation (ROP) of cyclic monomers must be carried out under dry conditions in order to produce polymers with high, controlled molecular weights.⁵³ The use of dry conditions necessitates the complete exclusion of water, which requires the time-consuming extensive drying of all glassware and reagents. However, since polymers of low molecular weight are desired for the formulation of printable resins with low viscosities, it was envisioned that water could be used as the initiating species for the polymerisation, in a similar manner to that described by Barker *et al.* for the preparation of PMAC-based printable resins.¹⁸ The use of water as initiator would negate the need for thorough exclusion of water from the reaction, thus simplifying the synthesis of large quantities of polymer for resin formulation. As such, the AOMEK monomer was synthesised as previously described in Chapter 2 of this thesis, and dried simply with MgSO₄ to remove excess water.

An initial test polymerisation was performed to determine the level of residual water in the polymer. The polymerisation was conducted in CDCl₃ ([AOMEK] = 2 M), using triazabicyclodecene (TBD, 1 mol%) as a bifunctional organic catalyst (Scheme 4.1). Conversion of the polymerisation was monitored by ¹H NMR spectroscopy, with the monomer achieving 84% conversion in 90 h. The polymerisation was quenched by addition of acidic Amberlyst A15 resin, and purified by flash column chromatography, first using methylene chloride as eluent to remove unreacted monomer, followed by

ethyl acetate for the collection of PAOMEC. ^1H NMR spectroscopy was used to determine the molecular weight of the polymer by comparison of the integral for the side-group methylene resonance of the chain-end unit at $\delta = 3.56$ ppm with the side-group methylene resonances of the main polymer chain at $\delta = 3.32$ ppm, which indicates that the polymer possessed a number-average molecular weight (M_n) of *ca.* 8,000 g mol^{-1} , with degree of polymerisation (DP) = 40 (Figure 4.2). Size exclusion chromatography (SEC) revealed that the polymer possessed a small amount of tailing at low molecular weight, with dispersity (D_M) = 1.37 (Figure 4.3).



Scheme 4.1. Synthesis of PAOMEC *via* TBD-catalysed ROP, using water as the initiating species.

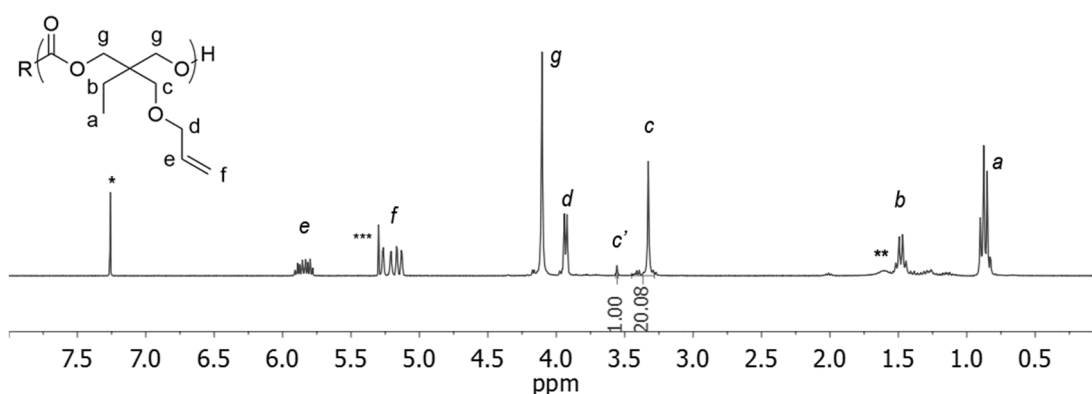


Figure 4.2. ^1H NMR spectrum of DP40 PAOMEC initiated from water, using 1 mol% TBD as catalyst (400 MHz, 293 K; * = CHCl_3 , ** = H_2O , *** = DCM , c' = chain end unit).

In an attempt to reduce the reaction time, the polymerisation was repeated using an increased TBD loading of 5 mol%. This successfully accelerated the rate of polymerisation, with 82% conversion achieved in under 30 minutes. However, the polymerisation proceeded with poor control, with an increase of M_n to 20,500 g mol⁻¹ and of D_M to 1.83 (Figure 4.3).

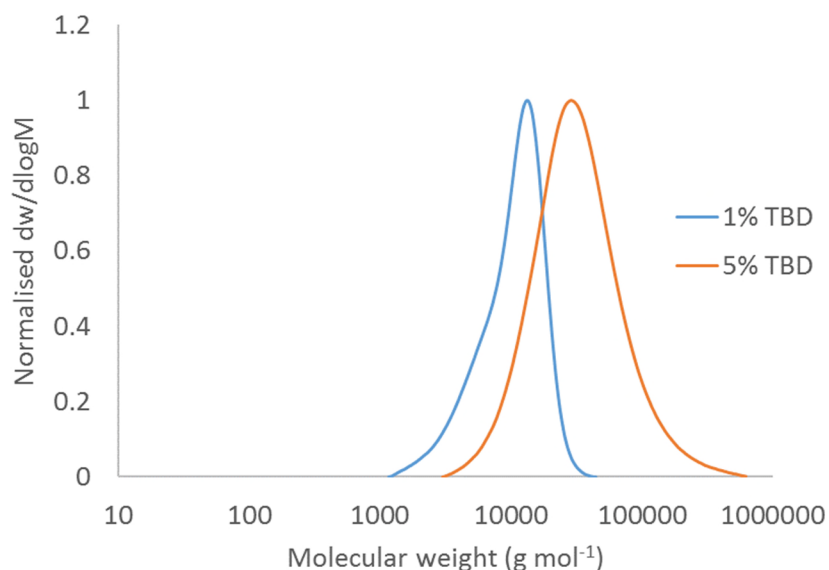
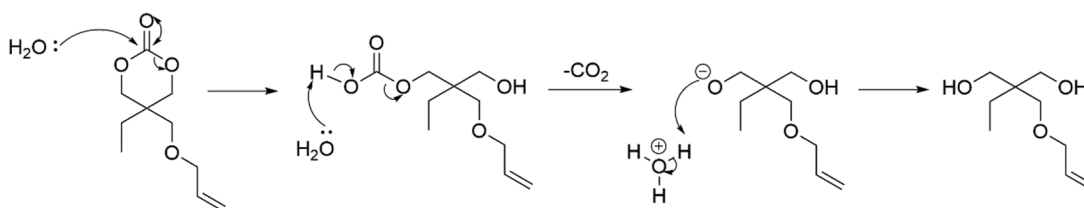


Figure 4.3. Size exclusion chromatograms of PAOMECE initiated from water, using 1 mol% TBD ($M_n = 8,200$ g mol⁻¹, $D_M = 1.37$) and 5 mol% TBD ($M_n = 21,000$ g mol⁻¹, $D_M = 1.83$) as catalyst. Samples measured against polystyrene standards using CHCl₃ as eluent.

The lack of control displayed for the polymerisation catalysed by 5% TBD is proposed to be a consequence of the water-initiated polymerisation mechanism. Water-initiated ROP of cyclic carbonates has previously been shown to proceed firstly by the ring-opening of a single monomer unit to generate an intermediate species bearing carbonic acid and hydroxyl functionality, followed by decarboxylation to yield a bifunctional alcohol species.⁵⁴ Propagation of the polymerisation then proceeds *via* nucleophilic attack of this bifunctional alcohol on additional monomer units, which leads to the generation of telechelic alcohol-terminated polymers (Scheme 4.2).⁵⁴ The nucleophilic

attack of water and subsequent decarboxylation of the carbonic acid species occur at a slower rate than nucleophilic attack by the telechelic chain ends, resulting in propagation proceeding much more quickly than the formation of the bifunctional initiating species (*i.e.* rate of propagation (k_{prop}) > rate of initiation (k_{init})). For the 5 mol% TBD reaction, it is proposed that this effect is exacerbated to the point that the monomer is largely consumed by a small number of propagating chains initiated from decarboxylated AOMEAC units before significant initiation can take place, resulting in the unexpectedly high molecular weight observed. The slight broadening of dispersity observed for the polymerisation catalysed by 1 mol% TBD is also proposed to be the result of this mechanism, however the effect is not as pronounced as a result of the lower catalyst loading and resultant reduced rate of propagation.



Scheme 4.2. Mechanism of nucleophilic attack of AOMEAC by water followed by subsequent decarboxylation of the intermediate carbonic acid-functional species, to yield a bifunctional alcohol initiator.

From the 1 mol% TBD-catalysed polymerisation, the water content was calculated to be roughly 0.8 $\mu\text{L}/\text{mL}$ reaction mixture (*i.e.* 2 mg $\text{H}_2\text{O}/1$ g AOMEAC). To adjust the molecular weight of the polymer, additional water was inserted into the reaction mixture, thereby adjusting the $[\text{M}]_0:[\text{I}]_0$ ratio of the polymerisation. Using this method, PAOMEAC polymers were synthesised targeting M_n values of 1,000, 2,000 and 3,000 g mol^{-1} , resulting in materials with M_n values of 1,500, 2,200 and 3,300 g mol^{-1} . Analysis by SEC indicated that the dispersities of the polymers were 2.43, 1.33, and

1.29 respectively (Figure 4.4). The broad dispersity and higher than expected M_n of the 1,500 g mol⁻¹ polymer is again proposed to be an effect of the slow rate of AOMEC ring-opening by water and subsequent decarboxylation, with the effect becoming more pronounced as a result of the relatively large volume of water added to the reaction (*i.e.* $k_{\text{prop}} > k_{\text{init}}$).

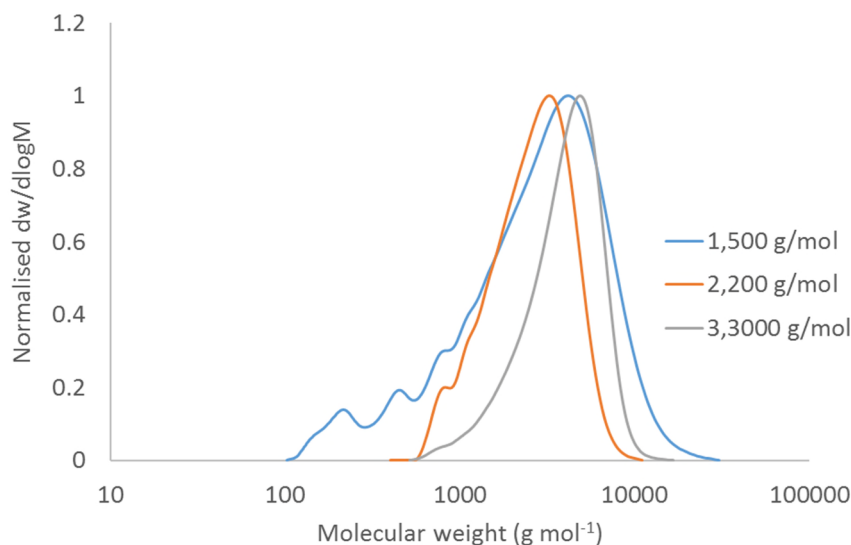


Figure 4.4. Size exclusion chromatograms of PAOMEC initiated from H₂O, with $M_n = 1,500, 2,200$ and $3,300 \text{ g mol}^{-1}$, and \bar{M}_w values of 2.43, 1.33 and 1.29 respectively. Samples measured against polystyrene standards using CHCl₃ as eluent.

The ability to print objects with good feature fidelity is highly dependent on the viscosity of the photocurable resin used. Generally, low-viscosity materials are favoured for SLA/ μ SL as the resins require less time to flow and settle between layer exposures, spread more easily to provide uniform layer thicknesses, flow more readily from the cured material, and require shorter overall exposure times leading to less overcure, thereby reducing build times and increasing feature fidelity.^{33,34,55} As such, rheological testing was performed on the polymers initiated from water to determine their viscosities *via* a shear rate sweep test using a rotational rheometer. As a result of

the viscous nature of the PAOMEK samples, the instrument was equipped with a rotating cone and fixed plane, in order to ensure that the applied shear rates remained constant across the whole of the sample. The polymer samples were subjected to shear rates ranging from 0 to 10 s^{-1} , with each test performed in triplicate and viscosity measured through ascending and descending shear rates. PAOMEK with $M_n = 3,300 \text{ g mol}^{-1}$ was found to have a viscosity ranging from 45,000 to 44,000 mPa s^{-1} , and demonstrated a slight shear-thinning tendency (Figure 4.5). As the upper viscosity limit for printable resins is *ca.* $5,000 \text{ mPa s}^{-1}$, and commercial resins for SLA typically possess viscosities of less than $3,000 \text{ mPa s}^{-1}$, this material was deemed to be too viscous for resin formulation.^{33,56} In comparison, $2,200 \text{ g mol}^{-1}$ and $1,500 \text{ g mol}^{-1}$ PAOMEK possess viscosities of *ca.* $7,900$ and $9,700 \text{ mPa s}^{-1}$ respectively. No change in viscosity was observed over the range of shear rates for both ascending and descending shear rate sweeps, which indicates both Newtonian and non-thixotropic fluid behaviour for both polymers (Figure 4.5). The greater viscosity of the $1,500 \text{ g mol}^{-1}$ polymer in comparison to the $2,200 \text{ g mol}^{-1}$ polymer is likely the result of the broader dispersity and higher weight-average molecular weight (M_w) of the material ($3,700 \text{ g mol}^{-1}$ vs $2,800 \text{ g mol}^{-1}$) resulting in greater chain entanglement. As the $2,200 \text{ g mol}^{-1}$ material possessed the lowest viscosity of the polymers tested, this material was selected for the formulation of printable resins.

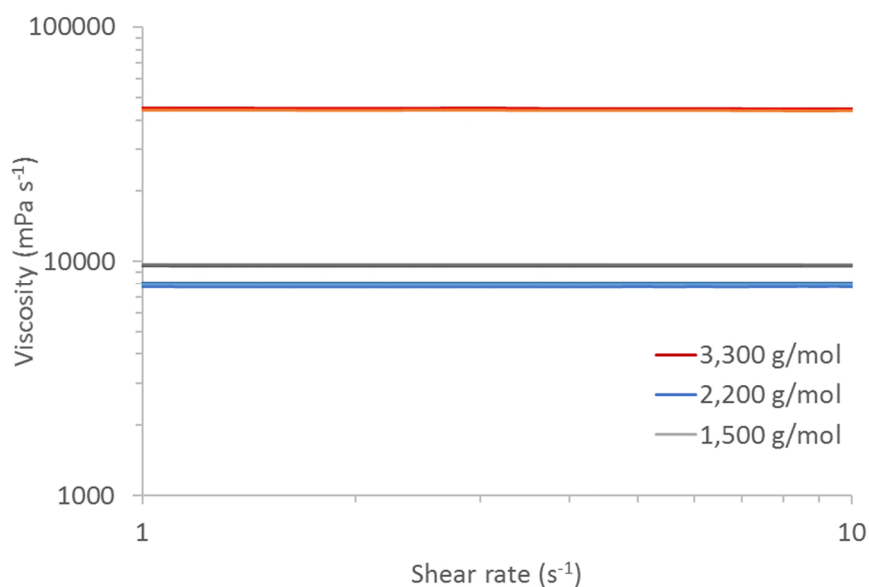


Figure 4.5. Plot of viscosity ($mPa s^{-1}$) against ascending and descending shear rate (s^{-1}) for PAOMEK homopolymers initiated from water with $M_n = 3,300$, $2,200$, and $1,500$ $g mol^{-1}$.

Resins were formulated using PAOMEK as the alkene-functional polymer and pentaerythritol tetrakis(3-mercaptopropionate) (henceforth referred to as tetrathiol) as a 4-arm thiol-functional crosslinker, in a 1:1 molar ratio of pendent alkene to thiol groups. Propylene carbonate (PC) was added as a non-reactive viscosity modifier in loadings of 5, 10 and 20 wt%, and butylated hydroxytoluene (BHT, 0.5 wt%) was included in each mixture as a radical inhibitor, in order to limit unwanted crosslinking on the rheometer plate. Each formulation was then subjected to a shear rate sweep test from 1 to 10 s^{-1} , the results of which are displayed in Figure 4.6.

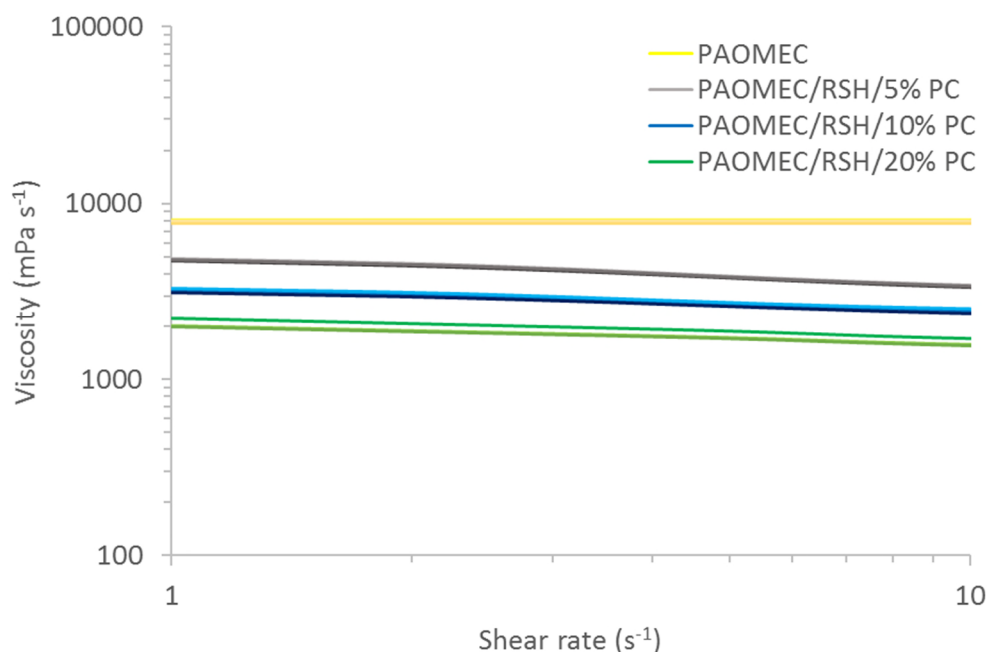


Figure 4.6. Plot of viscosity (mPa s^{-1}) against ascending and descending shear rate (s^{-1}) for PAOMEK homopolymer ($M_n = 2,200 \text{ g mol}^{-1}$) and resin formulations containing PAOMEK, tetrathiol crosslinker (RSH) and 5, 10 and 20 wt% propylene carbonate (PC) as viscosity modifier.

The viscosity of the materials decreases with the addition of the thiol crosslinker and propylene carbonate, with each of the formulations displaying slight shear-thinning behaviour. The effect is consistent across triplicate runs for each sample, and becomes less pronounced with increasing PC content. This shear-thinning behaviour was postulated to be the result of a minimal amount of light-induced resin crosslinking, even in the presence of BHT and absence of photoinitiator. As such, rheometry was repeated using increased loadings of radical inhibitor, however similar results were obtained. Alternatively, the observed shear-thinning behaviour may result from the difficulty associated with measuring low-viscosity fluids at low shear rates, and is therefore potentially simply an artefact of the rheology measurement process.

Resins containing 20 wt% PC were shown to have the lowest, and therefore most suitable viscosity for printing (viscosity = $1,792 \pm 94$ mPa s⁻¹ at shear = 5 s⁻¹). As such, an attempt was made to prepare uniform dogbone-shaped samples for mechanical testing using this formulation. The formulation was mixed with a UV-sensitive photoinitiator, bis(η -5-2,4-cyclopentadien-1-yl)-bis(2,6-difluoro-3-(1H-pyrrol-1-yl)-phenyl) titanium (Irgacure 784) in the absence of light to generate a photocurable resin. The resin was loaded into a 1.5 mm-thick stainless steel plate containing dogbone-shaped templates backed with a removable polypropylene transparent film. The loaded plate was then exposed to UV light to photocure the resin into dogbone-shaped samples with uniform length, width and height. Following postcuring of the resin, the poly(propylene) film was removed from the metal plate, and the crosslinked PAOMECEC/tetrathiol resin stamped from the stencils. However, it was immediately apparent that this resin formulation was not suitable for use as a photopolymerisable resin, as the cured dog-bone samples were not able to maintain their form following removal from the stencil. The low mechanical strength is likely a consequence of the high PC diluent content of the materials preventing the formation of a contiguous crosslinked network throughout the sample.

The experiment was repeated using the formulation containing 10 wt% PC (viscosity = $2,694 \pm 69$ mPa s⁻¹ at shear = 5 s⁻¹). Whilst more viscous than the formulation containing 20 wt% PC and most commercial resins, a viscosity of *ca.* $2,700$ mPa s⁻¹ is still within acceptable viscosity limits for printing.³⁰ Using this resin formulation, uniform dogbone-shaped samples were successfully cured, and the mechanical strength of the material was assessed through uniaxial tensile testing. The materials were stretched at a rate of 2 mm min⁻¹ until failure on a Tensiometric M100-1CT tensiometer, displaying an ultimate tensile strength of 1.8 ± 0.2 MPa and strain at break

of $17.5 \pm 2.4\%$, with an average Young's modulus of 10.6 ± 0.8 MPa (Figure 4.7). The material also displayed elastic deformation until failure, and cyclic extension/relaxation tests repeated 10 times up to 12% strain demonstrated that the material repeatedly returned to its original dimensions with no observed permanent deformation or loss of mechanical strength (Figure 4.8). As this resin formulation possessed an acceptably low viscosity and provided cured materials with reasonable mechanical properties, it was selected for the preparation of 3D-printed porous materials.

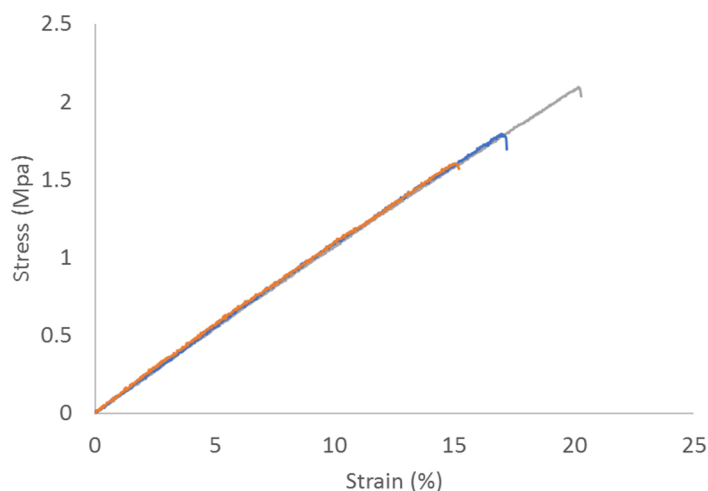


Figure 4.7. Plot of stress (MPa) against strain (%) for photocured resin samples, displaying elastic deformation until failure.

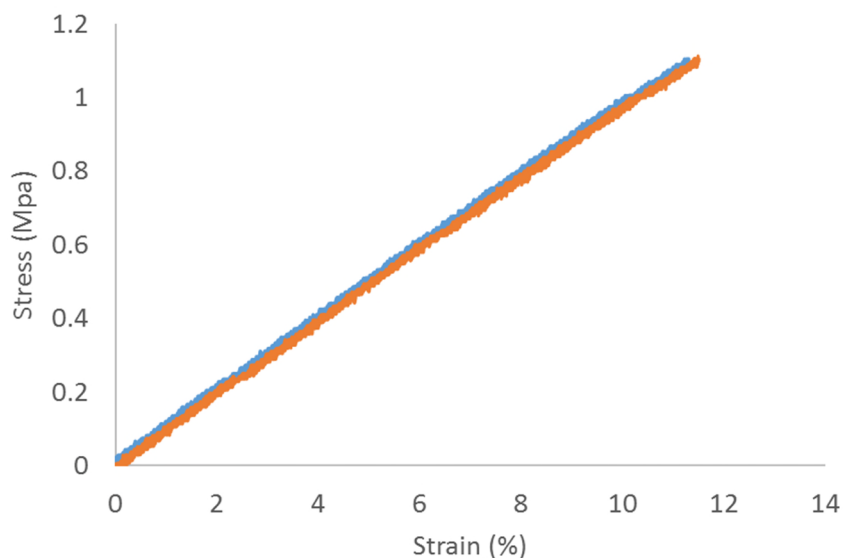


Figure 4.8. Plot of stress (MPa) against strain (%) for cyclic extension tests of photocured resin samples, displaying no deformation or loss of modulus over 10 cycles.

4.2.2 3D Printing

Prior to building 3D structures, it was necessary to obtain a resin composition possessing suitable curing times under exposure to a purple light source (peak output = 415 nm). A series of resins based on formulations containing 10 wt% PC were prepared with different loadings of photoinitiator and photoinhibitor. Bis(2,4,6-trimethylbenzoyl)-phenylphosphine-oxide (Irgacure 819) was selected as the photoinitiator, as it has previously demonstrated low cytotoxicity and absorbs strongly in the UV and purple regions of the electromagnetic spectrum (200-420 nm).⁵⁷ In contrast, other photoinitiators which absorb light strongly in the purple region of the spectrum typically also absorb light at higher wavelengths (*e.g.* > 500 nm for Irgacure 784), thus making them more prone to unwanted initiation from ambient light. A photoinhibitor was included as it is often necessary to limit the cure depth of the resin in order to maintain feature fidelity during the printing process.^{58,59} Kalsec Durabrite Oleoresin Paprika Extract NS was selected as the photoinhibitor as its absorption

spectrum extends across the transmission spectrum of the purple light engine used.¹⁸ The different resin formulations were loaded onto glass slides and exposed to a rectangular projection of purple light for different exposure times, before removal of uncured resin by rinsing the slides with isopropanol followed by acetone, thus enabling the determination of cure times necessary for the generation of rectangular cured materials with uniform cure depths and well-defined edges. Initial tests were performed using loadings of 0.5-2 wt% photoinitiator and 0.25 wt% photoinhibitor. For formulations containing 0.5 wt% photoinitiator, exposure times of 60 s were required to cure a material with approximately defined edges and corners. Increasing photoinitiator loading to 1 wt% resulted in a similarly-defined rectangle being afforded in 30 s, whilst increasing loadings to 2 wt% enabled the curing of a well-defined rectangle in the same time (Figure 4.9, images A-C). Additional experiments were performed using 0.5 wt% photoinitiator in the absence of inhibitor. In contrast to the resins containing paprika extract, these resins unexpectedly produced sharply-defined rectangles following 30 s exposure to the purple light source (Figure 4.9, image D). As such, this inhibitor-free resin was selected for initial printing tests.

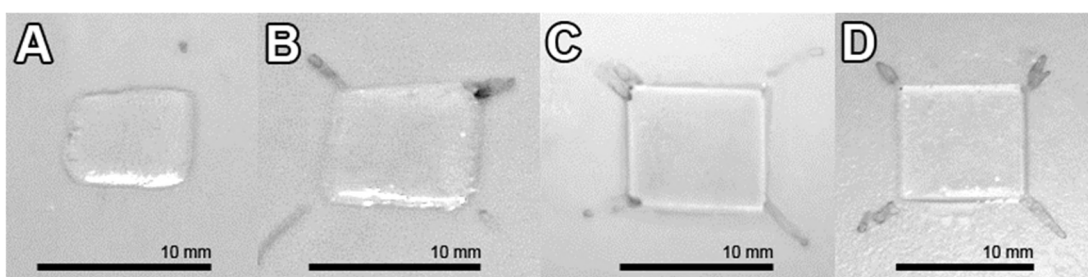


Figure 4.9. Photographs of resin formulations cured by exposure to rectangular projections of purple light. All samples pictured were exposed for 30 s, using photoinitiator/inhibitor loadings of (A) 0.5/0.25 wt%, (B) 1.0/0.25 wt%, (C) 2.0/0.25 wt% and (D) 0.5/0 wt%.

A layer-by-layer, projection-based curing method was used to cure the resin into 3D structures. The system was comprised of a commercially available DMD video projector (BenQ W1000+) modified by replacement of the light source with a purple light engine (peak output = 415 nm) and replacement of the built-in colour wheel with a monochromatic purple light filter. A 45° mirror was used to direct the projected image vertically through a transparent-bottomed polydimethylsiloxane (PDMS) resin tray, and a build platform attached to linear motion stage moveable along the Z-axis was employed to control layer thickness (Aerotech ATS100-100_UF). The printing setup was enclosed in a light-proof box (including a removable access door, formed from transparent orange perspex acrylic in order to enable observation of builds in-progress whilst excluding UV and purple light from the system), thus ensuring no unwanted cross-linking was induced by ambient light during the printing process. The motion of the Z-stage was computer-controlled using Aerotech Ensemble Motion Composer Suite, with the Z-stage moved up by the desired resolution distance in between layers. CAD representations of the desired structures were cut into 2D-slices of desired thickness using Perfactory RP 2.6 software. These slices were then rendered as black and white slides in PowerPoint to create a dynamic pattern mask, and projected layer-by-layer in sequence onto the resin in order to generate the desired 3D structure in solid form. The setup of the printing system is displayed in Figure 4.10.

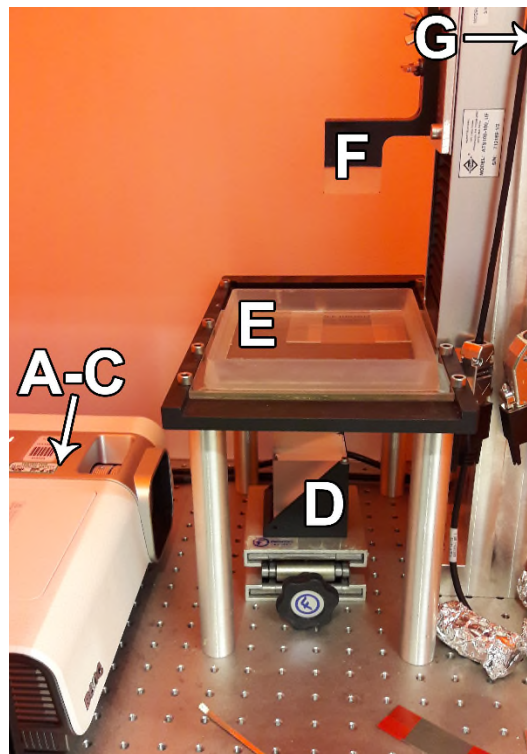
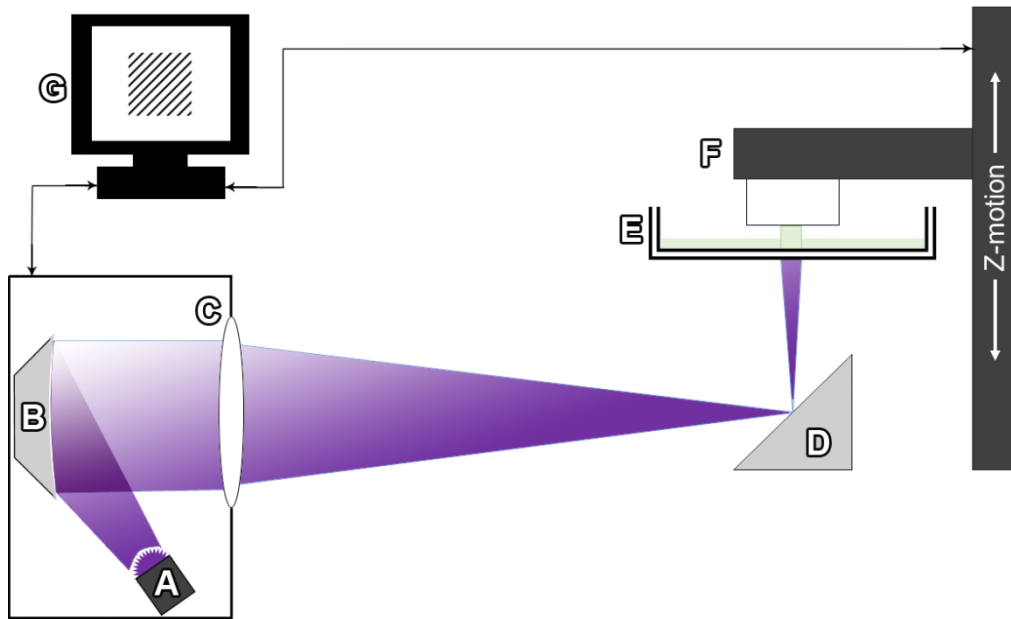
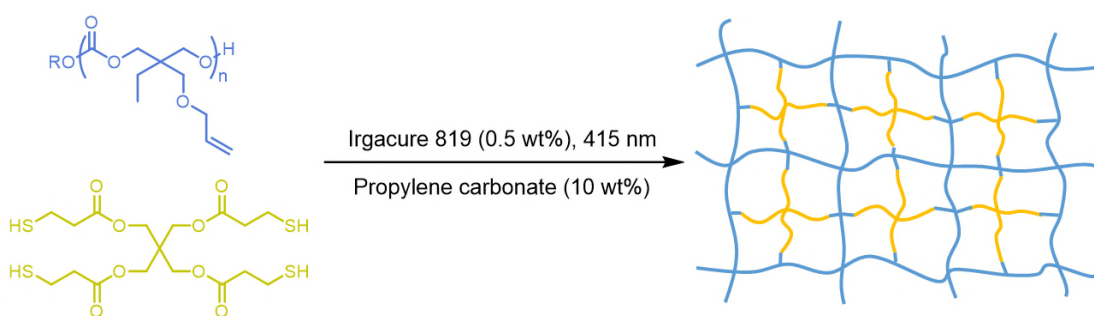


Figure 4.10. Schematic and photographic representation of μ SL setup. A = purple light engine with peak output at 415 nm; B = digital mirror device for mask projection; C = focussing optics; D = 45° mirror; E = transparent silicone resin tray; F = build platform mounted on a motion stage moveable along the Z-axis; G = computer system for control of exposure times and build platform movement.

The first stage of each print was to construct a 400 μm -high baseplate of the crosslinked PAOMEC/tetrathiol resin, in order to provide a favourable surface for adhesion of more complex structures to the build plate during printing. This was achieved by loading the resin formulation into the resin tray and lowering the Z-stage to a height of 100 μm above the base of the tray, followed by projection of purple light through a rectangular area of resin for 30 s (Scheme 4.3). The Z-stage was then moved up by 500 μm in order to allow the resin to refill the void created by curing the initial layer, before being lowered by 400 μm (*i.e.* its initial position minus 100 μm) and exposing a second resin layer to light for 30 s, thus growing the baseplate by a height of 100 μm . The time allowed for Z-stage movement and resin refilling between exposures totalled 45 s. The process was repeated twice more to generate the 400 μm -high rectangular baseplate.



Scheme 4.3. Synthesis of 3D crosslinked networks by radical thiol-ene addition, using Irgacure 819 as photoinitiator, propylene carbonate as viscosity modifier, and purple light with a peak output at 415 nm to initiate crosslinking.

Whilst the large area and low detail required allowed exposure times of 30 s to be used for the construction of the baseplate, the cure time required for good adhesion between layers for intricate structures remained to be established. The required cure time was determined through the building of parallel 100 μm -thick and 1 mm-high walls through sequential exposure of resin layers to the purple light source. As an initial test,

a height of 100 μm per layer was selected for the building of walls, with purple light projected for different lengths of time for each wall (starting at 15 s and increasing in 5 s intervals). Only when sufficient curing and adhesion had taken place could the walls be printed. Following the test build, the minimum cure time required to ensure good adhesion between layers and therefore for the successful building of detailed structures was determined to be 40 s per layer (Figure 4.11 and 4.12). Furthermore, the use of a layer height of 100 μm was found to provide well-resolved structures, with no observed defects in the X and Y axes, and no overcure observed in the Z-axis, indicating that the cure depth is roughly equal to this layer height. No further optimisation of the layer height was performed in this proof-of-concept study.



Figure 4.11. Exposure pattern progression used for the building of 1 mm-high walls. Each 100 μm resin layer was exposed to all 5 projections sequentially, with the pattern progressing every 5 seconds.

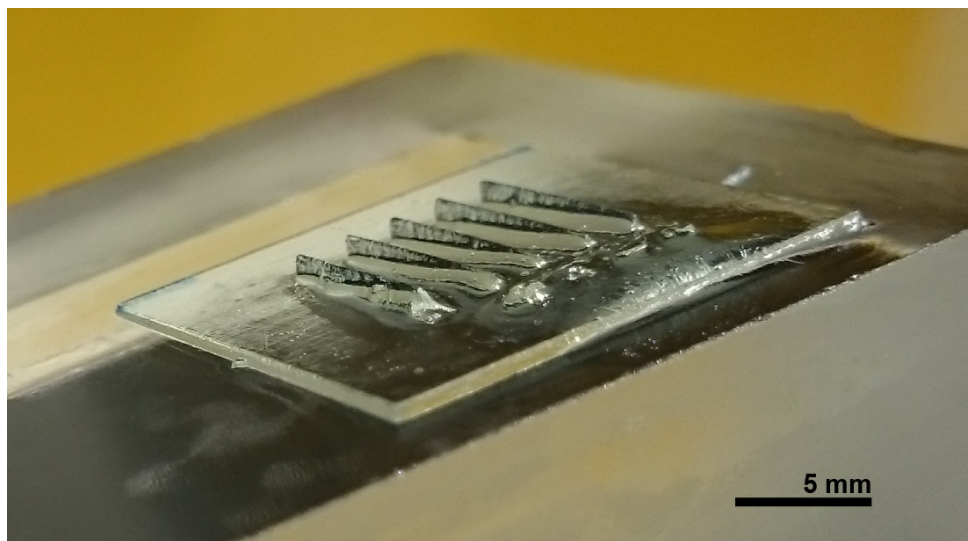


Figure 4.12. Photograph of 1 mm-high walls produced by μSL using exposure times of (left to right) 35, 40, 45, 50 and 55 seconds.

The established resin formulation and cure time were applied to an attempted print of a 0.9 cm³ (10,3)-a porous mathematical network, using a CAD model retrieved from the website of Prof. George. W. Hart,⁶⁰ in order to demonstrate the potential of the resin for the synthesis of complex structures through μ SL. The sample was constructed on a 400 μ m baseplate by exposure of 100 sequential layers to purple light, with each layer totalling 100 μ m in height. Each layer was cured for 40 s, with 45 s allowed between each layer for Z-stage movement and resin filling, resulting in a total build time of *ca.* 145 minutes. Following completion of the build, the structure was rinsed with isopropanol and acetone to remove residual resin from the construct, and post-cured by exposure to UV light for 20 minutes to yield the final structure, which possessed good feature fidelity and interconnected pores running throughout the structure (Figure 4.13). The dimensions of the cured structure were measured to be 8.90 \times 8.96 \times 8.70 mm, indicating overall shrinkage of the material of 5% during the curing process, however this shrinkage can be compensated for by changing the scale of the CAD model in the Perfactory software. Analysis by micro-computed tomography (micro-CT) demonstrated that the construct possessed an interconnected porous network running through all three axes of the structure (Figure 4.14). The ability to successfully print a complete (10,3)-a porous network using a PAOMEK-based resin in the absence of photoinhibitor represents a significant improvement on the partial (10,3)-a network fabricated using a MAC-based thiol-ene resin as previously reported by Barker *et al.*, which also required the use of a photoinhibitor to reduce significant overcure in the vertical axis of the structure.¹⁸

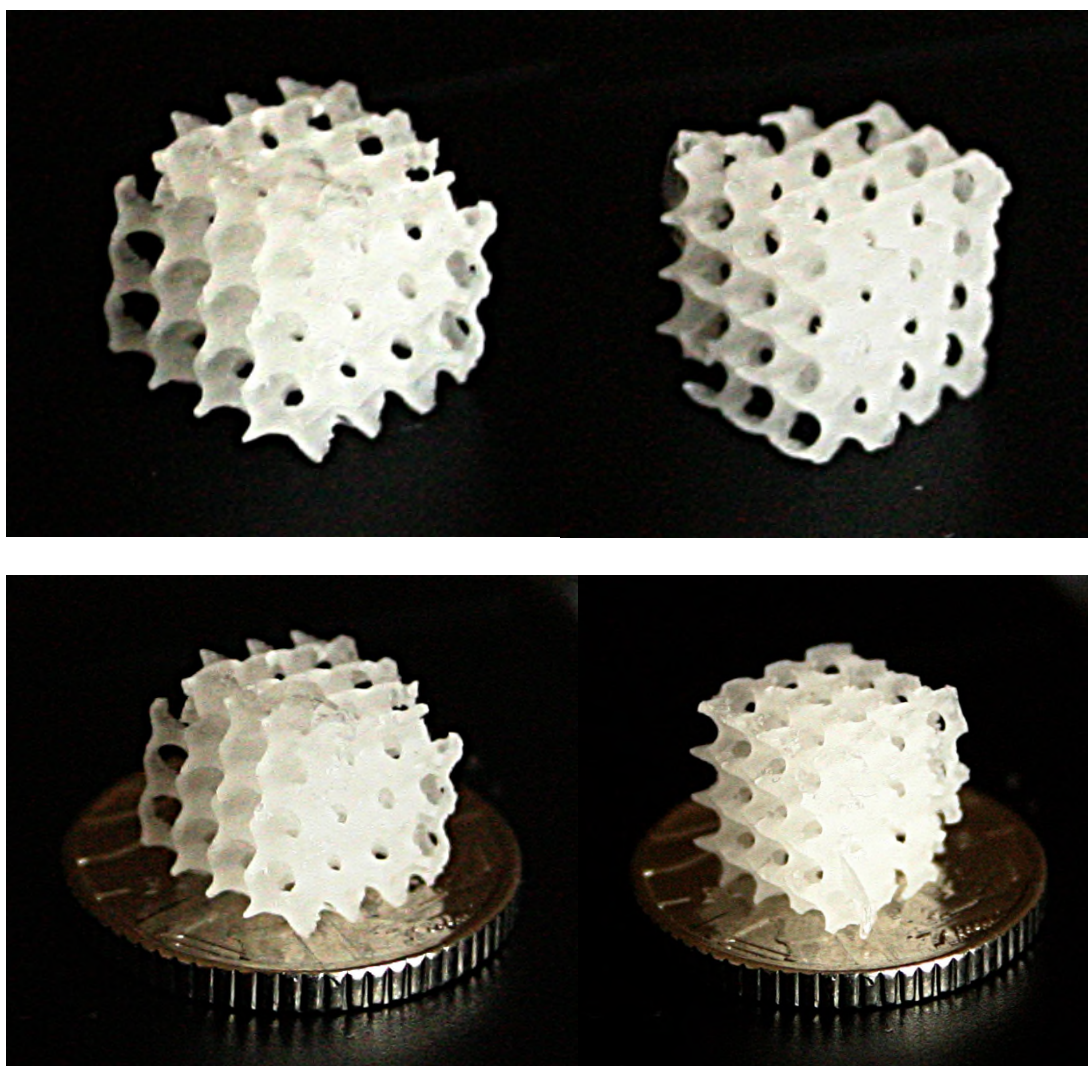


Figure 4.13. Photographs of (10,3)-a mathematical network produced by μ SL of PAOMEC-based resin, displaying good feature fidelity and interconnected pores running through structure, with structure placed on a 5 pence piece in lower photographs to illustrate scale.

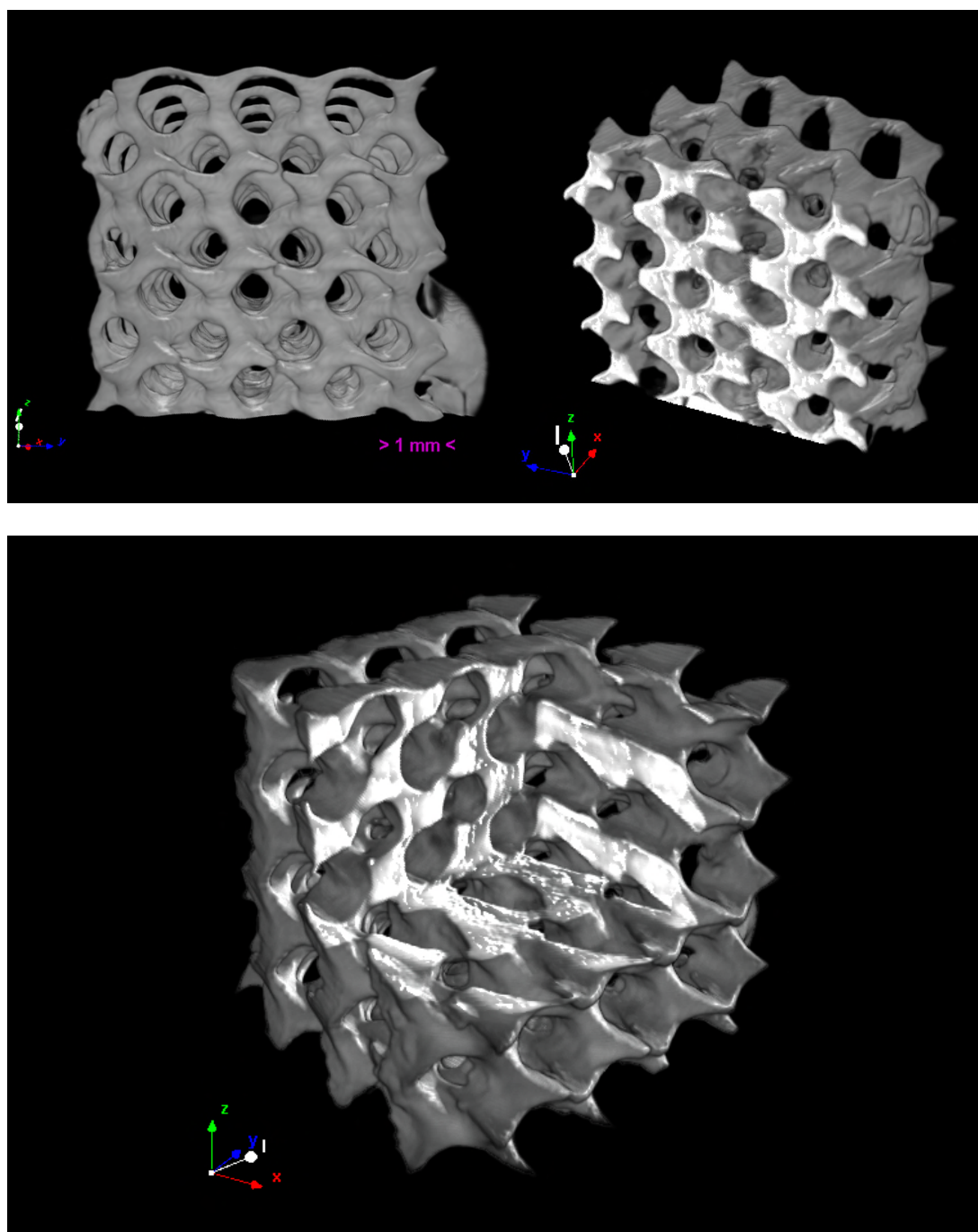


Figure 4.14. Micro-CT images of (10,3)-a mathematical network produced by μ SL of PAOMEC-based resin. Top left: image of complete structure viewed along a single axis. Top right: image of interior structure, showing the presence of interconnected pores in a single plane. Bottom: rectangular cutaway of structure, showing the porous nature of the construct through all three axes.

As the cured resin is insoluble in common deuterated solvents, characterisation of the structure was not possible using NMR spectroscopy, therefore the structure was analysed using FT-IR spectroscopy. The appearance of an ester C=O stretch at 1800 cm^{-1} confirms the presence of the tetrathiol linker in the cured and washed structure, and the success of the crosslinking reaction was evidenced by observed decreases in the intensity of absorptions associated with the monosubstituted alkene group (sp-hybridised C-H stretch at 3080 cm^{-1} and sp^2 -hybridised C-H bend at 943 cm^{-1}). The absence of any absorbance from $2650\text{--}2550\text{ cm}^{-1}$ associated with S-H bond stretching indicates the absence of free thiol groups, suggesting that the crosslinking reaction proceeds with near-quantitative conversion (Figure 4.15).

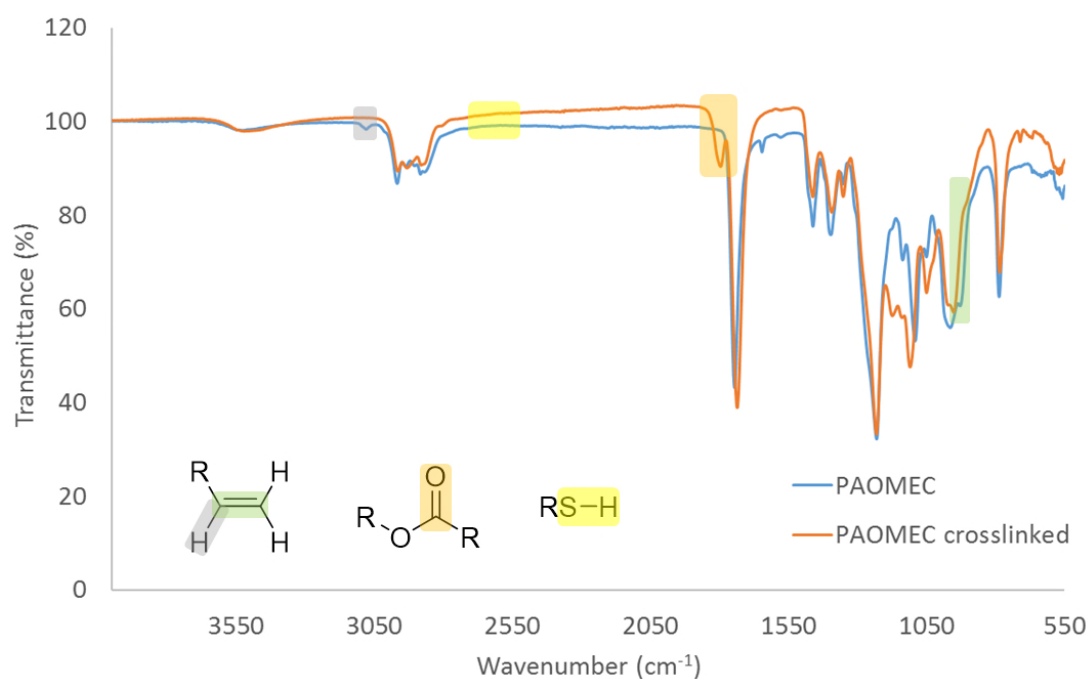
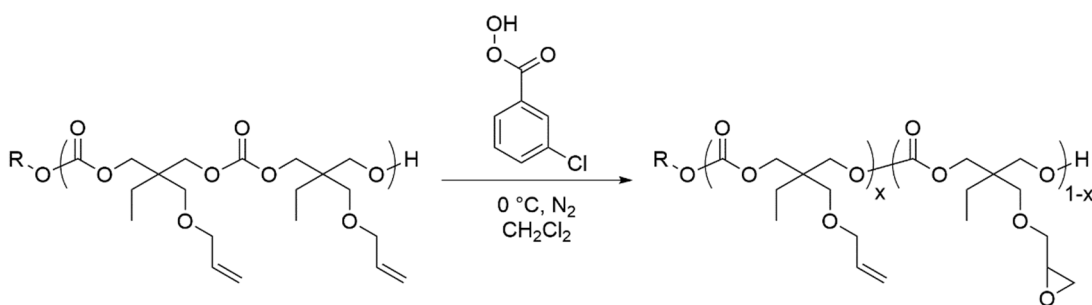


Figure 4.15. FT-IR spectra of PAOMEC and crosslinked PAOMEC-based resin, with key absorptions and absences highlighted.

4.2.3 Synthesis and printing of materials bearing epoxide functionality

Several research groups have demonstrated the potential of modifying alkene-functional polycarbonates through the epoxidation of pendent allyl groups, thus providing a method of functionalising the polymer without requiring the use of radical thiol-ene addition.⁶¹⁻⁶⁵ As such, it was envisaged that partially epoxidising low molecular weight PAOMEK may afford a resin which could be photocured through radical thiol-ene addition, whilst leaving the epoxide functionality available for post-fabrication modification of the 3D constructs.

PAOMEK ($2,100 \text{ g mol}^{-1}$) was epoxidised by addition of meta-chloroperoxybenzoic acid (mCPBA) at 0°C under an inert atmosphere, using an alkene:mCPBA molar ratio of 2:1.1 and methylene chloride as solvent. After 6 h, the reaction mixture was filtered and washed with saturated sodium hydrogen carbonate solution, before precipitation into *n*-hexane to yield the alkene- and epoxide-functional poly(2-allyloxymethyl-2-ethyltrimethylene carbonate)-*co*-(2-(oxiranyloxy)methyl-2-ethyl trimethylene carbonate) (P(AOMEK-*co*-OOMEK) (Scheme 4.4).



Scheme 4.4. Synthesis of polymer bearing both alkene and epoxide pendent functionalities (P(AOMEK-*co*-OOMEK)) by post-polymerisation modification of PAOMEK.

The composition of the copolymer was determined by ^1H NMR spectroscopy. Comparison of the integrals of the resonances corresponding to the ethylene proton of

the alkene group at $\delta = 5.85$ ppm, and the methine proton of the epoxide group at $\delta = 3.10$ ppm indicated that the copolymer possessed an alkene:epoxide ratio of 50:50 (Figure 4.16), with SEC indicating that the polymer was not degraded during the reaction (Figure 4.17).

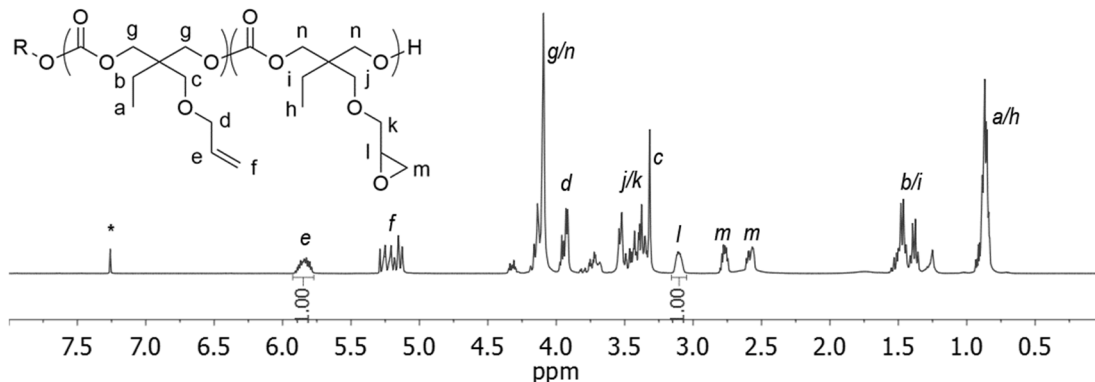


Figure 4.16. ¹H NMR spectrum of P(AOMEC₅-co-OOMEC₅) synthesised by partial epoxidation of PAOMEC₁₀ with mCPBA (400 MHz, 293 K, CDCl₃; * = CHCl₃).

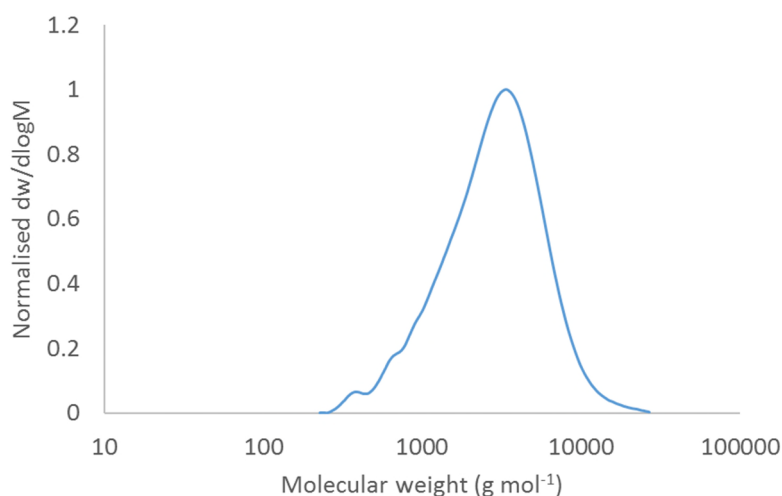


Figure 4.17. Size exclusion chromatogram of P(AOMEC₅-co-OOMEC₅), with $M_n = 2,700$ g mol⁻¹ and $\mathcal{D}_M = 1.31$. Sample measured against polystyrene standards using CHCl₃ as eluent.

Comparison of the FT-IR spectra of the homo and copolymer further confirmed the presence of the epoxide functionality. The majority of absorptions associated with epoxides are obscured by absorptions associated with either the ether functionality,

(1089 cm^{-1}), monosubstituted alkene functionality (943 cm^{-1}), or general C-H stretching signals (2970 cm^{-1}), however there is a distinct absorption in the epoxidised polymer sample visible at 800 cm^{-1} , which corresponds to the C-O-C stretching of the oxirane group (Figure 4.18).

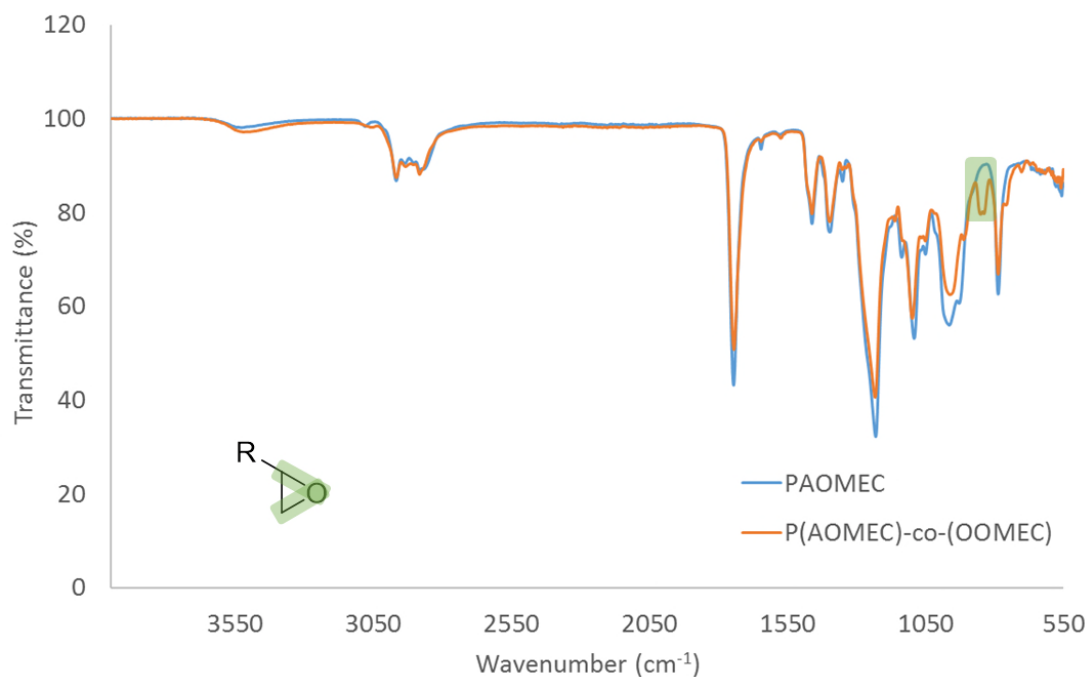


Figure 4.18. FT-IR spectra of PAOMECE and P(AOMECE-co-OOMECE), with oxirane C-O-C stretch highlighted.

A photocurable resin was formulated using P(AOMECE₅-co-OOMECE₅) and tetrathiol crosslinker, using a 1:1 molar ratio of alkene:thiol groups. Propylene carbonate was incorporated as a viscosity modifier (10 wt%), and Irgacure 819 used as photoinitiator (0.5 wt%). Following formulation, a 400 μm baseplate was successfully printed using μSL through sequential curing of 100 μm -thick layers. However, exposure times of 120 s per layer were required for the formation of a reasonably uniform baseplate, representing considerably longer curing times in comparison to the PAOMECE homopolymer-based resin. In order to determine the curing times required to adhere detailed structures to the baseplate, a print of parallel 100 μm -thick and 100 μm -high

lines was attempted, with each line cured for different lengths of time (starting at 115 s and increasing in intervals of 10 s). A well-defined line was cured following exposure to the purple light source for 155 s (Figure 4.19).

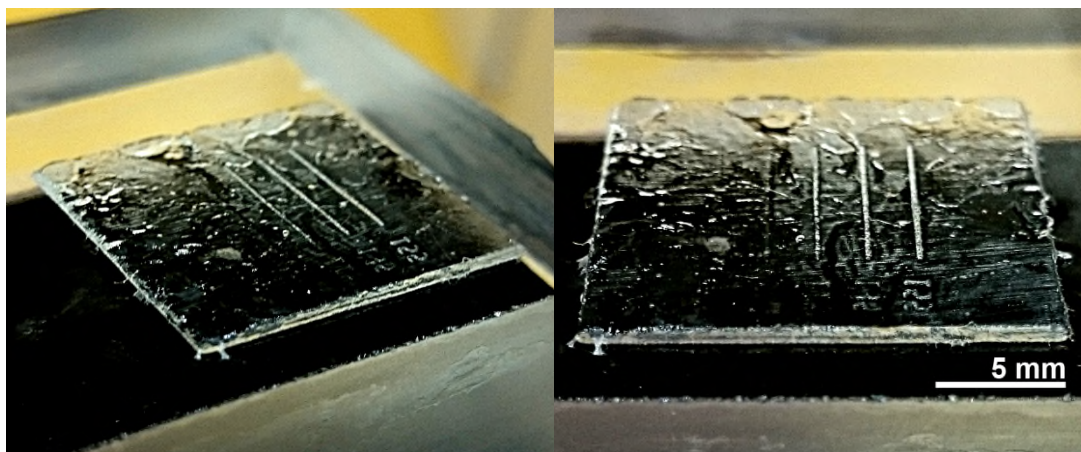


Figure 4.19. Photographs of a 400 μm -thick baseplate bearing 100 μm -high lines, produced by μSL of P(AOMECE-co-OOMECE)-based resin. Exposure times for lines (left to right): 115, 125, 135, 145 and 155 seconds.

The extended curing times required for resins formulated from the copolymer in comparison to those formulated using the homopolymer are likely the result of the lower concentration of alkene and thiol groups in the resin. Possible strategies for reducing cure times include decreasing the amount of propylene carbonate used as diluent (in order to increase the relative concentration of thiol/alkene groups), replacing the propylene carbonate with a reactive diluent, or simply by increasing the concentration of photoinitiator in the sample. Further work to investigate the effect of changing these parameters, and to subsequently optimise the epoxide-functional resin formulation for printing is ongoing.

Comparison of the FT-IR spectra for P(AOMECE₅-co-OOMECE₅) pre-and post-curing indicates that the epoxide functionality remains unaffected by the crosslinking reaction, as evidenced by the presence of the C-O-C oxirane stretch at 800 cm^{-1} in both

samples (Figure 4.20). P(AOMECE-co-OOMECE) therefore represents the first example of a polycarbonate-based resin for SLA/ μ SL bearing free functionality for modification post-fabrication.

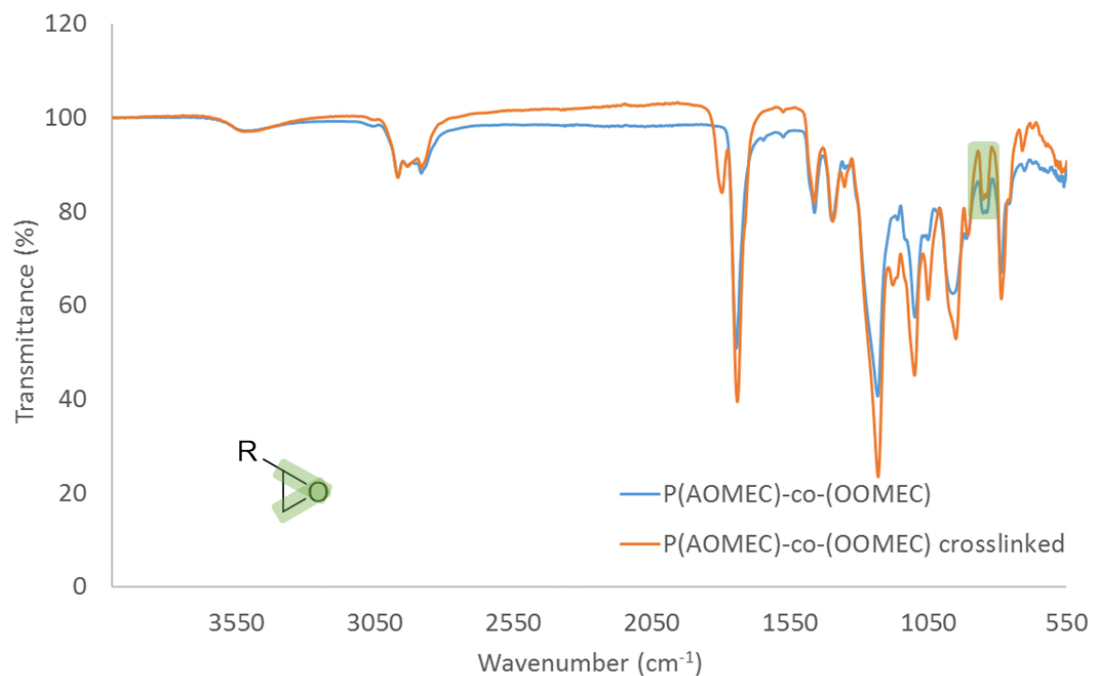


Figure 4.20. FT-IR spectra of P(AOMECE-co-OOMECE) and cured P(AOMECE-co-OOMECE)-based resin, indicating that the epoxide group remains unaffected by the thiol-ene crosslinking reaction.

4.3 Conclusion

The formulation of a photocrosslinkable resin based on a degradable alkene-functional polycarbonate (PAOMEK), and its subsequent curing by μ SL to form a porous 3D network has been described. The previously discussed ease of synthesis of AOMEK from a low-cost precursor (Chapter 2), in combination with the degradability of the polymer (Chapter 3) results in PAOMEK being an attractive material for the preparation of photocurable resins. Furthermore, the use of water as the initiating species, and the low cost and commercial availability of the crosslinker, viscosity modifier and photoinitiator make this resin formulation both low-cost and scalable. Structures displaying good feature fidelity and reasonable layer cure times were prepared using a custom-built μ SL system employing purple light, offering a low cost alternative to UV-curing systems and representing an improvement on previously reported alkene-functional polycarbonate-based resins.¹⁵

In addition, a photocrosslinkable resin was prepared using partially-epoxidised PAOMEK, with the epoxide group shown to remain intact following curing of the resin by μ SL. Whilst additional work is required to optimise resin formulations and cure times, to the best of our knowledge this represents the first demonstrated SLA/ μ SL fabrication of a 3D structure composed of a degradable polycarbonate bearing functionality available for modification post-fabrication. As such, these materials represent a promising advance in the development of photocurable biomedical devices.

4.4 References

- (1) Gross, B. C.; Erkal, J. L.; Lockwood, S. Y.; Chen, C. P.; Spence, D. M. *Anal. Chem.* **2014**, *86*, 3240.
- (2) Ventola, C. L. *Pharmacy and Therapeutics* **2014**, *39*, 704.
- (3) Wang, X.; Ao, Q.; Tian, X.; Fan, J.; Wei, Y.; Hou, W.; Tong, H.; Bai, S. *Materials* **2016**, *9*, 802.
- (4) Sun, J.; Vijayavenkataraman, S.; Liu, H. *Materials* **2017**, *10*, 29.
- (5) Hutmacher, D. W.; Sittinger, M.; Risbud, M. V. *Trends Biotechnol.* **2004**, *22*, 354.
- (6) Melchels, F. P. W.; Feijen, J.; Grijpma, D. W. *Biomaterials* **2010**, *31*, 6121.
- (7) Bártolo, P. J. In *Stereolithography*; 1 ed.; Bártolo, P. J., Ed.; Springer: 2011, p 1.
- (8) Munoz-Abraham, A. S.; Rodriguez-Davalos, M. I.; Bertacco, A.; Wengerter, B.; Geibel, J. P.; Mulligan, D. C. *Curr. Transpl. Rep.* **2016**, *3*, 93.
- (9) Laurent, C. P.; Durville, D.; Vaquette, C.; Rahouadj, R.; Ganghoffer, J.-F. In *Biomechanics of Cells and Tissues*; 1 ed.; Lecca, P., Ed.; Springer: Dordrecht, 2013, p 1.
- (10) Cooke, M. N.; Fisher, J. P.; Dean, D.; Rimmnac, C.; Mikos, A. G. *J. Biomed. Mater. Res. B Appl. Biomater.* **2003**, *64B*, 65.
- (11) Yeong, W. Y.; Chua, C. K.; Leong, K. F.; Chandrasekaran, M. *Trends Biotechnol.* **2004**, *22*, 643.

- (12) Billiet, T.; Vandenhaute, M.; Schelfhout, J.; Van Vlierberghe, S.; Dubruel, P. *Biomaterials* **2012**, *33*, 6020.
- (13) Bertsch, A.; Renaud, P. In *Stereolithography*; 1 ed.; Bártolo, P. J., Ed.; Springer: 2011, p 81.
- (14) Li, X. M.; Cui, R. R.; Sun, L. W.; Aifantis, K. E.; Fan, Y. B.; Feng, Q. L.; Cui, F. Z.; Watari, F. *Int. J. Polym. Sci.* **2014**.
- (15) Chae, M. P.; Rozen, W. M.; McMenamin, P. G.; Findlay, M. W.; Spychal, R. T.; Hunter-Smith, D. J. *Front. Surg.* **2015**, *2*, 1.
- (16) Bajaj, P.; Schweller, R. M.; Khademhosseini, A.; West, J. L.; Bashir, R. *Annu. Rev. Biomed. Eng.* **2014**, *16*, 247.
- (17) Chia, H. N.; Wu, B. M. *J. Biol. Eng.* **2015**, *9*.
- (18) Barker, I. A.; Ablett, M. P.; Gilbert, H. T. J.; Leigh, S. J.; Covington, J. A.; Hoyland, J. A.; Richardson, S. M.; Dove, A. P. *Biomater. Sci.* **2014**, *2*, 472.
- (19) Skoog, S. A.; Goering, P. L.; Narayan, R. J. *J. Mater. Sci. Mater. Med.* **2014**, *25*, 845.
- (20) Gauvin, R.; Chen, Y. C.; Lee, J. W.; Soman, P.; Zorlutuna, P.; Nichol, J. W.; Bae, H.; Chen, S. C.; Khademhosseini, A. *Biomaterials* **2012**, *33*, 3824.
- (21) Bertsch, A.; Renaud, P.; Vogt, C.; Bernhard, P. *Rapid Prototyping J.* **2000**, *6*, 259.
- (22) Yang, H.; Tsiklos, G.; Ronaldo, R.; Ratchev, S. In *Micro-Assembly Technologies and Applications*; 1 ed.; Ratchev, S., Koelemeijer, S., Eds.; Springer: 2008, p 171.

- (23) Ortega, I.; Deshpande, P.; Gill, A. A.; MacNeil, S.; Claeysens, F. *Biofabrication* **2013**, *5*.
- (24) Chu, T. M. G.; Orton, D. G.; Hollister, S. J.; Feinberg, S. E.; Halloran, J. W. *Biomaterials* **2002**, *23*, 1283.
- (25) Lee, S. J.; Kang, H. W.; Park, J. K.; Rhie, J. W.; Hahn, S. K.; Cho, D. W. *Biomed. Microdevices* **2008**, *10*, 233.
- (26) Wang, W. In *Reverse Engineering: Technology of Reinvention*; 1 ed.; Taylor & Francis: Boca Raton, 2010, p 25.
- (27) Méndez-Ramos, J.; Ruiz-Morales, J. C.; Acosta-Moraa, P.; Khaidukovc, N. M. *J. Mater. Chem. C* **2016**, *4*, 801.
- (28) O'Neill, W. In *Rapid Prototyping Casebook*; 1 ed.; McDonald, J. A., Ryall, C. J., Wimpenny, D. I., Eds.; Professional Engineering Publishing: London, 2001, p 243.
- (29) Boehm, R. D.; Jaipan, P.; Yang, K.-H.; Stewart, T. N.; Narayan, R. J. *Int. J. Bioprinting* **2016**, *2*, 72.
- (30) Elomaa, L.; Pan, C. C.; Shanjani, Y.; Malkovskiy, A.; Seppala, J. V.; Yang, Y. *Z. J. Mater. Chem. B* **2015**, *3*, 8348.
- (31) Leigh, S. J.; Purssell, C. P.; Bowen, J.; Hutchins, D. A.; Covington, J. A.; Billson, D. R. *Sensor. Actuat. A-Phys.* **2011**, *168*, 66.
- (32) Morris, V. B.; Nimbalkar, S.; Younesi, M.; McClellan, P.; Akkus, O. *Ann. Biomed. Eng.* **2016**, *1*.

- (33) Corbel, S.; Dufaud, O.; Roques-Carnes, T. In *Stereolithography: Materials, Processes and Applications*; 1 ed.; Bártolo, P. J., Ed.; Springer: New York, 2011, p 141.
- (34) Choi, J. W.; Wicker, R.; Lee, S. H.; Choi, K. H.; Ha, C. S.; Chung, I. *J. Mater. Process. Tech.* **2009**, *209*, 5494.
- (35) Lu, Y. F.; Mantha, S. N.; Crowder, D. C.; Chinchilla, S.; Shah, K. N.; Yun, Y. H.; Wicker, R. B.; Choi, J. W. *Biofabrication* **2015**, *7*.
- (36) Fisher, J. P.; Dean, D.; Mikos, A. G. *Biomaterials* **2002**, *23*, 4333.
- (37) Lee, K. W.; Wang, S. F.; Fox, B. C.; Ritman, E. L.; Yaszemski, M. J.; Lu, L. *C. Biomacromolecules* **2007**, *8*, 1077.
- (38) Luo, Y. Y.; Dolder, C. K.; Walker, J. M.; Mishra, R.; Dean, D.; Becker, M. L. *Biomacromolecules* **2016**, *17*, 690.
- (39) Elomaa, L.; Teixeira, S.; Hakala, R.; Korhonen, H.; Grijpma, D. W.; Seppala, J. V. *Acta Biomater.* **2011**, *7*, 3850.
- (40) Gill, A. A.; Claeysens, F. In *3D Cell Culture: Methods and Protocols*; Haycock, J. W., Ed.; Springer: New York, 2011; Vol. 695, p 309.
- (41) Kweon, H.; Yoo, M. K.; Park, I. K.; Kim, T. H.; Lee, H. C.; Lee, H. S.; Oh, J. S.; Akaike, T.; Cho, C. S. *Biomaterials* **2003**, *24*, 801.
- (42) Matsuda, T.; Mizutani, M. *J. Biomed. Mater. Res.* **2002**, *62*, 395.
- (43) Melchels, F. P. W.; Feijen, J.; Grijpma, D. W. *Biomaterials* **2009**, *30*, 3801.
- (44) Miao, S. D.; Zhu, W.; Castro, N. J.; Nowicki, M.; Zhou, X.; Cui, H. T.; Fisher, J. P.; Zhang, L. G. *Sci. Rep.* **2016**, *6*.

- (45) Schuller-Ravoo, S.; Feijen, J.; Grijpma, D. W. *Macromol. Biosci.* **2011**, *11*, 1662.
- (46) Serrine, J. M.; Pekkanen, A. M.; Nelson, A. M.; Chartrain, N. A.; Williams, C. B.; Long, T. E. *Aust. J. Chem.* **2015**, *68*, 1409.
- (47) Oskui, S. M.; Diamante, G.; Liao, C. Y.; Shi, W.; Gan, J.; Schlenk, D.; Grover, W. H. *Environ. Sci. Technol. Lett.* **2016**, *3*, 1.
- (48) Heller, C.; Schwentenwein, M.; Russmueller, G.; Varga, F.; Stampfl, J.; Liska, R. *J. Polym. Sci. A: Polym. Chem.* **2009**, *47*, 6941.
- (49) Jansen, J.; Melchels, F. P. W.; Grijpma, D. W.; Feijen, J. *Biomacromolecules* **2009**, *10*, 214.
- (50) Oesterreicher, A.; Wiener, J.; Roth, M.; Moser, A.; Gmeiner, R.; Edler, M.; Pinter, G.; Griesser, T. *Polym. Chem.* **2016**, *7*, 5169.
- (51) Lee, J. W.; Jung, J. H.; Kim, D. S.; Lim, G.; Cho, D. W. *Microelectron. Eng.* **2009**, *86*, 1451.
- (52) Shin, J. H.; Lee, J. W.; Jung, J. H.; Cho, D. W.; Lim, G. *J. Mater. Sci.* **2011**, *46*, 5282.
- (53) Dove, A. P. In *Handbook of Ring-Opening Polymerization*; 1 ed.; Dubois, P., Coulembier, O., Raquez, J.-M., Eds.; Wiley-VCH: Weinheim, 2009, p 357.
- (54) Delcroix, D.; Martin-Vaca, B.; Bourissou, D.; Navarro, C. *Macromolecules* **2010**, *43*, 8828.
- (55) Madou, M. J. In *Manufacturing Techniques for Microfabrication and Nanotechnology*; 3 ed.; CRC Press: Boca Raton, 2011, p 509.

- (56) Esposito Corcione, C.; Greco, A.; Licciulli, A.; Martena, M.; Maffezzoli, A. In *AMST '02 Advanced Manufacturing Systems and Technology*; 1 ed.; Kuljanic, E., Ed.; Springer-Verlag Wien: New York, 2002, p 731.
- (57) Comeau, B. M.; Umar, Y.; Gonsalves, K. E.; Henderson, C. L. In *Mater. Res. Soc. Symp. Proc.*; Laurencin, C. T., Botchwey, E., Eds.; Cambridge University Press: Boston, 2005; Vol. 845, p AA4.4.1.
- (58) Choi, J. W.; Wicker, R. B.; Cho, S. H.; Ha, C. S.; Lee, S. H. *Rapid Prototyping J.* **2009**, *15*, 59.
- (59) Bail, R.; Hong, J. Y.; Chin, B. D. *J. Ind. Eng. Chem.* **2016**, *38*, 141.
- (60) Hart, G. W. George W. Hart's Rapid Prototyping Web Page, <http://www.georgehart.com/rp/rp.html> (accessed Jan 22, 2017)
- (61) Wang, C.-F.; Lin, Y.-X.; Jiang, T.; He, F.; Zhuo, R.-X. *Biomaterials* **2009**, *30*, 4824.
- (62) He, F.; Wang, C.-F.; Jiang, T.; Han, B.; Zhuo, R.-X. *Biomacromolecules* **2010**, *11*, 3028.
- (63) Jiang, T.; Li, Y.-M.; Lv, Y.; Cheng, Y.-J.; He, F.; Zhuo, R.-X. *Colloids Surf., B* **2013**, *111*, 542.
- (64) Jiang, T.; Li, Y.; Lv, Y.; Cheng, Y.; He, F.; Zhuo, R. *J. Mater. Sci. Mater. Med.* **2014**, *25*, 131.
- (65) Stevens, D. M.; Tempelaar, S.; Dove, A. P.; Harth, E. *Acs Macro Lett.* **2012**, *1*, 915.

5 Copolymers of Cyclic Esters and an Alkene-
Functional Carbonate for the Synthesis of
Thermoplastic Elastomers

5.1 Introduction

Biodegradable polymers have found use in a range of biomedical applications, including surgical sutures, drug delivery vehicles, and temporary scaffolds for hard and soft tissue regeneration.¹⁻⁴ Materials used for tissue regeneration scaffolds should be degradable at a rate concordant with the formation of new tissue, and produce non-toxic and resorbable or excretable degradation products. The materials should also be readily processable and possess suitable mechanical properties for their intended application.⁵⁻⁷ Advances in polymerisation techniques have widened the range of materials available for such applications, however challenges still remain in the development of biodegradable materials for soft tissue repair, particularly in developing materials with suitable mechanical properties.⁵ The mechanical properties of implants are not only important for structural support as tissue regenerates, but also for biocompatibility, with implants only interfacing correctly with host tissues if the mechanical properties of both are similar.^{8,9} For example, differences in Young's moduli between implanted vascular grafts and host arteries have been shown to result in significant adverse effects, including thrombosis and anastomotic intimal hyperplasia (a thickening of the arterial wall), leading to eventual failure of the graft.⁹⁻

12

The majority of synthetic biodegradable polymers available for biomedical application are linear thermoplastics based on homo- and copolymers of α -hydroxy acids, in particular poly(*L*-lactide) and poly(*D,L*-lactide) (PLLA and PDLLA), poly(glycolide) (PGA), poly(ϵ -caprolactone) (PCL), and poly(3-hydroxybutyrate) or poly(4-hydroxybutyrate) (P3HB and P4HB).^{5,13-20} Whilst these materials possess high tensile strength and tuneable degradation rates, they are typically limited by their high rigidity and low elongations at break in comparison to soft tissues.^{19,21} By way of example,

PLLA possesses a Young's modulus (E) of 1,200-3,000 MPa, whereas those of myocardium and articular cartilage lie below 1 MPa and between 1-10 MPa respectively.²¹⁻²⁴ Conversely, biodegradable, resorbable materials which display good flexibility and elongations at break are typically limited by inadequate tensile strength. For example, poly(trimethylene carbonate) (PTMC) and poly(glycerol sebacate) (PGS) are rubbery, amorphous materials possessing low Young's moduli (3 and 0.3 MPa respectively) and moderate elongations at break (ϵ_b) (up to 160 and 448%), however both materials possess an ultimate tensile strength (UTS) of only 0.5 MPa.^{21,25,26}

Thermoplastic elastomers (TPEs) are materials that combine the flexibility and elasticity of elastomers with the processability and mechanical strength of thermoplastic polymers, and as such have generated significant interest as materials for tissue engineering applications.²⁷⁻³² The deformation of a TPE is typically elastic in nature up to its yield stress and is viscoelastic thereafter, with the material exhibiting time-dependent recovery and a small amount of permanent deformation.^{28,33} TPEs can be generated by the synthesis of A-B-A-type triblock and multiblock copolymers, wherein the A segments typically consist of polymers possessing high tensile strength and high glass transition temperature (T_g), and the B segments consist of rubbery amorphous polymers with low T_g (Figure 5.1). The tough A segments provide mechanical strength and form physical crosslinks through hydrogen bonding, co-crystallisation of semi-crystalline domains or hydrophobic interactions to generate robust networks throughout the material.^{28,34,35} The central B block typically comprises a rubbery domain of coiled polymer chains, and extending these chains leads to a drop in entropy in the amorphous domain. As the material is stretched, an entropic force grows to counteract the decreasing entropy and regain the coiled (higher

entropy) configuration, conferring elastomeric behaviour on the material.^{35,36} The immiscibility of the A and B blocks results in microphase separation of the incompatible polymer domains, thus preserving the mechanical strength and elasticity of the hard and rubbery segments respectively.^{35,37}

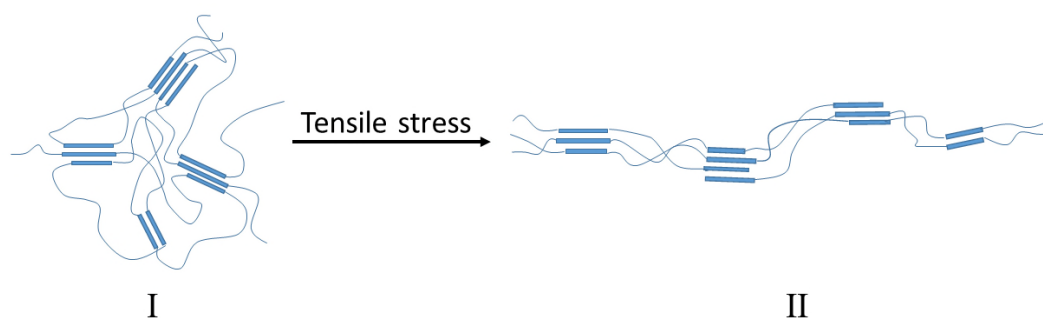


Figure 5.1. Schematic representation of a multiblock thermoplastic elastomer with semi-crystalline hard domains. (I) Polymer in relaxed state and (II) under uniaxial tensile stress. Upon removal of stress, configuration I is regained.

Several researchers have reported the synthesis of A-B-A triblock copolymers through the sequential ring-opening polymerisation (ROP) of cyclic esters and carbonates in order to generate elastomeric biomaterials. The majority of these materials employ PLLA as the hard domain, owing to its high tensile strength, its proven biocompatibility and biodegradability, its processability, its low cost and ready availability, and its ability to form reversible physical crosslinks by co-crystallisation between polymer chains.³⁸⁻⁴¹ Poly(α -hydroxy acids) with low T_g are most commonly employed as the central soft block, with reported midblocks including PCL,⁴²⁻⁴⁴ poly(1,5-dioxepan-2-one) (PDXO),^{45,46} poly(menthane) (PMI),⁴⁷⁻⁴⁹ poly(ϵ -decalactone) (PDL)⁵⁰⁻⁵² and methyl-substituted poly(valerolactone) (PMVL) (Figure 5.2).^{53,54} Triblock copolymers utilising PLLA as the terminal hard blocks and aliphatic polycarbonates as the amorphous midblock have also been reported. Of these, only

materials containing PTMC as the central soft block have been prepared exclusively by ROP to date, with the remainder prepared either by the copolymerisation of epoxides with CO₂ or by chain extension of commercially available oligomers with diphenyl carbonate (DPC).⁵⁵⁻⁶⁰ Hydroxyl-terminated A-B-A triblock copolymers can also be chain extended through the use of diisocyanates, thus generating multiblock copolymers with high molecular weights and improved mechanical properties. Several researchers have utilised this approach to produce lactide-based multiblock copolymers containing amorphous segments including PCL, PTMC, PDLLA, PDL, poly(ethylene glycol) (PEG), and random copolymers thereof.^{9,31,50,61-66}

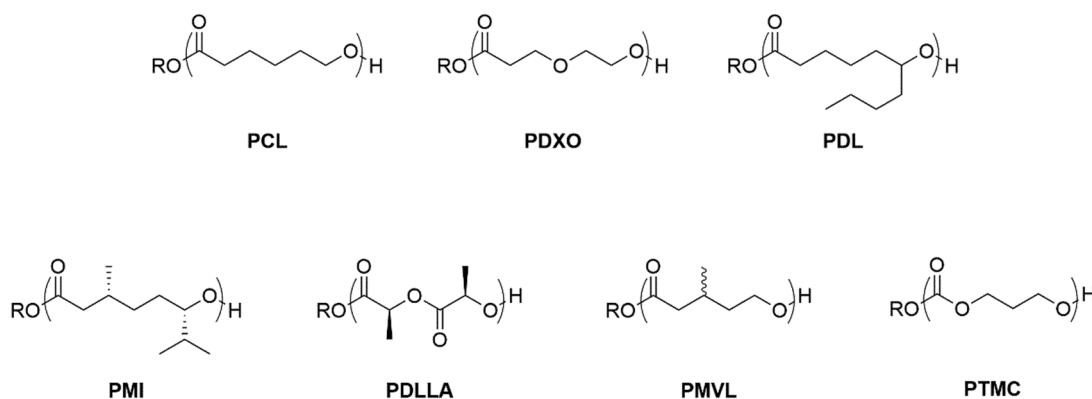


Figure 5.2. Examples of aliphatic polymers prepared by ROP and employed as amorphous segments of A-B-A triblock and multiblock copolymers.

By varying the relative incorporation of hard and soft blocks, the tensile strength and elastomeric nature of TPEs can be readily modified, as such potentially allowing materials based on a single A-B-A system to be used as scaffolds in multiple tissue environments. As an example, Zhang and co-workers prepared a series of PLLA-*b*-PTMC-*b*-PLLA triblock copolymers with PLLA contents ranging from *ca.* 15 to 60 wt%, generating materials with ultimate tensile strengths ranging from 0.05 to 19.8 MPa, Young's moduli of 0.84 to 408 MPa and elongation at break values of 120 to 1,800%.⁵⁷ Cohn *et al.* synthesised a series of multiblock copolymers by chain

extension of PLLA-*b*-PCL-*b*-PLLA triblocks with hexamethylene diisocyanate (HDI). The length of the PCL midblock was kept constant at 2,000 g mol⁻¹ and the length of the PLLA segments was varied from 550 to 6,000 g mol⁻¹. The use of relatively short block lengths ensured that the PCL blocks remained amorphous, as higher molecular weight PCL is semi-crystalline. Whilst all of the polyester/urethanes displayed similar UTS values (*ca.* 32 MPa), varying the hard block incorporation of the materials had a marked effect on the flexibility and ductility of the materials, with *E* increasing from 30 to 800 MPa and elongation at break decreasing from > 1600 to 100% with increasing PLLA content.⁹

The properties of TPEs can be further modified through the use of statistical copolymers as the amorphous midblock. Widjada and co-workers successfully demonstrated that by varying the incorporation of ϵ -caprolactone (CL) and trimethylene carbonate (TMC) in PLLA-*b*-P(CL-*co*-TMC)-*b*-PLLA triblock copolymers containing a statistical copolymer midblock, materials could be produced with UTS ranging from 4.5 to 29.5 MPa, *E* ranging from 12.5 to 72.3 MPa and ϵ_b of 67 to 1,084%. Increasing the TMC content of the midblock also reduced the amount of permanent deformation experienced by the materials when strained to 300% elongation.^{58,67} Similarly, Schneiderman *et al.* demonstrated that varying the ratio of CL and ϵ -decalactone (DL) in a statistical copolymer midblock, PLLA-*b*-P(CL-*co*-DL)-*b*-PLLA triblock copolymers could be prepared with UTS and strain at break values ranging from 0.24 to 18 MPa and 218 to 1200% respectively.⁶⁸

Polymers bearing pendent functionality on the soft segment present an attractive proposition, as they enable the properties of the material to be modified post-polymerisation. Several researchers have used this concept to prepare non-degradable triblock copolymers *via* reversible-deactivation radical polymerisation (RDRP) or

cationic polymerisation of acrylate and vinyl based monomer systems, generating materials bearing functionalities including ether,⁶⁹ ester,⁶⁹ bicycloalkenyl,⁷⁰ *tert*-butyldimethylsilyl (TBDMS),⁷¹ furfuryl,⁷² and nucleobase⁷³ groups for post-polymerisation modification. However, lactide-based triblock and multiblock copolymers bearing reactive functionalities on the amorphous segments are less common, with only a small number of materials reported. Xie *et al.* have reported the synthesis of anthracene-functional multiblock polyesterurethanes consisting of PLLA hard segments and soft segments comprising short PEG segments interspersed with *N,N*-bis(2-hydroxyethyl)-9-anthracene-methanamine (BHEAA). The researchers were able to demonstrate that the materials exhibited reversible light-induced shape memory properties, with [4 + 4] cycloaddition between the pendent anthracene groups triggered by irradiation with 365 nm light, and photocleavage of the crosslinked anthracene groups under irradiation with 254 nm light. The materials were also shown to demonstrate thermoplastic elastomer character, exhibiting Young's moduli as low as 15.9 MPa and elongations at break of up to 1612%.⁷⁴ Similar work was reported by Wu *et al.*, utilising hydrolysable soft segments comprised of short PCL blocks interspersed with *N,N*-bis(2-hydroxyethyl) cinnamamide (BHECA). Light-induced crosslinking of the cinnamamide groups was utilised to generate shape-memory materials, with wavelengths > 260 nm triggering a [2 + 2] cycloaddition between alkene functionalities, and wavelengths < 260 nm cleaving the crosslinkages. By varying the ratio of hard to soft segments, the researchers were able to produce a material with good mechanical strength (UTS = 21.3 MPa, ϵ_b = 476%) and flexibility (E = 21.0 MPa).⁷⁵

To date, functionality in the soft segments of lactide-based A-B-A triblock copolymers prepared exclusively by ROP appears to be limited only to polyesters bearing alkyl

groups.^{47,51,53} Despite the ease of synthesis and post-polymerisation modification of functional aliphatic polycarbonates, to our knowledge none have as yet been applied as the central soft block of A-B-A triblock copolymers. In this chapter, the synthesis of amorphous copolymers based on statistical copolymers of δ -valerolactone (VL) and an alkene-functional carbonate, 2-allyloxymethyl-2-ethyltrimethylene carbonate (AOMECC) is described. These materials are then used as macroinitiators for the polymerisation of *L*-lactide, thus generating A-B-A triblock copolymers displaying elastomeric character without the use of diisocyanate chain extenders. The effect of changing the composition of the soft block and the ratio of soft to hard segments on the thermal and mechanical properties of the materials is investigated, and the materials characterised by differential scanning calorimetry (DSC), dynamic mechanical thermal analysis (DMTA) and uniaxial tensile testing.

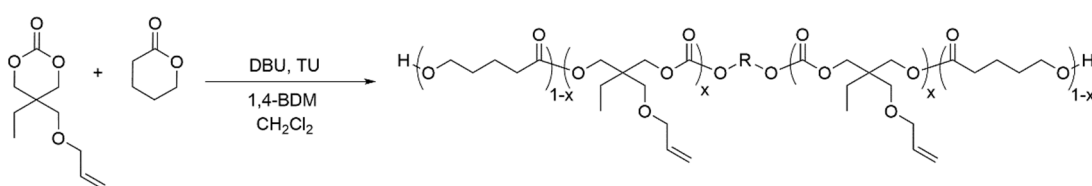
5.2 Results and discussion

5.2.1 Initial experiments

PLLA was selected as the hard block component of the A-B-A triblock copolymers, owing to the previously reported high tensile strength, biodegradability, and biocompatibility of the material.⁷⁶ In addition, the *L*-lactide monomer has previously been shown to undergo organocatalysed ROP with good control.⁷⁷ Random copolymers of AOMECEC and VL were selected for use as the midblock component. As discussed in Chapter 3, P(AOMECEC-*co*-VL) copolymers are completely amorphous at room temperature, are hydrolytically degradable, and the incorporation of alkene functionality in the polymer can be readily modified by changing the molar ratio of AOMECEC:VL in the monomer feed. In addition, the incorporation of pendent alkene functionality offers a potential route to post-polymerisation modification of these materials.

P(AOMECEC-*co*-VL) copolymers were prepared by the organocatalysed ROP of AOMECEC and VL, using methylene chloride as polymerisation solvent (overall monomer concentration = 2 M) and a dual organocatalyst system of 1,8-diazabicyclo[5.4.0]undec-7-ene (DBU, 5 mol%) and 1-(3,5-bis(trifluoromethyl)phenyl)-3-cyclohexylthiourea (TU, 5 mol%) (Scheme 5.1). 1,4-Benzenedimethanol (BDM) was used as a bifunctional initiator in order to generate telechelic polymers, targeting an initial overall degree of polymerisation (DP) of 30. As discussed in Chapter 3 of this thesis, AOMECEC is consumed more rapidly than VL in copolymerisations, therefore an AOMECEC:VL monomer feed ratio of 30:70 was used to target copolymers containing an AOMECEC:VL ratio of *ca.* 50:50. The polymerisation of AOMECEC became significantly retarded past 80% monomer conversion (as

described in Chapter 2 of this thesis), therefore the polymerisations were quenched at *ca.* 80% AOMECC conversion by addition of acidic Amberlyst A15 ion exchange resin, in order to ensure a statistical distribution of AOMECC and VL throughout the copolymer. Purification was performed by repeated precipitation into cold *n*-hexane, to yield a DP 27 copolymer containing an AOMECC:VL ratio of 62:38 (number-average molecular weight (M_n) = 4,500 g mol⁻¹, dispersity (D_M) = 1.11). (Figure 5.3 and 5.5).



Scheme 5.1. General reaction scheme for the synthesis of P(AOMECC-*co*-VL) macroinitiators *via* ring-opening polymerisation, using DBU (5 mol%) and TU (5 mol%) as polymerisation catalysts and 1,4-benzenedimethanol (BDM) as initiator.

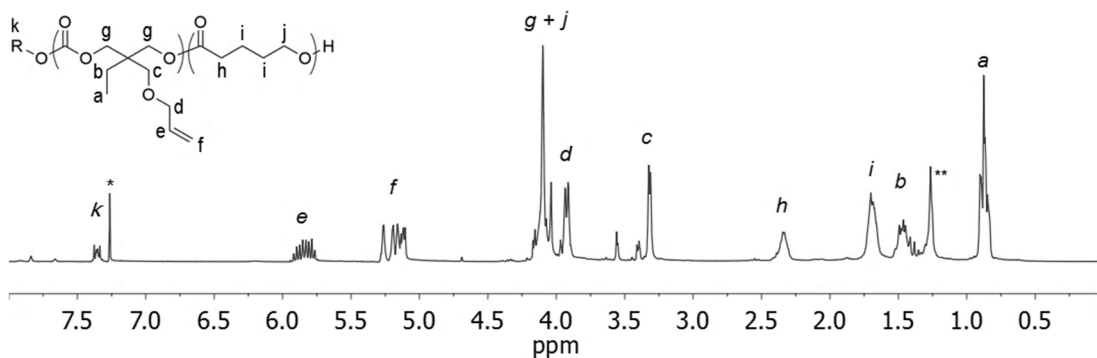
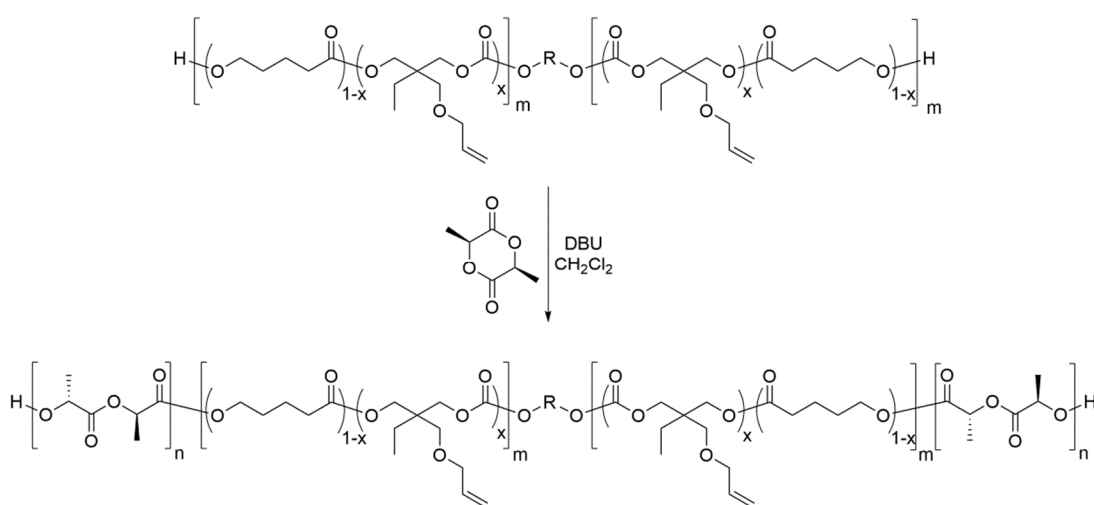


Figure 5.3. ¹H NMR spectrum of P(AOMECC₁₆-*co*-VL₁₁) initiated from BDM (400 MHz, 293 K; * = CHCl₃).

Following purification, the P(AOMECC₁₆-*co*-VL₁₁) copolymer was dissolved in dry methylene chloride, and the polymer solution dried extensively over molecular sieves (pore size = 3 Å). Following removal of the solvent under reduced pressure, the dry copolymer was used as a macroinitiator for the polymerisation of *L*-lactide. Polymerisations were performed using methylene chloride as solvent ([LLA] = 1 M)

and 0.5 mol% DBU as polymerisation catalyst (Scheme 5.2). DPs of lactide ranging from 10 to 40 were targeted by varying the $[\text{LLA}]_0:[\text{macroinitiator}]_0$ ratio, to yield materials containing 27-60 mol% PLLA. Polymerisations were quenched by addition of acidic Amberlyst A15 ion exchange resin, with purification performed by repeated precipitation into cold *n*-hexane followed by precipitation into cold methanol to yield the desired PLLA-*b*-P(AOMECCo-VL)-*b*-PLLA triblock copolymers. Analysis by ^1H NMR spectroscopy demonstrated that polymers with M_n values ranging from 5,500 to 9,900 g mol^{-1} were successfully produced (Figure 5.4). In addition, analysis by size exclusion chromatography (SEC) showed that narrow dispersities were maintained across the range of targeted triblock copolymer compositions ($D_M < 1.16$ for all samples), which indicates that the chain extension proceeds with good control (Figure 5.5).



Scheme 5.2. General reaction scheme for the synthesis of PLLA-*b*-P(AOMECCo-VL)-*b*-PLLA triblock copolymers *via* ring-opening polymerisation using DBU (0.5 mol%) as polymerisation catalyst.

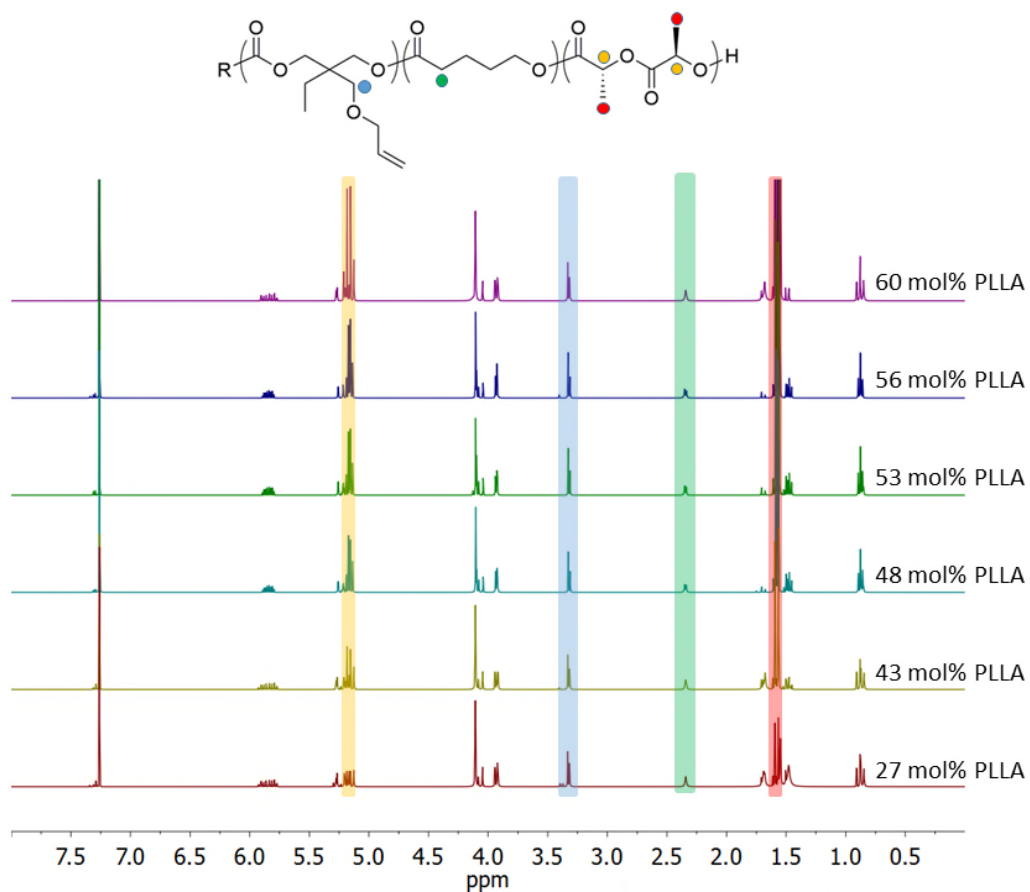


Figure 5.4. Stacked and deconvoluted ¹H NMR spectra of PLLA-*b*-P(AOMEC-*co*-VL)-*b*-PLLA triblock copolymers, showing the change in intensity of the PLLA methine proton ($\delta = 5.16$ ppm) with varying PLLA block incorporation (400 MHz, 293 K, CDCl₃).

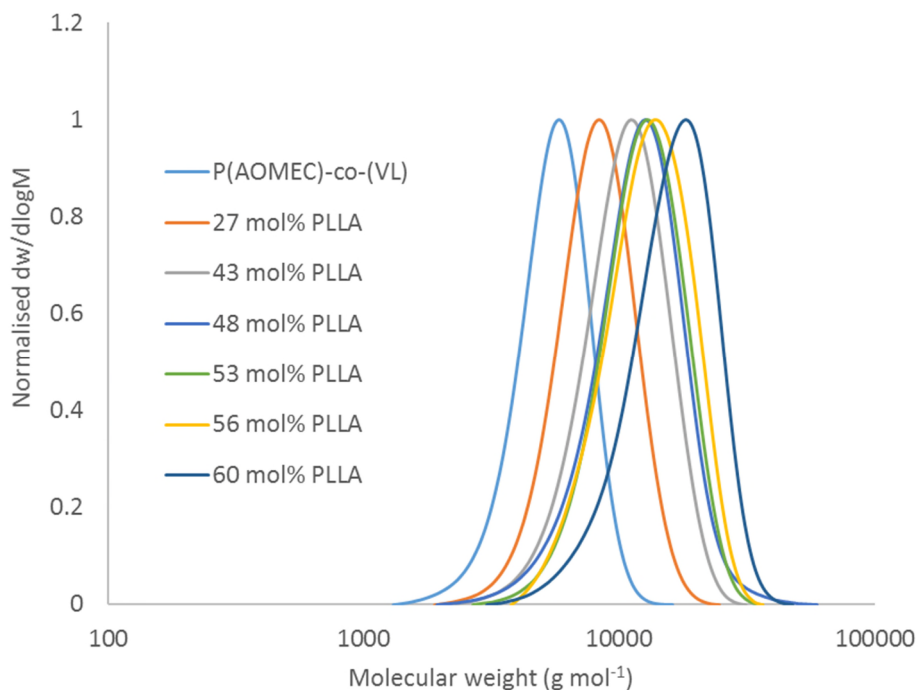


Figure 5.5. Size exclusion chromatograms for P(AOME C₁₆-co-VL₁₁) macroinitiator and PLLA-*b*-P(AOME C-co-VL)-*b*-PLLA triblock copolymers with different PLLA block incorporations. $M_n = 5,500 - 9,900 \text{ g mol}^{-1}$, $D_M \leq 1.16$ for all samples. Samples measured against polystyrene standards using CHCl_3 as eluent.

Materials containing $\leq 48 \text{ mol\% PLLA}$ were found to be liquids or tacky amorphous solids at room temperature, whilst those containing 60 mol\% lactide appeared hard, inflexible and brittle. Samples containing 53 and 56 mol\% lactide were softer, whilst still able to maintain their own form under gentle manual stretching. Samples comprising 56 mol\% PLLA were therefore analysed by uniaxial tensile testing in order to determine their mechanical properties. The polymer was formed into dogbone-shaped samples with uniform length, height and width by compression moulding in PTFE moulds, using a hydraulic press equipped with heated plates set to $100 \text{ }^\circ\text{C}$. The dogbone-shaped samples were then thermally annealed at $37 \text{ }^\circ\text{C}$ for 5 days to allow phase separation to take place between the semi-crystalline PLLA and amorphous P(AOME C-co-VL) block domains. Following annealing, the materials were loaded

into a tensiometer and stretched at a rate of 2 mm min^{-1} until failure. However, this material was found to exhibit poor mechanical properties, with negligible strain at break ($1.6 \pm 0.4\%$), low ultimate tensile strength ($2.7 \pm 0.3 \text{ MPa}$) and high elastic modulus ($179.4 \pm 40 \text{ MPa}$). These properties are likely the result of the low molecular weight of the material, with the short length of the amorphous midblock segment resulting in low flexibility and elongation at break, and the short PLLA blocks resulting in poor mechanical strength owing to the small size of the semi-crystalline segments limiting co-crystallisation between the polymer chains.

In an attempt to improve the mechanical properties of the materials, a triblock copolymer synthesis was attempted using a macroinitiator of higher molecular weight. A polymerisation was performed targeting a P(AOMECCO-VL) copolymer with a DP of 100, successfully producing a DP 98 copolymer with an AOMECCO:VL ratio of 46:54 ($M_n = 14,300 \text{ g mol}^{-1}$, $D_M = 1.17$, Figure 5.7). This copolymer was then used as a macroinitiator for the polymerisation of *L*-lactide, targeting a material with *ca.* 55 mol% PLLA incorporation. The polymerisation proceeded with good control, with analysis by ^1H NMR spectroscopy revealing a triblock copolymer comprising 56 mol% PLLA ($M_n = 32,200 \text{ g mol}^{-1}$) and a narrow molecular weight distribution observed by SEC ($D_M = 1.09$) (Figure 5.6 and 5.7).

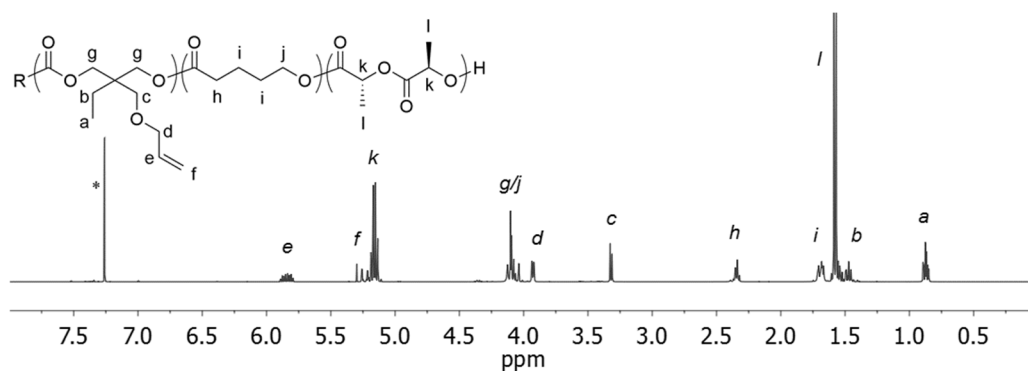


Figure 5.6. ^1H NMR spectrum of PLLA-*b*-P(AOMECCo-VL)-*b*-PLLA triblock copolymer (56 mol% PLLA) initiated from P(AOMECCo-VL₅₃), using 0.5 mol% DBU as polymerisation catalyst (400 MHz, 293 K, CDCl_3 ; * = CHCl_3).

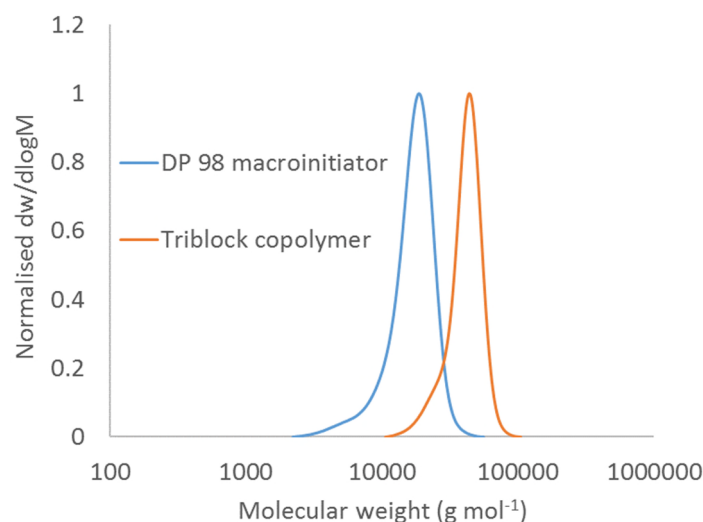


Figure 5.7. Size exclusion chromatogram of P(AOMECCo-VL₅₃) macroinitiator (DP 98, $M_n = 15,000 \text{ g mol}^{-1}$, $\bar{D}_M = 1.17$) and corresponding PLLA-*b*-P(AOMECCo-VL)-*b*-PLLA triblock copolymer (56 mol% PLLA, $M_n = 38,800 \text{ g mol}^{-1}$, $\bar{D}_M = 1.09$). Samples measured against polystyrene standards with CHCl_3 as eluent.

Dogbone-shaped samples with uniform dimensions were prepared by compression moulding, thermally annealed at $37 \text{ }^\circ\text{C}$ for 5 days, and subjected to uniaxial tensile testing at an elongation rate of 2 mm min^{-1} . These materials demonstrated significantly improved mechanical properties in comparison to those based on DP 27 macroinitiators, with E reduced to $34.4 \pm 2.6 \text{ MPa}$ and ε_b increasing to $247 \pm 13\%$

(Figure 5.8). This improvement is likely the result of better microphase separation between PLLA and midblock domains, and increased chain entanglement of the amorphous domain.

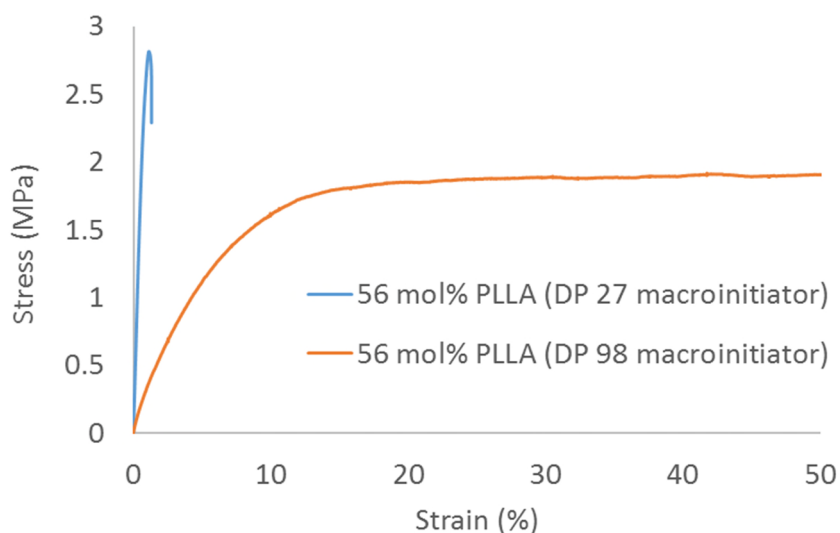


Figure 5.8. Example plots of stress (MPa) against strain (%) for triblock copolymers based on DP 27 and DP 98 macroinitiators up to 50% strain. Full extension data for ABA triblock based on DP 98 macroinitiator is shown in Figure 5.15 (P 209).

5.2.2 Variation of AOMEK:VL midblock composition

Polymers possessing midblocks of *ca.* DP 100 were selected to investigate the effect of changing the composition of the midblock on the thermal and mechanical properties of the materials. P(AOMEK-*co*-VL) midblocks consisting of AOMEK:VL ratios of 26:74, 46:54, and 83:17 were prepared, purified, and dried thoroughly over 3 Å molecular sieves in CHCl₃. These materials were then used as macroinitiators for the polymerisation of *L*-lactide (as described previously in this chapter), targeting similar molar ratios of PLLA to midblock (*ca.* 55 mol% PLLA). Triblock copolymers of PLLA-*b*-PAOMEK-*b*-PLLA and PLLA-*b*-PVL-*b*-PLLA were also prepared using a one-pot approach. In separate reaction vessels, PAOMEK and PVL were synthesised *via* ROP of their respective cyclic monomers in CHCl₃ ([M] = 2 M), using BDM as

initiator ($[\text{PAOMEC}]_0:[\text{I}]_0 = 125:1$, $[\text{VL}]_0:[\text{I}]_0 = 100:1$) and a dual organocatalyst system of DBU (5 mol%) and TU (5 mol%). Separate small scale reactions were prepared using CDCl_3 as solvent, and conversion of these samples monitored by ^1H NMR spectroscopy in order to determine the time required for the homopolymerisation reactions to reach equilibrium. At 83% AOMEC and 97% VL conversion, a 1 M solution of *L*-lactide in CHCl_3 was added to each of the polymerisation vessels. The reaction mixtures were then immediately removed from the glovebox and the polymerisations quenched by addition of acidic Amberlyst 15 ion exchange resin. Purification was performed by repeated precipitation into cold *n*-hexane and cold methanol to yield the triblock copolymers. Each of the triblock copolymer samples was then analysed by ^1H NMR spectroscopy and SEC to determine their composition (Table 5.1, Figure 5.9 and 5.10).

Table 5.1. Composition of triblock copolymers prepared from macroinitiators with varying AOMEC:VL ratios.^a

Polymer	A-B-A (DP) ^b	AOMEC:VL (midblock) ^b	f_{PLLA}	M_n PLLA (g mol^{-1}) ^b	M_n (g mol^{-1}) ^b	D_M^c
1	64-111-64	0:100	53	18,300	29,388	1.05
2	41-94-41	26:74	46	11,600	23,500	1.11
3	63-98-63	46:54	56	18,000	32,200	1.09
4	68-102-68	83:17	57	19,600	38,200	1.18
5	72-98-72	100:0	58	20,600	41,700	1.13

^a Polymerisations performed in CHCl_3 at 25 °C, $[\text{LLA}] = 1.0 \text{ M}$. ^b Polymer composition and number-average molecular weight determined by ^1H NMR spectroscopy. ^c Determined by SEC analysis in CHCl_3 .

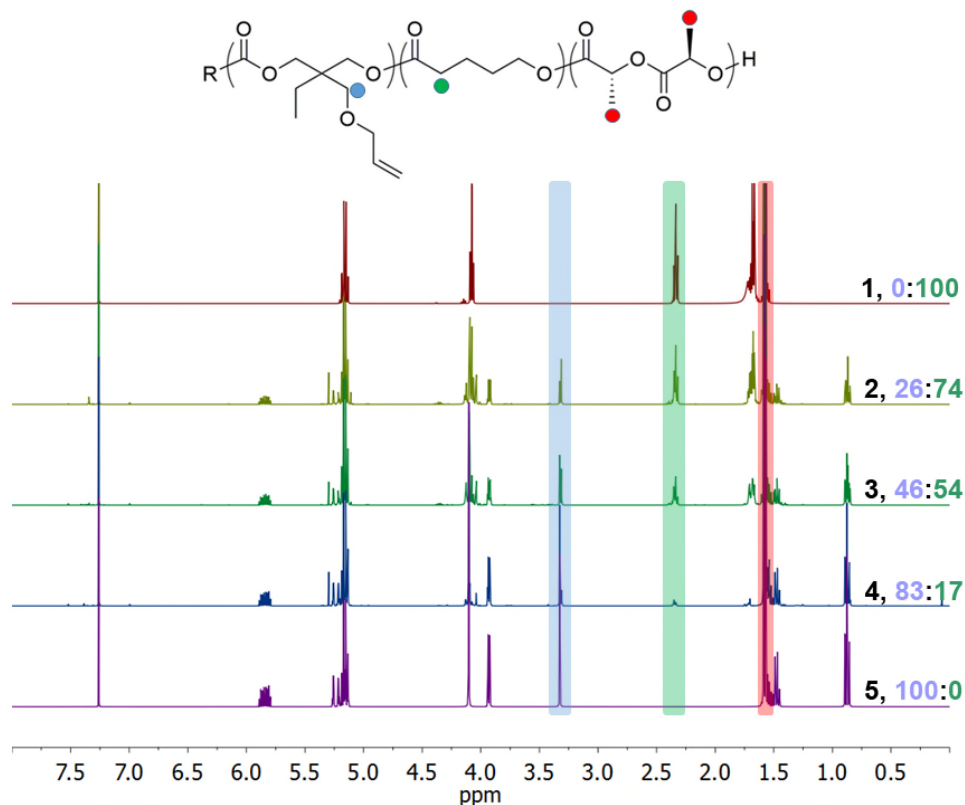


Figure 5.9. Stacked and deconvoluted ^1H NMR spectra of PLLA-*b*-P(AOMECCo-VL)-*b*-PLLA triblock copolymers, showing the change in intensity of the PAOMECCo and PVL methylene resonances with varying AOMECCo:VL midblock composition (400 MHz, 293 K, CDCl_3).

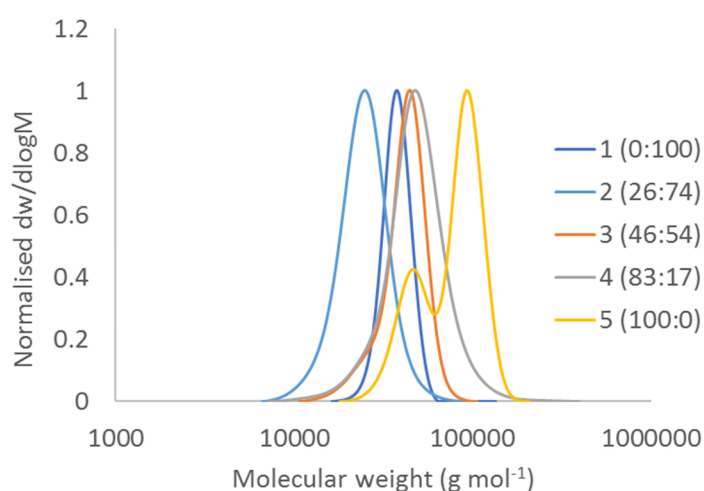


Figure 5.10. Size exclusion chromatograms of PLLA-*b*-P(AOMECCo-VL)-*b*-PLLA triblock copolymers with varying AOMECCo:VL midblock composition. $M_n = 22,900 - 49,200 \text{ g mol}^{-1}$, $\mathcal{D}_M \leq 1.18$ for all polymers. Samples measured against polystyrene standards using CHCl_3 as eluent.

Analysis by SEC demonstrated that polymers 1-4 possessed a narrow molecular weight distribution (D_M values of 1.18 or below), which indicates that the midblock and triblock polymerisations proceed with good control. PLLA-*b*-PAOMEC-*b*-PLLA (polymer **5**) displayed a bimodal molecular weight distribution, which may be indicative of a degree of initiation by residual water in the polymerisation system. In addition, polymer **5** possessed a slightly higher hard:soft block ratio in comparison to the other triblock copolymers, attributed to marginally lower than expected AOMEC monomer conversion during homopolymerisation. For polymer **2**, the molar ratio of hard:soft segments was unexpectedly low. Whilst this material was analysed to determine its thermal properties, the copolymer was excluded from mechanical testing as the lower than expected hard block incorporation resulted in materials which displayed poor mechanical properties.

Polymers 1-5 were subjected to thermal analysis by DSC and DMTA (full thermograms may be found in the Supplementary Information (SI) section of this thesis, Figures A-31 to A-35 and A-38 to A-42). Thermal analysis by DSC demonstrated that the materials typically display two T_g s, with a clear transition observed at low temperature corresponding to the soft segment, and a much weaker transition at higher temperatures corresponding to the hard segments (Figure 5.11 and 5.12). The T_g of the midblock varied markedly with changing composition, with higher temperatures observed for greater AOMEC incorporations. For midblocks composed entirely of VL (polymer **1**), the material displays a single T_g at -59.8 °C and a melting endotherm at *ca.* 40 °C, both corresponding to the PVL segment.⁷⁸ In this case, the T_g of the PLLA segment is obscured by the melting endotherm of the PVL block. The T_g of the amorphous midblock then ranges from -41.5 to -25.0 °C with increasing AOMEC content, with midblocks comprising entirely of AOMEC possessing a T_g of

-23.2 °C. For each material, the T_g of the hard segment was observed to be several °C lower than that of pure PLLA (60-65 °C),⁷⁹ characteristic of segmented elastomers with partially mixed phases.⁸⁰ Whilst polymer **2** did not possess an observable T_g for the hard segment (SI, Figure A-32), increasing the AOMECE content of the midblock generally resulted in an increase in T_g for the PLLA segments of the triblock copolymers, ranging from 40.7 to 50.2 °C for polymers **3** and **5** respectively. This trend is indicative of enhanced phase separation between the semi-crystalline and amorphous midblock domains with increasing carbonate content in the midblock.⁸⁰

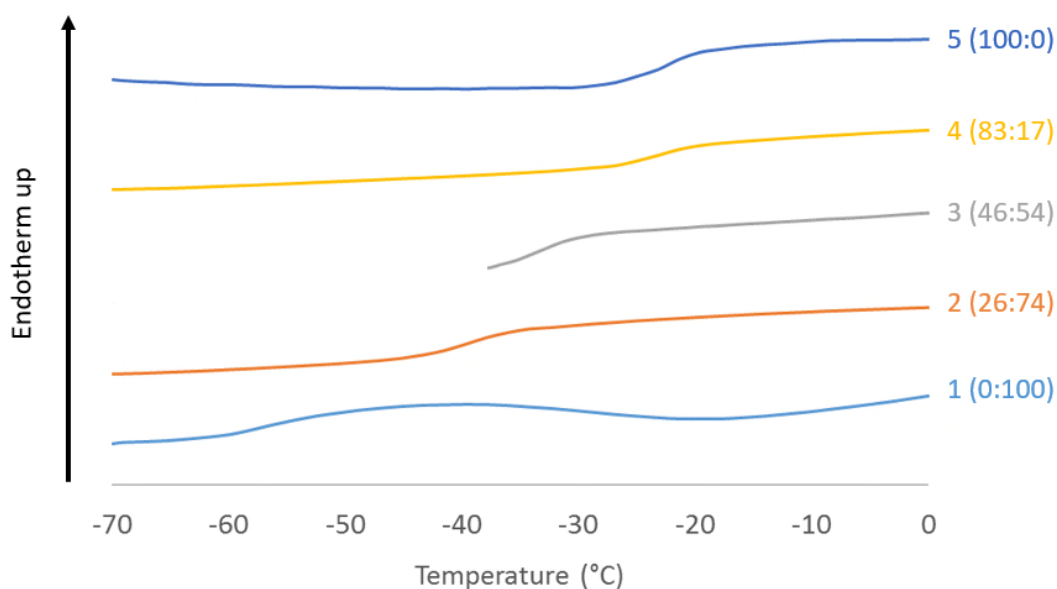


Figure 5.11. Expanded DSC thermograms of PLLA-*b*-P(AOMECE-*co*-VL)-*b*-PLLA triblock copolymers showing the change in soft block T_g with varying AOMECE:VL midblock composition. N.B. Polymer 3 measured from -50 to 80 °C, with tail region omitted for clarity.

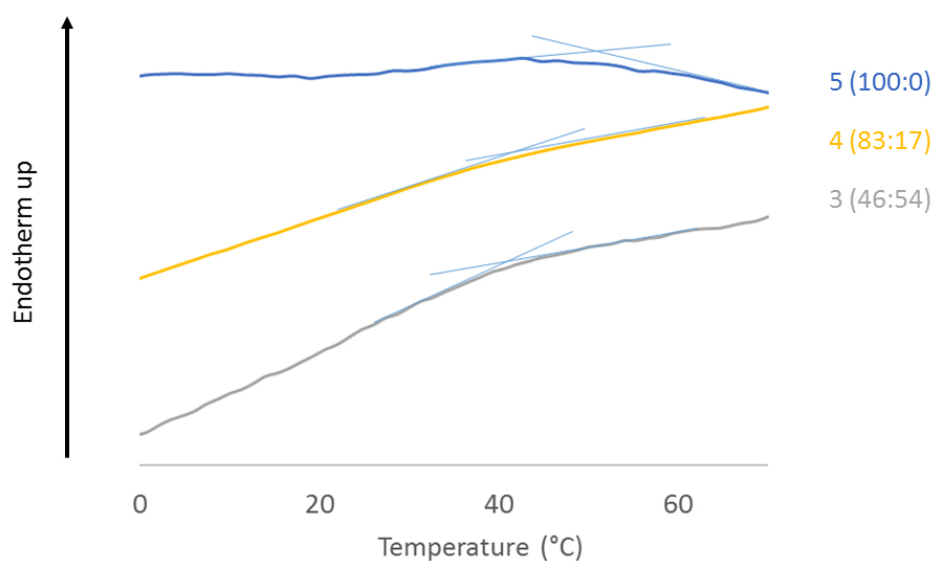


Figure 5.12. Expanded DSC thermograms of PLLA-*b*-P(AOMECE-*co*-VL)-*b*-PLLA triblock copolymers showing the change in hard block T_g with varying AOMECE:VL midblock composition. Tangent lines included to highlight the change in gradient of each thermogram.

Dynamic mechanical thermal analysis (DMTA) of the materials displayed a trend in T_g in good agreement with the DSC data, as determined by the peak in $\tan \delta$ and storage modulus (Table 5.2, Figure 5.13). The storage modulus (E') of the materials was found to decrease with increasing AOMECE content in the midblock when measured at 298 K, and the loss modulus (E'') peak was shifted to higher temperatures, indicating that the materials became more flexible with increasing AOMECE content in the midblock (Figure 5.14).

Table 5.2. Glass transition temperatures of PLLA-*b*-P(AOMECCo-VL)-*b*-PLLA triblock copolymers with varying AOMECCo:VL midblock composition.

Polymer	T_{g1} (°C)			T_{g2} (°C)		
	DSC ^a	Tan δ^b	E'^b	DSC ^a	Tan δ^b	E'^b
1	-59.8	-42.5	-48.4	– ^c	– ^c	– ^c
2	-41.5	-25.1	-36.5	– ^d	6.53	8.12
3	-35.3	-21.4	-29.9	40.7	37.2	24.7
4	-25.0	-12.3	-17.7	42.8	45.4	35.5
5	-23.2	-11.1	-20.1	50.2	54.3	51.9

^a Determined by differential scanning calorimetry using data from the second heating cycle, with a heating rate of 2 °C min⁻¹. ^b Determined by dynamic mechanical thermal analysis using a heating rate of 2 °C min⁻¹ and an oscillation rate of 0.5 Hz, with values taken from peaks in tan δ and E' curves. ^c T_g obscured by melting endotherm for PVL segment. ^d T_g not observed by DSC.

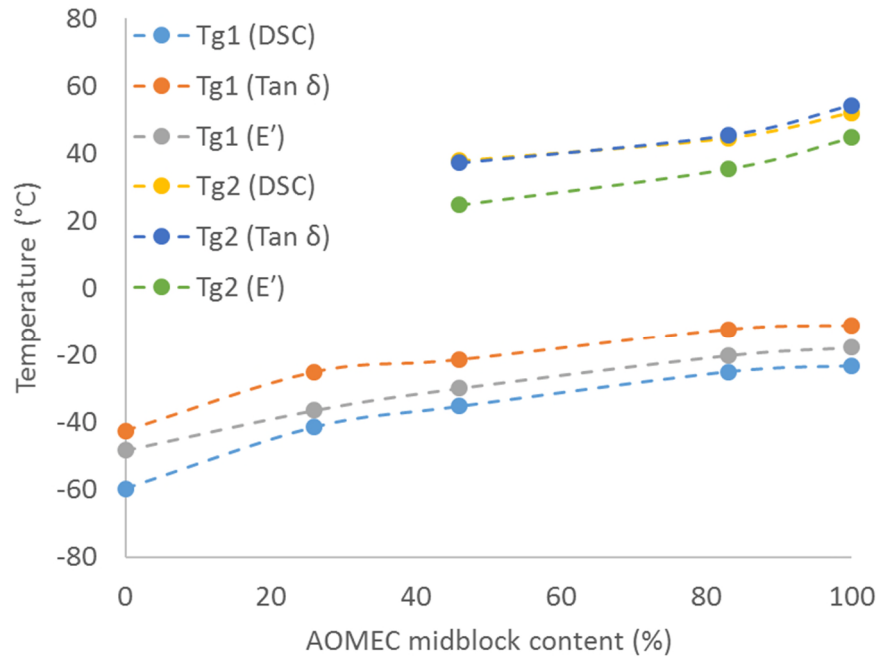


Figure 5.13. Graphical representation of changing glass transition temperatures of PLLA-*b*-P(AOMECCo-VL)-*b*-PLLA triblock copolymers with varying AOMECCo-VL midblock composition.

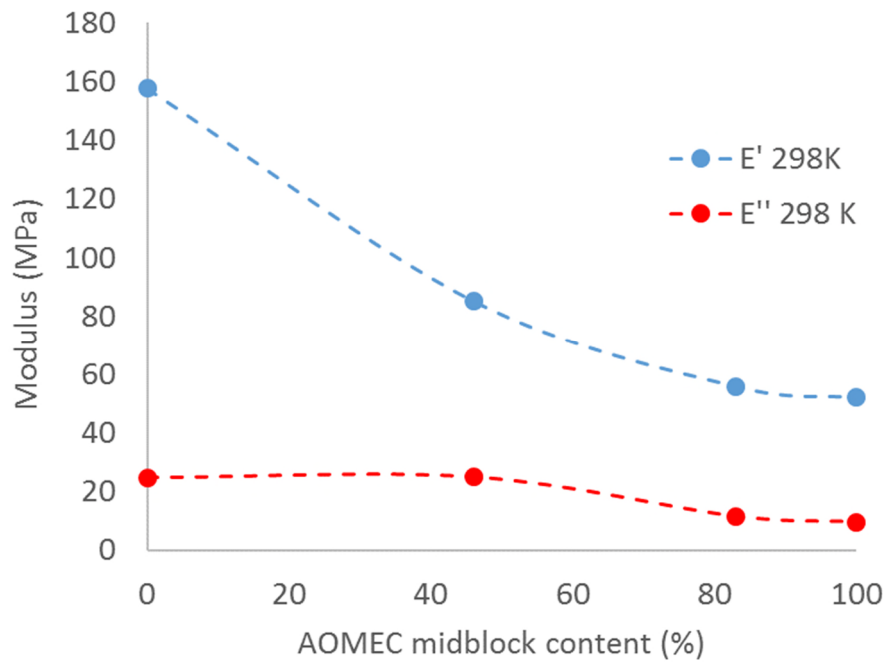


Figure 5.14. Plot of elastic and loss moduli of PLLA-*b*-P(AOMECCo-VL)-*b*-PLLA triblock copolymers (MPa) against AOMECCo-VL midblock content (%), determined by dynamic mechanical thermal analysis using a heating rate of 2 °C min⁻¹ and an oscillation rate of 0.5 Hz.

Uniaxial tensile testing of the polymers demonstrated that increasing the AOMECE content of the midblock resulted in reduced Young's moduli for the materials and improved elongations at break (Table 5.3, Figure 5.15 and 5.16). Polymer **1** (containing a midblock of 100% VL) was found to be tough and relatively inflexible, possessing a Young's modulus of 40.3 ± 4.1 MPa and UTS of 14.7 ± 3.0 MPa. These properties can be attributed to the semi-crystalline and relatively rigid nature of the PVL midblock. The Young's modulus of the materials was observed to decrease with increasing AOMECE midblock content, ranging from 34.4 ± 2.6 MPa for polymer **3** (46% AOMECE midblock content) to as low as 17.1 ± 3.6 MPa for polymer **5** (100% AOMECE midblock content). Increasing the incorporation of AOMECE in the midblock also resulted in improved elongation at break values, with strain at break values increasing from $247 \pm 14\%$ for polymer **3** to $484 \pm 88\%$ for PLLA-*b*-PAOMECE-*b*-PLLA triblocks. It is worth noting that none of the materials tested display a sharp yield point prior to failure, with each polymer possessing stress vs strain curves typical of viscoelastic materials (Figure 5.15).

Table 5.3. Mechanical properties of PLLA-*b*-P(AOME₂C-co-VL)-*b*-PLLA triblock copolymers with varying AOME₂C:VL midblock composition.

Polymer	UTS (MPa) ^a	ϵ_b (%) ^a	E (MPa) ^{a,b}	E' (MPa) ^c	E'' (MPa) ^c
1	14.7 ± 3.0	168 ± 47.9	40.3 ± 4.1	157.7	24.7
3	2.83 ± 0.3	247 ± 14	34.4 ± 2.6	85.3	24.9
4	10.0 ± 0.7	413 ± 59	24.4 ± 2.5	55.9	11.6
5	17.1 ± 3.6	484 ± 88	19.2 ± 5.6	52.1	9.6

^a Average values of a minimum of five samples as determined by uniaxial tensile testing, using a constant elongation rate of 2 mm min⁻¹. ^b Determined from the initial gradient of the tensile curve over 2% strain. ^c Determined by dynamic mechanical thermal analysis using a heating rate of 2 °C min⁻¹ and an oscillation rate of 0.5 Hz, with values taken at 298 K.

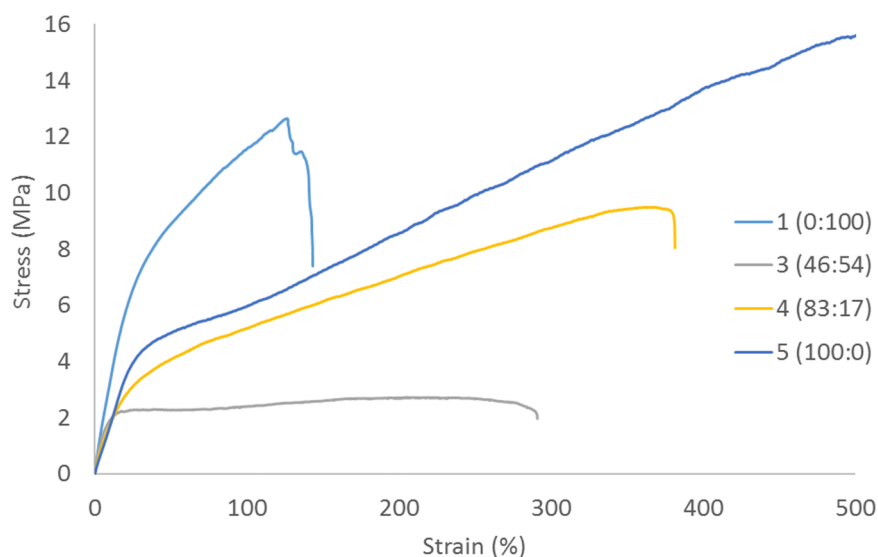


Figure 5.15. Example plots of stress (MPa) against strain (%) for PLLA-*b*-P(AOME₂C-co-VL)-*b*-PLLA triblock copolymers with varying AOME₂C:VL midblock composition.

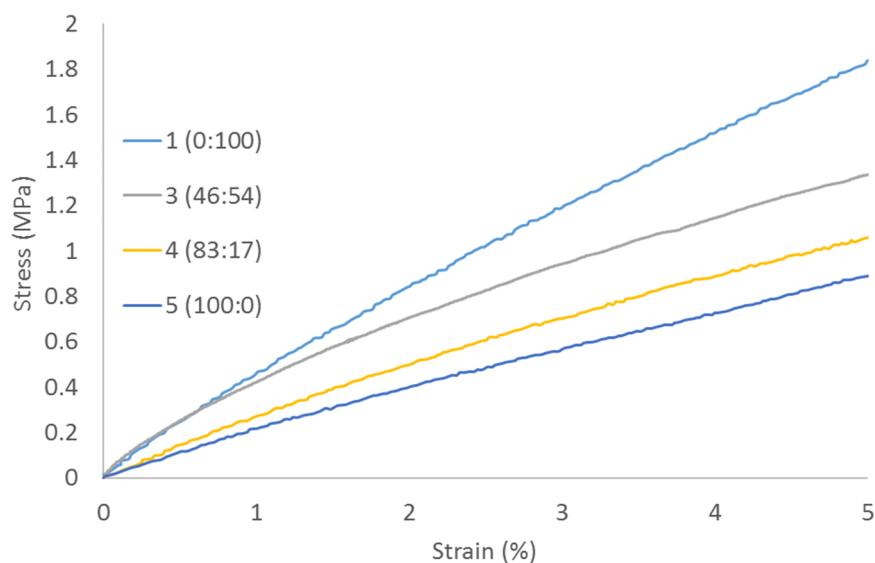


Figure 5.16. Initial stress (MPa) vs strain (%) curves for PLLA-*b*-P(AOMECCo-VL)-*b*-PLLA triblock copolymers with varying AOMECCo:VL midblock composition, highlighting the difference in stiffness between materials.

Interestingly, increasing the AOMECCo content of the midblock also appears to result in improved UTS values. This is proposed to be the result of two factors. Firstly, the molar ratio of PLLA to midblock increases slightly as the incorporation of AOMECCo in the midblock increases. Increased hard block incorporations have been shown to result in increased UTS,⁸¹ however this is typically also accompanied by an increase in stiffness which is not observed for the PLLA-*b*-P(AOMECCo-VL)-*b*-PLLA triblock copolymer series. A second potential influence is the degree of phase separation occurring between hard and soft segments in the copolymers. The chemical composition of midblock segments is known to have an effect on the degree of phase separation that occurs in segmented copolymers, and consequently the mechanical properties of the material.⁸⁰ Increasing the AOMECCo content of the midblock results in an increase in the T_g of the hard PLLA segment as observed by DMTA and DSC, indicative of a greater separation of the midblock and PLLA segments. It is therefore proposed that the improving UTS and elongation at break values are partially the result

of increased co-crystallisation of PLLA segments owing to more efficient phase separation between hard and soft domains with increasing AOMECE midblock content. As UTS and strain at break are known to improve with increasing molecular weight,⁸² it is also worth considering that the high UTS and elongation at break values observed for polymer **5** may partially result from the bimodal molecular weight distribution evidenced by SEC, with the higher molecular weight polymer distribution conferring improved mechanical properties on the material.

Triblock copolymers containing midblocks comprised of 83:17 and 100:0 AOMECE:VL copolymers displayed the greatest flexibility and elongations at break, and were therefore assessed for their elastomeric character by cyclic extension testing. Samples were stretched to 200% strain at a rate of 5 mm min⁻¹ and allowed to relax, and the degree of recovery measured over ten cycles (Figure 5.17).

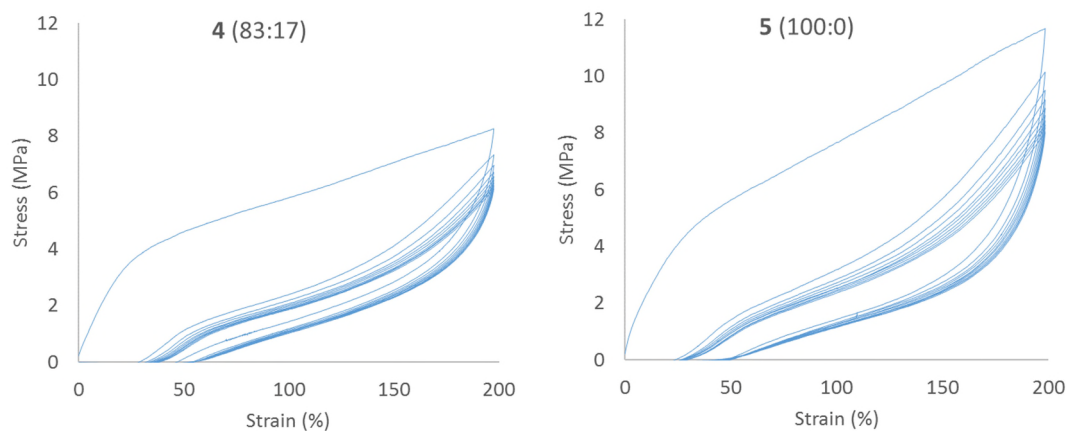


Figure 5.17. Plots of stress (MPa) against strain (%) for PLLA-*b*-P(AOMECE-*co*-VL)-*b*-PLLA triblock copolymers under repeated application of 200% strain, using an elongation rate of 5 mm min⁻¹.

Both materials demonstrate good elastomeric character, with polymer **4** exhibiting *ca.* 80% recovery and polymer **5** exhibiting 86% recovery following ten extension cycles. The mechanical properties of both materials are significantly affected by the repeated application tensile load. Both materials exhibit a large mechanical hysteresis for the

first loading cycle, and an accompanying permanent deformation (15.3 and 11.6% for polymers **4** and **5** respectively). This large initial hysteresis in thermoplastic elastomers has previously been attributed to the reorientation of macromolecules in the semi-crystalline microphase, leading to a decrease in elastic modulus.⁸³ The area of the hysteresis curve is significantly larger for polymer **5**, suggesting improved phase separation and subsequent formation of crystalline domains in this material in comparison to polymer **4**. The mechanical hysteresis is markedly reduced for cycles 2-10 for both polymers, accompanied by a reduction in additional permanent deformation with each cycle which becomes negligible for cycles 8-10. The high recovery exhibited by these materials following repeated loadings demonstrates the potential of these materials for use in applications where good elastomeric character is required.

5.2.3 Variation of PLLA:midblock composition

In order to investigate the effect of changing the PLLA:midblock ratio on the mechanical properties of the triblock copolymers, the 83:17 AOMEC:VL copolymer (DP 102) was selected as a macroinitiator for the synthesis of A-B-A triblock copolymers with different PLLA block lengths. In addition to polymer **4** (57 mol% PLLA), samples were prepared comprising 68 mol% PLLA (Table 5.4). An additional polymer was prepared containing 44 mol% PLLA based on the 46:54 AOMEC:VL macroinitiator (DP 98), and the thermal and mechanical properties of the materials assessed. Analysis by SEC demonstrated that each of the polymerisations proceeded with good control, with $D_M = 1.18$ or below for all three samples (Figure 5.18).

Table 5.4. Composition of triblock copolymers with PLLA:midblock ratios.

Polymer (mol% PLLA)	A-B-A (DP) ^c	f_{PLLA}	M_n PLLA (g mol ⁻¹) ^c	M_n (g mol ⁻¹) ^c	D_M ^d
44^a	40-98-40	44	11,520	14,200	1.09
57^b	68-102-68	57	19,600	38,200	1.18
68^b	105-102-105	68	30,300	48,900	1.18

^a Polymerisations performed in CHCl₃ at 25 °C using P(AOMECC₄₅-co-VL₅₃) as macroinitiator 0.5 mol% DBU as polymerisation catalyst, and [LLA] = 1.0 M. Polymerisations performed in CHCl₃ at 25 °C using P(AOMECC₈₅-co-VL₁₇) as macroinitiator, 0.5 mol% DBU as polymerisation catalyst, and [LLA] = 1.0 M.^c Polymer composition and number-average molecular weight determined by ¹H NMR spectroscopy.^d Determined by SEC analysis in CHCl₃.

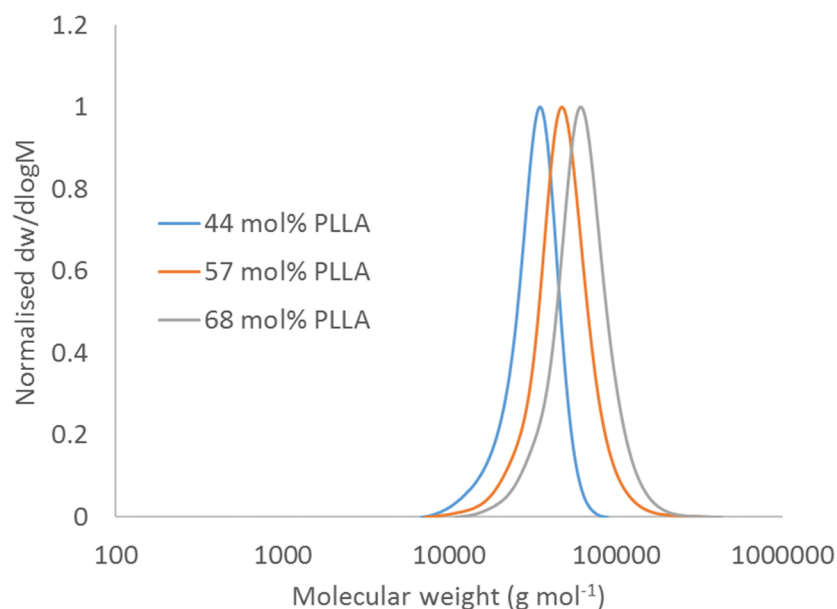


Figure 5.18. Size exclusion chromatograms of PLLA-*b*-P(AOMECC-*co*-VL)-*b*-PLLA triblock copolymers with varying PLLA:midblock composition. $M_n = 25,700 - 55,600$ g mol⁻¹, $D_M \leq 1.18$ for all polymers. Samples measured against polystyrene standards using CHCl₃ as eluent.

Polymers with varying PLLA:midblock composition were analysed by DSC and DMTA (full DSC thermograms may be found in SI Figures A-33, A-36 and A-37, full DMTA thermograms are shown in SI Figures A-40, A-43 and A-44). Analysis by DSC demonstrated that increasing the PLLA block length improved the phase separation of the PLLA and midblock, primarily evidenced by the change in T_g for the hard segment (Table 5.5). The polymer containing 44% PLLA (based on a P(AOMECC₄₅-co-VL₅₃ macroinitiator) displayed only a single T_g corresponding to the soft block at -32.0 °C, whilst all polymers containing higher mol% PLLA (based on a P(AOMECC₈₅-co-VL₁₇) macroinitiator) possessed two distinct T_g s corresponding to the hard and soft segments. The T_g of the soft segment decreases slightly from -25.0 to -26.8 °C with an increase in PLLA content from 57 to 68 mol%. This is accompanied by an increase in T_g for the hard segment from 43.9 to 48.3 °C for 57 and 68 mol% PLLA respectively. This trend was corroborated by DMTA, indicating that increasing hard block incorporation results in more effective microphase separation between the semi-crystalline and amorphous segments of the triblock copolymers.

Table 5.5. Glass transition temperatures of PLLA-*b*-P(AOMECA-*co*-VL)-*b*-PLLA triblock copolymers with varying PLLA:midblock composition.

Polymer (mol% PLLA)	T_{g1} (°C)			T_{g2} (°C)		
	DSC ^a	Tan δ^b	E'^b	DSC ^a	Tan δ^b	E'^b
44	-32.0	-19.1	-30.3	– ^c	– ^c	– ^c
57	-25.0	-12.3	-17.7	43.9	45.4	24.7
68	-26.8	-11.6	-18.3	48.3	56.5	35.5

^a Determined by differential scanning calorimetry using data from the second heating cycle, with a heating rate of 2 °C min⁻¹. ^b Determined by dynamic mechanical thermal analysis using a heating rate of 2 °C min⁻¹ and an oscillation rate of 0.5 Hz, with values taken from peaks in tan δ and E' curves. ^c T_g not observed by DSC or DMTA.

Uniaxial tensile testing demonstrated that the weight percentage of hard block in the copolymers had a significant effect on the mechanical properties of the materials (Table 5.6, Figure 5.19). Materials comprising 44 mol% PLLA displayed exceptionally low E (5.4 ± 0.8 MPa), but also demonstrated poor tensile strength and elongation at break (1.5 ± 0.1 MPa and $60 \pm 7\%$). In contrast, polymers comprising 68 mol% PLLA provided materials which possessed high tensile strength but were relatively inflexible (UTS = 17.4 ± 2.3 MPa, $E = 83.7 \pm 2.6$ MPa).

Table 5.6. Mechanical properties of PLLA-*b*-P(AOMEC-*co*-VL)-*b*-PLLA triblock copolymers with varying PLLA:midblock composition.

Polymer (mol% PLLA)	UTS (MPa) ^a	ϵ_b (%) ^a	E (MPa) ^{a,b}	E' (MPa) ^c	E'' (MPa) ^c
44	1.5 ± 0.1	60 ± 7	5.4 ± 0.8	11.4	3.2
57	10.0 ± 0.7	413 ± 59	24.4 ± 2.5	55.9	11.6
68	17.4 ± 2.3	328 ± 53	83.7 ± 2.6	205.4	24.3

^a Average values of a minimum of five samples as determined by uniaxial tensile testing, using a constant elongation rate of 2 mm min⁻¹. ^b Determined from the initial gradient of the tensile curve over 2% strain. ^c Determined by dynamic mechanical thermal analysis using a heating rate of 2 °C min⁻¹ and an oscillation rate of 0.5 Hz, with values taken at 298 K.

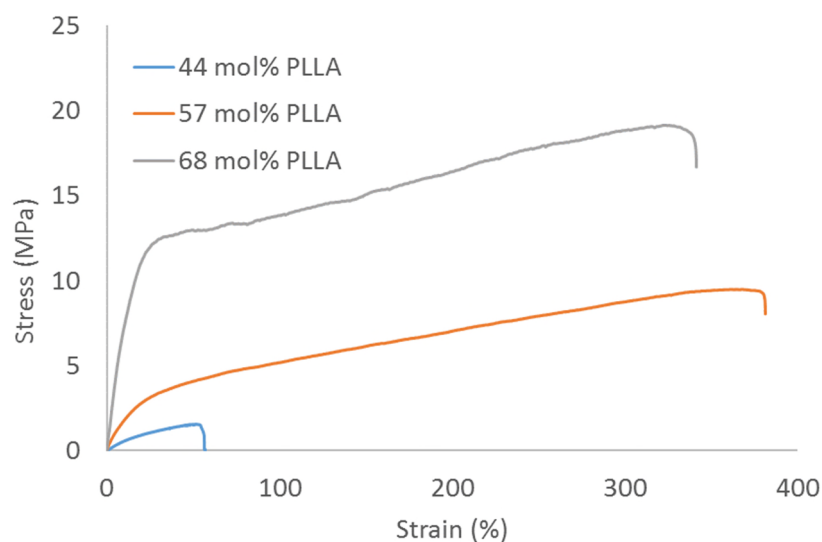


Figure 5.19. Example plots of stress (MPa) against strain (%) for PLLA-*b*-P(AOMEC-*co*-VL)-*b*-PLLA triblock copolymers with varying PLLA:midblock composition.

Whilst materials comprising 44 mol% PLLA possess a low Young's modulus, their low elongation at break values render them unsuitable for application as elastomers.⁶

In contrast, whilst materials comprising 68 mol% PLLA possess high ultimate strength and display good elongation at break, their relatively high rigidity is a limiting factor. In addition, the stress vs strain curve for this material displays a more clearly defined yield point in comparison to the other materials tested, beyond which the material primarily undergoes plastic deformation. Straining the polymer to 200% and allowing the material to relax further evidenced this increased plastic deformation (Figure 5.20). Whilst materials possessing 57 mol% PLLA demonstrate an immediate recovery of *ca.* 75% when stretched to 200% strain even after 10 extension/relaxation cycles, materials possessing 68 mol% PLLA display an immediate recovery of only *ca.* 60% from a single application of 200% strain. This demonstrates that PLLA-*b*-P(AOMECCo-VL)-*b*-PLLA copolymers with a high PLLA:midblock ratio possess significantly reduced elastomeric character, and are therefore not suitable for applications in which a high degree of elasticity is required.⁶⁷

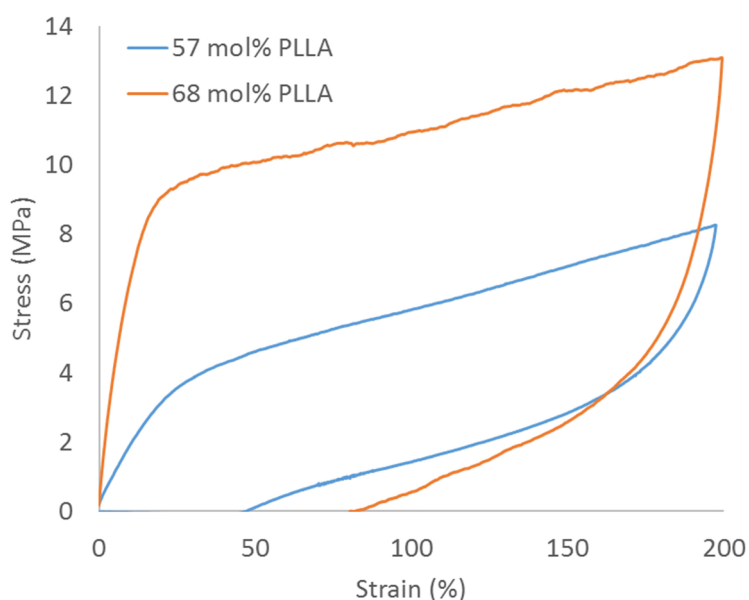


Figure 5.20. Plot of stress (MPa) against strain (%) for PLLA-*b*-P(AOMECCo-VL)-*b*-PLLA triblock copolymers with varying PLLA:midblock composition under single application and removal of 200% strain, using an elongation rate of 5 mm min⁻¹.

5.3 Conclusions

A-B-A triblock copolymers possessing good elastomeric character have been synthesised, using PLLA as terminal semi-crystalline blocks and a degradable copolymer of an alkene-functional carbonate and cyclic ester as the amorphous midblock. The mechanical properties of these triblock copolymers were readily modified both by changing the ratio of hard and soft segments, and by changing the ratio of carbonate:ester in the midblock. It was determined that increasing the incorporation of alkene-functional carbonate in the midblock reduced the rigidity and enhanced the elastomeric nature of the materials, and also promoted phase separation between the hard and soft polymer domains (as evidenced by thermal analysis data). It is proposed that this enhanced phase separation results in improved crystallisation of the hard domains, leading to the observed increase in ultimate tensile strength and elongation at break of the triblock copolymers. The mechanical properties of the triblock copolymers were also readily modified by changing the length of the hard block segment, with polymers comprising below 44 mol% PLLA possessing poor mechanical strength and those comprising above 68 mol% PLLA displaying inadequate elastomeric behaviour. However, materials consisting of 57 mol% PLLA displayed good tensile strength, flexibility, and elastomeric character. Further studies are required to optimise the mechanical properties and characterise the degradability of these materials. However, the readily tuneable flexibility and elastomeric nature of these polymers, the previously described hydrolytic degradability of the midblock segment (Chapter 3), and the potential to functionalise the triblock copolymers post-polymerisation makes these materials promising candidates for applications in the field of regenerative biomedicine.

5.4 References

- (1) Hutmacher, D. W. *Biomaterials* **2000**, *21*, 2529.
- (2) Kohane, D. S.; Langer, R. *Pediatr. Res.* **2008**, *63*, 487.
- (3) Pillai, C. K. S.; Sharma, C. P. *J. Biomater. Appl.* **2010**, *25*, 291.
- (4) Tateishi, T. C., Guoping; Ushida, Takashi; Murata, Toshimi; Mizuno, Shuichi
In *Tissue Engineering and Biodegradable Equivalents*; 1 ed.; Lewandrowski, K.-U. W., Donald L.; Trantolo, Debra J.; Gresser, Joseph D.; Yaszemski, Michael J.; Altobelli, David E., Ed.; Marcel Dekker: New York, 2002, p 99.
- (5) Ulery, B. D.; Nair, L. S.; Laurencin, C. T. *J. Polym. Sci. B: Polym. Phys.* **2011**, *49*, 832.
- (6) Shi, R.; Chen, D. F.; Liu, Q. Y.; Wu, Y.; Xu, X. C.; Zhang, L. Q.; Tian, W. *Int. J. Mol. Sci.* **2009**, *10*, 4223.
- (7) O'Brien, F. J. *Mater. Today* **2011**, *14*, 88.
- (8) Parthasarthy, M.; Sethuraman, S. In *Natural and Synthetic Biomedical Polymers*; 1 ed.; Kumbar, S. G., Laurencin, C. T., Deng, M., Eds.; Elsevier: San Diego, 2014, p 33.
- (9) Cohn, D.; Salomon, A. F. *Biomaterials* **2005**, *26*, 2297.
- (10) Salacinski, H. J.; Goldner, S.; Giudiceandrea, A.; Hamilton, G.; Seifalian, A. M.; Edwards, A.; Carson, R. J. *J. Biomater. Appl.* **2001**, *15*, 241.
- (11) Ballyk, P. D.; Walsh, C.; Butany, J.; Ojha, M. *J. Biomech.* **1998**, *31*, 229.
- (12) Stewart, S. F. C.; Lyman, D. J. *J. Biomech.* **1992**, *25*, 297.

- (13) Gupta, A. P.; Kumar, V. *Eur. Polym. J.* **2007**, *43*, 4053.
- (14) Gentile, P.; Chiono, V.; Carmagnola, I.; Hatton, P. V. *Int. J. Mol. Sci.* **2014**, *15*, 3640.
- (15) Jagur-Grodzinski, J. *Polymer. Adv. Tech.* **2006**, *17*, 395.
- (16) Dash, T. K.; Konkimalla, V. B. *J. Control. Release* **2012**, *158*, 15.
- (17) Nair, L. S.; Laurencin, C. T. *Prog. Polym. Sci.* **2007**, *32*, 762.
- (18) Ozdil, D.; Aydin, H. M. *J. Chem. Technol. Biotechnol.* **2014**, *89*, 1793.
- (19) Martin, D. P.; Williams, S. F. *Biochem. Eng. J.* **2003**, *16*, 97.
- (20) Chen, G. Q.; Wu, Q. *Biomaterials* **2005**, *26*, 6565.
- (21) Domb, A. J. K., Neeraj; Sheskin, Tzviel; Bentolila, Alfonso; Slager, Joram; Teomim, Doron In *Polymeric Biomaterials*; 2 ed.; Dumitriu, S., Ed.; CRC Press: Boca Raton, 2001.
- (22) Nagueh, S. F.; Shah, G.; Wu, Y. M.; Torre-Amione, G.; King, N. M. P.; Lahmers, S.; Witt, C. C.; Becker, K.; Labeit, S.; Granzier, H. L. *Circulation* **2004**, *110*, 155.
- (23) Mansour, J. M. In *Kinesiology: The Mechanics and Pathomechanics of Human Movement*; 2 ed.; Oatis, C. A., Ed.; Lippincott Williams and Wilkins: Baltimore, 2009, p 69.
- (24) Camarero-Espinosa, S.; Rothen-Rutishauser, B.; Foster, E. J.; Weder, C. *Biomater. Sci.* **2016**, *4*, 734.
- (25) Chen, Q. Z.; Bismarck, A.; Hansen, U.; Junaid, S.; Tran, M. Q.; Harding, S. E.; Ali, N. N.; Boccaccini, A. R. *Biomaterials* **2008**, *29*, 47.

- (26) Frydrych, M.; Roman, S.; Green, N. H.; MacNeil, S.; Chen, B. Q. *Polym. Chem.* **2015**, *6*, 7974.
- (27) Drobny, J. G. In *Handbook of Thermoplastic Elastomers*; 2 ed.; Elsevier: San Diego, 2014, p 1.
- (28) Shanks, R.; Kong, I. In *Thermoplastic Elastomers*; 1 ed.; El-Sonbati, A. Z., Ed.; InTech: Rijeka, 2012, p 137.
- (29) Kear, K. E. In *Developments in Thermoplastic Elastomers*; Rapra: Shrewsbury, 2003, p 3.
- (30) Chen, Q. Z.; Liang, S. L.; Thouas, G. A. *Prog. Polym. Sci.* **2013**, *38*, 584.
- (31) Sobczak, M. *Polym. Plast. Technol. Eng.* **2015**, *54*, 155.
- (32) Chauvel-Lebret, D. J.; Auroy, P.; Bonnaure-Mallet, M. In *Polymeric Biomaterials*; 2 ed.; Dumitriu, S., Ed.; CRC Press: Boca Raton, 2001, p 311.
- (33) Painter, P. C.; Coleman, M. M. In *Fundamentals of Polymer Science*; Painter, P. C., Coleman, M. M., Eds.; Technomic: Lancaster, PA, 1997, p 395.
- (34) Hamley, I. W. In *Developments in Block Copolymer Science and Technology*; 1 ed.; Hamley, I. W., Ed.; John Wiley & Sons: Chichester, 2004, p 1.
- (35) Bates, F. S.; Fredrickson, G. H. *Phys. Today* **1999**, *52*, 32.
- (36) Ravve, A. In *Principles of Polymer Chemistry*; 3 ed.; Springer: 2012, p 17.
- (37) Jones, R. A. L.; Richards, R. W. In *Polymers at Surfaces and Interfaces*; 1 ed.; Cambridge University Press: Cambridge, 1999, p 127.
- (38) Lendlein, A.; Langer, R. *Science* **2002**, *296*, 1673.
- (39) Frick, E. M.; Zalusky, A. S.; Hillmyer, M. A. *Biomacromolecules* **2003**, *4*, 216.

- (40) Gramlich, W. M. *Macromol. Chem. Phys.* **2015**, *216*, 145.
- (41) MacDonald, J. P.; Parker, M. P.; Greenland, B. W.; Hermida-Merino, D.; Hamley, I. W.; Shaver, M. P. *Polym. Chem.* **2015**, *6*, 1445.
- (42) Kong, J. F.; Lipik, V.; Abadie, M. J. M.; Deen, G. R.; Venkatraman, S. S. *Polym. Int.* **2012**, *61*, 43.
- (43) Lipik, V. T.; Kong, J. F.; Chattopadhyay, S.; Widjaja, L. K.; Liow, S. S.; Venkatraman, S. S.; Abadie, M. J. M. *Acta Biomater.* **2010**, *6*, 4261.
- (44) Qian, H. T.; Bei, J. Z.; Wang, S. G. *Polym. Degrad. Stab.* **2000**, *68*, 423.
- (45) Arias, V.; Olsén, P.; Odelius, K.; Höglund, A.; Albertsson, A. C. *Polym. Degrad. Stab.* **2016**.
- (46) Ryner, M.; Albertsson, A. C. *Biomacromolecules* **2002**, *3*, 601.
- (47) Hillmyer, M. A.; Tolman, W. B. *Acc. Chem. Res.* **2014**, *47*, 2390.
- (48) Wanamaker, C. L.; O'Leary, L. E.; Lynd, N. A.; Hillmyer, M. A.; Tolman, W. B. *Biomacromolecules* **2007**, *8*, 3634.
- (49) Wanamaker, C. L.; Tolman, W. B.; Hillmyer, M. A. *Biomacromolecules* **2009**, *10*, 443.
- (50) Lin, J.-O.; Chen, W.; Shen, Z.; Ling, J. *Macromolecules* **2013**, *46*, 7769.
- (51) Martello, M. T.; Schneiderman, D. K.; Hillmyer, M. A. *ACS Sustain. Chem. Eng.* **2014**, *2*, 2519.
- (52) Olsen, P.; Borke, T.; Odelius, K.; Albertsson, A.-C. *Biomacromolecules* **2013**, *14*, 2883.
- (53) Schneiderman, D. K.; Hillmyer, M. A. *Macromolecules* **2016**, *49*, 2419.

- (54) Xiong, M.; Schneiderman, D. K.; Bates, F. S.; Hillmyer, M. A.; Zhang, K. *Proc. Natl. Acad. Sci. U.S.A.* **2014**, *111*, 8357.
- (55) Guerin, W.; Helou, M.; Carpentier, J.-F.; Slawinski, M.; Brusson, J.-M.; Guillaume, S. M. *Polym. Chem.* **2013**, *4*, 1095.
- (56) Tyson, T.; Finne-Wistrand, A.; Albertsson, A.-C. *Biomacromolecules* **2009**, *10*, 149.
- (57) Zhang, Z.; Grijpma, D. W.; Feijen, J. *Macromol. Chem. Phys.* **2004**, *205*, 867.
- (58) Widjaja, L. K.; Kong, J. F.; Chattopadhyay, S.; Lipik, V. T.; Liow, S. S.; Abadie, M. J. M.; Venkatraman, S. S. *J. Mech. Behav. Biomed. Mater.* **2012**, *6*, 80.
- (59) Paul, S.; Romain, C.; Shaw, J.; Williams, C. K. *Macromolecules* **2015**, *48*, 6047.
- (60) Kobayashi, K.; Kanmuri, S.; Kimura, Y.; Masutani, K. *Polym. Int.* **2015**, *64*, 641.
- (61) Cohn, D.; Hotovely-Salomon, A. *Polymer* **2005**, *46*, 2068.
- (62) Kricheldorf, H. R.; Rost, S. *Macromolecules* **2005**, *38*, 8220.
- (63) Nakayama, Y.; Aihara, K.; Yamanishi, H.; Fukuoka, H.; Tanaka, R.; Cai, Z. G.; Shiono, T. *J. Polym. Sci. A: Polym. Chem.* **2015**, *53*, 489.
- (64) Trinca, R. B.; Felisberti, M. I. *Eur. Polym. J.* **2015**, *62*, 77.
- (65) Liow, S. S.; Lipik, V. T.; Widjaja, L. K.; Venkatraman, S. S.; Abadie, M. J. M. *Express Polym. Lett.* **2011**, *5*, 897.

- (66) Navarro-Baena, I.; Marcos-Fernandez, A.; Fernandez-Torres, A.; Kenny, J. M.; Peponi, L. *RSC Adv.* **2014**, *4*, 8510.
- (67) Widjaja, L. K.; Kong, J. F.; Chattopadhyay, S.; Lipik, V. T.; Liow, S. S.; Abadie, M. J. M.; Venkatraman, S. S. *J. Biomed. Mater. Res. A* **2011**, *99A*, 38.
- (68) Schneiderman, D. K.; Hill, E. M.; Martello, M. T.; Hillmyer, M. A. *Polym. Chem.* **2015**, *6*, 3641.
- (69) Hashimoto, T.; Imaeda, T.; Irie, S.; Urushisaki, M.; Sakaguchi, T. *J. Polym. Sci. A: Polym. Chem.* **2015**, *53*, 1114.
- (70) Mandal, P.; Choudhury, S.; Singha, N. K. *Polymer* **2014**, *55*, 5576.
- (71) Ren, P.; Wu, Y. B.; Guo, W. L.; Li, S. X.; Chen, Y. *Chin. J. Polym. Sci.* **2013**, *31*, 285.
- (72) Kavitha, A. A.; Singha, N. K. *Macromolecules* **2010**, *43*, 3193.
- (73) Zhang, K. R.; Aiba, M.; Fahs, G. B.; Hudson, A. G.; Chiang, W. D.; Moore, R. B.; Ueda, M.; Long, T. E. *Polym. Chem.* **2015**, *6*, 2434.
- (74) Xie, H.; He, M. J.; Deng, X. Y.; Du, L.; Fan, C. J.; Yang, K. K.; Wang, Y. Z. *ACS Appl. Mater. Interfaces* **2016**, *8*, 9431.
- (75) Wu, L. B.; Jin, C. L.; Sun, X. Y. *Biomacromolecules* **2011**, *12*, 235.
- (76) Matthew, H. W. T. In *Polymeric Biomaterials*; 2 ed.; Dumitriu, S., Ed.; CRC Press: Boca Raton, 2001, p 167.
- (77) Lohmeijer, B. G. G.; Pratt, R. C.; Leibfarth, F.; Logan, J. W.; Long, D. A.; Dove, A. P.; Nederberg, F.; Choi, J.; Wade, C.; Waymouth, R. M.; Hedrick, J. L. *Macromolecules* **2006**, *39*, 8574.

- (78) Aubin, M.; Prudhomme, R. E. *Polymer* **1981**, 22, 1223.
- (79) Mano, J. F.; Ribelles, J. L. G.; Alves, N. M.; Sanchez, M. S. *Polymer* **2005**, 46, 8258.
- (80) Drobny, J. G. In *Handbook of Thermoplastic Elastomers*; 2 ed.; Elsevier: San Diego, 2014, p 255.
- (81) Dutta, N. K.; Bhowmick, A. K.; Choudhury, N. R. In *Handbook of Thermoplastics*; 1 ed.; Olabisi, O., Ed.; Marcel Dekker: New York, 1997, p 349.
- (82) Nunes, R. W.; Martin, J. R.; Johnson, J. F. *Polym. Eng. Sci.* **1982**, 22, 205.
- (83) Andronova, N.; Albertsson, A. C. *Biomacromolecules* **2006**, 7, 1489.

6 Conclusions and Future Perspectives

6.1 Conclusions

The purpose of the research carried out for this thesis was to modify the physical and mechanical properties of an alkene-functional polycarbonate prepared by organocatalysed ring-opening polymerisation (ROP), both through post-polymerisation modification of the polymer and copolymerisation of the monomer with non-functional cyclic esters, in order to develop materials with tuneable properties for potential applications in the field of biomedicine. The key objectives listed to achieve this aim were; 1) to introduce additional functionality through post-polymerisation modification of the material, 2) to prepare stimuli-responsive materials, 3) to prepare random copolymers of the alkene-functional carbonate and a non-functional monomer with a view to controlling their degradation rates, 4) to prepare materials with potential applications as tissue scaffolds through a stereolithographic process, and 5) to synthesise thermoplastic elastomers with tuneable mechanical properties.

The first two of these objectives were successfully achieved in Chapter 2, in which the alkene-functional polycarbonate, poly(2-allyloxymethyl-2-ethyltrimethylene carbonate) (AOMECC) was prepared by ROP using highly active amidine and guanidine-based catalysts and a variety of alcohol-functional initiators. Post-polymerisation modification of the pendent alkene groups *via* radical thiol-ene addition chemistry enabled the preparation of polycarbonates bearing a wide range of chemical functionalities including alkyl, benzyl, acid and alcohol groups, and enabled the grafting of thiol-functional poly(ethylene glycol) chains to the polymer backbone to generate polymers with tuneable thermoresponsive properties.

Chapter 3 was successful in preparing random copolymers of AOMECE and the non-functional cyclic ester δ -valerolactone (VL), and terpolymers of AOMECE, VL and an alkyl-functional analogue of AOMECE to allow the independent tuning of alkene functional group density and ester:carbonate composition. However, the ability to modify the degradation rates of these materials could not be demonstrated, as the methodology devised for the degradation study of the liquid polymers was proved to be unsuitable for monitoring the hydrolysis of these materials.

The fourth objective was achieved in Chapter 4, with a porous 3D network prepared by microstereolithography of a resin based on PAOMECE and a tetrathiol-based crosslinker. Further, through partial epoxidation of PAOMECE prior to 3D printing, basic structures could be printed bearing free epoxide functionality for potential modification to enhance hydrophilicity or cell compatibility post-fabrication.

The final objective was achieved in Chapter 5, with thermoplastic elastomers prepared by polymerisation of *L*-lactide (LLA) using random copolymers of AOMECE and VL as macroinitiators to generate ABA triblock copolymers. The mechanical properties of the materials were successfully modified by variation of both midblock and ABA composition, thus demonstrating the potential of preparing materials with specific properties for different applications.

As such, the majority of the planned objectives were successfully realised. The development and potential of the work detailed in this thesis provides a platform for further research in a wide range of areas, a selection of which are suggested herein.

6.2 Further work

Additional investigations are currently ongoing in the optimisation of the 3D-printable resins and thermoplastic elastomers described above. In the case of the former, work is currently focussed on reducing both build times and overcure along the Z-axis of the printed materials. In particular, this work involves attempts to reduce the viscosity of the printable resin, as lower viscosity resins require less time to settle following the dipping of the build plate into the resin, thus decreasing dwell time (improving build speed) and defects arising from unwanted resin adherence (improving feature fidelity).^{1,2} Current strategies under consideration are variation of temperature, incorporation of reactive diluents, or synthesising PAOMEC polymers with lower viscosity. Whilst the latter method has to date proven challenging (as discussed in Chapter 4), this may be achieved by increasing the initiator content of the reaction and simultaneously reducing the catalyst loading, thus reducing the rate of propagation relative to initiation. In the case of thermoplastic elastomers, work is primarily focussed on expanding the range of hard block incorporations investigated, and increasing the molecular weight of the amorphous segment. The latter approach is known to improve elongations and elastomeric character as a consequence of the longer polymer chains and resultant increase in entropy, and also results in the degree of phase separation between segments increasing up to a threshold chain length, thus improving mechanical strength.^{3,4}

In addition to this work, an important avenue of further investigation should be the determination of the cytocompatibility of the PAOMEC-based materials described above, as the use of these material for biomedical applications is critically dependent on their biocompatibility, which remains to be determined. It is proposed that these cytocompatibility studies should be carried out by cell viability and proliferation tests,

for example by cell spreading assays using MC3T3 pre-osteoblasts, and additionally by cell differentiation tests using human mesenchymal stem cells.

An effective method of monitoring the degradation rates of PAOMEC and P(AOMEC-co-VL) copolymers should be developed, in order to monitor the effect of changing ester:carbonate composition on the degradation rate of the polymers. Providing that this can be achieved, the enzyme-catalysed hydrolysis of P(AOMEC-co-VL) copolymers should also be investigated. Aliphatic polycarbonates have previously been shown to be susceptible to accelerated hydrolysis under enzyme-catalysed conditions, such as those found in the extracellular matrix *in vivo*.⁵ As extracellular enzymes are too large to penetrate the polymer matrix, only the exterior of the polymer matrix is subjected to accelerated hydrolysis, leading to the materials degrading *via* a surface erosion mechanism, a desirable property for several biomedical applications.^{5,6} The susceptibility of aliphatic polyesters and polycarbonates to enzymatic hydrolysis is highly dependent on the structure of the polymer and its repeat unit, with rigid, highly ordered, semi-crystalline polymers less able to conform to the active site of the enzyme than more flexible, amorphous polymers.⁵ The effect of changing the ester to carbonate ratio of P(AOMEC-co-VL) copolymers on degradation rates and behaviour under enzymatic hydrolysis is therefore of significant interest.

The facile synthesis of materials bearing dual functionality should also be further investigated. As demonstrated in Chapter 4, PAOMEC can be readily partially functionalised by epoxidation to yield materials bearing both alkene and epoxide functionalities. The preparation of polycarbonates bearing dual functionality could enable the sequential modification of these polymers by radical thiol-ene addition and epoxide ring-opening reactions. Such an approach could be used to generate materials

simultaneously bearing multiple functional groups incompatible with ROP, or may enable the functionalisation density of the polymers to be readily tuned, *e.g.* by functionalising either the alkene or epoxide group with a non-reactive functionality. The latter method is of particular interest for the attachment of cell-promoting functionalities, where the functionalisation density of these bioactive groups has proven to be crucial in determining the ability of cells to proliferate.⁷ In addition, with regards to the work described in Chapter 2, this approach could be used to modify the grafting density of poly(ethylene glycol) (PEG) onto the polymer backbone, and further fine-tune the lower critical solution temperature (LCST) of these materials as a result. An additional approach which is currently under investigation is the use of the epoxide functionality for 3D printing, using either a photoacid generator or a multi-functional amine crosslinker, thus generating 3D constructs bearing free alkene functionality for post-fabrication modification. This would enable the preparation of 3D printed materials either through the epoxide or alkene functionality, leaving the other functionality free for post-fabrication modification depending on the desired application.

6.3 References

- (1) Bártolo, P. J. In *Stereolithography*; 1 ed.; Bártolo, P. J., Ed.; Springer: 2011, p 1.
- (2) Choi, J. W.; Wicker, R.; Lee, S. H.; Choi, K. H.; Ha, C. S.; Chung, I. J. *Mater. Process. Tech.* **2009**, *209*, 5494.
- (3) Drobny, J. G. In *Handbook of Thermoplastic Elastomers*; 2 ed.; Elsevier: San Diego, 2014, p 1.
- (4) Dutta, N. K.; Bhowmick, A. K.; Choudhury, N. R. In *Handbook of Thermoplastics*; 1 ed.; Olabisi, O., Ed.; Marcel Dekker: New York, 1997, p 349.
- (5) Artham, T.; Doble, M. *Macromol. Biosci.* **2008**, *8*, 14.
- (6) Lyu, S. P.; Untereker, D. *Int. J. Mol. Sci.* **2009**, *10*, 4033.
- (7) Griffith, L. G.; Naughton, G. *Science* **2002**, *295*, 1009.

7 Experimental

7.1 Materials

All chemicals and solvents, unless otherwise stated, were ordered from Sigma-Aldrich or Fisher Scientific and used without further purification. Silica gel (pore size = 40 Å) was obtained from Fischer Scientific and used as received. Dry toluene, tetrahydrofuran and methylene chloride were obtained by purification over an Innovative Technology SPS alumina column and degassed by repeated freeze-pump-thawing prior to use. 3-Mercaptopropionic acid was ordered from Alfa Aesar and used as received. 1,8-diazabicyclo[5.4.0]undec-7-ene (DBU) and δ -valerolactone (VL) (Alfa Aesar) were dried over CaH₂, distilled, and stored under an inert atmosphere of N₂. 1,5,7-triazabicyclo[4.4.0]dec-5-ene (TBD) was dried by sublimation and stored under an inert atmosphere of N₂. CHCl₃, CDCl₃, benzyl alcohol and 1,4-butanediol were dried over 3 Å molecular sieves and stored under an inert atmosphere of N₂. 1,4-benzenedimethanol (BDM) (Tokyo Chemical Industry) and poly(ethylene glycol) (PEG) (number-average molecular weight (M_n) = 2,000 g mol⁻¹) were dried over 3 Å molecular sieves in dry methylene chloride, and stored under an inert atmosphere of N₂ following the removal of sieves by cannula filtration and the removal of solvent under reduced pressure. Pentaerythritol dibenzyl ether (PDE) was synthesised as reported,¹ and sublimed three times before storage under an inert atmosphere of N₂. 1-(3,5-bis(trifluoromethyl)phenyl)-3-cyclohexylthiourea (TU)² and 5-methyl-5-allyloxycarbonyl-1,3-dioxan-2-one (MAC)³ were synthesised as previously reported and dried over CaH₂ in dry tetrahydrofuran. TU and MAC were isolated by removal of the drying agent *via* cannula filtration, followed by removal of the solvent under reduced pressure, and stored under an inert atmosphere of N₂. *L*-lactide (Corbion Purac) was purified by passing a solution of the material in methylene chloride through a silica plug and recrystallising from toluene, followed by dissolution in dry methylene

chloride and drying over two sets of 3 Å molecular sieves. The solution was then removed from sieves by cannula filtration, followed by removal of the solvent under reduced pressure. The *L*-lactide was recrystallised from dry toluene and the solvent removed thoroughly under reduced pressure before storage in an N₂ glovebox. Acidic Amberlyst 15 and Dowex 50WX8 ion exchange resins were washed repeatedly with methanol and air-dried prior to use. Irgacure 369, 714 and 819 photoinitiators were obtained from BASF and stored in a light-free environment prior to use.

7.2 General Considerations

All polymerisations were performed under an inert nitrogen atmosphere in a glovebox unless otherwise stated.

7.2.1 NMR spectroscopy

NMR spectra were recorded on a Bruker Avance III 400 MHz, Avance III HD 400 MHz or Avance III HD 500 MHz spectrometer at 293 K. Chemical shifts are reported as δ in parts per million (ppm) and referenced to the residual solvent signal (CDCl₃: ¹H, δ = 7.26 ppm, ¹³C, δ = 77.16 ppm, (CD₃)₂SO: ¹H, δ = 2.50 ppm, ¹³C, δ = 39.52 ppm, (CD₃)₂CO: ¹H, δ = 2.05 ppm, ¹³C, δ = 29.84 ppm (CD₃), 206.26 ppm (CO).

7.2.2 Mass spectrometry

High resolution mass spectrometry was performed on a Bruker UHR-Q-ToF MaXis spectrometer with electrospray ionisation. MALDI-ToF (matrix-assisted laser desorption ionisation-time of flight) mass spectrometry analysis was performed on a Bruker Daltonics Ultraflex II mass spectrometer using a nitrogen laser delivering 2 ns pulses at 337 nm with positive ion ToF detection performed using an accelerating voltage of 25 kV. Trans-2-[3-(4-tertbutylphenyl)-2-methyl-2-propylidene]malonitrile (DCTB) was used as a matrix (0.6 μ L of a 10 g L⁻¹ solution in tetrahydrofuran), with

sodium trifluoroacetate used as a cationisation agent (0.6 μL of a 10 g L^{-1} solution in tetrahydrofuran). Analyte (0.3 μL of a 5 g L^{-1} solution in tetrahydrofuran) was applied in between separate loadings of DCTB and sodium trifluoroacetate, with solvent being allowed to evaporate between applications, to form a thin matrix-analyte-matrix film. All samples were measured in reflectron mode and calibrated against a 2000 g mol^{-1} poly(ethylene glycol) standard.

7.2.3 Size exclusion chromatography

Size exclusion chromatography (SEC) was conducted on systems composed of a Varian 390-LC-Multi detector suite fitted with differential refractive index (RI), light scattering, and ultraviolet detectors, equipped with a guard column (Varian Polymer Laboratories PLGel 5 μM , 50 \times 7.5 mm) and two mixed D columns (Varian Polymer Laboratories PLGel 5 μM , 300 \times 7.5 mm). The mobile phase was either CHCl_3 (HPLC grade) with 0.5% triethylamine, or dimethylformamide (DMF), with a flow rate of 1.0 mL min^{-1} . SEC samples were calibrated against either Varian Polymer Laboratories Easi-Vials linear poly(styrene) standards (162 – 2.4 $\times 10^5$ g mol^{-1}) (CHCl_3 SEC), or linear poly(methyl methacrylate) standards (556 – 1.8 $\times 10^6$ g mol^{-1}) (DMF SEC) using Cirrus v3.3 software.

7.2.4 FT-IR spectroscopy

IR spectra were obtained using a Perkin-Elmer Spectrum 100 FT-IR spectrometer. Observed spectra were an accumulation of 16 scans with a background scan subtracted.

7.2.5 UV light source for post-polymerisation modifications

Photoinitiated post-polymerisation functionalisations were carried out in a Metalight QX1 light box equipped with 12 \times 9 W bulbs with a peak output at $\lambda = 365$ nm.

Samples were typically placed 10 cm away from the source with the bulbs arranged concentrically around them.

7.2.6 Determination of lower critical solution temperatures (LCST)

Lower critical solution temperature (LCST) measurements were recorded using a Perkin-Elmer UV-Vis Spectrometer (Lambda 35) equipped with a Peltier temperature control system, using a wavelength of 500 nm and a heating/cooling rate of 1 °C min⁻¹. Reported values were taken at 50% of normalised transmittance.

7.2.7 Rheometry

Rheological testing was carried out using an Anton Parr MCR 302 rheometer equipped with a cone and plate configuration with a diameter of 60 mm. Samples were subjected to rotational shear stress across shear rates of 0.1 to 10 s⁻¹, with a Peltier system used to maintain the temperature at 25 °C throughout the study. Data was analysed using RheoCompass software.

7.2.8 Degradation studies

Degradation studies were performed by weighing samples (50 mg) into individual glass vials and adding 10 mL of 5 M KOH solution. The vials were then sealed and incubated at 37 °C with constant agitation at 60 rpm. Sample recovery was performed by extraction into CHCl₃, and the change in molecular weight monitored by SEC.

7.2.9 Mechanical testing

Uniaxial tensile testing was performed at ambient temperature using a Tensiometric M100-1CT system with a load cell capacity of 1 kN and a crosshead speed of 2 mm min⁻¹ (5 mm min⁻¹ for cyclic extension testing) with a pre-measured grip-to-grip separation. Uniform dog-bone samples were prepared either by compression moulding samples in PTFE moulds at 95 °C using a Specac Atlas Manual 15T hydraulic press

equipped with heated platens, or by photocuring samples in a stainless steel template backed with transparent polypropylene film, using 200 pulses of UV light delivered by an Envisiontec Otofash unit equipped with 2×100 W lamps with peak output at $\lambda = 365$ nm. Block copolymer samples were thermally annealed at 37 °C in an incubator for 5 days prior to tensile testing, in order to allow complete microphase separation to occur. Samples were loaded axially into the apparatus, with a minimum of 5 samples of each material tested, and results recorded using winTest v4.3.2 software.

7.2.10 Dynamic mechanical thermal analysis (DMTA)

Dynamic mechanical thermal analysis (DMTA) was performed by single cantilever bending using a Mettler Toledo DMA 1 Star system. Samples were shaped into rectangular bars by compression moulding and allowed to anneal at 37 °C in an incubator over 5 days, before analysis using an oscillation frequency of 5.0 and 0.5 MHz and a displacement of 10 mm across a temperature range of -80 to 80 °C at a heating rate of 2 °C min^{-1} . Data was analysed using STARe V13.00a software (build 6917).

7.2.11 Thermal analysis

Differential scanning calorimetry (DSC) and thermogravimetric analysis (TGA) were performed using Mettler Toledo DSC1 Star and TGA/DSC Star systems. DSC heating and cooling cycles were run in triplicate in series between -80 and 100 °C under a nitrogen atmosphere at a heating rate of ± 2 °C min^{-1} in a 40 μL aluminium crucible. TGA was conducted between 20 and 300 °C at a heating rate of 10 °C min^{-1} in a 40 μL aluminium crucible.

7.2.12 Microstereolithography (μ SL)

Microstereolithography (μ SL) was performed using a custom-built system mounted on an optics bench. The system comprised of a BenQ W1000+ DMD projector equipped with a purple light engine (peak output at source $\lambda = 415$ nm, peak output at build plate $\lambda = 415$ nm) and monochromatic purple light filter, a 45° mirror to direct the projected image, a polydimethylsiloxane (PDMS) resin tray, and a build platform mounted on a linear motion stage (Aerotech ATS100-100_UF). Computer-aided design (CAD) representations of the desired structures were cut into 2D-slices of desired thickness using Perfactory RP 2.6 software. These slices were then rendered as black and white slides in Microsoft PowerPoint to create a dynamic pattern mask, and projected layer-by-layer in sequence onto the resin in order to generate the desired 3D structure in solid form. The motion of the build platform was controlled using Aerotech Ensemble Motion Composer Suite, with the platform raised by $100 \mu\text{m}$ between each layer.

7.2.13 Computed tomography

Micro CT scans were performed on a Bruker Skyscan 1174 Compact X-ray Microtomography system. Scans were carried out using small camera pixels for a 180° scan with a step rotation of 0.3° and an averaging of 3 frames in the Skyscan1174v2 software. The X-ray source was set to a maximum voltage and current of 50kV and $800\mu\text{A}$ respectively with no filter applied in this instance. The 3D reconstruction was carried out using NRcon software taking advantage of smoothing, a misalignment compensation of 2.5, a ring artefact reduction set to 16 and beam hardening set to 65% before being analysed and imaged using the CTVox software.

7.3 Experimental protocols

7.3.1 Synthesis of 2-allyloxymethyl-2-ethyltrimethylene carbonate (AOMEC)

Trimethylolpropane allyl ether diol (60 mL, 348 mmol) was dissolved in methylene chloride (1 L) in a 2 L round-bottomed flask, which was cooled to 0 °C. Ethyl chloroformate (99 mL, 1.038 mol) was then added and the solution stirred at 0 °C for 30 minutes. Triethylamine (145.2 mL, 1.038 mol) was added dropwise over a period of 1 h. The reaction was then allowed to warm to room temperature and stirred for 12 h, at which point the reaction mixture was filtered and concentrated under reduced pressure. The resulting oil was dissolved in ethyl acetate (200 mL) and washed with 1 M HCl (2 × 200 mL) followed by water (2 × 200 mL). The organic fraction was dried with anhydrous magnesium sulfate, filtered and concentrated under reduced pressure to yield the crude product as a yellow oil. The crude product was purified by vacuum distillation twice to yield pure AOMEC as a colourless oil (yield = 50.9 g, 254 mmol, 73%). The product was dried over CaH₂, recovered by vacuum distillation and stored in a glovebox for use as monomer. Literature contains information on ¹H and ¹³C NMR spectra only, which are in agreement with acquired data.⁴ ¹H NMR (CDCl₃, 400 MHz): δ = 5.84-5.74 (m, 1H, CH₂-CH=CH₂), 5.22-5.11 (m, 2H, CH=CH₂), 4.28-4.01 (dd, ²J_{H-H} = 72.9 Hz, ³J_{H-H} = 10.9 Hz, 4H, O-CH₂-C-CH₂-O), 3.91 (d, ³J_{H-H} = 5.6 Hz, 2H, O-CH₂-CH), 3.34 (s, 2H, C-CH₂-O), 1.49 (q, ³J_{H-H} = 7.6 Hz, 2H, C-CH₂-CH₃), 0.85 (t, ³J_{H-H} = 7.6 Hz, 3H, -CH₂-CH₃). ¹³C NMR (125 MHz, CDCl₃): δ 148.5 (O-C(O)-O), 134.0 (CH₂-CH=CH₂), 117.4 (CH=CH₂), 72.8 (O-CH₂-C), 72.3 (O-CH₂-CH), 68.2 (C-CH₂-O), 35.4 (C(CH₂)₄), 23.2 (CH₃-CH₂), 7.3 (CH₃-CH₂). MS (ESI, +ve): *m/z* 200.1039 (M⁺). Anal. calcd for C₁₀H₁₆O₄: C 60.0; H 8.1; N 0.0%. Found: C 59.9; H 8.0; N 0.1%. FT-IR: max/cm⁻¹ 2910 (C=C(H)₂) 1746 (O-C(O)-O), 1170 (H₂C-O-CH₂), 1109 and 1090 (C-C(H)=C(H)₂).

^1H NMR and ^{13}C NMR spectra are shown in Figure 2.1 and A-11 respectively.

7.3.2 General procedure for the synthesis of poly(2-allyloxymethyl-2-ethyltrimethylene carbonate (PAOMEC) by DBU/TU-catalysed ring-opening polymerisation (ROP)

In a typical experiment, the alcohol initiator (0.35-10 mol% to monomer dependent on $[\text{M}]_0:[\text{I}]_0$), 1,8-diazabicyclo[5.4.0]undec-7-ene (5 mol% to monomer) and 1-(3,5-bis(trifluoromethyl)phenyl)-3-cyclohexylthiourea (5 mol% to monomer) catalysts were dissolved in dry CDCl_3 or methylene chloride. AOMEC was dissolved separately in the same solvent and added to the initiator/catalyst solution (overall AOMEC concentration = 2 M). Conversion of monomer to polymer was monitored by ^1H NMR spectroscopy. At 80% monomer conversion, the polymerisation was quenched either by addition of acidic Amberlyst A15 ion exchange resin or by addition of benzoic acid (5 mg per 1 mg of DBU). Polymers were purified either by repeated precipitations into cold *n*-hexane, or by column chromatography using methylene chloride as eluent to remove trace thiourea, followed by ethyl acetate to recover the pure polymer, and subsequent precipitation into cold *n*-hexane. ^1H NMR (400 MHz, CDCl_3): δ 5.91-5.77 (m, 1H, $\text{CH}_2\text{-CH}=\text{CH}_2$), 5.28-5.08 (m, 2H, $\text{CH}=\text{CH}_2$), 4.13-4.05 (m, 4H, $\text{O-CH}_2\text{-C-CH}_2\text{-O}$), 3.91 (dd, $^3J_{\text{H-H}} = 5.4$ Hz, $^2J_{\text{H-H}} = 1.7$ Hz, 2H, $\text{O-CH}_2\text{-CH}=\text{CH}_2$), 3.31 (s, 2H, $\text{C-CH}_2\text{-O}$), 1.47 (q, $^3J_{\text{H-H}} = 7.5$ Hz, 2H, $\text{C-CH}_2\text{-CH}_3$), 0.86 (t, $^3J_{\text{H-H}} = 7.6$ Hz, 3H, $\text{CH}_2\text{-CH}_3$). ^{13}C NMR (125 MHz, CDCl_3): δ 155.0 (O-C(O)-O), 134.6 ($\text{CH}_2\text{-CH}=\text{CH}_2$), 116.6 ($\text{CH}=\text{CH}_2$), 72.1 ($\text{O-CH}_2\text{-CH}$), 69.3 (C(O)-O-CH_2), 67.7 ($\text{C-CH}_2\text{-O}$), 41.8 ($\text{C}(\text{CH}_2)_4$), 22.5 ($\text{CH}_3\text{-CH}_2$), 7.3 ($\text{CH}_3\text{-CH}_2$). For $[\text{M}]_0:[\text{I}]_0 = 24$, $M_n = 3,800$ g mol^{-1} (DP 19, determined by ^1H NMR, 400 MHz, CDCl_3). $M_n = 4,100$ g mol^{-1} , $D_M = 1.09$ (determined by SEC using RI detection and CHCl_3 as eluent).

^1H NMR spectrum and size exclusion chromatograms are shown in Figure 2.4 and 2.7 respectively, ^{13}C NMR spectrum is shown in Figure A-12.

7.3.3 Synthesis of poly(*L*-lactide)-*b*-poly(AOMECE)-*b*-poly(*L*-lactide) (PLLA-*b*-PAOMECE-*b*-PLLA)

PAOMECE (50 mg, 3.2 μmol , $M_n = 15,800 \text{ g mol}^{-1}$) and *L*-lactide (42 mg, 300 μmol) were dissolved in CDCl_3 (500 μL). DBU (1 mol% to lactide) was then added to catalyse the polymerisation of lactide. The polymerisation was monitored by ^1H NMR spectroscopy. At completion, the polymerisation was quenched by addition of acidic Amberlyst A15 ion exchange resin. The resulting copolymer was then purified by repeated precipitations into cold *n*-hexane to yield pure PLLA-*b*-PAOMECE-*b*-PLLA. ^1H NMR (400 MHz, CDCl_3): δ 5.91-5.77 (m, 1H, $\text{CH}_2\text{-CH}=\text{CH}_2$), 5.28-5.08 (m, 2H, + 1H, $\text{CH}_2\text{-CH}=\text{CH}_2$, $\text{C(O)-C(CH}_3\text{)H-O}$), 4.13-4.05 (m, 4H, $\text{O-CH}_2\text{-C-CH}_2\text{-O}$), 3.91 (dd, $^3J_{\text{H-H}} = 5.4 \text{ Hz}$, $^2J_{\text{H-H}} = 1.7 \text{ Hz}$, 2H, $\text{O-CH}_2\text{-CH}$), 3.31 (s, 2H, $\text{C-CH}_2\text{-O}$), 1.65 (d, $^3J_{\text{H-H}} = 1.6 \text{ Hz}$ 2H, C(O)-CH-CH_3), 1.47 (q, $^3J_{\text{H-H}} = 7.5 \text{ Hz}$, 2H, $\text{C-CH}_2\text{-CH}_3$), 0.86 (t, $^3J_{\text{H-H}} = 7.6 \text{ Hz}$, 3H, $\text{CH}_2\text{-CH}_3$). ^{13}C NMR (125 MHz, CDCl_3): δ 169.6 (CH-C(O)-CO), 155.0 (O-C(O)-O), 134.6 ($\text{CH}_2\text{-CH}=\text{CH}_2$), 116.6 ($\text{C-CH}=\text{CH}_2$), 72.1 ($\text{O-CH}_2\text{-CH}$), 69.3 (C(O)-O-CH_2), 67.7 ($\text{C-CH}_2\text{-O}$), 41.8 ($\text{C(CH}_2\text{)}_4$), 22.5 ($\text{CH}_3\text{-CH}_2\text{-C}$), 16.7 ($\text{CH}_3\text{-CH-C(O)}$), 7.3 ($\text{CH}_3\text{-CH}_2\text{-C}$). $M_n = 29,400 \text{ g mol}^{-1}$ (determined by ^1H NMR, 400 MHz, CDCl_3). $M_n = 30,100 \text{ g mol}^{-1}$, $D_M = 1.12$ (determined by SEC using RI detection and CHCl_3 as eluent).

^1H NMR spectrum and size exclusion chromatogram are shown in Figure 2.11 and 2.12 respectively, ^{13}C NMR spectrum is shown in Figure A-13.

7.3.4 Synthesis of PAOME**C**-*b*-PEG-*b*-PAOME**C**

PEG (40 mg, 2×10^{-5} mol, $M_n = 2,000$ g mol⁻¹, $D_M = 1.04$) and AOME**C** (200 mg, 1 mmol) were dissolved in CDCl₃ (250 μL). DBU (5 mol% to monomer) and thiourea (5 mol% to monomer) catalysts were dissolved in the same solvent (250 μL) in a separate vessel and added to the initiator/monomer solution. The conversion of AOME**C** to PAOME**C** was monitored by ¹H NMR spectroscopy. At 80% monomer conversion, the polymerisation was quenched by addition of acidic Amberlyst A15 ion exchange resin. The resulting copolymer was then purified by repeated precipitation into cold *n*-hexane to yield pure PAOME**C**-*b*-PEG-*b*-PAOME**C**. ¹H NMR (400 MHz, CDCl₃): δ 5.92-5.78 (m, 1H, CH₂-CH=CH₂), 5.28-5.08 (m, 2H, CH=CH₂), 4.13-4.05 (m, 4H, O-CH₂-C-CH₂-O), 3.91 (dd, ³J_{H-H} = 5.4 Hz, ²J_{H-H} = 1.7 Hz, 2H, O-CH₂-CH=CH₂), 3.66-3.64 (m, ³J_{H-H} = 1.7 Hz, 2H, PAOME**C**-O-CH₂(PEG)), 3.64 (s, 4H, O-CH₂-CH₂-O(PEG)), 3.31 (s, 2H, C-CH₂-O), 1.47 (q, ³J_{H-H} = 7.5 Hz, 2H, C-CH₂-CH₃), 0.86 (t, ³J_{H-H} = 7.6 Hz, 3H, CH₂-CH₃). $M_n = 9,200$ g mol⁻¹ (determined by ¹H NMR, 400 MHz, CDCl₃), $M_n = 13,300$ g mol⁻¹, $D_M = 1.07$ (determined by SEC using RI detection and CHCl₃ as eluent).

¹H NMR spectrum and size exclusion chromatogram are shown in Figure 2.9 and 2.10 respectively.

7.3.5 General procedure for synthesis of P(AOME**C**-*co*-VL) by organocatalysed ring-opening copolymerisation

In a typical experiment, the alcohol initiator (0.35-10 mol% to monomer dependent on target M_n), DBU (5 mol% to monomer) and TU (5 mol% to monomer) catalysts were dissolved in CDCl₃ or methylene chloride. Monomer feed ratios were varied according to the copolymer composition targeted. AOME**C** and VL were dissolved in

a separate container using the same solvent and added to the initiator/catalyst solution (overall monomer concentration = 2 M). Conversion of monomer to polymer was monitored by ^1H NMR spectroscopy. At 80% conversion of either monomer, the polymerisation was quenched by addition of acidic Amberlyst A15 ion exchange resin or by addition of benzoic acid (5 mg per 1 mg of DBU). Polymers were purified by precipitations into cold *n*-hexane, or by column chromatography using methylene chloride as eluent to remove trace thiourea, followed by ethyl acetate to recover the pure polymer, and subsequent precipitation into cold *n*-hexane. ^1H NMR (400 MHz, CDCl_3): δ 5.93-5.77 (m, 1H, $\text{CH}_2\text{-CH}=\text{CH}_2$), 5.29-5.09 (m, 2H, $\text{CH}=\text{CH}_2$), 4.15-4.06 (m, 2H + 4H, $\text{CH}_2\text{-O-C(O)}_{(\text{PVL})}$, $\text{O-CH}_2\text{-C-CH}_2\text{-O}_{(\text{PAOMECE})}$), 3.92 (dd, $^3J_{\text{H-H}} = 5.4$ Hz, $^2J_{\text{H-H}} = 1.7$ Hz, 2H, $\text{O-CH}_2\text{-CH}$), 3.31 (s, 2H, $\text{C-CH}_2\text{-O}$), 2.42 – 2.29 (m, 2H, $\text{O-CH}_2\text{-CH}_2$), 1.70 (m, 4H, $\text{CH}_2\text{-CH}_2\text{-CH}_2\text{-CH}_2$), 1.47 (q, $^3J_{\text{H-H}} = 7.5$ Hz, 2H, $\text{C-CH}_2\text{-CH}_3$), 0.86 (t, $^3J_{\text{H-H}} = 7.6$ Hz, 3H, $\text{CH}_2\text{-CH}_3$). ^{13}C NMR (125 MHz, CDCl_3): δ 173.4-173.0 ($\text{CH}_2\text{-C(O)-O}$), 155.4-155.3 (O-C(O)-O), 134.7 ($\text{CH}_2\text{-CH}=\text{CH}_2$), 116.7 ($\text{CH}=\text{CH}_2$), 72.3 ($\text{O-CH}_2\text{-CH}$), 69.5 (C(O)-O-CH_2), 67.8 ($\text{O-CH}_2\text{-C}$, $\text{O-CH}_2\text{-CH}_2$), 64.3 ($\text{CH}_2\text{-O-C(O)}$), 41.9 ($\text{C}(\text{CH}_2)_4$), 33.7 ($\text{O-CH}_2\text{-CH}_2\text{-CH}_2$), 28.2 ($\text{C(O)-CH}_2\text{-CH}_2\text{-CH}_2$), 22.5 ($\text{O-CH}_2\text{-CH}_2\text{-CH}_2$), 21.2 ($\text{CH}_3\text{-CH}_2$), 7.5 ($\text{CH}_3\text{-CH}_2$). For $\text{P}(\text{AOMECE}_{47\text{-}co\text{-}}\text{VL}_{31})$, $M_n = 12,500$ g mol^{-1} (DP 98, determined by ^1H NMR, 400 MHz, CDCl_3), $M_n = 13,400$ g mol^{-1} , $D_M = 1.09$ (determined by SEC using RI detection and CHCl_3 as eluent).

^1H NMR spectrum and size exclusion chromatogram are shown in Figure 3.4 and 3.5 respectively, ^{13}C NMR spectrum is shown in Figure A-14.

7.3.6 General procedure for the synthesis of PAOMECE by TBD-catalysed ROP

In a typical experiment, the alcohol initiator (0.35-10 mol% to monomer dependent on target $[\text{M}]_0:[\text{I}]_0$), and triazabicyclo[4.4.0]dec-5-ene (0.5 mol% to monomer) were dissolved in dry CDCl_3 . AOMECE was dissolved separately using the same solvent and

added to the initiator/catalyst solution (overall AOMECE concentration = 4 M). Conversion of monomer to polymer was monitored by ^1H NMR spectroscopy, and the polymerisation quenched by addition of acidic Amberlyst A15 ion exchange resin at 80% monomer conversion. Polymers were purified by repeated precipitation into cold *n*-hexane. ^1H NMR (400 MHz, CDCl_3): δ 5.91-5.77 (m, 1H, $\text{CH}_2\text{-CH}=\text{CH}_2$), 5.28-5.08 (m, 2H, $\text{CH}=\text{CH}_2$), 4.13-4.05 (m, 4H, $\text{O-CH}_2\text{-C-CH}_2\text{-O}$), 3.91 (dd, $^3J_{\text{H-H}} = 5.4$ Hz, $^2J_{\text{H-H}} = 1.7$ Hz, 2H, $\text{O-CH}_2\text{-CH}$), 3.31 (s, 2H, $\text{C-CH}_2\text{-O}$), 1.47 (q, $^3J_{\text{H-H}} = 7.5$ Hz, 2H, $\text{C-CH}_2\text{-CH}_3$), 0.86 (t, $^3J_{\text{H-H}} = 7.6$ Hz, 3H, $\text{CH}_2\text{-CH}_3$). ^{13}C NMR (101 MHz, CDCl_3): δ 155.0 (O-C(O)-O), 134.6 ($\text{CH}_2\text{-CH}=\text{CH}_2$), 116.6 ($\text{CH}=\text{CH}_2$), 72.1 ($\text{O-CH}_2\text{-CH}$), 69.3 (C(O)-O-CH_2), 67.7 ($\text{C-CH}_2\text{-O}$), 41.8 ($\text{C}(\text{CH}_2)_4$), 22.5 ($\text{CH}_3\text{-CH}_2$), 7.3 ($\text{CH}_3\text{-CH}_2$). For $[\text{M}]_0:[\text{I}]_0 = 100$, $M_n = 18,000$ g mol $^{-1}$ (DP 90, determined by ^1H NMR, 400 MHz, CDCl_3), $M_n = 19,300$ g mol $^{-1}$, $D_M = 1.10$ (determined by SEC using RI detection and CHCl_3 as eluent).

^1H NMR and size exclusion chromatograms are shown in Figure 2.3 and 2.13 respectively, ^{13}C NMR spectrum is shown in Figure A-12.

7.3.7 Post-polymerisation functionalisation of PAOMECE with 1-dodecanethiol (DDT)

PAOMECE (20 mg, DP 20, 5 μmol) and 1-dodecanethiol (2 equivalents to polymer alkene groups, 202 mg, 1 mmol) were dissolved in 1,4-dioxane (0.4 mL). The radical photoinitiator, 2-benzyl-2-(dimethylamino)-4'-morpholinobutyrophenone (0.37 mg, 1 μmol) was dissolved separately in the same solvent (0.1 ml) and added to the polymer/thiol solution. The solution was then transferred to an NMR tube, sealed, placed in a UV light box and irradiated with light ($\lambda = 365$ nm) for 30 minutes. The functionalised polymer was purified by repeated precipitations into cold methanol to

yield the purified product. ^1H NMR (400 MHz, CDCl_3): δ 4.02 (m, 4H, O- CH_2 -C- CH_2 -O), 3.40 (t, $^3J_{\text{H-H}} = 5.4$ Hz, 2H, O- CH_2 - CH_2), 3.25 (s, 2H, C- CH_2 -O), 2.48 (t, 2H, O- CH_2 - CH_2 - CH_2 -S), 2.42 (t, 2H, S- CH_2 - CH_2 - CH_2 - CH_2), 1.74 (dt, 2H, O- CH_2 - CH_2 - CH_2 -S), 1.58-1.45 (m, 2H, S- CH_2 - CH_2 - CH_2), 1.40 (q, $^3J_{\text{H-H}} = 7.5$ Hz, 2H, C- CH_2 - CH_3), 1.34-1.19 (m, 20H, S- CH_2 - CH_2 -(CH_2) $_{10}$ - CH_3), 0.81 (t, $^3J_{\text{H-H}} = 7.6$ Hz, 6H, CH_3 - CH_2). ^{13}C NMR (125 MHz, CDCl_3): δ 155.3 (O-C(O)-O), 70.3-70.0 (C- CH_2 -O- CH_2 - CH_2), 68.0 (O- CH_2 -C- CH_2 -O), 42.0 (O- CH_2 -C- CH_2 -O), 32.3 (O- CH_2 - CH_2 - CH_2 -S- CH_2 - CH_2), 32.1 (O- CH_2 - CH_2 - CH_2 -S- CH_2 - CH_2), 29.8-28.9 (O- CH_2 - CH_2 - CH_2 -S- CH_2 -(CH_2) $_{10}$ - CH_2 - CH_3), 22.8 (CH_3 - CH_2 -C, S- CH_2 -(CH_2) $_{10}$ - CH_2 - CH_3), 14.3 (S- CH_2 -(CH_2) $_{10}$ - CH_2 - CH_3), 7.7 (CH_3 - CH_2 -C). For DP 24 polymer, $M_n = 9,000$ g mol $^{-1}$ (determined by ^1H NMR, 400 MHz, CDCl_3), $M_n = 10,600$ g mol $^{-1}$, $D_M = 1.13$ (determined by SEC using RI detection and CHCl_3 as eluent).

^1H NMR spectrum and size exclusion chromatogram are displayed in Figure 2.14 and 2.15 respectively, ^{13}C NMR spectrum is shown in Figure A-15.

7.3.8 Post-polymerisation functionalisation of PAOMEC with 3-mercaptopropionic acid (3-MPA)

Functionalisation of PAOMEC with 3-mercaptopropionic acid (3-MPA) was carried out using the method listed in section 7.3.7, with the exceptions of the use of ten equivalents of thiol to alkene groups, and purification which was carried out by repeated precipitations into cold *n*-hexane. ^1H NMR (400 MHz, $(\text{CD}_3)_2\text{CO}$): δ 4.14 (m, 4H, O- CH_2 -C- CH_2 -O), 3.53 (t, $^3J_{\text{H-H}} = 5.4$ Hz, 2H, O- CH_2 - CH_2), 3.38 (s, 2H, C- CH_2 -O), 2.77 (dt, $^4J_{\text{H-H}} = 12.7$, $^3J_{\text{H-H}} = 6.6$ Hz, 2H, CH_2 -C(O)OH), 2.66 – 2.59 (m, 4H, CH_2 -S- CH_2), 1.84 (dt, 2H, O- CH_2 - CH_2 - CH_2 -S), 1.48 (q, $^3J_{\text{H-H}} = 7.5$ Hz, 2H, C- CH_2 - CH_3), 0.87 (t, $^3J_{\text{H-H}} = 7.6$ Hz, 6H, CH_3 - CH_2). For DP 79 polymer, $M_n = 24,800$ g mol $^{-1}$

1 (determined by ^1H NMR, 400 MHz, $(\text{CD}_3)_2\text{CO}$), $M_n = 19,800 \text{ g mol}^{-1}$, $D_M = 1.10$ (determined by SEC using RI detection and DMF as eluent).

^1H NMR spectrum and size exclusion chromatogram are shown in Figure A-1 and A-27 respectively.

7.3.9 Post-polymerisation functionalisation of PAOMEC with benzyl mercaptan (BnSH)

Functionalisation of PAOMEC with benzyl mercaptan was carried out using the method described for functionalisations using 3-MPA in section 7.3.8. ^1H NMR (400 MHz, $(\text{CD}_3)_2\text{CO}$): δ 7.42-7.18 (m, 5H, ArH), 4.20-4.07 (m, 4H, O-CH₂-C-CH₂-O), 3.75 (s, 2H, S-CH₂-Ar), 3.58-3.40 (t, $^3J_{\text{H-H}} = 5.4 \text{ Hz}$, 2H, O-CH₂-CH₂), 3.34 (s, 2H, C-CH₂-O), 2.51 (t, $^3J_{\text{H-H}} = 7.2 \text{ Hz}$, 2H, CH₂-CH₂-S), 1.87-1.71 (dt, 2H, O-CH₂-CH₂-CH₂-S), 1.46 (q, $^3J_{\text{H-H}} = 7.5 \text{ Hz}$, 2H, C-CH₂-CH₃), 0.88 (t, $^3J_{\text{H-H}} = 7.6 \text{ Hz}$, 6H, CH₃-CH₂). For DP 79 polymer, $M_n = 25,600 \text{ g mol}^{-1}$ (determined by ^1H NMR, 400 MHz, $(\text{CD}_3)_2\text{CO}$), $M_n = 16,800 \text{ g mol}^{-1}$, $D_M = 1.16$ (determined by SEC using RI detection and DMF as eluent).

^1H NMR spectrum and size exclusion chromatogram are shown in Figure A-2 and A-27 respectively.

7.3.10 Post-polymerisation functionalisation of PAOMEC with 1-thioglycerol

Functionalisation of PAOMEC with 1-thioglycerol was carried out using the method described for functionalisations using 3-MPA in section 7.3.8. ^1H NMR (400 MHz, $(\text{CD}_3)_2\text{CO}$): δ 4.16-4.03 (m, 4H, O-CH₂-C-CH₂-O), 3.77-3.66 (m, 1H), 3.47 (t, $^3J_{\text{H-H}} = 5.4 \text{ Hz}$, 2H, O-CH₂-CH₂), 3.32 (s, 2H, C-CH₂-O), 2.74-2.53 (m, 4H, CH₂-CH₂-S-CH₂-CH), 2.42 (s, 2H, OH), 1.90-1.76 (dt, 2H, O-CH₂-CH₂-CH₂-S), 1.46 (q, $^3J_{\text{H-H}} = 7.5 \text{ Hz}$, 2H, C-CH₂-CH₃), 0.89 (t, $^3J_{\text{H-H}} = 7.6 \text{ Hz}$, 6H, CH₃-CH₂). For DP 79 polymer,

$M_n = 21,900 \text{ g mol}^{-1}$ (determined by $^1\text{H NMR}$, 400 MHz, $(\text{CD}_3)_2\text{CO}$), $M_n = 26,700 \text{ g mol}^{-1}$, $D_M = 1.10$ (determined by SEC using RI detection and DMF as eluent).

$^1\text{H NMR}$ spectrum and size exclusion chromatogram are shown in Figure A-3 and A-27 respectively.

7.3.11 General procedure for synthesis of thiol-functional poly(ethylene glycol) monomethyl ether (MeO-PEG-SH)

The synthesis was performed according to a previously reported procedure.⁵ PEG monomethyl ether (9.1 mmol) and 3-MPA (18 mmol) were weighed into a 100 mL round-bottomed flask equipped with a stirrer bar and dissolved in toluene (50 mL), with the solution heated to 80 °C to ensure complete dissolution. 2 drops of H_2SO_4 (18.4 M) were added as catalyst, and the reaction vessel connected to a Dean-Stark trap equipped with condenser. The reaction mixture was then heated to reflux for 12 h. Upon cooling, the solvent was removed under reduced pressure, and the crude product dissolved in methylene chloride (25 mL) and washed with saturated aqueous sodium hydrogen carbonate solution ($3 \times 20 \text{ mL}$). The organic layer was dried with anhydrous magnesium sulfate, filtered, and the solvent removed under reduced pressure to yield the purified product as a viscous pale yellow oil (for MeO-PEG₅₅₀-SH, yield = 3.87 g, 6.64 mmol, 73%). $^1\text{H NMR}$ (400 MHz, CDCl_3): δ 4.20 (t, $^3J_{\text{H-H}} = 4.8 \text{ Hz}$, 2H, $\text{CH}_2\text{-CH}_2\text{-O-C(O)}$), 3.64-3.48 (m, 44H, $\text{CH}_3\text{-O-(CH}_2\text{-CH}_2\text{-O)}_{10}\text{-CH}_2\text{-CH}_2$), 3.37 (s, 3H, $\text{CH}_3\text{-O-CH}_2$), 2.76 (q, $^3J_{\text{H-H}} = 7.3 \text{ Hz}$, 2H, $\text{CH}_2\text{-CH}_2\text{-SH}$), 2.68 (t, $^3J_{\text{H-H}} = 6.7 \text{ Hz}$, 2H, $\text{C(O)-CH}_2\text{-CH}_2\text{-SH}$), 1.67 (t, $^3J_{\text{H-H}} = 8.3 \text{ Hz}$, 1H, $\text{CH}_2\text{-CH}_2\text{-SH}$). $^{13}\text{C NMR}$ (125 MHz, CDCl_3): δ 171.4 (O-C(O)-CH_2), 71.8-68.9 ($\text{CH}_3\text{-O-(CH}_2\text{-CH}_2\text{-O)}_{10}\text{-CH}_2\text{-CH}_2$), 63.7 ($\text{CH}_2\text{-CH}_2\text{-O-C(O)}$), 58.9 ($\text{CH}_3\text{-O-(CH}_2\text{-CH}_2\text{)}_{10}$), 32.3 ($\text{C(O)-CH}_2\text{-CH}_2\text{-SH}$), 19.6 ($\text{C(O)-CH}_2\text{-CH}_2\text{-SH}$). For MeO-PEG₅₅₀-SH, $M_n = 650 \text{ g mol}^{-1}$

(determined by ^1H NMR, 400 MHz, CDCl_3), $M_n = 1,100 \text{ g mol}^{-1}$, $D_M = 1.08$ (determined by SEC using RI detection and CHCl_3 as eluent).

^1H NMR spectrum and size exclusion chromatogram are shown in Figure 2.20 and 2.21 respectively, ^{13}C NMR spectrum is shown in Figure A-16.

7.3.12 General procedure for functionalisation of PAOMEC with thiol-functional PEG monomethyl ether

PAOMEC ($M_n = 16,400 \text{ g mol}^{-1}$, 40 mg, 2.44 μmol) and MeO-PEG-SH (5 eq. per PAOMEC alkene group) were weighed into a vial equipped with a stirrer bar and dissolved in 1,4-dioxane (0.9 mL). The radical photoinitiator, 2-benzyl-2-(dimethylamino)-4'-morpholinobutyrophenone (0.74 mg, 2 μmol) was dissolved separately using the same solvent (0.1 mL) and added to the polymer/thiol solution. The vial was then sealed, placed in a UV light box and irradiated with light ($\lambda = 365 \text{ nm}$) for 15 minutes. The reaction mixture was then transferred to a 1 mL dialysis vessel, and the solvent allowed to evaporate. The crude product was then immersed in $18.2 \text{ M}\Omega \text{ cm}^{-1}$ water, and the vessel covered with a semi-permeable membrane (molecular weight cutoff = $3,000 \text{ g mol}^{-1}$). The sample was then dialysed against $18.2 \text{ M}\Omega \text{ cm}$ water for 10 days, with the water changed twice daily. The contents of the dialysis vessel were then transferred to a vial and the water removed under reduced pressure to yield the purified polymer. ^1H NMR (400 MHz, CDCl_3): δ 4.20 (t, $^3J_{\text{H-H}} = 4.8 \text{ Hz}$, 2H, $\text{CH}_2\text{-CH}_2\text{-O-C(O)}$), 4.13-4.05 (m, 4H, $\text{O-CH}_2\text{-C-CH}_2\text{-O}$), 3.64-3.48 (m, 44H, $\text{CH}_3\text{-O-(CH}_2\text{-CH}_2\text{-O)}_{10}\text{-CH}_2\text{-CH}_2$), 3.46 (t, $^3J_{\text{H-H}} = 5.4 \text{ Hz}$, 2H, $\text{O-CH}_2\text{-CH}_2$), 3.38 (s, 3H, $\text{CH}_3\text{-O-CH}_2$), 3.31 (s, 2H, $\text{C-CH}_2\text{-O}$), 2.76 (t, $^3J_{\text{H-H}} = 7.5 \text{ Hz}$, 2H, $\text{C(O)-CH}_2\text{-CH}_2\text{-S}$), 2.64 (t, $^3J_{\text{H-H}} = 7.5 \text{ Hz}$, 2H, $\text{SH-CH}_2\text{-CH}_2\text{-C(O)}$), 2.57 (t, $^3J_{\text{H-H}} = 7.2 \text{ Hz}$, 2H, $\text{CH}_2\text{-CH}_2\text{-CH}_2\text{-S}$), 1.82 (q, $^3J_{\text{H-H}} = 7.1 \text{ Hz}$, 2H, $\text{CH}_2\text{-CH}_2\text{-CH}_2$), 1.47 (q, $^3J_{\text{H-H}} =$

7.5 Hz, 2H, C-CH₂-CH₃), 0.87 (t, ³J_{H-H} = 7.6 Hz, 3H, C-CH₂-CH₃). ¹³C NMR (125 MHz, CDCl₃): δ 172.0 (CH₂-C(O)-O), 155.2 (O-C(O)-O), 72.3-72.0 (C-CH₂-O-CH₂-CH₂), 70.6-69.8 (O-CH₂-C-CH₂-O, CH₃-O-(CH₂-CH₂-O)-CH₂-CH₂), 63.8 (CH₂-CH₂-O-C(O)-CH₂), 59.1 (CH₃-O-(CH₂-CH₂-O)), 42.0 (O-CH₂-C-CH₂-O), 34.8 (S-CH₂-CH₂-C(O)), 29.6 (O-CH₂-CH₂-CH₂-S), 28.9 (O-CH₂-CH₂-CH₂-S), 26.9 (S-CH₂-CH₂-C(O)), 22.7 (CH₃-CH₂-C), 7.6 (CH₃-CH₂-C). For polymers grafted with MeO-PEG₅₅₀-SH, *M_n* = 68,060 g mol⁻¹ (determined by ¹H NMR, 400 MHz, CDCl₃), *M_n* = 67,800 g mol⁻¹, *D_M* = 1.17 (determined by SEC using RI detection and CHCl₃ as eluent).

¹H NMR spectrum and size exclusion chromatogram are shown in Figure 2.22 and 2.23 respectively, ¹³C NMR spectrum is shown in Figure A-17.

7.3.13 Organocatalysed ring-opening copolymerisation of 5-methyl-5-allyloxycarbonyl-1,3-dioxan-2-one (MAC) with δ-valerolactone (VL)

A solution of benzyl alcohol (2.5 μL, 25 μmol), DBU (0.75 μL, 5 μmol) and TU (9.25 mg, 50 μmol) in CDCl₃ (0.5 mL) was prepared and added to a vial containing a mixture of VL (25 mg, 0.25 mmol) and MAC (50 mg, 0.25 mmol). The reaction mixture was then transferred to an NMR tube, and monomer conversion monitored by ¹H NMR spectroscopy. The reaction was quenched at 36% VL conversion by addition of acidic Amberlyst A15 ion exchange resin, and the polymer purified by repeated precipitation into cold *n*-hexane. ¹H NMR (400 MHz, CDCl₃): δ 5.92-5.83 (m, 1H, CH₂-CH=CH₂), 5.27 (m, 2H, CH₂-CH=CH₂), 4.62 (m, 2H, O-CH₂-CH), 4.36 – 4.24 (m, 4H, O-CH₂-C-CH₂-O), 4.10 (m, 2H, CH₂-CH₂-O-C(O)), 2.33 (m, 2H, O-C(O)-CH₂-CH₂), 1.68 (m, 4H, O-C(O)-CH₂-CH₂-CH₂), 1.26 (m, 3H, CH₃-C). *M_n* = 2,300 g mol⁻¹ (determined by ¹H NMR, 400 MHz, CDCl₃), *M_n* = 3,400 g mol⁻¹, *D_M* = 1.36 (determined by SEC using RI detection and CHCl₃ as eluent).

^1H NMR spectrum and size exclusion chromatogram are shown in Figure A-4 and A-28 respectively.

7.3.14 Synthesis of poly(δ -valerolactone) (PVL) by organocatalysed ring-opening polymerisation.

For a DP 78 polymer, δ -valerolactone (2.5 g, 25 mmol), BDM (43 mg, 312 μmol , $[\text{M}]_0:[\text{I}]_0 = 80$) and TU (462.5 mg, 1.25 mmol) were weighed into a vial equipped with a stirrer bar and dissolved in CHCl_3 (12.5 mL, $[\text{VL}] = 2.0 \text{ M}$). Upon complete dissolution, DBU (187.5 μL , 1.25 mmol) was added to catalyse the polymerisation. Aliquots of the reaction mixture were taken periodically and analysed by ^1H NMR spectroscopy in order to monitor monomer conversion, and the reaction quenched at 96% monomer conversion by addition of acidic Amberlyst A15 ion exchange resin. Purification was performed by repeated precipitation into cold *n*-hexane. ^1H NMR (400 MHz, CDCl_3): δ 4.14-3.97 (m, 2H, $\text{CH}_2\text{-CH}_2\text{-O-C(O)}$), 3.61 (m, 1H, $\text{CH}_2\text{-CH}_2\text{-OH}$), 2.43-2.19 (m, 2H, $\text{C(O)-CH}_2\text{-CH}_2$), 1.80-1.50 (m, 4H, $\text{C(O)-CH}_2\text{-CH}_2\text{-CH}_2\text{-CH}_2\text{-O}$). ^{13}C NMR (125 MHz, CDCl_3): δ 173.4 ($\text{CH}_2\text{-C(O)-O}$), 64.0 ($\text{CH}_2\text{-CH}_2\text{-O}$), 33.8 ($\text{C(O)-CH}_2\text{-CH}_2$), 28.1 ($\text{CH}_2\text{-CH}_2\text{-CH}_2\text{-O}$), 21.5 ($\text{C(O)-CH}_2\text{-CH}_2\text{-CH}_2$). $M_n = 7,800 \text{ g mol}^{-1}$ (determined by ^1H NMR, 400 MHz, CDCl_3), $M_n = 9,400 \text{ g mol}^{-1}$, $D_M = 1.09$ (determined by SEC using RI detection and CHCl_3 as eluent).

^1H NMR and ^{13}C NMR spectra are shown in Figure A-5 and A-18 respectively, size exclusion chromatogram is shown in Figure A-29.

7.3.15 Synthesis of 3-ethyl-3-hydroxymethyloxetane

The synthesis was performed according to a previously reported procedure.⁶ A round-bottom flask equipped with a stirrer bar was charged with trimethylolpropane (93.9 g, 0.7 mol), diethyl carbonate (85 mL, 700 mmol) and potassium carbonate (400 mg, 2.9

mmol), and the vessel equipped with distillation apparatus. The reaction mixture was heated, with a clear, homogenous solution formed at 110 °C and ethanol distilled from the reaction mixture at 130 °C. The pressure was gradually reduced to remove unreacted diethyl carbonate and any remaining ethanol. The temperature was then increased further, with the pure product distilled at 195 °C (40 mbar) (yield = 63.8 g, 546 mmol, 78%). ¹H NMR (400 MHz, CDCl₃): δ 4.44 (d, 2H, ³J_{H-H} = 5.6 Hz, C-CH₂-O), 4.40 (d, 2H, ³J_{H-H} = 5.6 Hz, C-CH₂-O), 3.71 (s, 2H, C-CH₂-OH), 1.70 (q, ³J_{H-H} = 7.5 Hz, 2H CH₃-CH₂-C), 0.87 (t, ³J_{H-H} = 7.4 Hz, 3H, CH₃-CH₂-C). ¹³C NMR (125 MHz, CDCl₃): δ 78.1 (CH₂-O-CH₂), 65.2 (C-CH₂-OH), 44.4 (C(CH₂)₄), 26.3(CH₃-CH₂-C), 8.2 (CH₃-CH₂-C).

¹H NMR spectrum shown in Figure A-6.

7.3.16 Synthesis of 2-(bromomethyl)-2-ethyl-1,3-propanediol

The synthesis was performed using a modified previously reported procedure.⁶ 3-ethyl-3-hydroxymethyloxetane (34.2 g, 300 mmol) was weighed into a round-bottom flask equipped with a stirrer bar, dissolved in tetrahydrofuran (300 mL), and the solution cooled to 0 °C. HBr solution (102 mL, 48% in H₂O) was added dropwise, and the reaction mixture allowed to warm to room temperature and stirred for 16 h. The reaction mixture was neutralised with saturated aqueous sodium hydrogen carbonate solution (750 mL) and extracted with diethyl ether (3 × 600 mL). The organic layers were combined, dried with anhydrous magnesium sulfate, filtered, and the solvent removed under reduced pressure to yield a white crystalline solid. The crude product was recrystallised from toluene to yield the pure product (yield = 52.6 g, 270 mmol, 90%). ¹H NMR (400 MHz, CDCl₃): δ 3.67 (s, 4H, HO-CH₂-C-CH₂-OH), 3.51 (s, 2H, C-CH₂-Br), 2.78 (s, 2H, HO-CH₂-C-CH₂-OH), 1.36 (q, ³J_{H-H} = 7.6 Hz, 2H, CH₃-CH₂-C), 0.86 (t, ³J_{H-H} = 7.6 Hz, 3H, CH₃-CH₂-C). ¹³C NMR (125 MHz, CDCl₃): δ 66.4

(OH-CH₂-C-CH₂-OH), 42.9 (C(CH₂)₄), 36.7 (C-CH₂-Br), 23.5 (CH₃-CH₂-C), 7.27 (CH₃-CH₂-C).

¹H NMR and ¹³C NMR spectra are shown in Figure A-7 and A-19 respectively.

7.3.17 Synthesis of 5-(bromomethyl)-5-ethyl-2,2-dimethyl-1,3-dioxane

2-(bromomethyl)-2-ethyl-1,3-propanediol (30 g, 152 mmol) and 2,2-dimethoxypropane (24 g, 230 mmol) were weighed into a round-bottom flask equipped with a stirrer bar and dissolved in acetone (210 mL). *p*-Toluenesulfonic acid monohydrate (1.44 g, 7.5 mmol) was added, and the reaction mixture allowed to stir at room temperature for 16 h. The reaction mixture was neutralised by dropwise addition of aqueous 5 M sodium hydroxide solution, and the solvent removed under reduced pressure. The residue was dissolved in methylene chloride (750 mL) and washed with water (3 × 300 mL). The organic layer was dried with anhydrous magnesium sulfate, filtered, and the solvent removed under reduced pressure to yield the pure product as a white solid (yield = 29.4 g, 125 mmol, 82%). ¹H NMR (400 MHz, CDCl₃): δ 3.70 (s, 4H, O-CH₂-C-CH₂-O), 3.65 (s, 2H, C-CH₂-Br), 1.41-1.39 (m, 6H, CH₃-C-CH₃), 1.39-1.33 (m, 2H, CH₃-CH₂-C), 0.82 (t, ³J_{H-H} = 7.6 Hz, 3H, CH₃-CH₂-C). ¹³C NMR (125 MHz, CDCl₃): δ 98.6 (C(CH₃)₂(O)₂), 66.2 (O-CH₂-C-CH₂-O), 37.4 (C-CH₂-Br), 36.5 (C(CH₂)₄), 27.4 (CH₃-C(O)₂-CH₃), 24.9 (CH₃-CH₂-C), 20.2 (CH₃-C(O)₂-CH₃), 6.7 (CH₃-CH₂-C).

¹H NMR and ¹³C NMR spectra are shown in Figure A-8 and A-20 respectively.

7.3.18 Synthesis of 5-ethyl-2,2-dimethyl-5-(propoxymethyl)-1,3-dioxane

A three-necked round-bottom flask equipped with a stirrer bar was charged with 5-(bromomethyl)-5-ethyl-2,2-dimethyl-1,3-dioxane (15 g, 63.2 mmol) and a large excess of 1-propanol (125 mL, 1.67 mol), and cooled to 0 °C under a flow of N₂.

Sodium hydride (7.6 g of 60% dispersion in mineral oil, 190 mmol) was then gradually added, with the reaction mixture allowed to cool between additions. The reaction mixture was then allowed to warm to room temperature, and the reaction vessel equipped with a condenser. The reaction mixture was then heated to reflux for 24 h. The reaction mixture was cooled and neutralised by gradual addition of HCl, and the resulting precipitate removed by filtration. The excess 1-propanol was then removed under reduced pressure to yield the crude product as a colourless oil. The product was then purified by vacuum distillation (120 °C and 0.4 mbar pressure) to yield the pure product as a colourless oil (yield = 12.6 g, 58.8 mmol, 93%). ¹H NMR (400 MHz, CDCl₃): δ 3.73-3.53 (m, 4H, O-CH₂-C-CH₂-O), 3.41 (s, 2H, C-CH₂-O), 3.37 (t, ³J_{H-H} = 6.6 Hz, 2H, O-CH₂-CH₂) 1.57 (h, ³J_{H-H} = 6.5 Hz, 2H, CH₂-CH₂-CH₃), 1.43-1.38 (m, 6H, CH₃-C(O)₂-CH₃), 1.39-1.30 (m, 2H, CH₃-CH₂-C), 0.90 (t, ³J_{H-H} = 7.4 Hz, 3H, CH₂-CH₂-CH₃) 0.81 (t, ³J_{H-H} = 7.6 Hz, 3H, CH₃-CH₂-C). ¹³C NMR (125 MHz, CDCl₃): δ 98.1 (CH₃-C(O)₂-CH₃), 73.3 (C-CH₂-O-CH₂), 70.6 (O-CH₂-CH₂-CH₃), 65.5 (O-CH₂-C-CH₂-O), 36.8 (O-CH₂-C-CH₂-O), 26.3 (CH₃-C(O)₂-CH₃), 24.4 (O-CH₂-CH₂-CH₃), 23.0 (CH₃-CH₂-C), 21.6 (CH₃-C(O)₂-CH₃), 10.7 (O-CH₂-CH₂-CH₃), 7.3 (CH₃-CH₂-C).

¹H NMR and ¹³C NMR spectra are shown in Figure A-9 and A-21 respectively.

7.3.19 Synthesis of 2-ethyl-2-(propoxymethyl)propane-1,3-diol

5-ethyl-2,2-dimethyl-5-(propoxymethyl)-1,3-dioxane (9.5 g, 44 mmol) was weighed into a round-bottom flask equipped with a stirrer bar and dissolved in methanol (60 mL). Acidic Dowex 50W X8 ion exchange resin (9.5 g) was then added, and the reaction mixture stirred for 12 h. The Dowex resin was removed by filtration, and the solvent and by-products were removed under reduced pressure to yield the product as a clear oil, which was used without further purification (yield = 7.5 g, 42.2 mmol,

96%). ^1H NMR (400 MHz, CDCl_3): δ 3.75-3.53 (m, 4H, $\text{HO-CH}_2\text{-C-CH}_2\text{-OH}$), 3.40 (s, 2H, $\text{C-CH}_2\text{-O}$), 3.36 (t, $^3J_{\text{H-H}} = 6.5$ Hz, 2H, $\text{O-CH}_2\text{-CH}_2$), 2.88 (s, 2H, $\text{HO-CH}_2\text{-C-CH}_2\text{-OH}$), 1.56 (h, $^3J_{\text{H-H}} = 6.5$ Hz, 2H, $\text{CH}_2\text{-CH}_2\text{-CH}_3$), 1.30 (q, $^3J_{\text{H-H}} = 7.7$ Hz, 2H, $\text{CH}_3\text{-CH}_2\text{-C}$), 0.89 (t, $^3J_{\text{H-H}} = 7.4$ Hz, 3H, $\text{CH}_2\text{-CH}_2\text{-CH}_3$), 0.82 (t, $^3J_{\text{H-H}} = 7.6$ Hz, 3H, $\text{CH}_3\text{-CH}_2\text{-C}$). ^{13}C NMR (125 MHz, CDCl_3): δ 75.1 ($\text{C-CH}_2\text{-O-CH}_2$), 73.6 ($\text{O-CH}_2\text{-CH}_2\text{-CH}_3$), 65.9 ($\text{HO-CH}_2\text{-C-CH}_2\text{-OH}$), 42.8 ($\text{O-CH}_2\text{-C-CH}_2\text{-O}$), 23.2 ($\text{CH}_3\text{-CH}_2\text{-C}$), 22.8 ($\text{O-CH}_2\text{-CH}_2\text{-CH}_3$), 10.7 ($\text{O-CH}_2\text{-CH}_2\text{-CH}_3$), 7.6 ($\text{CH}_3\text{-CH}_2\text{-C}$).

^1H NMR and ^{13}C NMR spectra are shown in Figure A-10 and A-22 respectively.

7.3.20 Synthesis of 2-propyloxymethyl-2-ethyltrimethylene carbonate (POMEC)

2-ethyl-2-(propoxymethyl)propane-1,3-diol (7.0 g, 40 mmol) was weighed into a round-bottom flask equipped with a stirrer bar and dissolved in tetrahydrofuran (150 mL), and the solution cooled to 0 °C. Ethyl chloroformate (11.6 mL, 120 mmol) was then added and the solution stirred at 0 °C for 30 minutes. Triethylamine (17.0 mL, 122 mmol) was then added dropwise over a period of 1 h. The reaction mixture was allowed to warm to room temperature and stirred for 12 h, at which point the solution was filtered and concentrated under reduced pressure. The resulting oil was dissolved in ethyl acetate (150 mL) and washed with HCl (1M, 2 × 150 mL) and H_2O (2 × 150 mL). The organic layer was dried with anhydrous magnesium sulfate, filtered, and the solvent removed under reduced pressure to yield the crude product as a viscous yellow oil. The crude product was purified by vacuum distillation to yield the pure product as a colourless oil (yield = 5.8 g, 28.8 mmol, 72%). ^1H NMR (400 MHz, CDCl_3): δ 4.36-4.05 (m, 4H, $\text{O-CH}_2\text{-C-CH}_2\text{-O}$), 3.38-3.29 (m, 2H + 2H, $\text{C-CH}_2\text{-O-CH}_2\text{-CH}_2\text{-CH}_3$), 1.61-1.41 (m, 2H + 2H, $\text{CH}_3\text{-CH}_2\text{-C}$, $\text{O-CH}_2\text{-CH}_2\text{-CH}_3$), 0.94-0.79 (m, 3H + 3H, $\text{CH}_3\text{-}$

CH₂-C, O-CH₂-CH₂-CH₃). ¹³C NMR (125 MHz, CDCl₃): δ 148.7 (O-C(O)-O), 73.4 (C-CH₂-O-CH₂), 72.9 (O-CH₂-C-CH₂-O), 69.0 (O-CH₂-CH₂-CH₃), 35.5 (O-CH₂-C-CH₂-O), 23.4 (CH₃-CH₂-C), 22.7 (O-CH₂-CH₂-CH₃), 10.6 (O-CH₂-CH₂-CH₃), 7.4 (CH₃-CH₂-C).

¹H NMR and ¹³C NMR spectra are shown in Figure 3.15 and A-23 respectively.

7.3.21 General procedure for the synthesis of poly(2-propyloxymethyl-2-ethyltrimethylene carbonate) (PPOMEC) by organocatalysed ROP

POMEC, 1,4-benzenedimethanol (1-3.3 mol% to monomer dependent on [M]₀:[I]₀) and TU (5 mol% to monomer) were weighed into a vial equipped with a stirrer bar and dissolved in CDCl₃ ([POMEC] = 2M). DBU (5 mol% to monomer) was then added to catalyse the homopolymerisation, and conversion monitored by ¹H NMR spectroscopy. The polymerisation was quenched at 78% monomer conversion by addition of acidic Amberlyst A15 ion exchange resin, and the crude polymer was purified by repeated precipitation into cold *n*-hexane. ¹H NMR (400 MHz, CDCl₃): δ 4.16-1.05 (m, 4H, C(O)-O-CH₂-C-CH₂-O), 3.32 (t, ³J_{H-H} = 6.5 Hz, 2H, O-CH₂-CH₂-CH₃), 3.29 (s, 2H, C-CH₂-O), 1.53 (h, ³J_{H-H} = 7.0 Hz, 2H, O-CH₂-CH₂-CH₃), 1.46 (q, ³J_{H-H} = 7.6 Hz, 2H, CH₃-CH₂-C), 0.95-0.81 (m, 3H + 3H, CH₃-CH₂-C, O-CH₂-CH₂-CH₃). ¹³C NMR (125 MHz, CDCl₃): δ 155.2 (O-C(O)-O), 73.2 (O-CH₂-CH₂-CH₃), 70.0 (C-CH₂-O), 68.0 (O-CH₂-C-CH₂-O), 42.0 (O-CH₂-C-CH₂-O), 22.9 (CH₃-CH₂-C, O-CH₂-CH₂-CH₃), 10.7 (O-CH₂-CH₂-CH₃), 7.6 (CH₃-CH₂-C). For a DP 23 polymer, *M*_n = 4,700 g mol⁻¹ (determined by ¹H NMR, 400 MHz, CDCl₃), *M*_n = 5,100 g mol⁻¹, *D*_M = 1.14 (determined by SEC using RI detection and CHCl₃ as eluent).

¹H NMR spectrum, size exclusion chromatogram, and ¹³C NMR spectrum are shown in Figure 3.17, 3.18 and 3.23 respectively.

7.3.22 General procedure for the synthesis of P(AOME_c-co-POME_c) by organocatalysed ROP

AOME_c, POME_c, BDM (0.8 mol% to monomer, [AOME_c]₀:[POME_c]₀:[I]₀ = 62.5:62.5:1) and TU (5 mol% to monomer) were weighed into a vial equipped with a stirrer bar and dissolved in CHCl₃ (overall monomer concentration = 2.0 M). DBU (5 mol% to monomer) was then added to catalyse the polymerisation, and conversion monitored by ¹H NMR spectroscopy. At *ca.* 80% AOME_c conversion, the polymerisation was quenched by addition of acidic Amberlyst A15 ion exchange resin, and the polymer purified by repeated precipitation into cold *n*-hexane. ¹H NMR (400 MHz, CDCl₃): δ 5.90-5.78 (m, 1H, CH₂-CH=CH₂), 5.27-5.12 (m, 2H, CH₂-CH=CH₂), 4.19-4.04 (m, 4H + 4H, O-CH₂-C-CH₂-O_(PAOME_c), O-CH₂-C-CH₂-O_(PPOME_c)), 3.92 (dd, ³J_{H-H} = 5.4 Hz, ²J_{H-H} = 1.7 Hz, 2H, O-CH₂-CH=CH₂), 3.34-3.30 (m, 2H + 2H, C-CH₂-O_(PAOME_c), O-CH₂-CH₂-CH₃_(PPOME_c)), 3.29 (s, 2H, C-CH₂-O_(PPOME_c)), 1.54 (h, ³J_{H-H} = 7.0 Hz, 2H, O-CH₂-CH₂-CH₃), 1.50-1.43 (m, 2H + 2H, CH₃-CH₂-C_(PAOME_c), CH₃-CH₂-C_(PPOME_c)), 0.92-0.84 (m, 3H + 3H + 3H, CH₃-CH₂-C_(PAOME_c), CH₃-CH₂-C_(PPOME_c), O-CH₂-CH₂-CH₃). ¹³C NMR (125 MHz, CDCl₃): δ 155.3-155.2 (O-C(O)-O_(PAOME_c), O-C(O)-O_(PPOME_c)), 134.8 (O-CH₂-CH=CH₂), 116.8 (O-CH₂-CH=CH₂), 73.2 (O-CH₂-CH₂-CH₃), 72.4 (O-CH₂-CH=CH₂), 70.0 (C-CH₂-O_(PPOME_c)), 69.6 (C-CH₂-O_(PAOME_c)), 68.0-68.8 (O-CH₂-C-CH₂-O_(PAOME_c), O-CH₂-C-CH₂-O_(PPOME_c)), 42.0 (O-CH₂-C-CH₂-O_(PAOME_c), O-CH₂-C-CH₂-O_(PPOME_c)), 22.9-22.7 (CH₃-CH₂-C_(PAOME_c), CH₃-CH₂-C_(PPOME_c), O-CH₂-CH₂-CH₃), 10.7 (O-CH₂-CH₂-CH₃), 7.6 (CH₃-CH₂-C_(PAOME_c), CH₃-CH₂-C_(PPOME_c)). *M_n* = 20,100 g mol⁻¹ (determined by ¹H NMR, 400 MHz, CDCl₃), *M_n* = 21,200 g mol⁻¹, *D_M* = 1.14 (determined by SEC using RI detection and CHCl₃ as eluent).

^1H NMR and ^{13}C NMR spectra are shown in Figure 3.22 and 3.23 respectively, size exclusion chromatogram is shown in Figure A-30.

7.3.23 Synthesis of P(AOME c - c o-POME c - c o-VL) by organocatalysed ROP

POME c (320 mg, 1.58 mmol), AOME c (320 mg, 1.6 mmol), VL (1.68 g, 16.8 mmol), BDM (27.6 mg, 200 μmol) and TU (370 mg, 1 mmol) were weighed into a vial equipped with a stirrer bar and dissolved in CHCl_3 . DBU (150 μL , 1 mmol) was then added to catalyse the polymerisation, and conversion monitored by ^1H NMR spectroscopy. At 80% AOME c conversion, the polymerisation was quenched by addition of acidic Amberlyst A15 ion exchange resin, and the crude polymer purified by repeated precipitation into cold *n*-hexane. ^1H NMR (400 MHz, CDCl_3): δ 5.93-5.74 (m, 1H, $\text{CH}_2\text{-CH}=\text{CH}_2$), 5.28-5.09 (m, 2H, $\text{CH}_2\text{-CH}=\text{CH}_2$), 4.21-4.00 (m, 4H + 4H + 2H, $\text{O-CH}_2\text{-C-CH}_2\text{-O}_{(\text{PAOME}c)}$, $\text{O-CH}_2\text{-C-CH}_2\text{-O}_{(\text{PPOME}c)}$, $\text{CH}_2\text{-CH}_2\text{-O-C(O)}_{(\text{PVL})}$), 3.93 (dd, $^3J_{\text{H-H}} = 5.4$ Hz, $^2J_{\text{H-H}} = 1.7$ Hz, 2H, $\text{O-CH}_2\text{-CH}=\text{CH}_2$), 3.37-3.25 (m, 2H + 2H + 2H, $\text{C-CH}_2\text{-O}_{(\text{PAOME}c)}$, $\text{O-CH}_2\text{-CH}_2\text{-CH}_3_{(\text{PPOME}c)}$, $\text{C-CH}_2\text{-O}_{(\text{PPOME}c)}$), 2.43-2.26 (m, 2H, $\text{C(O)-CH}_2\text{-CH}_2$), 1.83-1.60 (m, 4H, $\text{C(O)-CH}_2\text{-CH}_2\text{-CH}_2\text{-CH}_2\text{-O}$), 1.60-1.35 (m, 2H + 2H + 2H, $\text{O-CH}_2\text{-CH}_2\text{-CH}_3$, $\text{CH}_3\text{-CH}_2\text{-C}_{(\text{PAOME}c)}$, $\text{CH}_3\text{-CH}_2\text{-C}_{(\text{PPOME}c)}$), 0.94-0.82 (m, 3H + 3H + 3H, $\text{CH}_3\text{-CH}_2\text{-C}_{(\text{PAOME}c)}$, $\text{CH}_3\text{-CH}_2\text{-C}_{(\text{PPOME}c)}$, $\text{O-CH}_2\text{-CH}_2\text{-CH}_3$). $M_n = 9,700$ g mol $^{-1}$ (determined by ^1H NMR, 400 MHz, CDCl_3), $M_n = 10,800$ g mol $^{-1}$, $D_M = 1.17$ (determined by SEC using RI detection and CHCl_3 as eluent).

^1H NMR spectrum and size exclusion chromatogram are shown in Figure 3.24 and 3.25 respectively.

7.3.24 Procedure for H₂O-initiated ROP of AOMECE

In a fume cupboard, a nitrogen-flushed Schlenk flask equipped with a stirrer bar was charged with AOMECE (20 g, 100 mmol), and the monomer was dissolved in CHCl₃ (50 mL, [AOMECE] = 2 M). H₂O (120 μL, 6.7 mmol) and TBD (140 mg, 1 mmol) were then added to the reaction vessel which was then sealed, and the contents allowed to stir for 90 h. The polymerisation was quenched by addition of acidic Amberlyst A15 ion exchange resin. The crude polymer was purified by flash column chromatography, using methylene chloride to remove unreacted monomer followed by ethyl acetate to recover the pure PAOMECE. ¹H NMR (400 MHz, CDCl₃): δ 5.93-5.77 (m, 1H, CH₂-CH=CH₂), 5.29-5.09 (m, 2H, CH=CH₂), 4.15-4.06 (m, 4H, O-CH₂-C-CH₂-O), 3.92 (dd, ³J_{H-H} = 5.4 Hz, ²J_{H-H} = 1.7 Hz, 2H, O-CH₂-CH), 3.31 (s, 2H, C-CH₂-O), 1.47 (q, ³J_{H-H} = 7.5 Hz, 2H, C-CH₂-CH₃), 0.86 (t, ³J_{H-H} = 7.6 Hz, 3H, CH₂-CH₃). ¹³C NMR (125 MHz, CDCl₃): δ 173.4-173.0 (CH₂-C(O)-O), ¹³C NMR (125 MHz, CDCl₃): δ 155.3 (O-C(O)-O), 134.6 (CH₂-CH=CH₂), 116.6 (CH=CH₂), 72.1 (O-CH₂-CH), 69.3 (C(O)-O-CH₂), 67.7 (C-CH₂-O), 41.8 (C(CH₂)₄), 22.5 (CH₃-CH₂), 7.3 (CH₃-CH₂). *M_n* = 2,200 g mol⁻¹ (determined by ¹H NMR, 400 MHz, CDCl₃), *M_n* = 2,800 g mol⁻¹, *D_M* = 1.33 (determined by SEC using RI detection and CHCl₃ as eluent).

¹H NMR spectrum and size exclusion chromatogram are shown in Figure 4.2 and 4.4 respectively, ¹³C NMR spectrum of PAOMECE is shown in Figure A-12.

7.3.25 Synthesis of poly(2-allyloxymethyl-2-ethyltrimethylene carbonate)-*co*-
 (2-(oxiranyloxy)methyl-2-ethyltrimethylene carbonate) (P(AOMECCO-
 OOMECCO))

A nitrogen-flushed 2-necked round-bottom flask equipped with a stirrer bar was charged with PAOMECCO ($M_n = 2,200 \text{ g mol}^{-1}$) (2.7 g, 1.23 mmol), and the polymer was dissolved in methylene chloride (60 mL). The reaction mixture was cooled to 0 °C, and 3-chloroperoxybenzoic acid (77%) (1.5 g, 67 mmol, 0.5 eq. to pendent alkene groups of PAOMECCO) was gradually added under a flow of N₂. The reaction mixture was then allowed to stir for 6 h under N₂. The solution was filtered and washed with saturated aqueous sodium hydrogen carbonate solution (2 × 100 mL). The organic layer was dried with anhydrous magnesium sulfate, filtered, and the solvent removed under reduced pressure. The polymer was then re-dissolved in a minimal amount of methylene chloride and precipitated into cold *n*-hexane to yield the purified polymer.

¹H NMR (400 MHz, CDCl₃): δ 5.93-5.77 (m, 1H, CH₂-CH=CH₂), 5.29-5.09 (m, 2H, CH=CH₂), 4.23-4.06 (m, 4H + 4H, O-CH₂-C-CH₂-O_(PAOMECCO), O-CH₂-C-CH₂-O_(POOMECCO)), 3.92 (dd, ³J_{H-H} = 5.4 Hz, ²J_{H-H} = 1.7 Hz, 2H, O-CH₂-CH), 3.64-3.50 (m, 2H + 2H, C-CH₂-O_(POOMECCO), O-CH₂-CH(CH₂)-O), 3.31 (s, 2H, C-CH₂-O_(PAOMECCO)), 3.19-3.05 (m, 1H, O-CH₂-CH(CH₂)-O), 2.77 (dd, ³J_{H-H} = 6.0 Hz, ²J_{H-H} = 3.0 Hz, 1H, O-CH₂-CH(C(H)-H)-O), 2.58 (dd, ³J_{H-H} = 5.6 Hz, ²J_{H-H} = 3.0 Hz, 1H, O-CH₂-CH(C(H)-H)-O), 1.56-1.43 (m, 2H, CH₃-CH₂-C_(POOMECCO)), 1.43-1.33 (m, 2H, CH₃-CH₂-C_(PAOMECCO)), 0.98-0.78 (m, 3H + 3H, CH₃-CH₂-C_(POOMECCO), CH₃-CH₂-C_(PAOMECCO)).

¹³C NMR (125 MHz, CDCl₃): δ 155.6-155.2 (O-C(O)-O_(PAOMECCO), O-C(O)-O_(POOMECCO)), 134.8-134.1 (O-CH₂-CH=CH₂), 117.7-116.8 (O-CH₂-CH=CH₂), 73.3-70.8 (C-CH₂-O-CH₂-C_(PAOMECCO), C-CH₂-O-CH₂-C_(POOMECCO)), 69.9-69.5 (C-CH₂-O-CH₂-C_(POOMECCO)),

68.3-67.9 (O-CH₂-C-CH₂-O_(PAOMEC), O-CH₂-C-CH₂-O_(POOMEC)), 65.5-64.6 (O-CH₂-C-CH₂-OH_(PAOMEC), O-CH₂-C-CH₂-OH_(POOMEC)), 50.9 (CH₂-CH(CH₂)-O), 44.1 (CH₂-CH(CH₂)-O), 43.0 (O-CH₂-C-CH₂-OH_(PAOMEC), O-CH₂-C-CH₂-OH_(POOMEC)), 42.0 (O-CH₂-C-CH₂-O_(PAOMEC), O-CH₂-C-CH₂-O_(POOMEC)), 23.5-22.7 (CH₃-CH₂-C_(PAOMEC), CH₃-CH₂-C_(POOMEC)), 7.53 (CH₃-CH₂-C_(PAOMEC), CH₃-CH₂-C_(POOMEC)). $M_n = 2,700 \text{ g mol}^{-1}$ (determined by ¹H NMR, 400 MHz, CDCl₃), $M_n = 2,700 \text{ g mol}^{-1}$, $D_M = 1.31$ (determined by SEC using RI detection and CHCl₃ as eluent).

¹H NMR spectrum and size exclusion chromatogram are shown in Figure 4.16 and 4.17 respectively, ¹³C NMR spectrum is shown in Figure A-24.

7.3.26 General procedure for 3D printing of structures by radical thiol-ene addition

Photocurable resins were prepared by mixing PAOMEC or P(AOMEC-*co*-OOMECE) with pentaerythritol tetrakis(3-mercaptopropionate) (1 eq. of thiol to pendent alkene groups), propylene carbonte (10 wt%) and Irgacure 819 (0.5 wt%) in the absence of light. The mixture was placed into the resin tray of the custom-built 3D printer, and 3D structures prepared by exposure of sequential 100 μm layers of resin to a dynamic pattern mask of purple light (peak output = 415 nm). Exposure times of 40 s per layer were required using the PAOMEC-based resin, and 155 s per layer for the P(AOMEC-*co*-OOMECE)-based resin. Following completion of the build, excess resin was removed from the constructs by gentle rinsing with 2-propanol followed by acetone, and the printed structures were post-cured by exposure to UV light for 10 minutes. For PAOMEC resin, FT-IR: max/cm⁻¹ 3610-3350 (CH₂-O-H), 1798 (O-C(O)-CH₂), 1736 (O-C(O)-O), 1170 (H₂C-O-CH₂). For P(AOMEC-*co*-OOMECE) resin, FT-IR: max/cm⁻¹

¹ 3610-3350 (CH₂-O-H), 1798 (O-C(O)-CH₂), 1736 (O-C(O)-O), 1170 (H₂C-O-CH₂), 799 (CH₂-HC-O-CH₂).

FT-IR spectra of cured PAOMEAC and P(AOMEAC-co-OOMEAC) resins are shown in Figure 4.15 and 4.20 respectively.

7.3.27 General procedure for the synthesis of PLLA-*b*-P(AOMEAC-co-VL)-*b*-PLLA triblock copolymers

In a typical experiment, PLLA and P(AOMEAC-co-VL) macroinitiator (0.48-10 mol% relative to PLLA) were weighed into a vial equipped with a stirrer bar, and dissolved in CHCl₃ ([PLLA] = 1 M). DBU (0.5 mol% to PLLA) was added to catalyse the polymerisation, and conversion monitored by ¹H NMR spectroscopy. At > 95% monomer conversion, the reaction was quenched by addition of acidic Amberlyst A15 ion exchange resin, and purified by repeated precipitation into cold *n*-hexane, followed by precipitation into cold methanol. ¹H NMR (400 MHz, CDCl₃): δ 5.91-5.78 (m, 1H, CH₂-CH=CH₂), 5.26-5.10 (m, 1H + 2H, C(O)-C(CH₃)H-O, CH₂-CH=CH₂), 4.14-4.04 (m, 2H + 4H, CH₂-O-C(O)_(PVL), O-CH₂-C-CH₂-O_(PAOMEAC)), 3.93 (dd, ³J_{H-H} = 5.4 Hz, ²J_{H-H} = 1.7 Hz, 2H, O-CH₂-CH=CH₃), 3.31 (s, 2H, C-CH₂-O), 2.38 – 2.31 (m, 2H, O-CH₂-CH₂), 1.73-1.65 (m, 4H, CH₂-CH₂-CH₂-CH₂), 1.58 (d, ³J_{H-H} = 7.1 Hz, 3H, C(O)-C(CH₃)H-O) 1.54-1.44 (m, 2H, C-CH₂-CH₃), 0.87 (t, ³J_{H-H} = 7.6 Hz, 3H, CH₂-CH₃). ¹³C NMR (125 MHz, CDCl₃): δ 173.4-173.0 (CH₂-C(O)-O), 169.7 (O-C(O)-C(CH₃)H), 155.4-155.3 (O-C(O)-O), 134.8 (CH₂-CH=CH₂), 116.8 (CH₂-CH=CH₂), 72.4 (O-CH₂-CH), 69.6 (C-CH₂-O), 69.1 (C(O)-C(CH₃)H), 67.9 (O-CH₂-C-CH₂-O), 64.4 (CH₂-CH₂-O), 42.0 (C(CH₂)₄), 33.8 (O-CH₂-CH₂-CH₂), 28.2 (C(O)-CH₂-CH₂-CH₂), 22.5 (O-CH₂-CH₂-CH₂), 21.6 (CH₃-CH₂), 7.6 (CH₃-CH₂). For PLLA₆₄-*b*-P(AOMEAC₄₅-co-VL₅₃)-*b*-PLLA₆₄, M_n = 32,200 g mol⁻¹ (determined by ¹H NMR, 400

MHz, CDCl₃), $M_n = 38,800 \text{ g mol}^{-1}$, $D_M = 1.09$ (determined by SEC using RI detection and CHCl₃ as eluent).

¹H NMR spectrum and size exclusion chromatogram are shown in Figure 5.7 and 5.8 respectively, ¹³C NMR spectrum is shown in Figure A-25. Differential scanning calorimetry thermograms are shown in Figure A-32, 33, 34, 35 and 37. Dynamic mechanical thermal analysis data are shown in Figure A-39, 40, 41, 43 and 44.

7.3.28 One-pot synthesis of PLLA-*b*-PAOMEC-*b*-PLLA triblock copolymer

AOMEC (2 g, 10 mmol), BDM (11 mg, 80 μmol) and TU (185 mg, 500 μmol) were weighed into a vial equipped with a stirrer bar, and dissolved in CHCl₃ (5 ml, [AOMEC] = 2 M) before addition of DBU (75 μL, 500 μmol) to catalyse the polymerisation. A second reaction was performed simultaneously on 1/10th scale using CDCl₃ as solvent, and monomer conversion of this reaction was monitored by ¹H NMR spectroscopy. At 80% monomer conversion, a solution of *L*-lactide (1.4 g, 9.7 mmol) in CHCl₃ (9.7 mL, [LLA] = 1 M) was added to the AOMEC homopolymerisation, and the reaction mixture immediately removed from the glovebox and quenched by addition of acidic Amberlyst A15 ion exchange resin. The crude polymer was purified by repeated precipitation in cold *n*-hexane followed by precipitation in cold methanol. ¹H NMR (400 MHz, CDCl₃): δ 5.91-5.77 (m, 1H, CH₂-CH=CH₂), 5.28-5.08 (m, 2H + 1H, CH₂-CH=CH₂, C(O)-C(CH₃)H-O), 4.13-4.05 (m, 4H, O-CH₂-C-CH₂-O), 3.91 (dd, ³J_{H-H} = 5.4 Hz, ²J_{H-H} = 1.7 Hz, 2H, O-CH₂-CH), 3.31 (s, 2H, C-CH₂-O), 1.65 (d, ³J_{H-H} = 1.6 Hz, 2H, C(O)-CH-CH₃), 1.47 (q, ³J_{H-H} = 7.5 Hz, 2H, C-CH₂-CH₃), 0.86 (t, ³J_{H-H} = 7.6 Hz, 3H, CH₂-CH₃). ¹³C NMR (125 MHz, CDCl₃): δ 169.6 (CH-C(O)-CO), 155.0 (O-C(O)-O), 134.6 (CH₂-CH=CH₂), 116.6 (CH₂-CH=CH₂), 72.1 (O-CH₂-CH), 69.3 (C(O)-O-CH₂), 67.7 (C-CH₂-O), 41.8

($C(CH_2)_4$), 22.5 (CH_3-CH_2-C), 16.7 ($CH_3-CH-C(O)$), 7.3 (CH_3-CH_2-C). $M_n = 41,700$ g mol⁻¹ (determined by ¹H NMR, 400 MHz, CDCl₃). $M_n = 49,200$ g mol⁻¹, $D_M = 1.12$ (determined by SEC using RI detection and CHCl₃ as eluent).

¹H NMR spectrum and size exclusion chromatogram are shown in Figure 5.9 and 5.10 respectively, ¹³C NMR spectrum of PLLA-*b*-PAOMEC-*b*-PLLA is shown in Figure A-13. Differential scanning calorimetry thermogram and dynamic mechanical thermal analysis data are shown in Figure A-35 and A-42 respectively.

7.3.29 One-pot synthesis of PLLA-*b*-PVL-*b*-PLLA triblock copolymer

VL (1.5 g, 15 mmol), BDM (20.7 mg, 150 μmol) and TU (277 mg, 750 μmol) were weighed into a vial equipped with a stirrer bar, and dissolved in CHCl₃ (7.5 ml, [VL] = 2 M) before addition of DBU (113 μL, 750 μmol) to catalyse the polymerisation. A second reaction was performed simultaneously on 1/10th scale using CDCl₃ as solvent, and monomer conversion of this reaction was monitored by ¹H NMR spectroscopy. At 95% monomer conversion, a solution of *L*-lactide (2.1 g, 14.6 mmol) in CHCl₃ (14.6 mL, [LLA] = 1 M) was added to the VL homopolymerisation, and the reaction mixture immediately removed from the glovebox and quenched by addition of acidic Amberlyst A15 ion exchange resin. The crude polymer was purified by repeated precipitation in cold *n*-hexane followed by precipitation in cold methanol. ¹H NMR (400 MHz, CDCl₃): δ 5.16 (q, ³J_{H-H} = 7.1 Hz, 1H, C(O)-C(CH₃)H-O), 4.12-4.04 (m, 2H, C(O)-O-CH₂-CH₂), 2.34 (t, ³J_{H-H} = 6.9 Hz, 2H, CH₂-CH₂-C(O)-O), 1.73-1.64 (m, 4H, O-CH₂-CH₂-CH₂-CH₂-C(O)), 1.58 (d, ³J_{H-H} = 7.1 Hz, 3H, C(O)-C(CH₃)H-O). ¹³C NMR (125 MHz, CDCl₃): δ 173.4 (CH₂-C(O)-O), 169.7 (O-C(O)-CH(CH₃)), 69.1 (O-C(O)-CH(CH₃)), 64.0 (CH₂-CH₂-O), 33.8 (C(O)-CH₂-CH₂), 28.2 (CH₂-CH₂-CH₂-O), 21.5 (C(O)-CH₂-CH₂-CH₂), 16.8 (O-C(O)-CH(CH₃)). $M_n = 29,400$ g mol⁻¹

(determined by ^1H NMR, 400 MHz, CDCl_3). $M_n = 36,600 \text{ g mol}^{-1}$, $D_M = 1.05$
(determined by SEC using RI detection and CHCl_3 as eluent).

^1H NMR spectrum and size exclusion chromatogram are shown in Figure 5.9 and 5.10 respectively, ^{13}C NMR spectrum is shown in Figure A-26. Differential scanning calorimetry thermogram and dynamic mechanical thermal analysis data are shown in Figure A-31 and A-38 respectively.

7.4 References

- (1) Weber, E. *J. Org. Chem.* **1982**, *47*, 3478.
- (2) Coulembier, O.; Sanders, D. R.; Nelson, A.; Hollenbeck, A. N.; Horn, H. W.; Rice, J. E.; Fujiwara, M.; Dubois, P.; Hedrick, J. L. *Angew. Chem. Int. Ed.* **2009**, *48*, 5170.
- (3) Hu, X.; Chen, X.; Xie, Z.; Liu, S.; Jing, X. *J. Polym. Sci. A: Polym. Chem.* **2007**, *45*, 5518.
- (4) He, Y.; Keul, H.; Moeller, M. *React. Funct. Polym.* **2011**, *71*, 175.
- (5) Truong, V. X.; Barker, I. A.; Tan, M.; Mespouille, L.; Dubois, P.; Dove, A. P. *J. Mater. Chem. B* **2013**, *1*, 221.
- (6) Mindemark, J.; Bowden, T. *Polymer* **2011**, *52*, 5716.

A Appendix – Supplementary Information

A.1 Supplementary ^1H NMR spectra

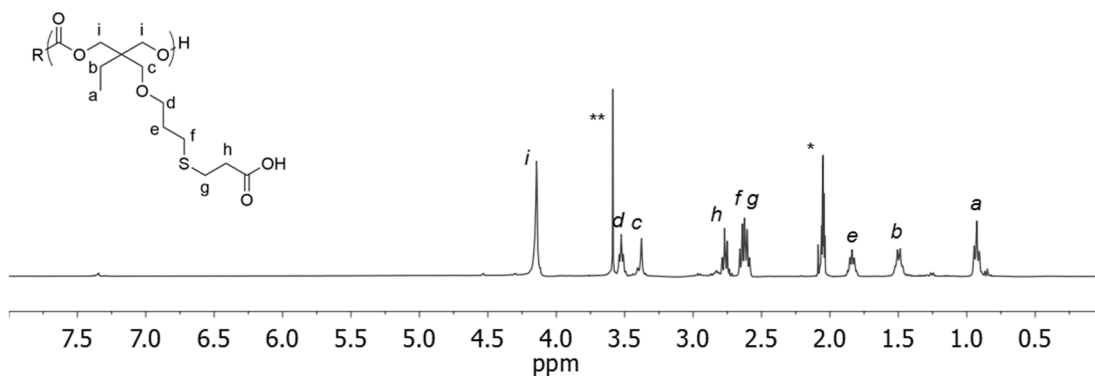


Figure A.1. ^1H NMR spectrum of PAOMEC₁₉ grafted with 3-MPA (400 MHz, 293 K, $(\text{CD}_3)_2\text{CO}$; * = $(\text{CH}_3)_2\text{CO}$, ** = residual 1,4-dioxane).

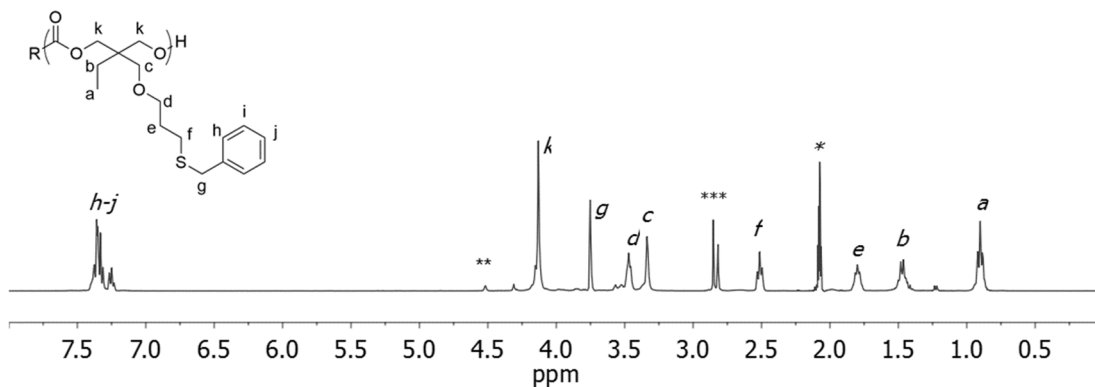


Figure A.2. ^1H NMR spectrum of PAOMEC₁₉ grafted with benzyl mercaptan (400 MHz, 293 K, $(\text{CD}_3)_2\text{CO}$; * = $(\text{CD}_3)_2\text{CO}$, ** = PDE initiator, *** = H_2O).

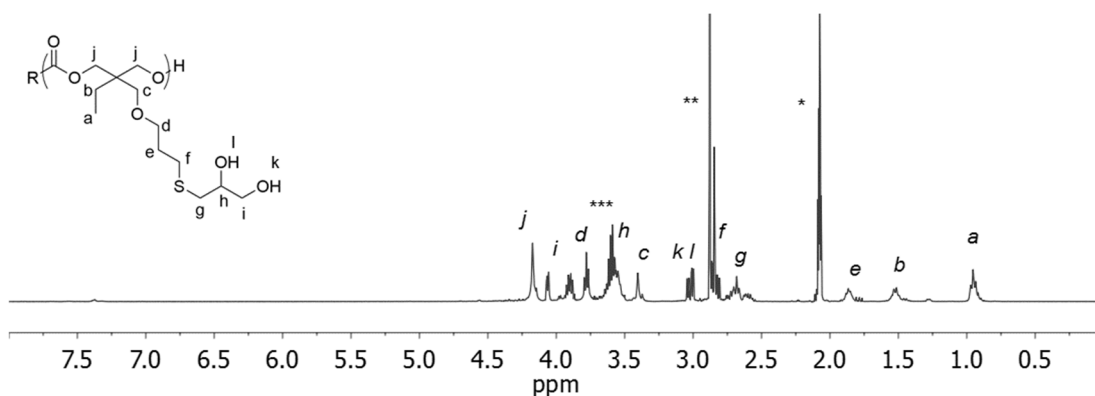


Figure A.3. ^1H NMR spectrum of PAOMEC₂₄ grafted with 1-thioglycerol (400 MHz, 293 K, $(\text{CD}_3)_2\text{CO}$; * = $(\text{CH}_3)_2\text{CO}$, ** = H_2O , *** = residual 1,4-dioxane).

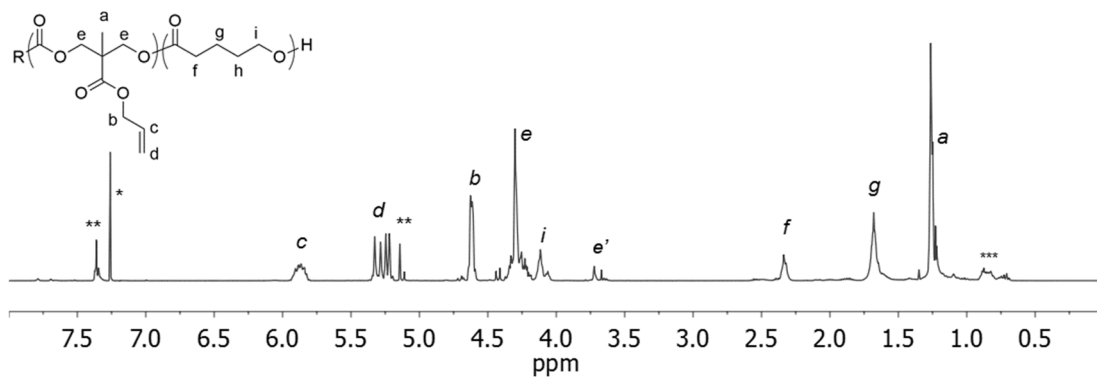


Figure A.4. ^1H NMR spectrum of P(MAC₉-co-VL₅) initiated from BnOH (400 MHz, 293 K, CDCl₃; * = CHCl₃, ** = BnOH initiator, *** = residual hexane from precipitation).

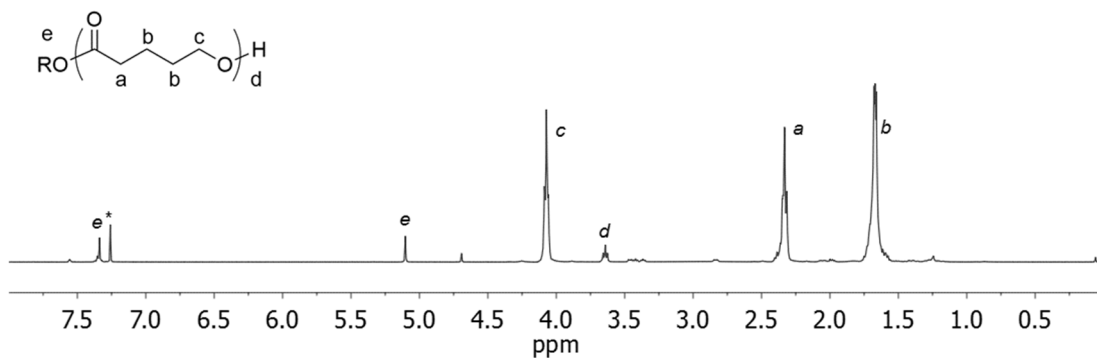


Figure A.5. ^1H NMR spectrum of PVL initiated from BDM (400 MHz, 293 K, CDCl₃; * = CHCl₃).

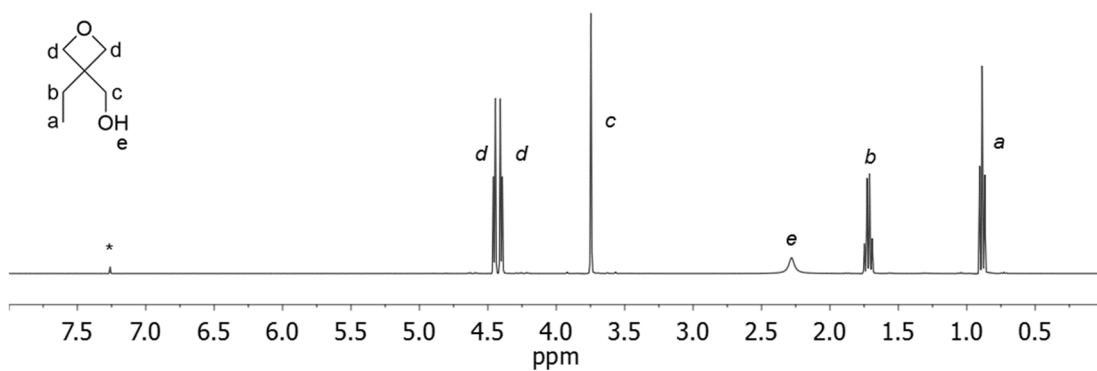


Figure A.6. ^1H NMR spectrum of 3-ethyl-3-hydroxymethyloxetane (400 MHz, 293 K, CDCl₃; * = CHCl₃).

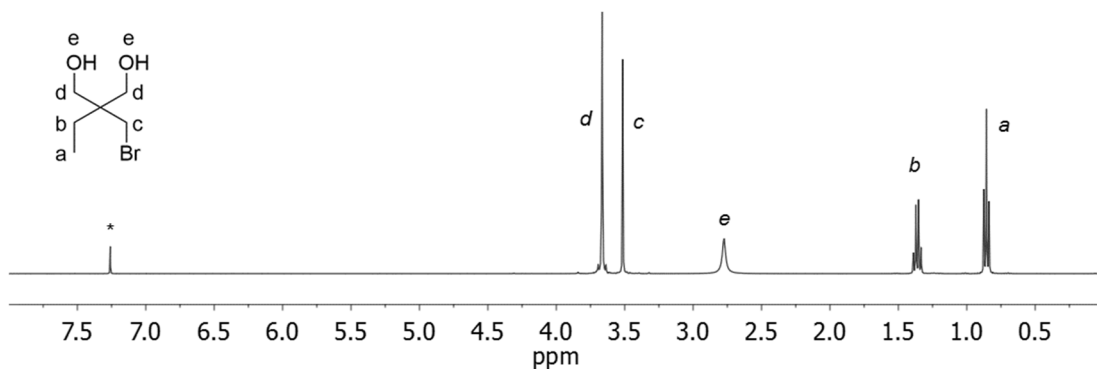


Figure A.7. ^1H NMR spectrum of 2-(bromomethyl)-2-ethyl-1,3-propanediol (400 MHz, 293 K, CDCl_3 ; * = CHCl_3).

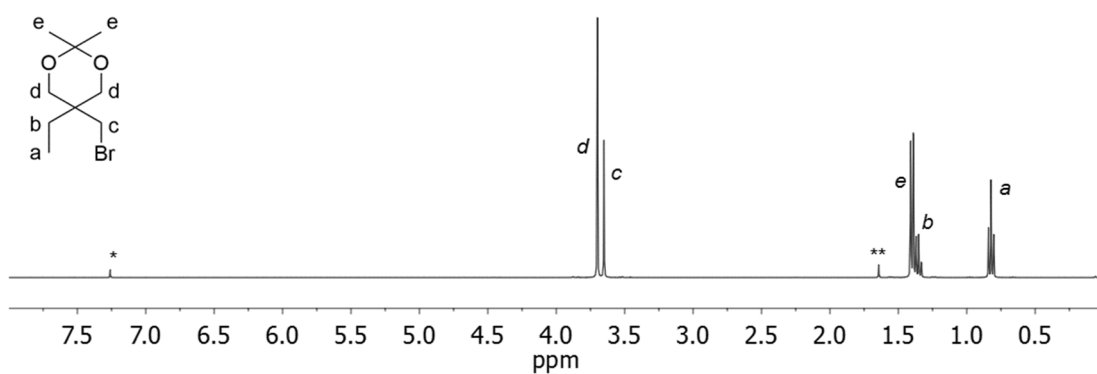


Figure A.8. ^1H NMR spectrum of 5-(bromomethyl)-5-ethyl-2,2-dimethyl-1,3-dioxane (400 MHz, 293 K, CDCl_3 ; * = CHCl_3 , ** = H_2O).

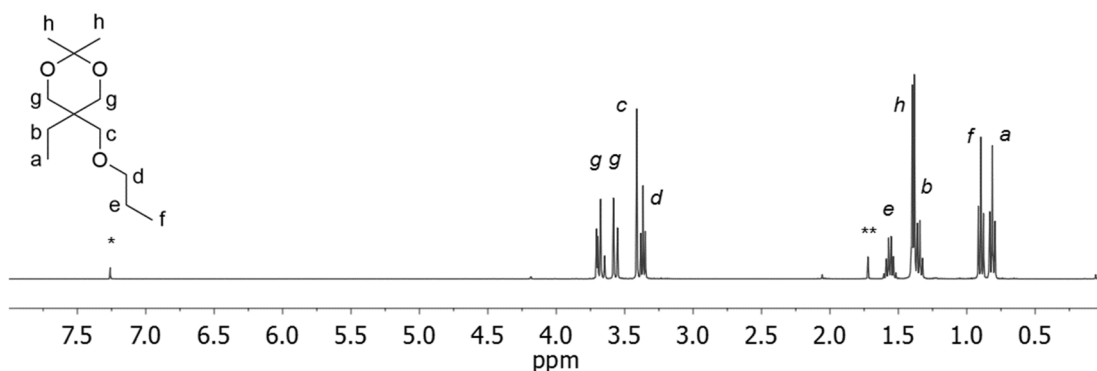


Figure A.9. ^1H NMR spectrum of 5-ethyl-2,2-dimethyl-5-(propoxymethyl)-1,3-dioxane (400 MHz, 293 K, CDCl_3 ; * = CHCl_3 , ** = H_2O).

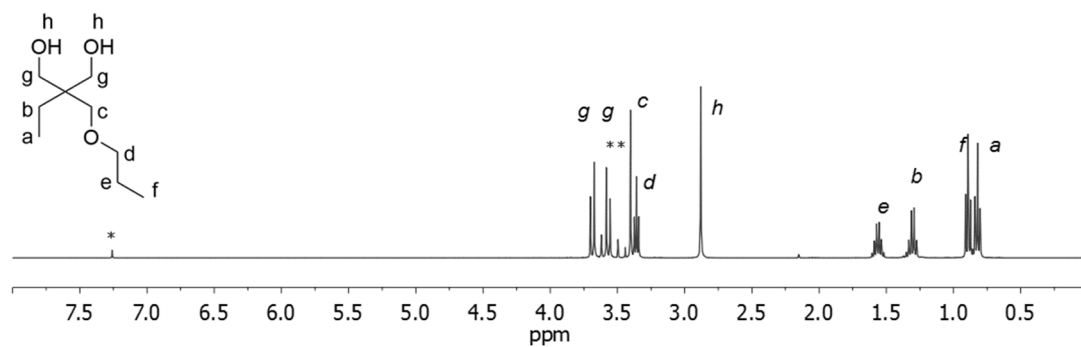


Figure A.10. ^1H NMR spectrum of 2-ethyl-2-(propoxymethyl)propane-1,3-diol (400 MHz, 293 K, CDCl_3 ;

* = CHCl_3 , ** = residual MeOH).

A.2 Supplementary ^{13}C NMR spectra

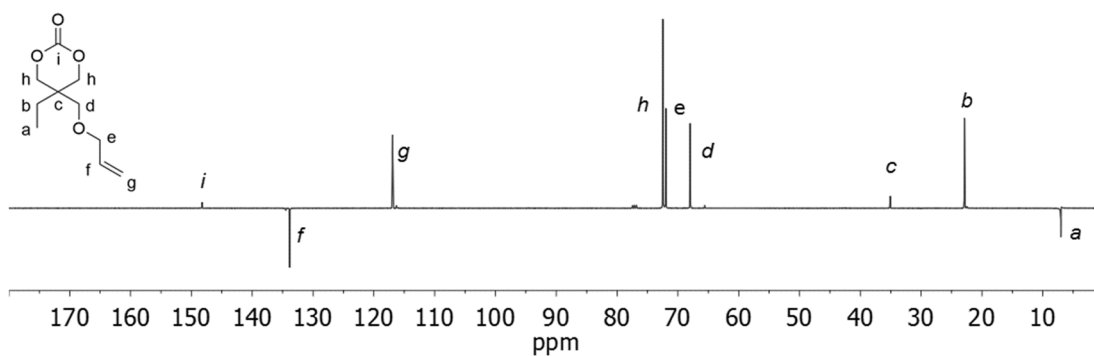


Figure A.11. ^{13}C NMR spectrum of AOMEAC (125 MHz, 293 K, CDCl_3).

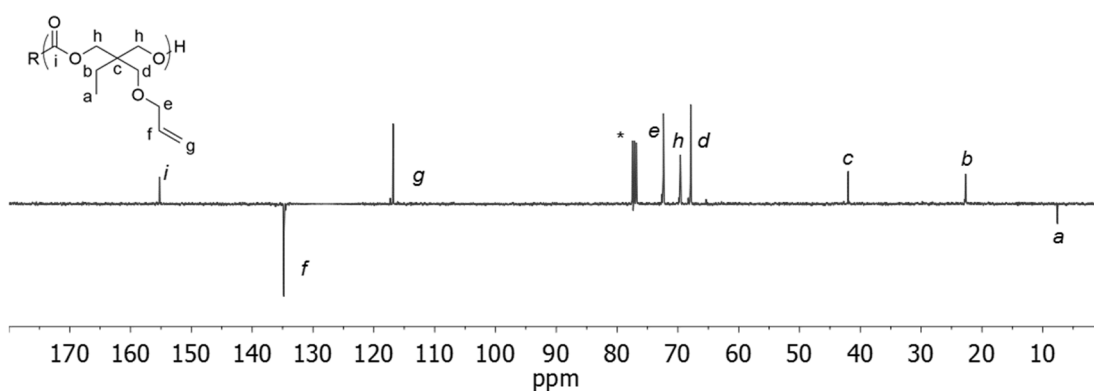


Figure A.12. ^{13}C NMR spectrum of PAOMEAC initiated from 1,4-benzenedimethanol (BDM) (125 MHz, 293 K, CDCl_3 ; * = CHCl_3).

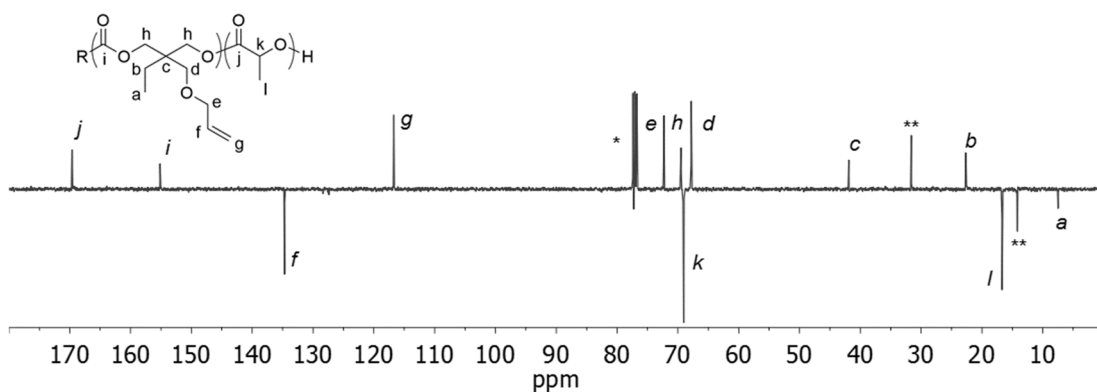


Figure A.13. ^{13}C NMR spectrum of PLLA-*b*-PAOMEC-*b*-PLLA (125 MHz, 293 K, CDCl_3 ; * = CHCl_3 , ** = residual *n*-hexane from precipitation).

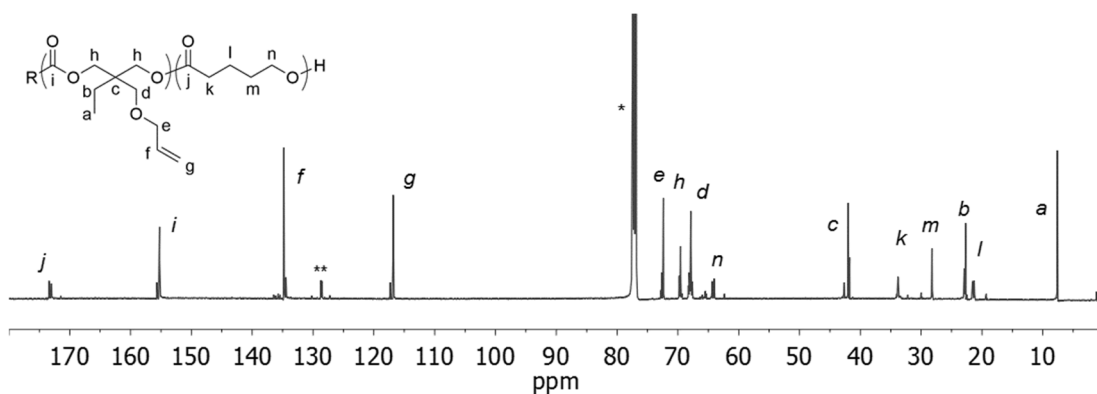


Figure A.14. ^{13}C NMR spectrum of P(AOMEC₂₁-co-VL₁₂) initiated from BDM (125 MHz, 293 K, CDCl_3 ; * = CHCl_3 , ** = BDM).

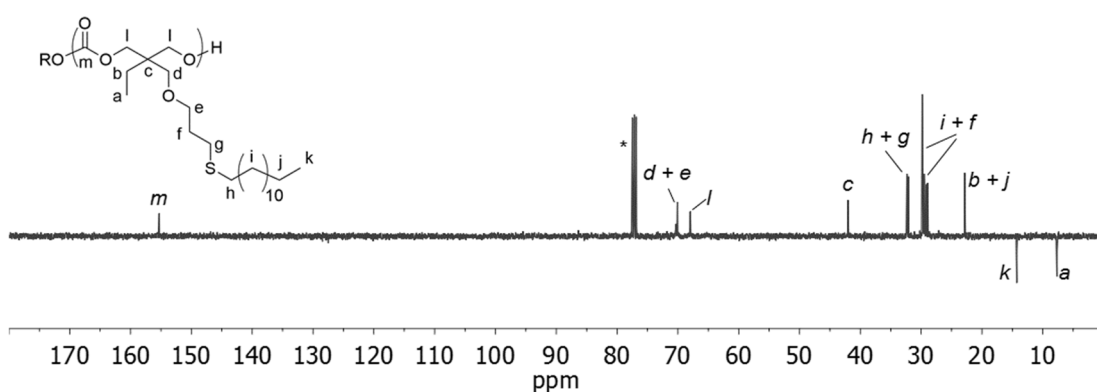


Figure A.15. ^{13}C NMR spectrum of PAOMEC₂₄ grafted with 1-dodecanethiol (125 MHz, 293 K, CDCl_3 ; * = CHCl_3).

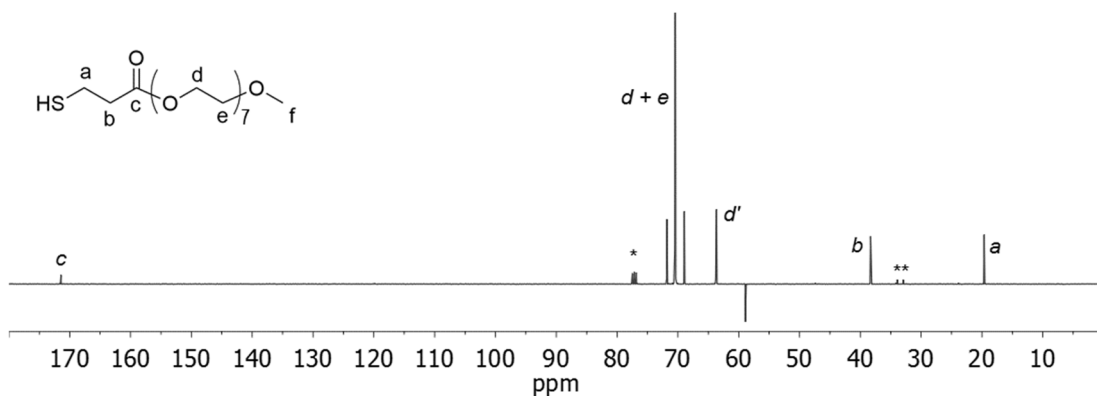


Figure A.16. ^{13}C NMR spectrum of mPEG₃₅₀-SH (125 MHz, 293 K, CDCl₃; * = CHCl₃, ** = disulfide impurity).

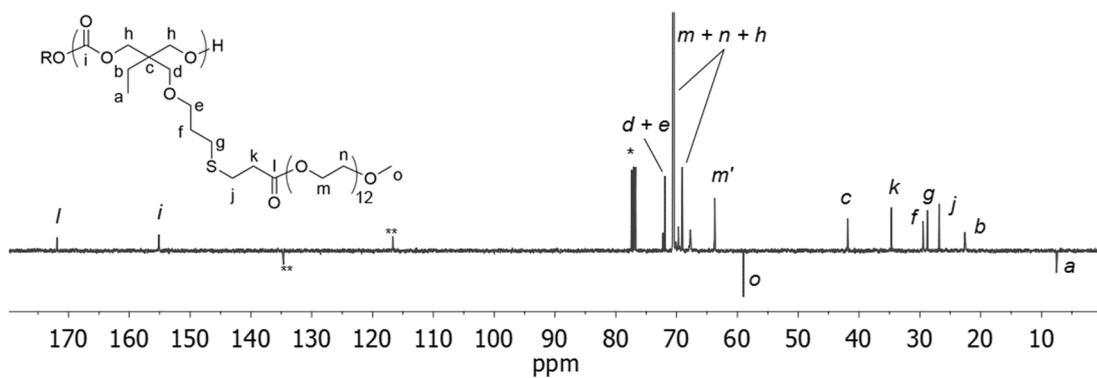


Figure A.17. ^{13}C NMR spectrum of PAOMEC₈₂-g-PEG₅₅₀-OMe (125 MHz, 293 K, CDCl₃; * = CHCl₃, ** = unreacted alkene functionality).

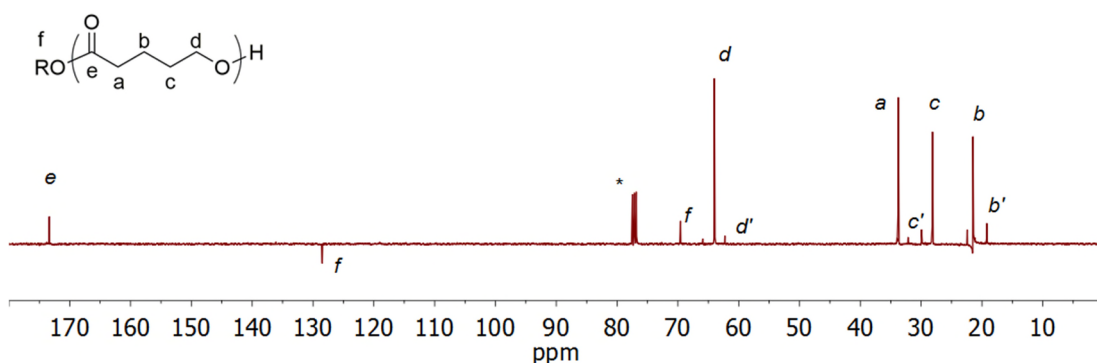


Figure A.18. ^{13}C NMR spectrum of PVL₇₈ initiated from BDM (125 MHz, 293 K, CDCl₃; * = CHCl₃).

Appendix – Supplementary Information

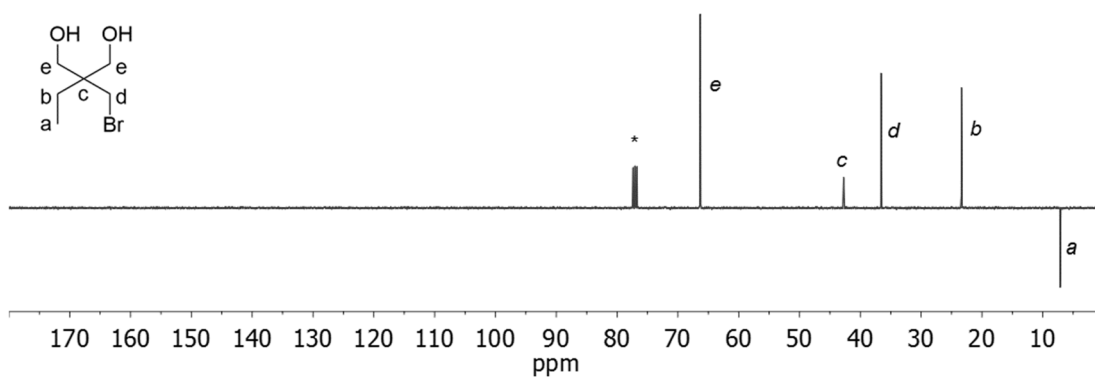


Figure A.19. ^{13}C NMR spectrum of 2-(bromomethyl)-2-ethyl-1,3-propanediol (125 MHz, 293 K, CDCl_3 ; * = CHCl_3).

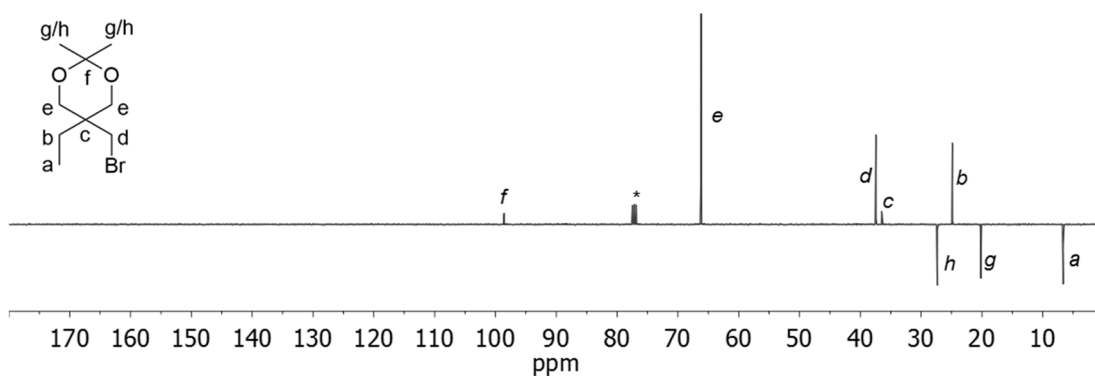


Figure A.20. ^{13}C NMR spectrum of 5-(bromomethyl)-5-ethyl-2,2-dimethyl-1,3-dioxane (125 MHz, 293 K, CDCl_3 ; * = CHCl_3).

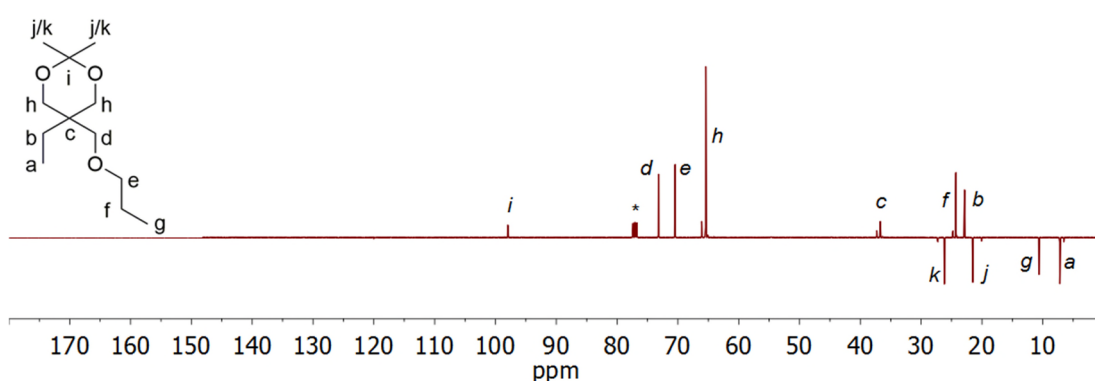


Figure A.21. ^{13}C NMR spectrum of 5-ethyl-2,2-dimethyl-5-(propoxymethyl)-1,3-dioxane (125 MHz, 293 K, CDCl_3 ; * = CHCl_3).

Appendix – Supplementary Information

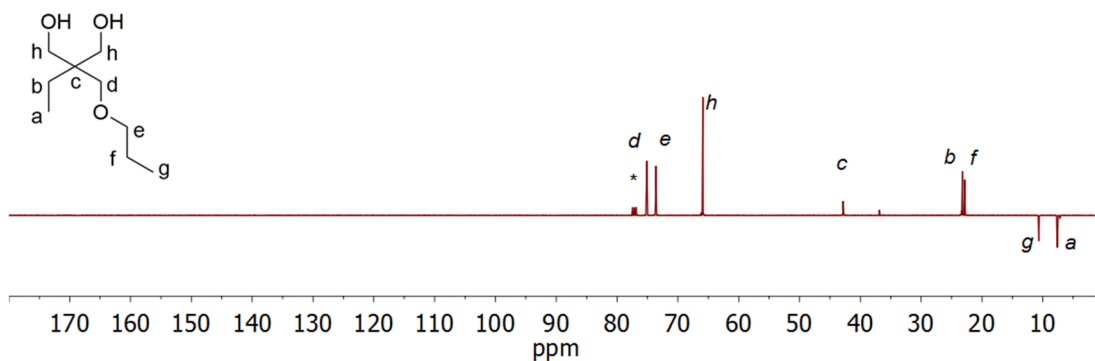


Figure A.22. ^{13}C NMR spectrum of 2-ethyl-2-(propoxymethyl)propane-1,3-diol (125 MHz, 293 K, CDCl_3 ;

* = CHCl_3).

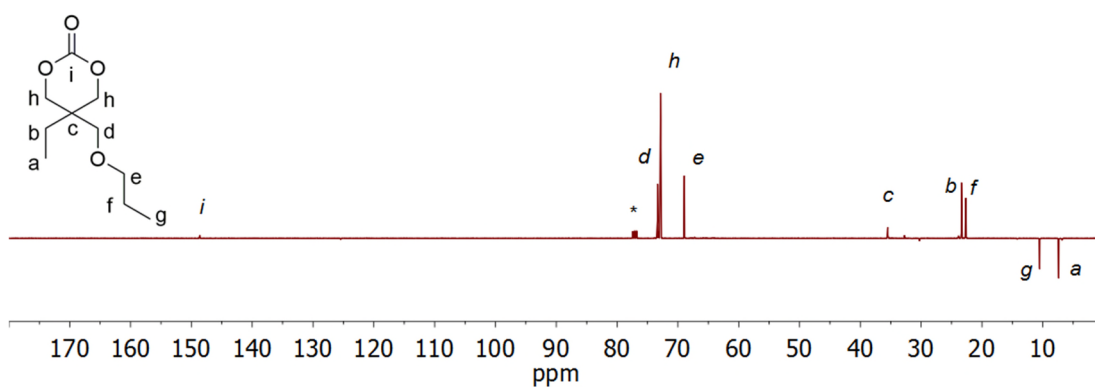


Figure A.23. ^{13}C NMR spectrum of POMEc (125 MHz, 293 K, CDCl_3 ; * = CHCl_3).

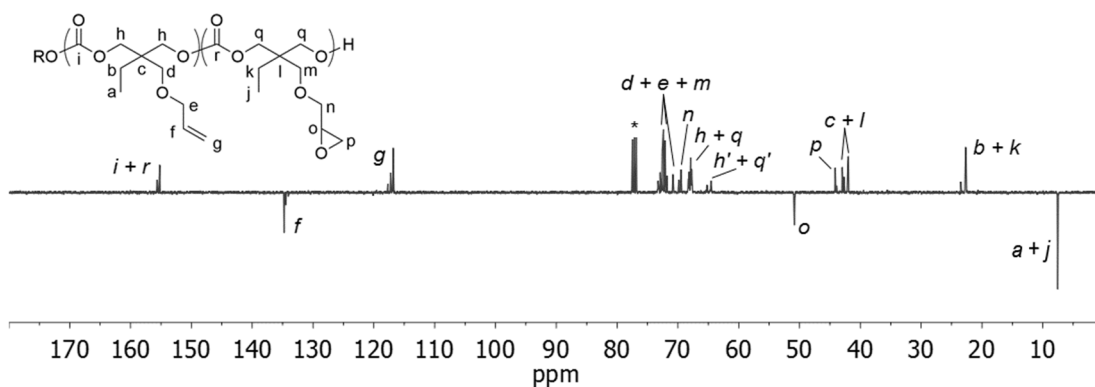


Figure A.24. ^{13}C NMR spectrum of P(AOMEc₅-co-OOMEc₅) (125 MHz, 293 K, CDCl_3 ; * = CHCl_3).

Appendix – Supplementary Information

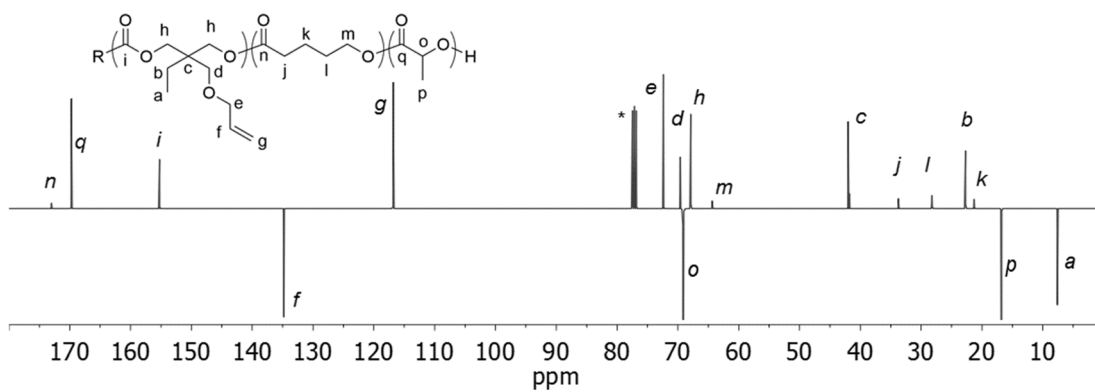


Figure A.25. ^{13}C NMR spectrum of PLLA₆₈-*b*-P(AOMECS₈₅-*co*-VL₁₇)-*b*-PLLA₆₈ triblock copolymer (125 MHz, 293 K, CDCl₃; * = CHCl₃).

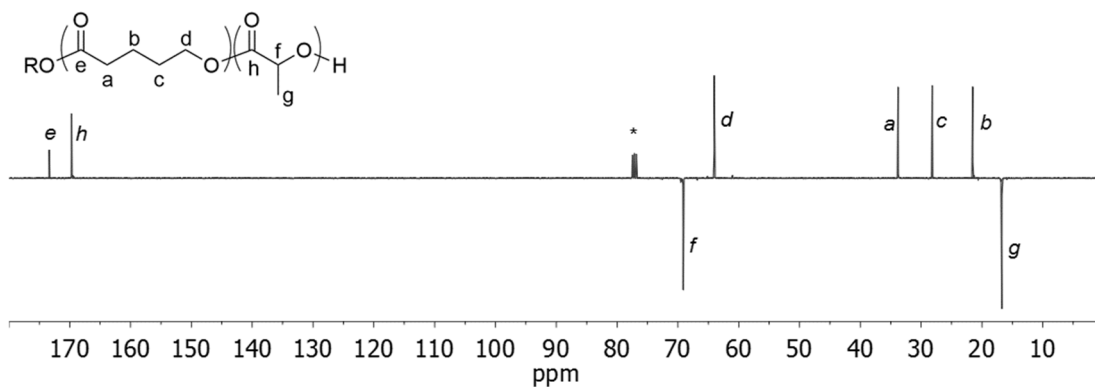


Figure A.26. ^{13}C NMR spectrum of PLLA₆₄-*b*-PVL₁₁₁-*b*-PLLA₆₄ (125 MHz, 293 K, CDCl₃; * = CHCl₃).

A.3 Supplementary size exclusion chromatograms

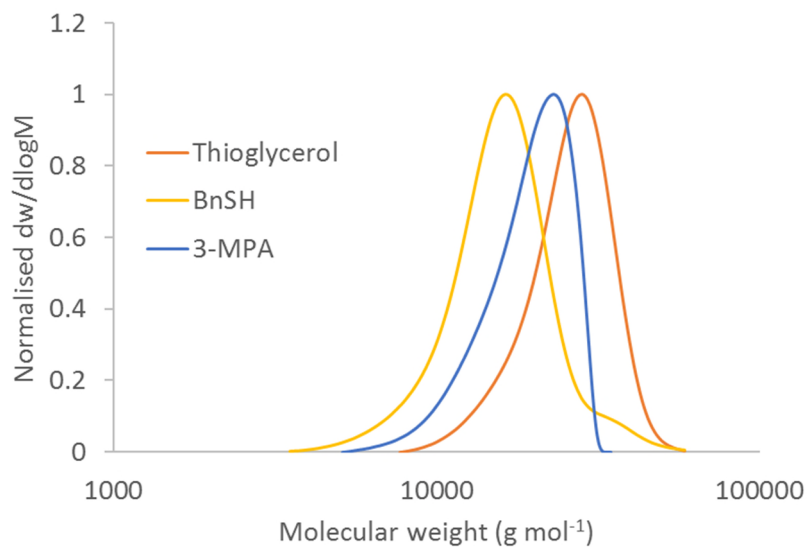


Figure A.27. Size exclusion chromatograms of PAOMEC₇₉ functionalised with 3-MPA, BnSH and 1-thioglycerol. Samples measured against poly(methyl methacrylate) standards using DMF as eluent.

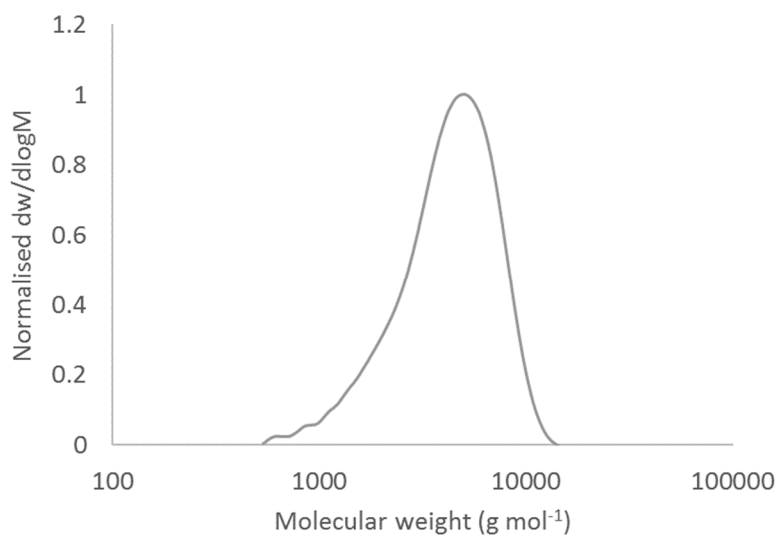


Figure A.28. Size exclusion chromatogram of P(MAC₉-co-VL₅) initiated from BDM. Sample measured against polystyrene standards using CHCl₃ as eluent.

Appendix – Supplementary Information

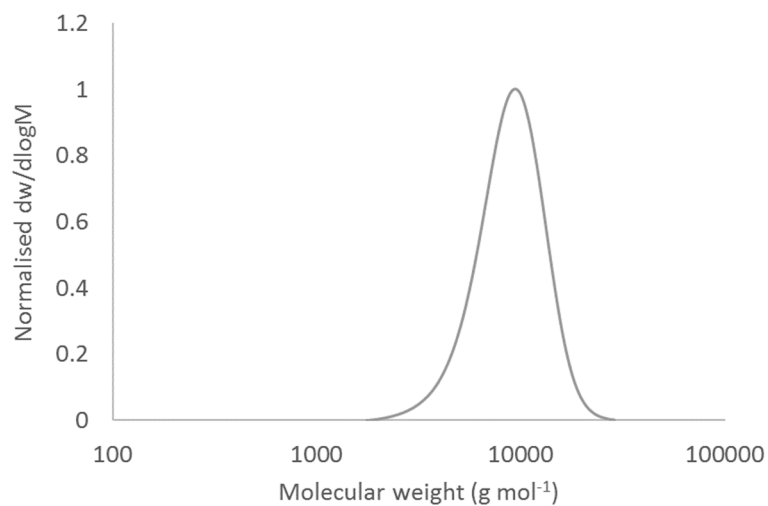


Figure A.29. Size exclusion chromatogram of PVL₇₈ initiated from BDM. Sample measured against polystyrene standards using CHCl₃ as eluent.

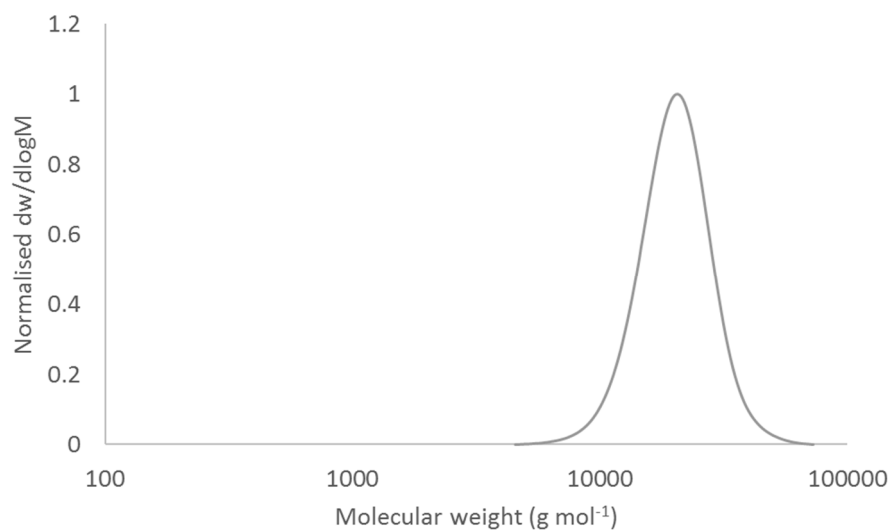


Figure A.30. Size exclusion chromatogram of P(POMEC₄₉-co-AOMEC₅₁). Sample measured against polystyrene standards using CHCl₃ as eluent.

A.4 Differential scanning calorimetry (DSC) thermograms for
 PLLA-*b*-P(AOMECCo-VL)-*b*-PLLA triblock copolymers

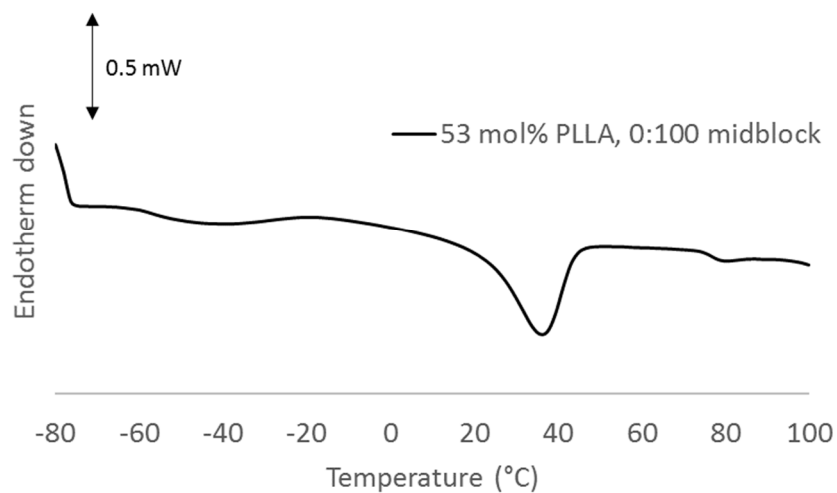


Figure A.31. DSC thermogram for PLLA₆₄-*b*-PVL₁₁₁-*b*-PLLA₆₄, measured at a heating rate of 2 °C min⁻¹.

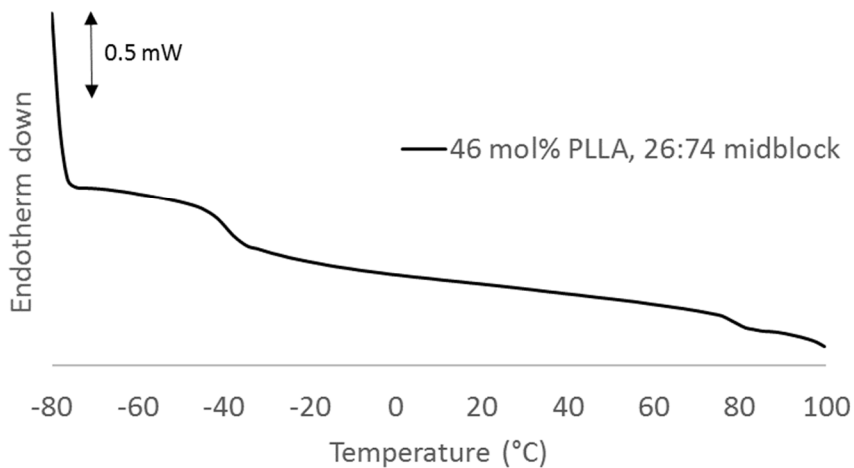


Figure A.32. DSC thermogram for PLLA₄₇-*b*-P(AOMECCo-VL₇₀)-*b*-PLLA₆₄, measured at a heating rate of 2 °C min⁻¹.

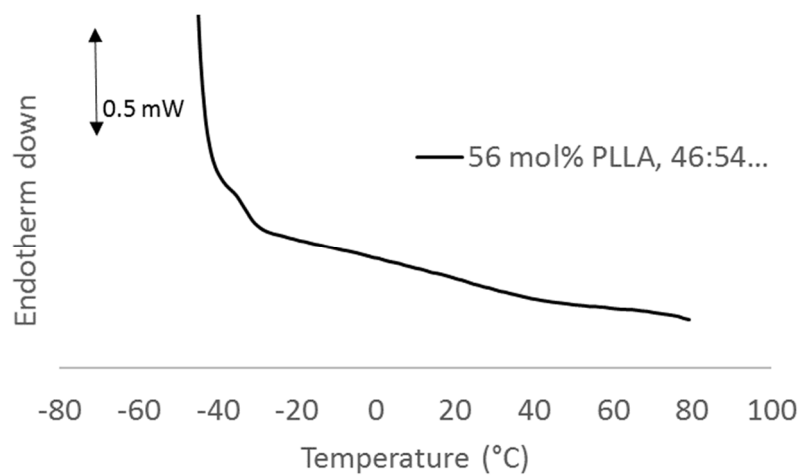


Figure A.33. DSC thermogram for PLLA₆₃-*b*-P(AOMECC₄₅-*co*-VL₅₃)-*b*-PLLA₆₃, measured at a heating rate of 2 °C min⁻¹. Sample analysed from -50 to 80 °C.

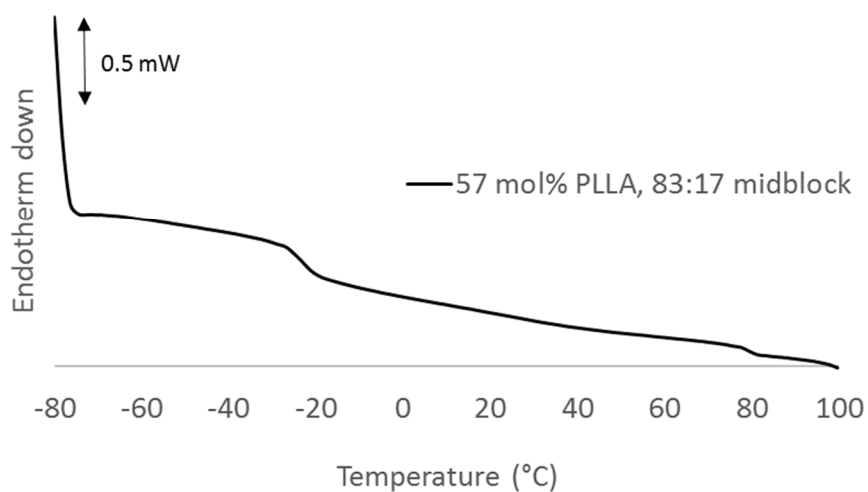


Figure A.34. DSC thermogram for PLLA₆₈-*b*-P(AOMECC₈₅-*co*-VL₁₇)-*b*-PLLA₆₈, measured at a heating rate of 2 °C min⁻¹.

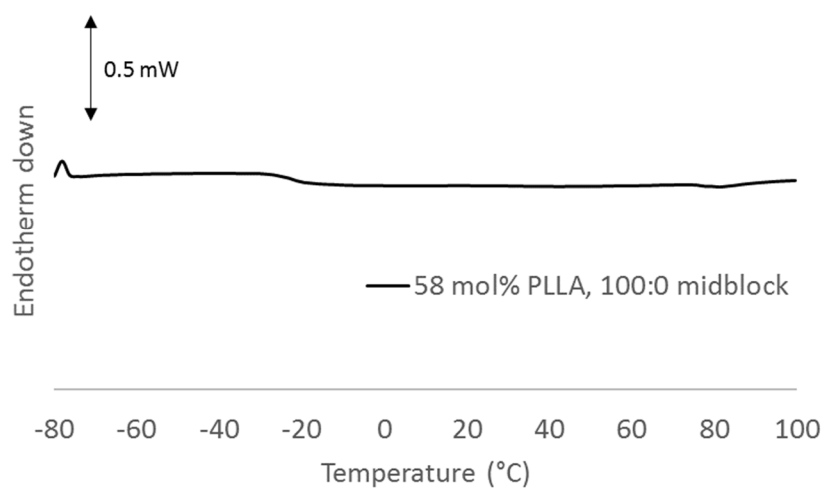


Figure A.35. DSC thermogram for PLLA₇₂-*b*-PAOMEC₉₈-*b*-PLLA₇₂, measured at a heating rate of 2 °C min⁻¹.

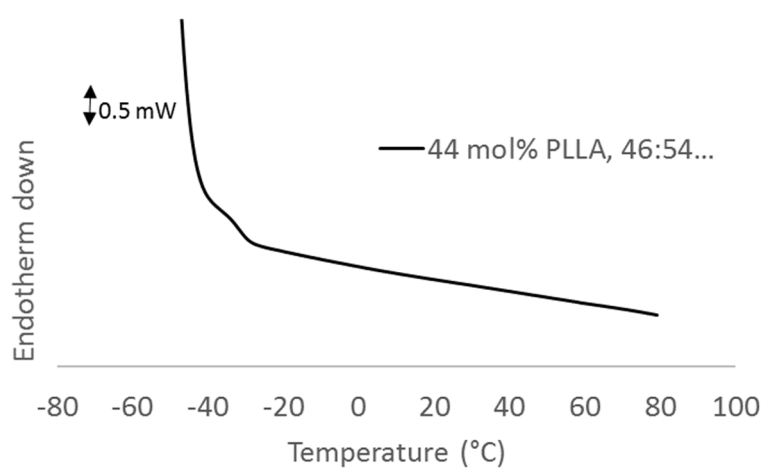


Figure A.36. DSC thermogram for PLLA₄₀-*b*-P(AOMEC₄₅-*co*-VL₅₃)-*b*-PLLA₄₀, measured at a heating rate of 2 °C min⁻¹. Sample analysed from -50 to 80 °C.

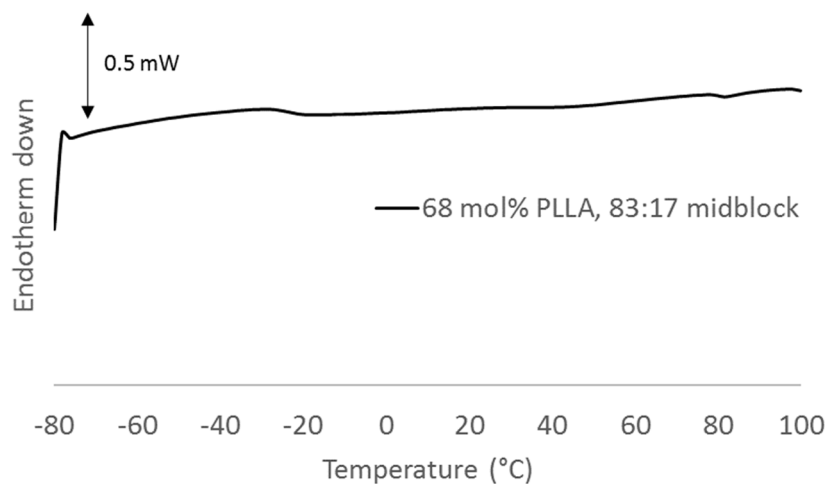


Figure A.37. DSC thermogram for PLLA₁₀₅-*b*-P(AOME₈₅-*co*-VL₁₇)-*b*-PLLA₁₀₅, measured at a heating rate of 2 °C min⁻¹.

A.5 Dynamic mechanical thermal analysis data for PLLA-*b*-P(AOME₈₅-*co*-VL)-*b*-PLLA triblock copolymers

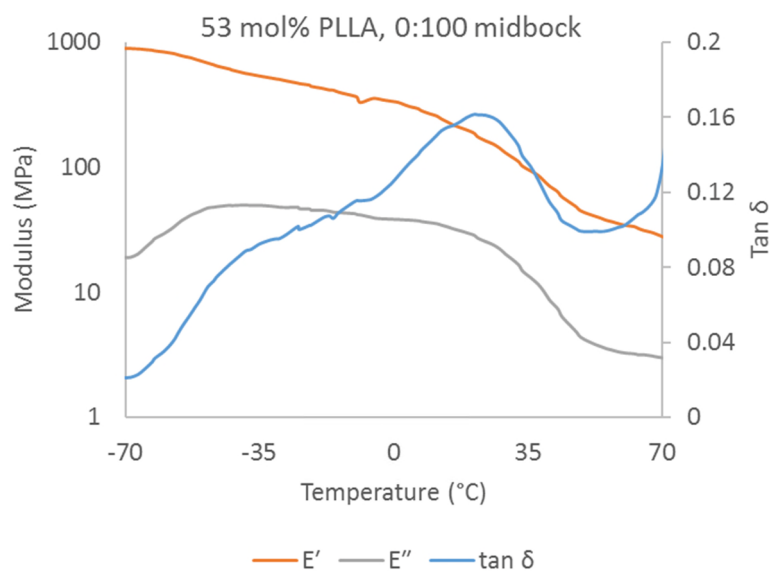


Figure A.38. E' , E'' and $\tan \delta$ for PLLA₆₄-*b*-PVL₁₁₁-*b*-PLLA₆₄, measured at an oscillation frequency of 0.5 Hz using a heating rate of 2 °C min⁻¹.

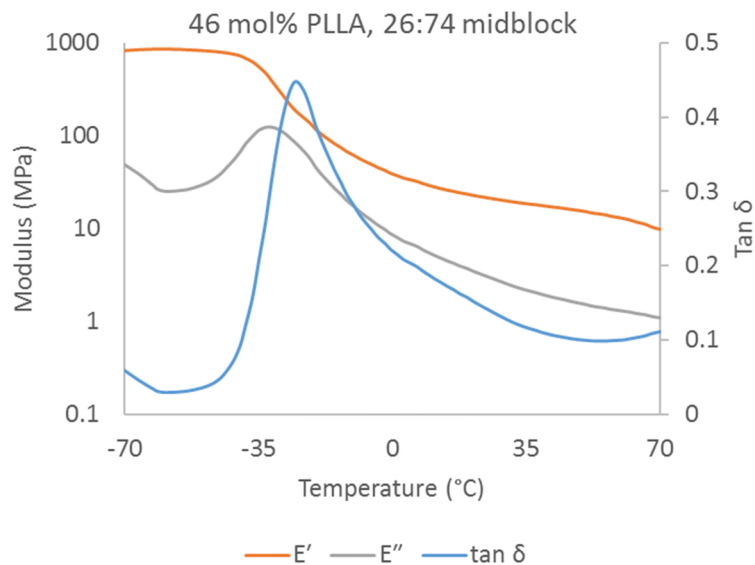


Figure A.39. E' , E'' and $\tan \delta$ for PLLA₄₇-*b*-P(AOMECL₂₄-co-VL₇₀)-*b*-PLLA₆₄, measured at an oscillation frequency of 0.5 Hz using a heating rate of 2 °C min⁻¹.

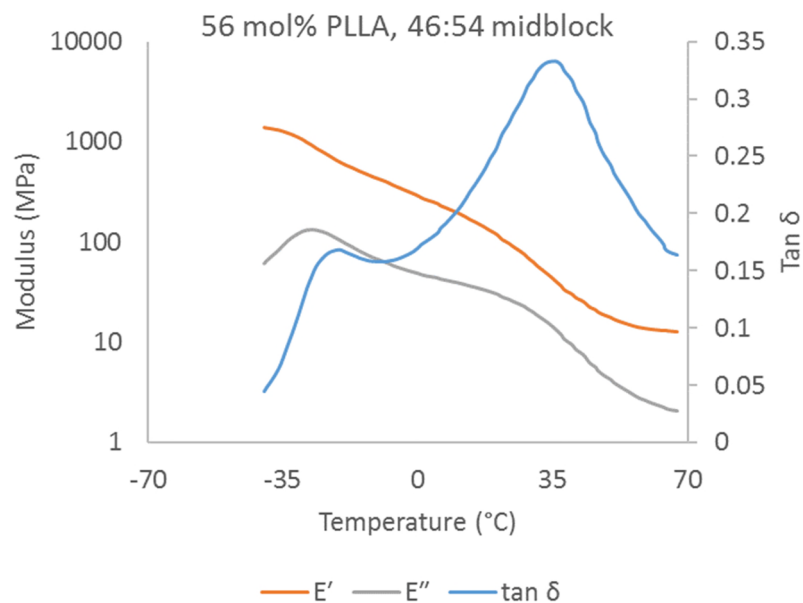


Figure A.40. E' , E'' and $\tan \delta$ for PLLA₆₃-*b*-P(AOMECL₄₅-co-VL₅₃)-*b*-PLLA₆₃, measured at an oscillation frequency of 0.5 Hz using a heating rate of 2 °C min⁻¹. Sample analysed from -40 to 70 °C.

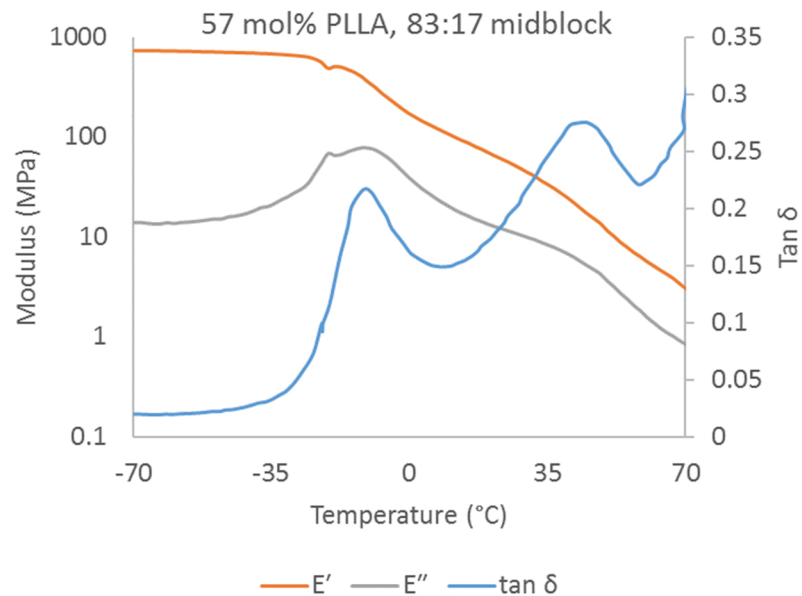


Figure A.41. E' , E'' and $\tan \delta$ for PLLA₆₈-*b*-P(AOME_{C85}-*co*-VL₁₇)-*b*-PLLA₆₈, measured at an oscillation frequency of 0.5 Hz using a heating rate of 2 °C min⁻¹.

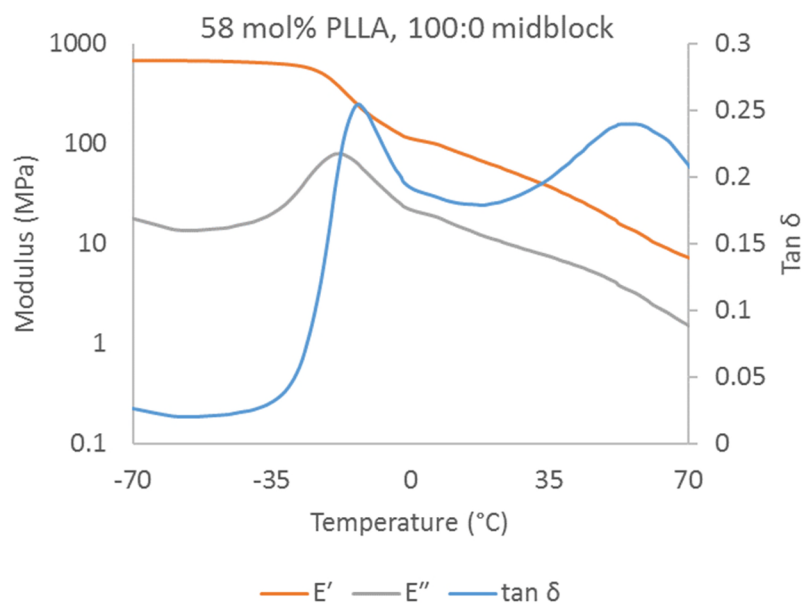


Figure A.42. E' , E'' and $\tan \delta$ for PLLA₇₂-*b*-PAOME_{C98}-*b*-PLLA₇₂, measured at an oscillation frequency of 0.5 Hz using a heating rate of 2 °C min⁻¹.

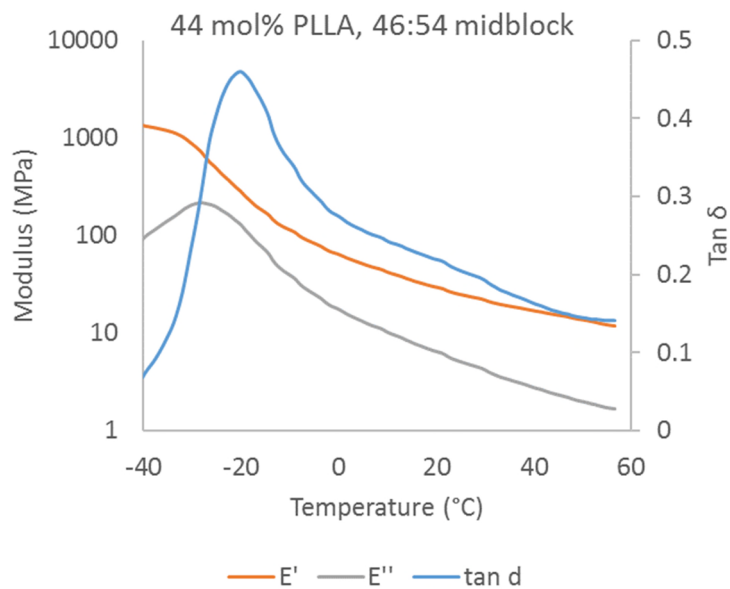


Figure A.43. E' , E'' and $\tan \delta$ for PLLA₄₀-*b*-P(AOMECC₄₅-co-VL₅₃)-*b*-PLLA₄₀, measured at an oscillation frequency of 0.5 Hz using a heating rate of 2 °C min⁻¹.

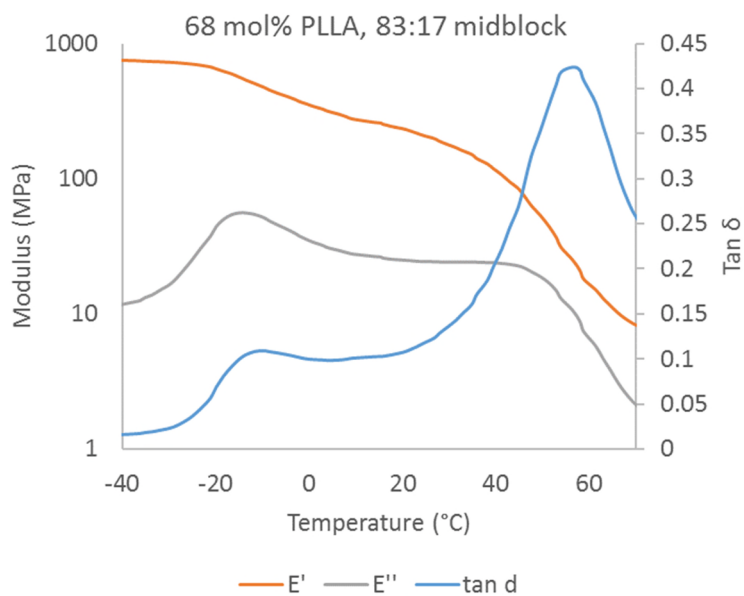


Figure A.44. E' , E'' and $\tan \delta$ for PLLA₁₀₅-*b*-P(AOMECC₈₅-co-VL₁₇)-*b*-PLLA₁₀₅, measured at an oscillation frequency of 0.5 Hz using a heating rate of 2 °C min⁻¹.